



# Electrodeposició de capes metàl·liques per a la seva incorporació en sensors i actuadors

## Metallic films deposition for their incorporation in sensors and actuators

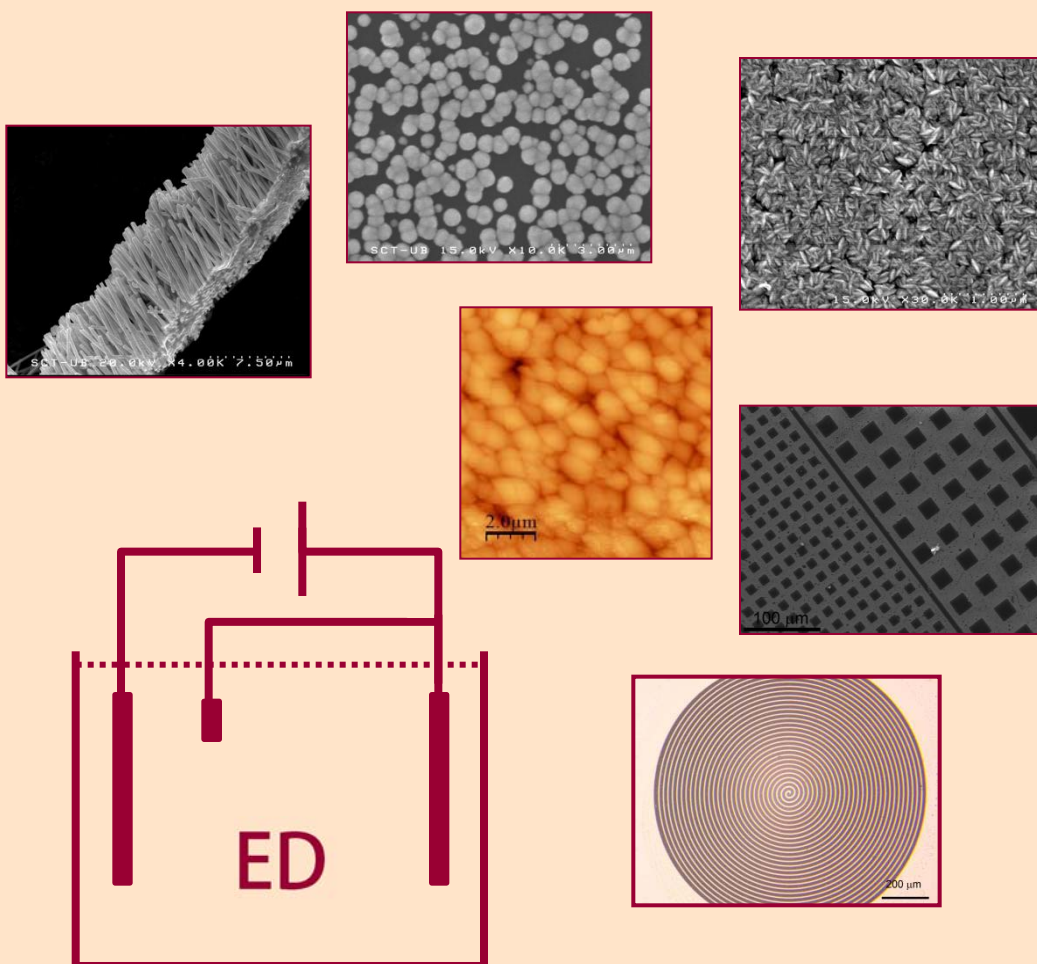
Meritxell Cortés Francisco

**ADVERTIMENT.** La consulta d'aquesta tesi queda condicionada a l'acceptació de les següents condicions d'ús: La difusió d'aquesta tesi per mitjà del servei TDX ([www.tdx.cat](http://www.tdx.cat)) ha estat autoritzada pels titulars dels drets de propietat intel·lectual únicament per a usos privats emmarcats en activitats d'investigació i docència. No s'autoritza la seva reproducció amb finalitats de lucre ni la seva difusió i posada a disposició des d'un lloc aliè al servei TDX. No s'autoritza la presentació del seu contingut en una finestra o marc aliè a TDX (framing). Aquesta reserva de drets afecta tant al resum de presentació de la tesi com als seus continguts. En la utilització o cita de parts de la tesi és obligat indicar el nom de la persona autora.

**ADVERTENCIA.** La consulta de esta tesis queda condicionada a la aceptación de las siguientes condiciones de uso: La difusión de esta tesis por medio del servicio TDR ([www.tdx.cat](http://www.tdx.cat)) ha sido autorizada por los titulares de los derechos de propiedad intelectual únicamente para usos privados enmarcados en actividades de investigación y docencia. No se autoriza su reproducción con finalidades de lucro ni su difusión y puesta a disposición desde un sitio ajeno al servicio TDR. No se autoriza la presentación de su contenido en una ventana o marco ajeno a TDR (framing). Esta reserva de derechos afecta tanto al resumen de presentación de la tesis como a sus contenidos. En la utilización o cita de partes de la tesis es obligado indicar el nombre de la persona autora.

**WARNING.** On having consulted this thesis you're accepting the following use conditions: Spreading this thesis by the TDX ([www.tdx.cat](http://www.tdx.cat)) service has been authorized by the titular of the intellectual property rights only for private uses placed in investigation and teaching activities. Reproduction with lucrative aims is not authorized neither its spreading and availability from a site foreign to the TDX service. Introducing its content in a window or frame foreign to the TDX service is not authorized (framing). This rights affect to the presentation summary of the thesis as well as to its contents. In the using or citation of parts of the thesis it's obliged to indicate the name of the author.

# Electrodeposició de capes metàl·liques per a la seva incorporació en sensors i actuadors



Tesi doctoral

**Meritxell Cortés Francisco**

Universitat de Barcelona 2012

UNIVERSITAT DE BARCELONA  
DEPARTAMENT DE QUÍMICA FÍSICA

Laboratori d'Electrodeposició i Corrosió (Electrodep)



**Electrodeposició de capes metàl·liques  
per a la seva incorporació  
en sensors i actuadors**

Meritxell Cortés Francisco

TESIS DOCTORAL

Barcelona, setembre 2012



UNIVERSITAT DE BARCELONA  
FACULTAT DE QUÍMICA  
DEPARTAMENT DE QUÍMICA FÍSICA

Programa de Doctorat Electroquímica. Ciència i Tecnologia  
Bienni 2006-2008

**Electrodeposició de capes metàl·liques  
per a la seva incorporació  
en sensors i actuadors**

Memòria que presenta MERITXELL CORTÉS FRANCISCO per  
optar al títol de Doctora per la Universitat de Barcelona

Directores de la tesi:

Dra. Elisa VALLÉS GIMÉNEZ	Dra. Elvira GÓMEZ VALENTÍN
Professora Titular de Química Física	Professora Titular de Química Física
Universitat de Barcelona	Universitat de Barcelona



**Electrodeposició de capes metàl·liques  
per a la seva incorporació  
en sensors i actuadors**

**Metallic films deposition  
for their incorporation  
in sensors and actuators**



# Contents

<b>1</b>	<b>Introduction</b>	<b>1</b>
1.1	Electrodeposition . . . . .	1
1.2	Additives . . . . .	4
1.3	Electrodeposition advantages and drawbacks . . . . .	5
1.4	History of electrodeposition . . . . .	7
1.5	Electrochemical deposition in actual industry . . . . .	10
1.6	New applications of electrodeposition . . . . .	13
<b>2</b>	<b>Objectives</b>	<b>19</b>
<b>3</b>	<b>Experimental Procedure</b>	<b>23</b>
3.1	Electrochemical experiments . . . . .	23
3.1.1	Experimental setup . . . . .	23
3.1.2	Electrochemical cells and electrodes . . . . .	23
3.1.3	Chemicals . . . . .	30
3.1.4	Electrochemical techniques . . . . .	33
3.2	Ex-situ characterisation techniques . . . . .	36
3.2.1	Morphological analysis . . . . .	36
3.2.2	Compositional analysis . . . . .	39
3.2.3	Structural characterisation . . . . .	40
3.2.4	Roughness and thickness measurements . . . . .	44
3.2.5	Magnetic measurements . . . . .	45
3.2.6	Contact angle measurements . . . . .	49
3.2.7	Electrical characterisation . . . . .	50
3.3	Etching . . . . .	52
3.4	Photolithography masks . . . . .	53
3.5	Simulations . . . . .	57

<b>4</b>	<b>Electrodeposition of Copper coils for inductive sensors</b>	<b>59</b>
4.1	Introduction . . . . .	59
4.2	Results presented in this chapter . . . . .	73
4.2.1	Optimisation of copper electrodeposition processes for Si technology based inductive microsystems . . . . .	75
4.2.2	Analysis of the texture and stress of the Cu deposits . . . . .	83
4.2.3	Implementation of the deposition conditions over plastic substrates . . . . .	93
4.2.4	Design and electrochemical preparation of inductive copper coils for magnetic particles detection . . . . .	99
4.3	Conclusions . . . . .	109
<b>5</b>	<b>Deposition of CoPt and CoPtP magnetic alloys for MEMS application</b>	<b>113</b>
5.1	Study of the electrodeposition process of the binary CoPt and the ternary CoPtP alloys . . . . .	113
5.2	Results of the preparation of thin films CoPt and CoPtP . . . . .	121
5.2.1	Ternary CoPtP electrodeposition process: Structural and magnetic properties of the deposits . . . . .	123
5.2.2	Magnetic properties of nanocrystalline CoPt electrodeposited films. Influence of P incorporation . . . . .	131
5.3	Electrodeposition of CoPt micro/nanostructures. Modulation of the magnetic properties . . . . .	141
5.4	Results of the micro/nanostructures preparation . . . . .	149
5.4.1	Magnetic CoPt (60-70 wt % Pt) microstructures fabricated by the electrochemical method . . . . .	151
5.4.2	Electrochemical growth of CoPt nanowires of different aspect ratio and their magnetic properties . . . . .	159
5.4.3	Electrochemical preparation and characterisation of CoPt magnetic particles . . . . .	167
5.4.4	CoPt nanoscale structures with different geometry prepared by electrodeposition for modulation of their magnetic properties . . . . .	173
5.4.5	Electrochemical preparation and magnetic properties of submicrometric core-shell CoPt-CoNi particles . . . . .	181
5.5	Conclusions . . . . .	187
<b>6</b>	<b>Formation of organic monolayers over electrodeposited magnetic materials as a first step for spintronics spin valves fabrication</b>	<b>193</b>

6.1	Introduction . . . . .	193
6.2	Results presented in this chapter . . . . .	203
6.2.1	Adsorption of organic layers over electrodeposited magnetite ( $\text{Fe}_3\text{O}_4$ ) thin films . . . . .	205
6.2.2	Analysis of the purity of magnetite deposits . . . . .	211
6.3	Conclusions . . . . .	223
<b>7</b>	<b>Conclusions</b>	<b>225</b>
<b>A</b>	<b>Resum en català</b>	<b>227</b>
	<b>Bibliography</b>	<b>265</b>



# Chapter 1

## Introduction

### 1.1 Electrodeposition

Electrodeposition involves chemical phenomena associated with charge separation and transfer that can occur homogeneously in solution, or heterogeneously over electrode surfaces. In order to assure electroneutrality at least two charge transfer half-reactions should take place. In the case of heterogeneous redox reactions, these half-reactions occur over two different electrodes immersed in a solution.

Electrodeposition is a process in which metal ions present in a solution are reduced to coat a conductive object with a thin layer of the material. The chemical reaction that takes place could be described as 1.1:



This process involves the application of an electric current through the solution containing the ions to reduce them onto the substrate. This reaction is heterogeneous and takes place in the interfacial region between electrode and solution. Each half-reaction has associated a standard electrode

potential  $E^\circ$ . For half-reactions at equilibrium, the equilibrium potential,  $E_{eq}$ , can be related to the standard electrode potential through the Nernst equation 1.2:

$$\mathbf{E}_{eq} = E^\circ - \frac{RT}{nF} \sum \nu_i \ln a_i \quad (1.2)$$

Where  $\nu_i$  are the stoichiometric numbers and  $a_i$  are the species activities.

There is a minimum energy that the transferable electrons from the electrode must have before transfer can occur, which corresponds to sufficiently negative potential. In most of the electrodeposition processes, it is necessary to apply a higher potential than equilibrium one in order to overcome the activation barrier and allow the reduction reaction to take place. This extra potential is called the overpotential,  $\eta$ . For that reason a basic electrochemical study is needed in order to establish the potentials at which each process takes place.

To perform the electrodeposition there are some basic elements, such as: the electrolyte, the electrolytic cell, the electrodes and the potentiostat/galvanostat. The electrolyte is the solution that contains the ions of the metal or metals that we want to deposit, usually known as electroactive species. It is generally an aqueous solution and it can contain other species either to control the pH or to increase the conductivity of the solution or to improve the characteristic of the deposits. The receptacle that contains the electrolyte is the electrolytic cell. In order to perform the electrodeposition, at least two electrodes are necessary: one working electrode which acts as the cathode and where the reduction of the metal ions takes place, it should be a conductive substrate in order to electrodeposition can occur.

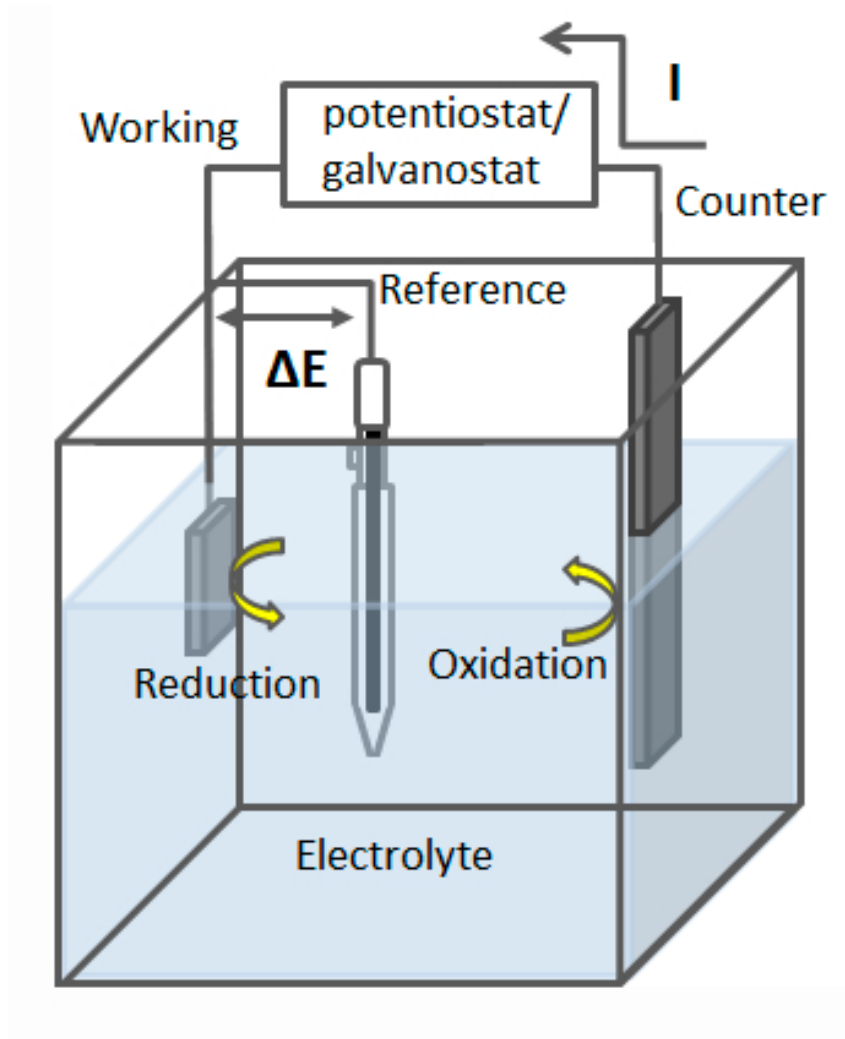


Figure 1.1: Schematic representation of the experimental set up

The second necessary electrode is the counter or auxiliary which acts as the anode of the process. In order to have a better control of the process a third electrode can be used, this is called reference electrode and allows controlling the potential of the working electrode. Finally, the potentiostat/galvanostat is the equipment used to apply and measure the signal during the electrodeposition (Figure 1.1).

Although electrodeposition technique seems an easy method to prepare

materials, a lot of processing parameters such as electrolyte composition, pH, temperature, agitation and applied potential or current should be controlled. The variation of any of these parameters can affect the characteristics of the films such as their thickness, composition, grain size or crystalline structure, among others, which at the same time affects the properties of the material, i.e. magnetic, electric or optic properties.

## 1.2 Additives

As mentioned before, in some occasions it is necessary to add some species to improve some of the deposit characteristics. These species are called additives and they are chemical substances added in a very small proportion to the bath, modifying the physic-mechanical properties of the deposits such as: morphology, roughness, hardness, structure, corrosion resistance...

The use of the appropriate additives in an adequate concentration leads to coatings with the desired requirements. However, an excess or a misuse of the additives can lead to opaque, fragile or tensioned deposits. There are lots of additives, the more commonly used are:

- Brightener. This kind of additives decrease the roughness of the deposit, modify the nucleation process generating fine-grained deposits.
- Leveller. They are adsorbed at points where the deposit is growing too fast, and they inhibit the growth. Modify the growth speed, making it slower.
- Structure modifiers. In this case the additives adjust the stress of the

deposits.

- Carrier. They accelerate the hydrogen output and reduce the surface tension of the deposit.
- Complexing agents. They complex the metal cations, which permits to control the arrival of ions to the surface electrode. This avoids undesired dendritic growth, which produce opaque, rough and porous deposits.

### 1.3 Electrodeposition advantages and drawbacks

Electrodeposition present several advantages over other methods commonly used to prepare films and structures which require vacuum conditions, physical or chemical vapor deposition (PVD or CVD), plasma enhanced deposition (PLD), sputtering... One of these advantages is its low cost and high simplicity of the experimental setup. The equipment used is cheap and maintenance is hardly required.

On the other hand, room temperature is commonly used to grow the material or, at least, temperatures lower than 100°C. This characteristic avoids mechanical stress and other problems induced during substrate cooling.

Another advantage is the higher deposition rate achieved with respect to vacuum techniques currently used in Si technology, which allows to obtain a very wide thickness range from values below 0.1  $\mu\text{m}$  up to more than 100  $\mu\text{m}$  instead of the typically limited thickness of about 1-2  $\mu\text{m}$  achieved in the vacuum techniques. It also permits an easy control of thickness

and chemical composition of the layer. This makes electroplating irreplaceable on certain applications like magnetic read-heads fabrication and magnetic nucleus for inductive systems [1] as well as in the piezoelectric-magnetostrictive sensors response improvement [2].

It is a very versatile technique that permits a wide range of different materials with very different applications to be obtained. But maybe one of the most important advantages of the electrodeposition and surely the characteristic that has greatly contributed to its incorporation in the microelectronic industry is the capacity to deposit the material over the conducting part of the substrate leaving the insulating zones free. In this sense, this technique allows achieving the designed pattern by growing the material by electrodeposition over a lithographic substrate without any subsequent treatment like chemical etching or lift-off. Moreover, a high quantity of the precursor material used in vacuum techniques is deposited on the chamber's walls, situation that does not occur in electrodeposition.

On the contrary, electrodeposition also presents some drawbacks. On one hand, the uniformity of the electrodeposited films (thickness and chemical composition) depends on not only the cell geometry but also the hydrodynamics of the process, these factors are sometimes difficult to control. On the other hand, the electrolyte composition depletion is also important to consider in such processes in which the concentration is a critical parameter.

## 1.4 History of electrodeposition

It is not possible to precisely determine its origins, but one can easily admit that they go back at least three thousand years. Indeed, the presence in the ancient tombs of Thebes and Memphis of various objects covered with a thin layer of copper, such as vases and statuettes in clay, sword blades and wood arrowheads, allows to assume that in ancient times, the Egyptians used methods similar to electroplating copper as it is still practiced today. It must be admitted that such works could not be carried out from a concentrated solution of a salt of the metal by using an external power source. Instead of that to perform the copper deposit, it was enough to take a carved wooden statue, whose surface had previously been metalized by applying fine-grained powdered gold or by application of gold (or silver) beaten into thin sheets, immerse it and a zinc plate in the copper solution and connect them both, which produced a ion exchange. When the copper deposit was thick enough the copper statue was removed from the bath, it was dried on low heat, then proceed to a progressive heating to finally remove the ashes of the wooden support. However, these are just guesses.

Modern electrochemical deposition was invented by Italian chemist Luigi V. Brugnatelli in 1805. Brugnatelli used the invention that made five years before his colleague Alessandro Volta, the voltaic pile, to perform the first electrodeposition. This phenomenon, which was ignored by the French Academy of Sciences, was investigated a few years later by Spencer in England, La Rive in Switzerland (1825) and Antoine Becquerel in France (1829), but nothing definite resulted of their work. On the other hand,

the Russian physicist Jacobi, taking the Delarue research on the functioning of the cell Daniell, invented in 1837 the processes currently used for electroplating copper.

Electroplating quickly became popular in Russia, with people like the inventor Peter Bagrationi, the scientist Heinrich Lenz and the science fiction author Vladimir Odyevski, they all contributed to the further development of technology. As an example of uses of electroplating during the mid-nineteenth century in Russia there are the giant electroplated sculptures in St. Isaac's Cathedral in St. Petersburg (figure 1.2) and the golden dome of the Cathedral of Christ the Savior in Moscow, the highest Orthodox Church of the world.



Figure 1.2: Copper sculptures in St. Isaac's Cathedral in St. Petersburg

Later, John Wright of Birmingham, England, discovered that potassium cyanide is a suitable electrolyte for electroplating gold and silver. By experiencing the effects of electric current on solutions of salts of gold or

silver, George and Henry Elkington, Wright's associates, and Count Henri de Ruolz-Montchal in France managed to obtain an adherent deposit of gold or silver on the electrode connected to negative pole of the current source.

That moment could be considered as the invention of gilding and silvering by electrolysis. It was truly the birth of electroplating. The first patents for electroplating were made in 1840 by George and Henry Elkington, for gold and silver electroplating. Then they founded the electroplating industry in Birmingham from where it spread around the world.

Some months later, Ruolz, who did not know, made one in France. From 1850 there took place the development of electroplating of precious metals, but as electrochemical science was developed, the electrodeposition process was understood and other undecorative electroplating processes were also developed. The commercial electroplating nickel, brass, tin and zinc were developed over the 1850s. The Norddeutsche Affinerie in Hamburg was the first modern electroplating plant starting its production in 1876. At that time, one of the drawbacks of the electroplating was that the deposition rates were extremely slow. Despite this, it was possible to obtain excellent results, because the slow deposition favored the weld metal grain fineness and cohesion.

By the XIX century, the modeling and study of electrochemistry, were clarified by Michael Faraday (laws of electrolysis) and John Daniell (single stack metal ion dependent Zinc-Copper).

The plating industry received a big boost from the advent of the development of electric generators in the late XIX century. Could therefore

perform electrodeposition without DC power limitation and everything become possible. With the higher currents, metal machine components, hardware, and automotive parts requiring corrosion protection and enhanced properties, along with better appearance, could be processed in bulk.

The two World Wars and the growing aviation industry gave impetus to further developments and refinements including processes such as hard chromium plating, bronze alloy plating, sulfamate nickel plating, along with numerous other plating processes. Plating equipment evolved from manually operated tanks to automated equipment, capable of processing thousands of kilograms per hour.

During the last part of the XX century from the actual time, the chemical and the electrochemical deposition have been extended to different applications in both industry and research work.

## **1.5 Electrochemical deposition in actual industry**

Nowadays electrodeposition is used in a wide range of applications as metal processing and finishing [3, 4]:

Electrolytic methods are used to extract and refine metals as for example: lead, tin, copper, gold and silver. The advantage of extracting or refining metals by electrolytic processes is that the deposited metal is of high purity. One major industrial application of electrolysis is the electric furnace, which is used for manufacturing aluminum that is one of the most abundant elements in earth's crust but it can only be extracted by electrolysis [5]. Other metals than can be extracted are magnesium and sodium.

In this oven, metal salts are heated until they melt and are ionized. Then the metal is deposited electrolytically.

Electroformation and electromechanical machining are two types of processing metals. In the first one, a metal is electrodeposited on top of a mould that is removed afterwards. The most commonly used metals are nickel and copper. Electromechanical machining also known as electroerosion is used when mechanical machining is not possible. It consists in dissolving the object that acts as anode by using a cathode with the form of a mould for that object. This is used in manufacturing of components such as blades for turbines [6].

Electroplating is a process widely used in industry for coating metal objects with a thin layer of a different metal. It is one of the most important in terms of volume of production, and it also has one of the greatest economic impacts. The purpose of these coatings is to provide the metal object with some desired property that the metal object does not have. For example chromium plating is done on many objects such as car parts, bath taps, kitchen gas burners, wheel rims and many others.

As mentioned before, common application of this procedure is in jewelry, where a piece made with cheap material is coated with a layer of gold or silver, to protect it from corrosion and to increase the value of the piece. In fact this was the first application of electroplating in the industry. To obtain coatings relatively pure chemicals are used, so that during electrodeposition pieces are completely recovered by the desired metals. Industrially this process is known as electroplating. Some examples of frequent electroplating processes are [6]: Electrolytic zinc, that consists in a

zinc coating that acts as a barrier which is sacrificed to prevent corrosion of the metal under it, tinning processes to prevent corrosion of cans and other containers for food use, chrome plating, used for its decorative appearance, provides corrosion resistance and facilitates cleaning procedures. It also increases surface hardness, and therefore is widely used for parts requiring wear resistance, figure 1.3. One sector of the industry that has successfully implemented this technique is the naval or automotive industry to coat sheet metal structures, bumpers, hydraulic pistons and cylinders, piston rings, engine components and similar applications. Electrodeposition can also be used on a smaller scale, for example, electrolytic nickel is used in watchmaking and electronics due to its corrosion resistance and its decorative appearance. It can also be used as base for other electroplated coatings.



Figure 1.3: Chrome plating on a wheel, on screws and on a faucet

A relatively new process is the electrodeposition of plastic parts with

metal layers, which ensures the plastic piece to have the properties of the metal on its surface.

## 1.6 New applications of electrodeposition

Electrodeposition has come a long way since its inception; developing new techniques that have increased the range of applications of the same. In this chapter a brief summary of some of these new applications is provided.

Electrochemistry can be used to synthesize conductive polymers (CP) by electrochemical oxidation polymerization. An increasing interest in the use of CP for corrosion protection has been observed in the last years. For that reason different attempts of synthesizing them electrochemically over active metals instead of noble ones have been performed, such as carry on electrodeposition in organic solvents, decreasing of the electropolymerization overpotential in the presence of electron mediators or by passivation of the metal before formation of the polymer layer [7]. Recent advancement in the synthesis and applications of CP/CCG (chemically converted graphenes) composites has also been achieved. For example, PANI (polyaniline)/CCCG composite films and PPy (polypyrrole)/CCG have been prepared by electrochemical polymerization. Due to the structure and properties of these composites, they exhibit a wide range of applications in electrochemical devices a part from the corrosion protection previously mentioned. They have been used as energy storage materials in supercapacitors, as energy conversion in third-generation solar cells and in electrochemical sensing due to its excellent electrocatalytic activities

towards various kinds of substrates [8].

Because of the great utility of nanostructures, the search for methods to obtain high quality nanostructures materials has continued. Since a few decades ago electrodeposition has been considered as a real alternative to the physical deposition methods to grow high quality nanostructured materials, i.e. films, multilayers, nanowires, among others [9–14]. Electrochemical deposition of Bi,  $\text{Bi}_2\text{Te}_3$ , CuNi,  $\text{PbSe}_{1-x}\text{Te}_x$  and  $\text{CoSb}_3$  nanowires has been performed to be used in thermoelectric power generators and coolers. For example, Lim et al. demonstrated the fabrication of nanowire based thermoelectric device by using electrodeposited n-type  $\text{Bi}_2\text{Te}_3$  and p-type  $\text{Bi}_{2-x}\text{Sb}_x\text{Te}_3$  nanowires [15]. In another example,  $\text{TiO}_2$  nanotube array films prepared by electrochemical oxidation were investigated for the photodegradation of phenol, methyl orange, methylene blue or gaseous acetaldehyde [16].

There are several examples of magnetic films and patterned deposits obtained by means of electrodeposition that have been used in microelectromechanical systems (MEMS). Leith et al. reported on the NiFe electrodeposition through a mould to obtain MEMS components with uniform composition [17]. Thin films of different alloys such as phosphorus, tungsten, platinum and cobalt alloys have been prepared by different authors [18,19]. The need of developing new hard magnetic materials capable of retaining their magnetic properties up to thicknesses of tens of microns using silicon-compatible deposition processes has led Kulkarni et al. to electrodeposit CoPtP films of 82  $\mu\text{m}$  thick [20]. The growth process and microstructures and magnetic properties correlations of magnetic alloys have been investigated by numerous groups [21–24]. A new method to im-

prove Ni films adhesion by using pulse reversed current has been presented by Wang et al. [25].

Another application for patterned deposits and arrays are high density non-volatile memories, some examples of this are  $\text{Ag}_2\text{Se}$  nanostructures obtained by Ann et al. [26],  $\text{Ni}_x\text{Pb}_{1-x}$  nanowire arrays fabricated by Ji et al. [27] and CoCu nanowire arrays prepared by Lin et al. [28].

Electrodeposition of multilayer films showing giant magnetoresistance (GMR) similar to that usually obtained by physical methods have permitted to use electrochemistry for spintronic device preparation. The majority of GMR studies on electrodeposited multilayer films were carried out on samples prepared by two-pulse plating from a single bath containing both the magnetic and non-magnetic species. An extended research activity on electrodeposited multilayer films with GMR behaviour has been performed in the last 15 years. A probe of this research is the high number of reports that have been on the subject and the wide range of multilayer films studied: CoCu/Cu, NiCu/Cu, CoAg/Ag, CoAu/Au, CoRu/Ru, CoNiCu/Cu, FeNiCu/Cu, FeCoCu/Cu, Co(Cu)Zn/Cu and FeCoNiCu/Cu [29].

On the other hand, the electrochemical preparation of magnetic composites has been achieved. The interest of preparing composites lies in the provision or the improvement of certain properties, such as mechanical resistance, corrosion protection, hydrophobicity, hardness or magnetism. The preparation of composites consisting of magnetic oxide nanoparticles embedded into a ductile metallic matrix has been studied in our group. Pané et al. prepared barium ferrite microparticles entrapped in electrodeposited CoNi films [30] and Roldan et al. studied copper-magnetite mag-

netic composite films [31].

Nowadays chemical and electrochemical deposition methods have been used as detection methods in some micro-total analysis systems ( $\mu$ -TAS) for biochemical assays. Microchips combining multiple detection strategies, one of them electrochemistry, have been reported. Lapos et al. [32] presented an electrophoresis microchip combining amperometric and fluorescence detection. Chips presenting both fluorescence/contactless conductivity detection and electrochemical and electrochemiluminescence detection in a single microchip have also been described [32,33]. However, this is not the only application of electrochemical deposition techniques in biochemical assays, microelectrodes have been employed in microfluidic chips and other microdevices to conduct electrical manipulation of fluids and biochemical analytes such as DNA, proteins, cells, microorganisms, nanoparticles, and possibly single molecules in aqueous solutions [32]. Finally, combining electrochemical methods with biological receptor substances (antibody, enzyme, DNA, nucleic acid,) a great variety of electrochemical biosensors have been documented [32,34,35]. But not only biological receptors have been used for electrochemical biosensors to be performed. More recently, nanoscale materials as electrodes or as biomolecular tracers have been applied in disease diagnostics, infectious organisms and biothreat agents' detection. Yu et al. [32] exploited carbon nanotube amplification strategies for highly sensitive immunodetection of cancer biomarkers. Nanoparticles have also played a crucial role in electrochemical biosensors based on nanomaterials [36].

Simultaneously, electrochemical techniques commonly used to perform electrodeposition can be also exploited to perform fundamental studies of

electron transfer kinetics for molecular electronics. For this purpose electrodes modified with self-assembled monolayers (SAM) and electrochemical techniques such as cyclic voltammetry, AC voltammetry, chronoamperometry and electrochemical impedance spectroscopy have been combined [37].



## Chapter 2

# Objectives

This thesis mainly focuses on the new applications and uses of electrodeposition as a tool of fabricating some materials that can be integrated in different kind of devices such as sensors and actuators. Electrodeposition presents several advantages respect to vacuum techniques. It has a high materials and structures versatility that can be obtained which permits its integration in lots of processes.

The specific objectives raised in this thesis are:

- The design, preparation and characterisation of planar coils to be implemented in inductive biosensors. The study of the optimum bath, electrodeposition conditions and fabrication processes to prepare robust, low resistant and adherent planar copper coils of different aspect ratios, which allow to detect magnetic particles. In order to do that, simulations of the main parameters based in previous designs to improve the sensitivity of the coils will be executed. The final objective is the fabrication of the new designed coils and perform the first tests of their sensing ability.

- Deposition of a hard magnetic alloy for MEMS application. Basic study of the electrodeposition process of the CoPt alloy to find the optimum bath. Preparation of structures with different shapes and geometries (films, thin films, lithographed microstructures, nanoparticles, nanowires...) over different substrates based on the previous electrochemical results. Study of the influence of the electrodeposition and preparation conditions on the properties of the CoPt alloy (morphology, composition, crystalline structure, magnetic properties) and analysis of the relationship among those properties.
- Organic monolayer formation on top of several electrodeposited magnetic substrates (magnetic/non-magnetic assembly) as the first step to fabricate a molecular spintronic device. Preparation of smooth thin films of magnetite and CoP by means of electrodeposition. Formation and study of octanethiol and acid oleic monolayers on top.

The present thesis is organized as follows. Chapter 3 summarizes the techniques employed to prepare the different classes of nanostructured materials as well as the techniques used to characterise them. In Chapter 4 the results concerning the design, preparation and characterisation of planar coils are presented. Chapter 5 focuses in the results of the magnetic alloy preparation. With several subsections: the study of the system and preparation and characterisation of the different structures. The results concerning the preparation and characterisation of monolayers over magnetic substrates are shown in Chapter 6. Chapter 7 briefly summarizes the main conclusions drawn in this thesis.

This thesis has been mainly developed in the *Laboratori d'Electrodeposi-*

*ció i Corrosió (Electrodep)* in the Physical Chemistry Department of the Universitat de Barcelona under the supervision of Dra. Elisa Vallés and Dra. Elvira Gómez. Part of this thesis was carried out in the Surface Physics group in the H.H. Wills Physics Laboratory of the University of Bristol in United Kingdom during two three-month research stays under the supervision of Dr. Walther Schwarzacher.



## Chapter 3

# Experimental Procedure

### 3.1 Electrochemical experiments

#### 3.1.1 Experimental setup

Electrochemical experiments and sample preparation were carried out using a microcomputer-controlled potentiostat/galvanostat Autolab with PGSTAT30 equipment and GPES software (figure 3.1A). In some experiments a booster BSTR10A was connected to the equipment to supply a higher current density (figure 3.1B).

#### 3.1.2 Electrochemical cells and electrodes

The electrochemical experiments were performed in a three-electrode cell configuration. Different cells geometries were used depending on the sample being prepared. The use of these different cell geometries implies employing two different arrangement of the working electrode, vertical or horizontal. The vertical arrangement was used to prepare all the samples except the nanowires. For this kind of arrangement three different cell

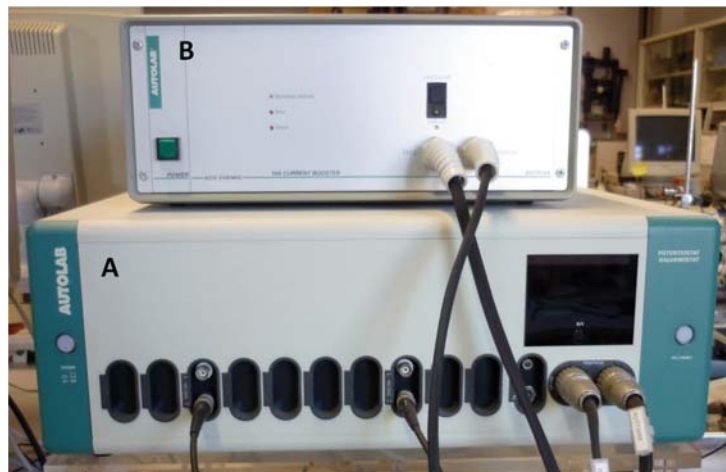


Figure 3.1: A) Potentiostat/galvanostat AUTOLAB. B) Booster BSTR10A

volumes were chosen depending on the size of the substrate used. For the smallest substrates a cylindrical cell of  $\varnothing$  (diameter) = 7.23 cm, 7.5 cm height and 250 ml capacity which permitted control of the temperature was selected (figure 3.2A). A Julabo thermostat was used to control the temperature of the bath. As the size of the substrate increased the size of the bath used was increased, as so did the cell containing it. In order to scale the process to the size of the half of a usual wafer of silicon, a rectangular cell with a 9x16 cm<sup>2</sup> base, 14 cm height and 1.5 litres of useful capacity was used (figure 3.2B). Finally, to be able to perform deposition over the whole wafer, a cell with a base of 13x16 cm<sup>2</sup>, 15 cm height and 2.5 litres of useful capacity was employed (figure 3.2C). To control the temperature in the two cells previously described, a methacrylate bath with a J.P. Selecta Microterm thermostat was needed. In all the cases a magnetic stirring of the bath was possible. As mentioned before, a different cell with horizontal working electrode arrangement was used to prepare the nanowires (figure 3.3); in this case no control of the temperature was possible and the stirring of the bath was performed by a flow of argon.

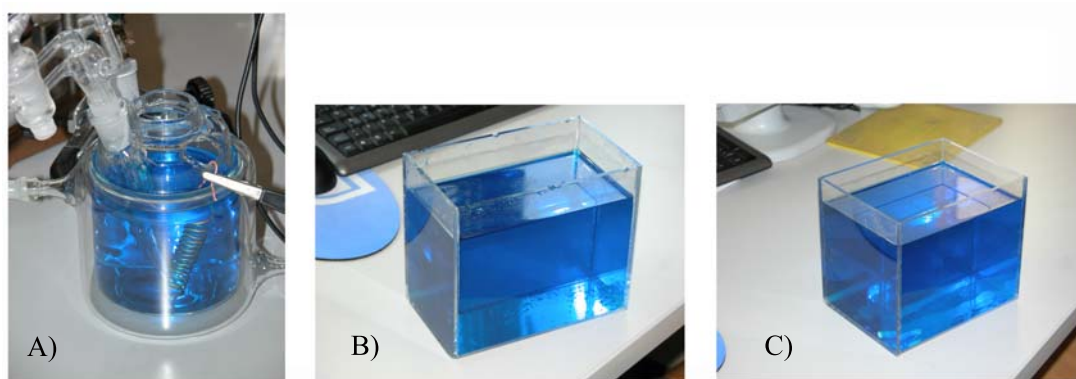


Figure 3.2: Electrochemical cells employed with vertical arrangement of the working electrode.  
 A) 250 ml B) 1.5 l C) 2.5 l

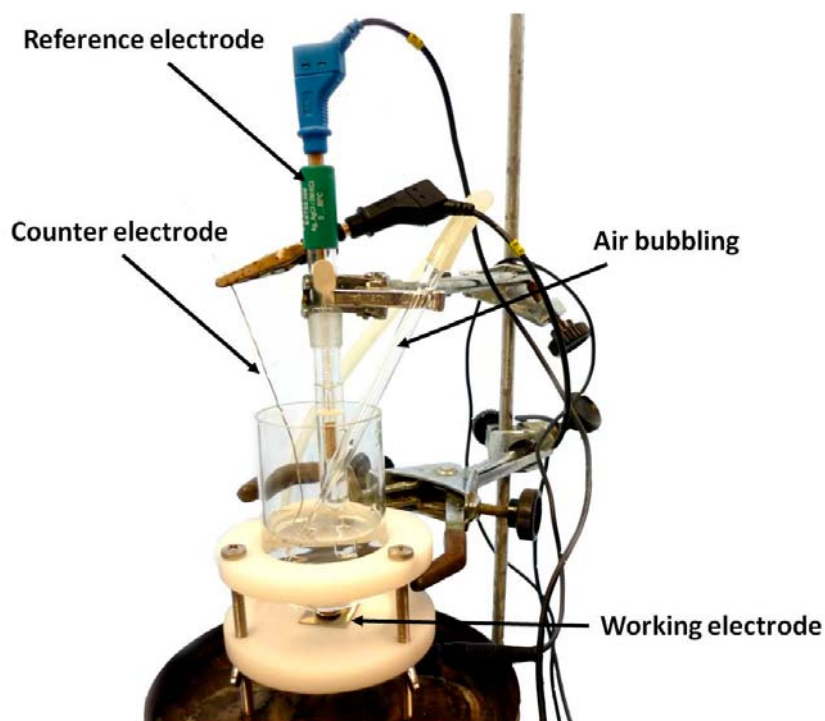


Figure 3.3: Electrochemical cell employed with horizontal arrangement of the working electrode

As reference electrode either  $\text{Ag}/\text{AgCl}/1 \text{ mol dm}^{-3} \text{ NaCl}$  and Saturated Calomel Electrode (SCE) were used.

The counter electrodes were either a platinum spiral or an alloy of copper-phosphorous. Because of its inert nature, a platinum spiral was

chosen when the contamination of the bath needed to be avoided. When the bath contained copper a copper-phosphorous alloy was employed. The samples performed using this bath had a high charge applied and then the concentration of copper in the bath might decrease after some time. Copper-phosphorous provided copper to the bath and made it possible to maintain a more constant concentration. The phosphorus is needed to facilitate the copper oxidation to ion copper (II) rather than ion copper (I). As so many different samples were prepared, very different working electrodes were employed, figure 3.4. The treatment performed to reach sample reproducibility was different in each case.

- A vitreous carbon (Metrohm) electrode of  $0.0314 \text{ cm}^2$  was used for the basic electrochemical study of the different deposition processes because it has a wide potential window where no redox activity takes place. Before each experiment the electrode was mechanically polished to a mirror finish using alumina of different grades ( $3.75$  and  $1.85 \mu\text{m}$ ) over polishing cloths DP-Mol and DP-Nap from Struers and cleaned ultrasonically for two minutes in Millipore water to be sure that all the alumina had been removed.
- Silicon/seed layer. p-type silicon electrodes of  $4\text{-}40 \Omega \text{ cm}$  and (100) orientation modified with sputtered Ti( $100 \text{ nm}$ )/Ni( $50 \text{ nm}$ ) seed layer were the substrates employed to carry out the first studies of the deposition process over a metal and to obtain thick samples of the materials studied to be characterised. The same substrates with an intermediate  $400 \text{ nm}$  thick  $\text{SiO}_2$  layer grown by plasma-enhanced chemical vapour deposition were tested in some cases to check if the new layer in-

duced any change in the grown deposits. In both cases the substrates were first washed with acetone, then with ethanol and finally rinsed in water before deposition. For copper deposits the Ti/Ni seed layer was changed to evaporated Ti(10 nm)/Cu(100 nm) because it was found that this new seed layer induced minimal stress in the electrodeposited copper. Substrates containing this seed layer were cleaned with ethanol and rinsed in water before deposition. These substrates were supplied by IMB-CNM.CSIC (Centro Nacional de Microelectrónica)

- Plastics/Ti(10 nm)/Cu(100 nm) supplied by the Parc Científic de Barcelona. Different plastics modified with an evaporated Ti/Cu seed layer to make them conductive were tested:
  - PEEK: Polyether ether ketone
  - PEN: Polyethylene Naphthalate
  - PMMA: Poly(methyl methacrylate)
  - PS: Polystyrene
  - Teflon: Polytetrafluoroethylene (PTFE)
  - Kapton: Polyimide film

These electrodes were employed to check the viability of obtaining deposits over a flexible substrate. In order to add the seed layer a RIE (Reactive ion etching) was applied to Kapton to increase the roughness and favour the adherence of the seed layer.

- Graphite rods (Alpha Aesar) of area =  $0.541 \text{ cm}^2$  were used to prepare submicrometric particles. They were polished using alumina of  $1.87 \mu\text{m}$  grit size over polishing cloths DP-Nap from Struers and cleaned ultrasonically for two minutes in water.

- Doped silicon (p-B Sitronix 11523-13012 with a resistivity of 0.008-0.012  $\Omega$  cm, supplied by IMB-CNM.CSIC) substrate. Silicon pieces of 0.6 cm x 0.3 cm were used as working electrodes to obtain the submicrometer particles and core-shell particles; they were chosen because they present a low conductivity, which permits the deposition, but favour a moderate nucleation rate, and do not interfere with the magnetic measurements. The silicon substrate was etched with a 5 % (p/v) HF solution for 60 s, to remove the native silicon oxide, before each experiment.
- Glass/ITO (Indium Tin Oxide) substrates. A 25 nm-thick layer of sputtered ITO over glass was used to obtain thin films. This substrate was selected because it allowed the magnetic properties of the prepared deposits to be measured directly as it does not affect the magnetic response of the deposits.
- Glass/Cr(30 nm)/Au(280 nm) electrodes (H.H. Wills Physics Laboratory, Bristol, United Kingdom). In these electrodes the seed layer was added by evaporation. Prior to deposition an annealing was performed to obtain a (111) Au orientation. Samples of 5 cm x 5 cm were used to obtain both magnetite and cobalt-phosphorous films over which organic monolayers were adsorbed.
- Photolithographed substrates. In some experiments a resin was added to some of the previously mentioned substrates in order to obtain different microstructures.

– Silicon/SiO<sub>2</sub>(1  $\mu$ m)/Ti(10 nm)/Cu(100 nm)/Photoresist(15  $\mu$ m).

Two resins were used with this substrate; MAP1275 was used to

check the suitability of the bath to obtain thick microstructures and deposit some square coils of test. AZ4562 was used to obtain the new design cooper coils to be used in the biosensors device

- Glass/ITO/Photoresist electrodes were used for the CoPt microstructures preparation. The preparation method consisted in first spinning a 1.2  $\mu\text{m}$ -thick HiPR 6512 photoresist (Fujifilm) layer over ITO and heating it at 100°C for 20 minutes to remove the moisture. Then, the photoresist was irradiated and soft baked at 110°C for 30 minutes. Finally, it was developed and hard baked at 115°C for 20 minutes.

These two substrates were supplied by IMB-CNM.CSIC (Centro Nacional de Microelectrónica).

- Plastics/Photoresist. AZ9260 was used to study the possibilities of obtaining microstructures over a flexible substrate. For this purpose square coil deposition was performed over these substrates. These substrates were supplied by the Parc Científic de Barcelona. All these substrates containing a photoresist were cleaned by rinsing them in water.

- Membrane templates

- Polycarbonate membranes (Millipore) 20  $\mu\text{m}$ -thick with pore diameters of 200 nm and 100 nm were used to grow nanowires. The pore density of the membranes goes from  $10^8$  to  $2.5 \cdot 10^9$  pores  $\text{cm}^{-2}$ . Vacuum evaporation was used to coat the membranes with around a 100 nm-thick gold layer, enabling conductivity. Prior to the electrodeposition the porous template was kept in distilled

water for several hours to make the pores hydrophilic for uniform filling of the pores, crucial step for obtaining homogeneous growth over the entire membrane.

- Alumina membranes (Whatman) 60  $\mu\text{m}$ -thick with pore diameter of 100 nm and density around  $8.5 \cdot 10^9$  pores  $\text{cm}^{-2}$  were used to obtain nanowires arrays with higher density. The treatment applied to these membranes before performing the electrochemical experiments was the same as applied to polycarbonate ones.

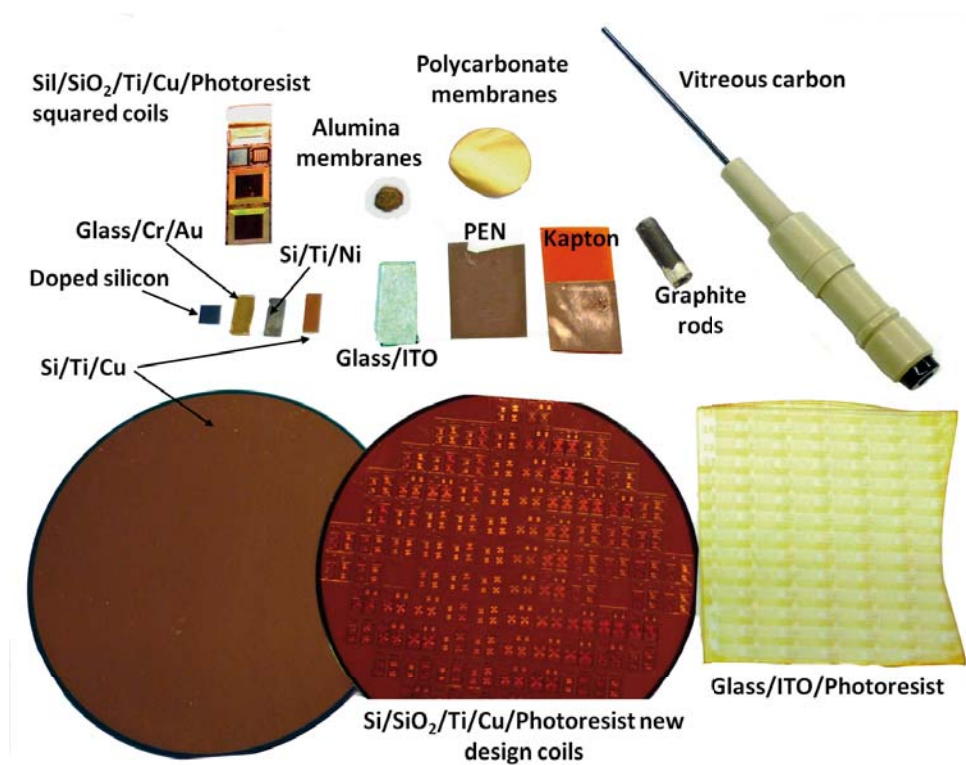


Figure 3.4: Working electrodes used during the thesis

### 3.1.3 Chemicals

All reagents used in the electrochemical experiments were of analytical grade. All solutions were prepared with water, which was first doubly distilled and then treated with a Millipore Milli Q system. Solutions were

de-aerated by argon bubbling before each experiment and maintained under argon atmosphere during it. Table 3.1 shows the chemicals used to prepare the solutions employed to obtain the different samples.

Table 3.1: Chemicals used to prepare the solutions employed to obtain the different samples

Samples	Solutions employed	
Cu Deposits and Coils	CuSO <sub>4</sub> · 5H <sub>2</sub> O	
	H <sub>2</sub> SO <sub>4</sub>	
	NaCl	
	Leveller*	
	Brightener*	
	Carrier*	
CoPtP Deposits	CoCl <sub>2</sub>	
	Na <sub>2</sub> PtCl <sub>6</sub>	
	Sodium hypophosphite	
	NaH <sub>2</sub> PO <sub>2</sub>	
	H <sub>3</sub> BO <sub>3</sub>	
	NH <sub>4</sub> Cl	
CoPt Deposits	pH=4.5 (NaOH)	
	CoCl <sub>2</sub>	
	Na <sub>2</sub> PtCl <sub>6</sub>	
	H <sub>3</sub> BO <sub>3</sub>	
	NH <sub>4</sub> Cl	
	pH=4.5 (NaOH)	
CoPt Submicrometrical particles	CoCl <sub>2</sub>	CoCl <sub>2</sub>
	Na <sub>2</sub> PtCl <sub>6</sub>	Na <sub>2</sub> PtCl <sub>6</sub>
	H <sub>3</sub> BO <sub>3</sub>	H <sub>3</sub> BO <sub>3</sub>
	NH <sub>4</sub> Cl	NH <sub>4</sub> Cl
		sodium citrate
	pH=4.5 (NaOH)	pH=4.5 (NaOH)

Samples	Solutions employed	
CoPt Thin films	CoCl <sub>2</sub>	
	Na <sub>2</sub> PtCl <sub>6</sub>	
CoPt Nanowires	H <sub>3</sub> BO <sub>3</sub>	
	NH <sub>4</sub> Cl	
CoPt Microstructures	sodium citrate	
	pH=4.5 (NaOH)	
CoNi Shell	CoCl <sub>2</sub>	
	NiCl <sub>2</sub>	
	H <sub>3</sub> BO <sub>3</sub>	
	saccharine	
	pH=3 (HCl)	
CoNi Shell	Fe <sub>2</sub> (SO) <sub>3</sub>	
	Triethanolamine (TEA)	
	NaOH	
CoP Deposits	H <sub>3</sub> PO <sub>3</sub>	
	H <sub>3</sub> PO <sub>4</sub>	
	CoCl <sub>2</sub> 6H <sub>2</sub> O	
	CoCO <sub>3</sub>	
Monolayers Preparation	Oleic acid in ethanol	Dodecanethiol in ethanol
Monolayers Study	Na <sub>2</sub> SO <sub>4</sub>	
	pH=3 (H <sub>2</sub> SO <sub>4</sub> )	

\*Supplied by MacDermid Company: Leveller (polymerized tiazine, XD7399)

Brightener (bis-(3-sulphopropyl)-disulphidesodium salt, XD7398)

Carrier (polyethyleneglycol of high molecular weight, XD7397)

Tropicoat (Ref :7361) acrylic-based varnish from Jelt was used to insulate the coils before the electrical characterisation.

### 3.1.4 Electrochemical techniques

**Cyclic voltammetry** Cyclic voltammetry was selected to study the electrochemical behaviour of the different solutions employed. It was performed under both quiescent and stirring conditions. A single cycle was run in all the experiments, initiating the scan in a potential at which no redox process took place and usually toward negative potentials (negative scan). During the negative scan, the reduction of the electroactive species took place. Once the cathodic limit is reached, the scan was reversed. During the scan toward positive potentials (positive scan) the total or partial oxidation of the species previously electrodeposited occurred. Special attention should be paid to the cathodic and anodic limits in order to avoid or minimize hydrogen evolution and oxygen evolution or substrate oxidation, respectively. Cyclic voltammetry was mainly carried out at 50 mVs<sup>-1</sup>. Cyclic voltammetry permits the charges recorded during both oxidation and reduction processes to be calculated. Comparing both charges ( $Q_{ox}/Q_{red}$ ) it is possible to have an idea of the difficulty of the oxidation of the deposits prepared and the presence of parallel reactions taking place simultaneously with electrodeposition.

**Linear sweep voltammetry (LSV)** LSV is an electrochemical technique that permits information about the reduction and oxidation processes to be obtained separately. The scan was initiated at a potential at which no redox process takes place till the cathodic or the anodic limit was reached. The LSV curves were carried out at 10 mVs<sup>-1</sup>. The information obtained by means of this technique is complementary to that obtained by cyclic voltammetry. In the cyclic voltammetry, contrary to what happens in the

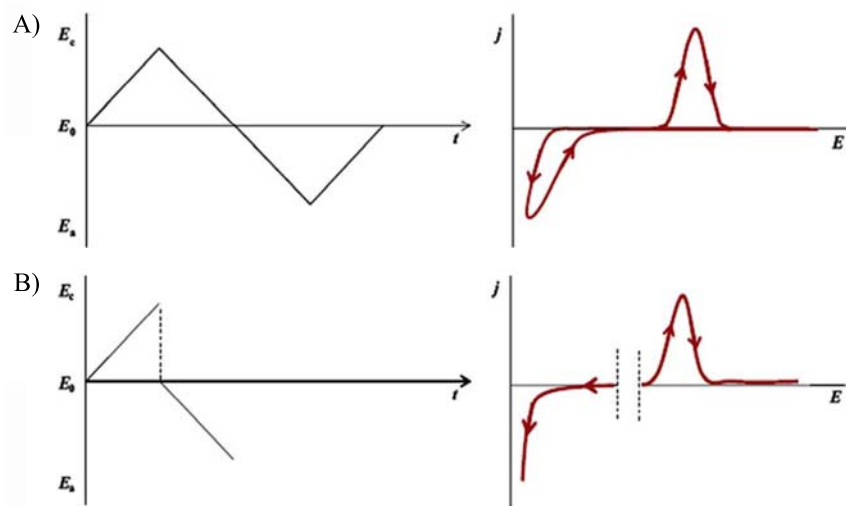


Figure 3.5: Scheme of the applied signal and the recorded response A) cyclic voltammetry and B) two combined linear sweep voltammeters where  $E_0$  is the starting potential;  $E_c$  is the cathodic potential;  $E_a$  is the anodic potential;  $t$  is the time and  $j$  is the current density

LSV, the reduction processes not only take place during the negative scan but also during the positive sweep until the current is zero (crossover). Figure 3.5 shows a comparison between the applied signals and the recorded responses for both techniques.

**Cronomethods** The electrodeposition processes and sample preparation were either studied potentiostatically or galvanostatically. The first of these cronomethods consists of applying a constant potential whilst the  $j$ - $t$  curve is recorded. In the second one a constant current is applied and the  $E$ - $t$  curve is recorded.

**Pulse plating deposition** The pulse plating deposition was used to prepare some of the CoPt alloy nanowires in potentiostatic control. The method allows applying series of discrete potential pulses rather than a constant potential value. The advantage of combining cathodic/anodic currents and being able to modify the duration of pulses/pauses when trying

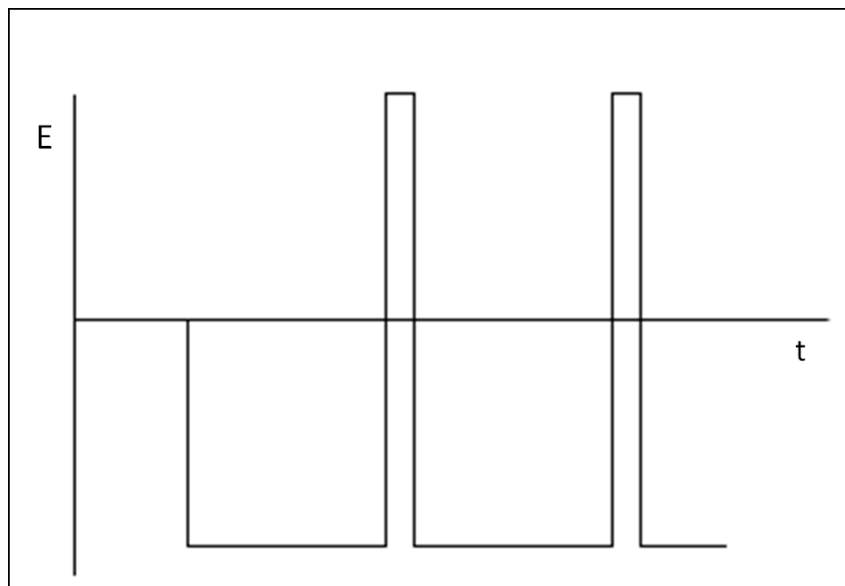


Figure 3.6: Scheme of the applied signal of a serie of pulse plating deposition

to deposit over a template is the reduction of the diffusion layer compared with conventional direct current deposition. In figure 3.6 a scheme of the applied signal is shown.

**Electrochemical quartz crystal micro-balance (EQCM)** EQCM (figure 3.7) was used to follow the monolayer formation process on top of the magnetic substrates. The EQCM contains a quartz crystal that oscillates at a specific frequency. When the monolayer was adsorbed or desorbed on top of the substrate the frequency decreased or increased respectively. This change in the resonant frequency can be recorded and used to calculate the rate of adsorption or desorption as well as to study the affinity of different organic molecules with the substrate.

**Corrosion measurements** Corrosion measurements were performed by means of electrochemical techniques. Corrosion tests were carried out at 25°C in a 5% NaCl solution. The samples were immersed in NaCl media for 3 h in order to determine the steady-state potential ( $E_{ss}$ ). Immediately



Figure 3.7: Photograph of EQCM and the support to work in liquids containing the quartz crystal resonators metallised with gold electrodes by vapour deposition

afterwards, a linear potentiodynamic sweep from  $E_{ss} - 300$  to  $E_{ss} + 300$  mV was performed at  $0.1 \text{ mV s}^{-1}$  to evaluate corrosion potential ( $E_{corr}$ ) and current density corrosion ( $j_{corr}$ ). No stirring was performed during both the polarisation and potentiodynamic scans.

## 3.2 Ex-situ characterisation techniques

### 3.2.1 Morphological analysis

As there was a wide variety of samples to be analysed different techniques were used in order to observe the morphology:

**Optical microscopy (OM)** An Olympus PMG 3 optical microscope was used for samples observation. It was mainly used to analyse the correct filling of the microstructures.

**Scanning electron microscope (SEM)** It was used to study the morphology and the grain of the deposits, as well as to look into detail microstructures or for nanostructures (nanoparticles and nanowires) ob-

servation. Several SEM were used: Quanta 200 FEI XTE 325/D8395, Hitachi S-2300, Leica Stereoscan S-360 (Centres Científics i tecnològics de la Universitat de Barcelona (CCiTUB)) and Jeol JSM 5600LV (H.H. Wills Physics Laboratory, Bristol, United Kingdom). Topography images of the surface of the samples were recorded. In some cases to obtain a higher resolution a Hitachi H-4100FE (FE-SEM: Field Emission Scanning Electron Microscope) with field emission was used, as the spatial resolution is from 3 to 6 times higher than conventional SEM equipment. In SEM an electron beam is used to scan the surface of a sample. Electrons interact with the atoms of the surface of the material and as a result of it, secondary electrons are emitted and detected. The processing of the signal permits to obtain information about the surface morphology and composition.

Samples have to be conductive and electrically grounded to avoid an excess of charge on top of the surfaces studied. Therefore, samples prepared over vitreous carbon and graphite could be directly examined by SEM without any prior treatment, except for mounting them on a stub. In samples prepared over non conductive substrates (glass or membranes) or substrates with low conductivity (silicon) covered with a seed layer (Ti/Ni or Ti/Cu or ITO or Au) it was necessary to apply a colloidal silver strip between the surface and the stub to make electrical contact in order to avoid artefacts. Membrane templates were necessary coated with an ultrathin film of carbon before being observed due to their isolating nature.

**Atomic Force microscope (AFM)** It was not possible to observe some of the samples with the SEM because they present very fine grain; when that happened morphological characterisation of the films was complete using AFM. Two different AFM equipments were used: Veeco Di-

mension V (H.H. Wills Physics Laboratory, Bristol, United Kingdom) and Extended multimode 8 with a Nanoscope V controller (Bruker, Germany) (CCiTUB, University of Barcelona).

AFM measures the interaction force between a cantilever with a very sharp tip and a sample by measuring the deflection of the cantilever caused when approaching them. To measure the deflection a laser is pointed into the cantilever and a photodiode detects its movements. The two main operation modes are contact or tapping. It is a very high-resolution technique on the order of fractions of a nanometer. AFM images were recorded in peak force tapping mode with triangular silicon cantilevers (nominal radius of 8 nm and spring constant 0.5N/m) at a scan rate of 1 Hz.

**Transmission electron microscopy (TEM)** TEM was used for the observation of shorter nanowires because it was not possible to see them with the other techniques. This technique requires the samples to be extremely thin, as an electron beam penetrates in the sample to interact with the material. The resulting electrons are collected with a CCD camera and processed to obtain an image. In our case a JEOL JEM 2100 TEM was used.

**Focused ion beam (FIB)** FIB from H.H. Wills Physics Laboratory, Bristol, United Kingdom was briefly used for some of the shorter nanowires observation as it was the equipment available there. It is similar to a SEM, but instead of using an electron beam it uses an ion beam to obtain the images.

### 3.2.2 Compositional analysis

The compositional analysis of the samples was performed in different grades of accuracy depending on the system studied and the desired information, for that reason different techniques were used:

**Energy dispersive X-ray spectroscopy (EDS)** Most of the samples composition was analysed by means of EDS connected to a Leica Stereoscan S-360 SEM. In SEM when scanning the sample with the electron beam, X-rays are emitted. The X-ray radiation emitted depends on the atomic structure and it is characteristic of each element. Analysing the X-rays emitted information about the elemental composition of a sample is obtained. Calibration of the equipment was performed with cobalt pattern before taking measurement.

**X-Ray photoelectron spectroscopy (XPS)** XPS is a more precise technique than EDS because a part of giving information of the elemental composition, it also gives information about the chemical state or electronic state of the elements of the material. It was used to study the manner the organic monolayer binds on top of the magnetic deposits used. Using the XPS only a few nanometers (10 nm) of the surface can be studied, the material is irradiated with an X-ray beam which produces the emission of electrons of the sample. The number and kinetic energy of the electrons emitted gives information about the bonding. XPS experiments were carried out in a PHI ESCA-5500 Multitechnique System from Physical Electronics and the recorded data was analysed with the program Multipak from Physical Electronics.

**Raman spectroscopy** Raman spectroscopy is based in the inelastic scattering of a laser produced when it interacts with a system. After being irradiated with the laser the system evolves to a new state with a different vibrating or rotating state and emits a photon with a different frequency than the initial one. This shift in the energy of the laser photons gives information about the vibration modes of the system that are related to the chemical bonds and the symmetry of the entities that form the system. Raman spectra were recorded at room temperature using a Renishaw Invia micro-Raman system. The samples were excited by the 488 nm line of an argon ion laser. The spectra were collected in a backscattering geometry with spectral resolution of  $2\text{ cm}^{-1}$ . The laser beam was focused on the sample by a x50 0.9NA (numerical aperture) objective to a spot size of 300 nm. The samples were exposed to both 3 mW and 0.5 mW incident laser powers, with unpolarised detection. One spectrum was recorded each time with an acquisition time of 300 s.

### 3.2.3 Structural characterisation

In order to determine the crystalline structure of the materials two complementary techniques were used: X-Ray diffraction (XRD) and Transmission electron microscopy (TEM). X-Ray diffraction (XRD) was also used to study other aspects of the structure, as the texture and the stress.

**X-Ray diffraction (XRD)** XRD allows the investigation of the fine structure of matter. This technique is based in the fact that crystals diffract X-rays. X-ray diffraction can be used not only to determine the crystal structure, but for chemical analysis, stress measurement, to determine the

grain size and to establish the orientation of crystals in polycrystalline aggregate. In our case a Philips MRD diffractometer with parallel optical geometry using Cu  $K_\alpha$  radiation ( $\lambda = 1.5418 \text{ \AA}$ ) and a texture goniometer that allows control of the sample rotation about the three axes was used applying different methods depending of the information required. In figure 3.8 a schematic representation of the rotation angles is shown.

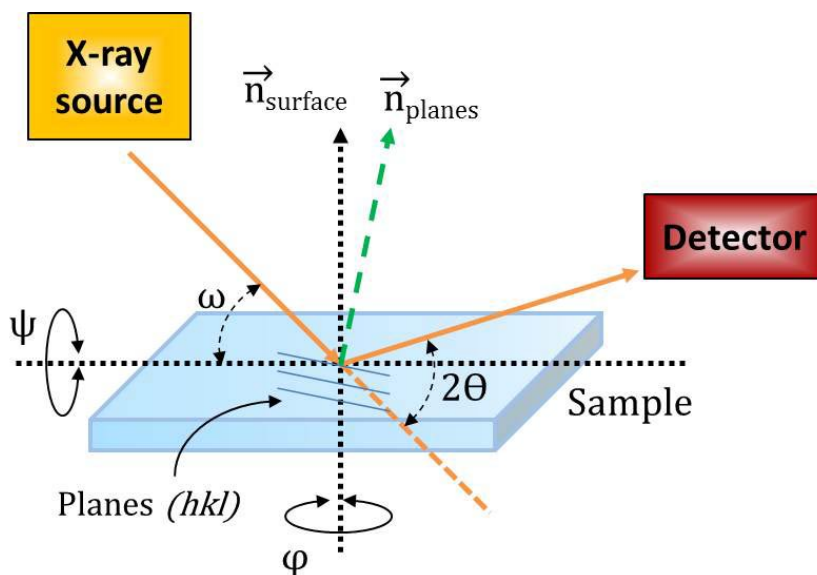


Figure 3.8: Schematic representation of the rotation angles

*Powder diffraction* has been mainly used to characterise the crystallographic structure. For the deposits presenting nanometric grain size it was possible to determine the crystalline size by using the Scherrer formula 3.1 [38]. In some cases the  $\theta/2\theta$  scan was performed at different  $\psi$  angles to study the preferred orientation in polycrystalline samples. Grazing incidence X-ray diffraction has also been employed to characterise the crystallographic structure and preferred orientation of the thinner samples in order to avoid substrate interferences. The  $2\theta$  range, step and measurement time were different depending on the sample analysed.

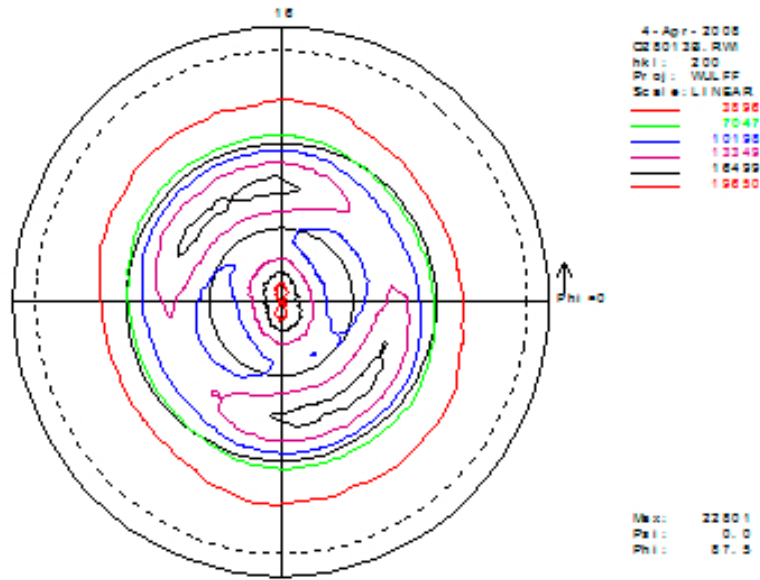


Figure 3.9: (200) pole figure of a Cu deposit over Si/Ti/Cu

$$\tau = \left( \frac{0.9\lambda}{W_{0.5} \cos \theta_B} \right) \quad (3.1)$$

Where  $\tau$  is the grain size,  $\lambda$  is the wavelength,  $W_{0.5}$  is the width of the peak at the half of the high and  $\theta_B$  is the Bragg angle for a specific orientation.

*Pole figures* were recorded in order to study the texture of the deposits. A pole figure is a stereographic projection which shows the variation of pole density with pole orientation for a selected set of crystal planes. The method used to obtain them consisted in performing a double scan in  $\psi$  (0-85°) and  $\varphi$  (0-360°) for a fix  $\theta$  angle. The fixed  $\theta$  corresponds to a crystallographic orientation of the material. The double scan permits to register the diffracted intensities of each crystallographic orientation in plane and out of plane revealing the orientation of all the grains of the material. In figure 3.9 an example of a pole figure is shown.

*Stress measurements.* Finally, it is important to determine the stress of the deposits when they have to be implemented in a device as it can lead to its malfunction. When there is strain present in a material, diffraction lines could be both shifted and broadened. From this shift the strain may be calculated and, knowing the strain of a specific direction at different  $\psi$  angles, elasticity theory gives the following relation for the difference between these strains, equation 3.2, so we can determine the stress present in this specific direction ( $\sigma_\varphi$ ) by applying the  $\sin^2 \psi$  method [38].

$$\sigma_\varphi = \left( \frac{E}{(1 + \nu) \sin^2 \psi} \right) \left( \frac{d_i - d_n}{d_n} \right) \quad (3.2)$$

Where  $d_n$  and  $d_i$  are the spacing of the planes reflecting at normal incidence and of the inclined reflecting planes respectively both under stress,  $E$  is Young's modulus and  $\nu$  is Poisson's ratio. Knowing the spacing between planes at two incidences, normal and forming an angle ( $\psi$ ) with the normal, the stress of the planes direction can be calculated. Measurements were performed in the  $\theta/2\theta$  range corresponding to each peak and with a  $\psi$  range of 0-70°.

### **High resolution transmission electron microscopy (HRTEM)**

HRTEM was used to obtain images of the crystallographic planes of the nanowires. The use of the fast Fourier transform (FFT) together with high resolution images allowed the study of their crystalline structures. It is a technique with atomic resolution. JEOL JEM 2100 equipment with DigitalMicrograph (Gatan) Software was used.

For sample preparation nanowires were extracted from the membrane by

dissolving first the gold layer with  $I_2/I^-$  solution and then the polycarbonate membrane with chloroform. After several washes, a diluted emulsion containing the specimen was directly cast onto a carbon-coated copper grid sample holder.

### 3.2.4 Roughness and thickness measurements

There are several techniques that were used to measure the roughness and the thickness of the deposits. There were two equipments that were mainly used; the interferometer and the confocal microscope.

**Interferometer** Both roughness (rms) and thickness of the coatings were measured using a Zygo NEW VIEW 100 white-light interferometer together with MetroPro Software and a Fogale-Nanotec ZoomSurf 3D interferometer. This technique is based in the principle of superposition of waves to obtain a dark and bright fringe pattern from which the surface profile can be obtained. It is a non-destructive technique and has nanometer resolution in the vertical range. Roughness is expressed by the rms (root-mean-squares) values, which are obtained by means of the equation 3.3:

$$\mathbf{rms} = \sqrt{\frac{1}{l} \int_0^l Z^2(X) dx} \quad (3.3)$$

Where  $Z(x)$  is the function that describes the height profile along a  $x$  axis of length  $l$ .

**Confocal** The confocal microscopy technique uses a focused beam of light to scan the surface of the samples. Moreover, the light is detected

by a photomultiplier tube through a pinhole or a slit in order to eliminate out of focus light. It has some advantages such as controlling how many parts of the sample is in focus by controlling the field depth, it only collects information from the focal plane to avoid degradation of the image, and it is possible to collect serial optical sections from thick specimens. These advantages permit 3D images of the samples to be obtained from which roughness (rms) or thickness of the samples can be calculated. The equipment used was a Leica DCM 3D Confocal.

Two techniques previously mentioned in this chapter were also used for these purposes. It is the example of the AFM, the images obtained were treated with Nanoscope analysis Software to obtain the films roughness. SEM was used to observe the cross section of the deposits. It required the sample to be frozen by immersing it into liquid nitrogen and breaking it in half afterwards.

### 3.2.5 Magnetic measurements

To magnetically characterise the deposits the hysteresis loops of the films at room temperature were recorded by means of either a Superconducting Quantum Interference Device (SQUID) magnetometer or a Vibrating Sample Magnetometer (VSM).

**Superconducting quantum interference device (SQUID) magnetometer** A SQUID is based on the principle that the magnetic field in a hole within a superconductor loop is quantized. It consists of a superconducting loop with one or two Josephson junctions. The Josephson junctions consist of two superconductors coupled by a thin insulating bar-

rier or a short section of non-superconducting metal. When applying a current to the superconducting loop, it will split in the two branches of the loop. If an external magnetic field is then applied, a different current will be apparent in each branch, causing a current phase difference in the junctions that is dependent of the magnetic flux. As a consequence, the voltage phase will oscillate, permitting the magnetic flux to be evaluated. In figure 3.10 a schematic representation is shown. It is very sensitive and can measure extremely small magnetic fields such as the ones created by living organisms.

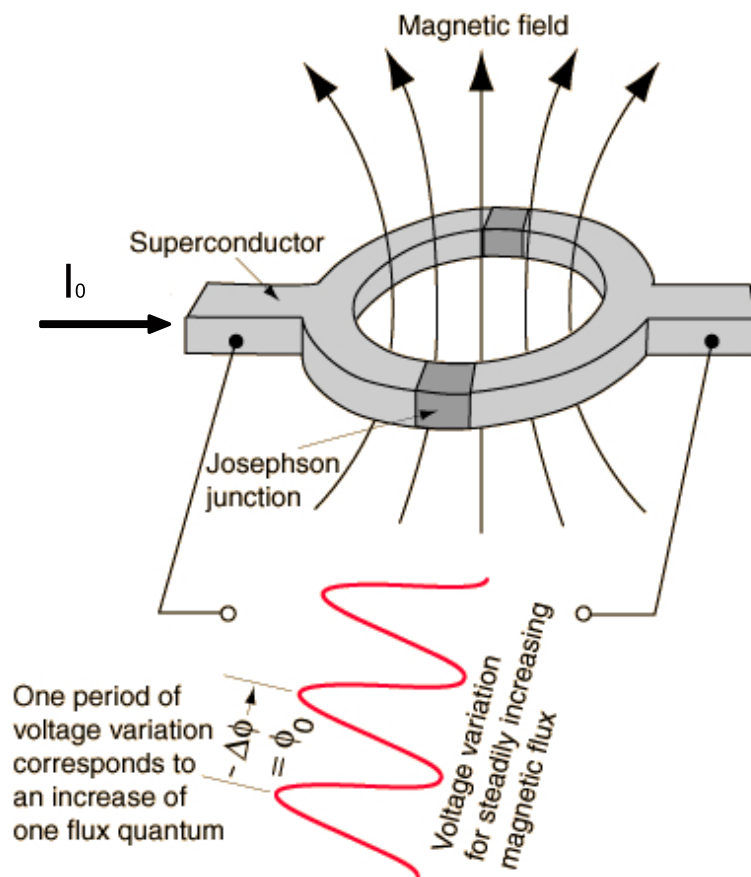


Figure 3.10: Schematic representation of the operation mode of a SQUID

The magnetization-magnetic field (M-H) curves were recorded at room temperature in helium atmosphere using a SQUID magnetometer Quantum

Design MPMS XL. They were recorded with the magnetic field applied parallel and perpendicular to the samples and in some cases it was applied in the two directions (x,y) in the plane of the sample in order to study the magnetic anisotropy of the material. When there was very little amount of sample, as in the case of the nanoparticles, the diamagnetic nature of some substrates (graphite) caused interferences, for that reason it was necessary to detach the particles of the surface of the substrate and placed them into a capsule for the magnetic characterisation. The effect of the soft Ni layer when measuring the magnetism of thick layers of CoPt is negligible, for thinner CoPt layers other substrates with no magnetic response were used.

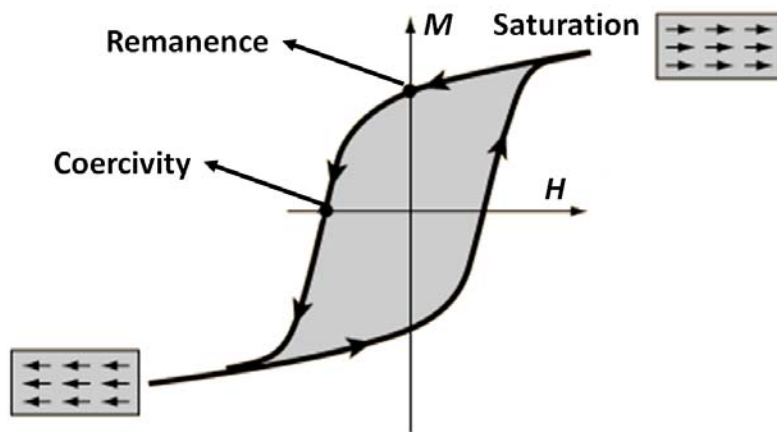


Figure 3.11: Example of a magnetization-magnetic field hysteresis loop

In figure 3.11 typical magnetization-magnetic field curves are shown. Where the saturation ( $M_s$ ) is the maximum possible magnetization of a material, the coercivity ( $H_c$ ) is the magnetic field required to reduce the magnetization of a material to zero after being magnetized, it gives an idea of the resistance of a ferromagnetic material to become demagnetized, and the remanence ( $M_r$ ) is the remaining magnetization when, after taking

the material to the magnetic saturation, the applied field is driven to zero. Another parameter to take into account is the magnetic susceptibility ( $\chi_m$ ), related to the M/H slope, that gives information about how easily the material reacts at the applied magnetic field.

**Vibrating sample magnetometer (VSM)** In a VSM the sample is vibrated inside a uniform magnetic field with two coils (pickup coils) in both sides, figure 3.12. A voltage proportional to the sample's magnetic moment, but not dependent of the extern magnetic field, is induced in the pickup coils.

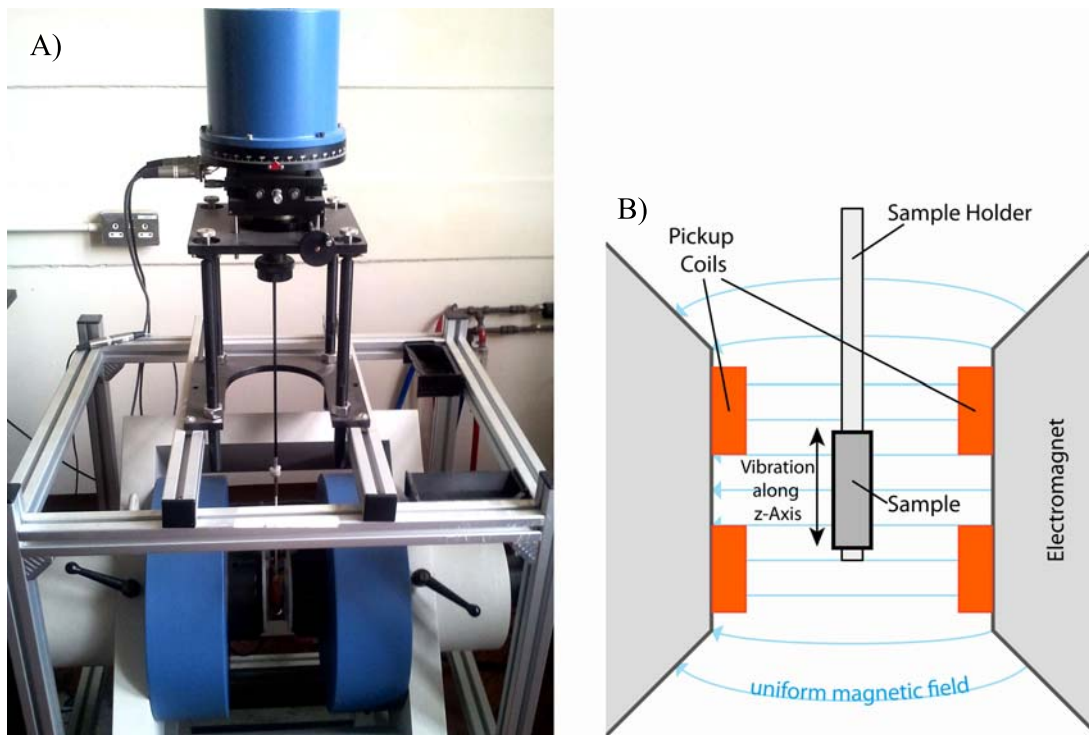


Figure 3.12: A) Photograph of the 7300 Lake Shore VSM and B) Schematic representation of the components of a VSM

By using a lock-in amplifier the induced voltage can be measured and knowing the external magnetic field the hysteresis loop of the material can be obtained. In this thesis a 7300 Lake Shore VSM from H.H. Wills

Physics Laboratory, Bristol, United Kingdom was used to perform some of the magnetic measurements.

### 3.2.6 Contact angle measurements

The contact angle of water measurements were performed using a home-built apparatus, figure 3.13, from the group: Self Organized Complexity and Self Assembled Materials, University of Barcelona. It consists in a moving platform where the sample is located and illuminated by a lamp, a webcam to register the images and a micropipette to place the water drop on top of the sample.

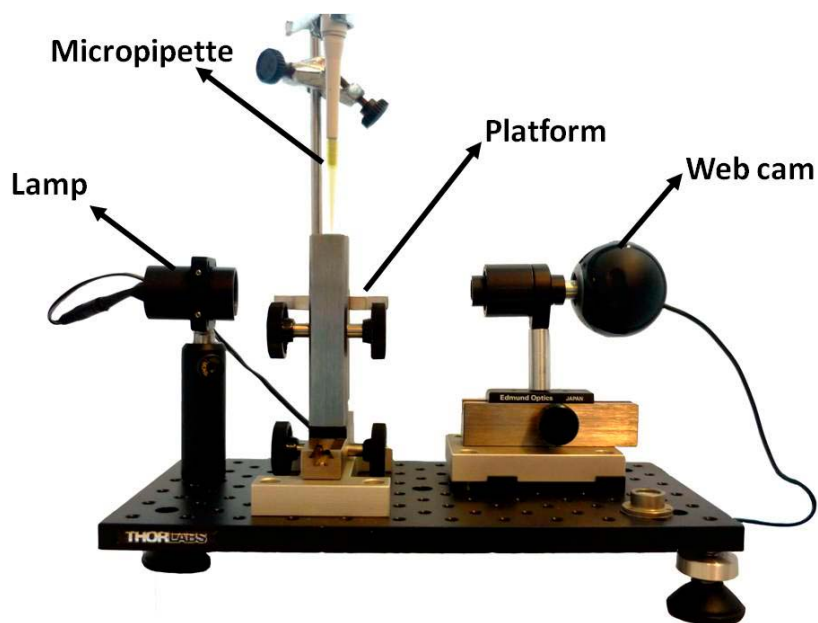


Figure 3.13: Contact angle home-built apparatus from the Self Organized Complexity and Self Assembled Materials group, University of Barcelona

First of all, a drop is formed and maintained in the tip of the micropipette, and then the sample is approached with the platform till it contacts the drop and moved away with the drop on top of the surface

instead of letting it fall from the micropipette. The amount that the drop wets the surface depends on its hydrophilic behaviour and not because of the fall. Drops should be smaller than  $10\ \mu\text{m}$  in order to avoid the flattening of the drop because of the gravity effect.

With a ImageJ Software the recorded images were processed and the contact was measured.

### 3.2.7 Electrical characterisation

A multimeter, a probe station for electrical and optical measurements and a magnifying glass to see the contacts were used to measure the resistance of the copper coils. (figure 3.14)

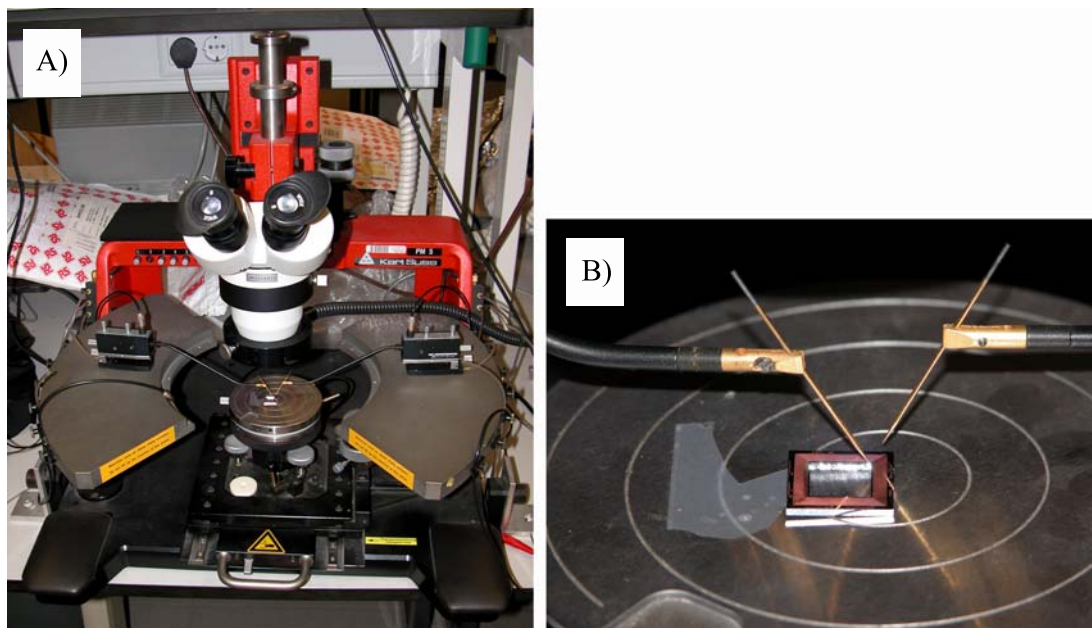


Figure 3.14: A) Probe station for electrical and optical measurements. B) Detail of the copper coil and the platinum tips when measuring the resistance

The chips were encapsulated and connected by gold wire bonds (figure

3.15) for practical electrical characterisation.

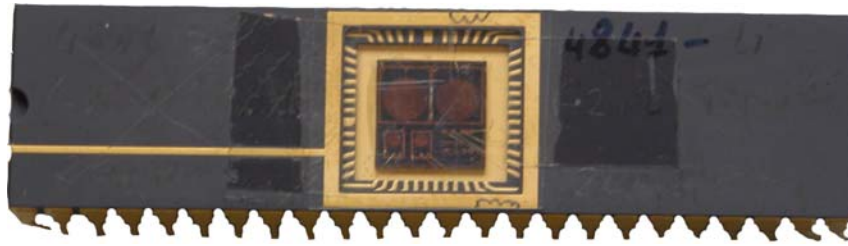


Figure 3.15: Encapsulated chip

In order to characterise their dynamic behaviour with respect to the targeted sensing applications, the coils have been connected in a RLC filter configuration with an external capacitor, and the resonant frequency and phase of the circuit were then characterised using an Agilent 4294A impedance analyser (figure 3.16).

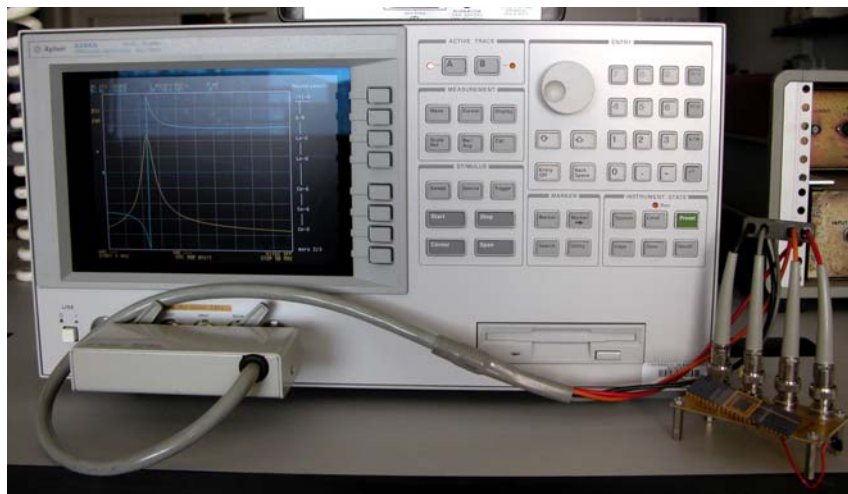


Figure 3.16: Agilent 4294A impedance analyser

Test structures included within the chips were used for open and short circuit calibration of the impedance analyser, providing a thorough compensation of the connections contribution as close as possible to the chip

under analysis.

Finally, a preliminary assessment of the sensing ability of the devices has been performed by measuring the RLC filter response to the presence of Neodymium Boron Iron powder (NdBFe). The powder particles were distributed to cover the entire sensing coil surface.

### 3.3 Etching

In some cases the photoresist or the seed layer of a sample had to be removed, depending on its applications. Two kinds of etching, chemical and physical, were employed in this thesis. They have been summarized in table 3.2

Table 3.2: Etchings employed in the preparation of the samples

Layers	Chemical etchings	Physical etchings
Photoresist	Acetone	
Kapton	Reactive Ion Etching (RIE)	
Si	5% (p/v) HF	
Ti	HF 10%:propylenglycol (1:3)	Ar/SF <sub>6</sub> Plasma
Ni	HNO <sub>3</sub> 70%:H <sub>2</sub> O (1:4)	Ar/SF <sub>6</sub> Plasma
Cu	0.02 M H <sub>3</sub> PO <sub>4</sub> ,4.7 M NH <sub>4</sub> Cl	
	5.7 M NH <sub>4</sub> OH	
Au	I <sub>2</sub> /I <sup>-</sup> saturated solution	
Polycarbonate Templates	Chloroform	
Alumina Templates	1 M NaOH	

### 3.4 Photolithography masks

Three different masks have been used:

- Square coil mask: This mask was designed by Dr. Emile Martinic from Université Paris Sud and Dr. Christophe Serre from EME/CERMAE, Departament d'Electrònica and Institut de Nanociència i Nanotecnologia (IN2UB), Universitat de Barcelona, within the framework of the project SENSATION (ref. FP6-507231).

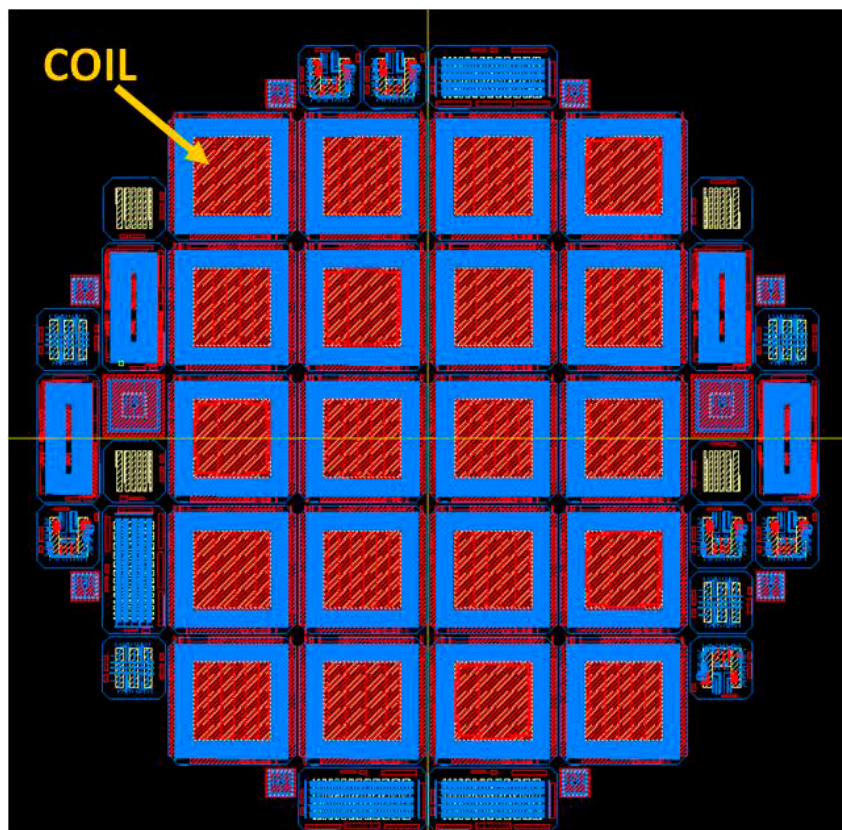


Figure 3.17: Design of the mask with square coils

The mask set designed for this fabrication process has three levels, but only two were used for the sample prepared in this thesis: The first level with bright field corresponds to the DRIE process and the second

with dark field corresponds to the thick photoresist lithography to be used as a mould for the electrodeposition step. It consists of twenty square coils of  $1 \text{ cm}^2$  with a hole in the centre of  $8 \times 8 \text{ mm}^2$ . The coils present different width of tracks, from  $15 \text{ }\mu\text{m}$  to  $30 \text{ }\mu\text{m}$ , and different separation between them, from  $10 \text{ }\mu\text{m}$  to  $20 \text{ }\mu\text{m}$ . The coils with the highest tracks width and separation contain 37 tracks and the ones with the lowest width and separation have 90 tracks. In figure 3.17 the design of the mask is shown. [39]

- Round coil mask: The mask was designed by myself supported by Christophe Serre, within the framework of the project Consolider Ingenio NANOBIO MED (ref. CSD 2006-12). The mask set designed for this fabrication process has three levels: The first level with bright field corresponds to the aluminium track for the centre contact with the coil (figure 3.18).

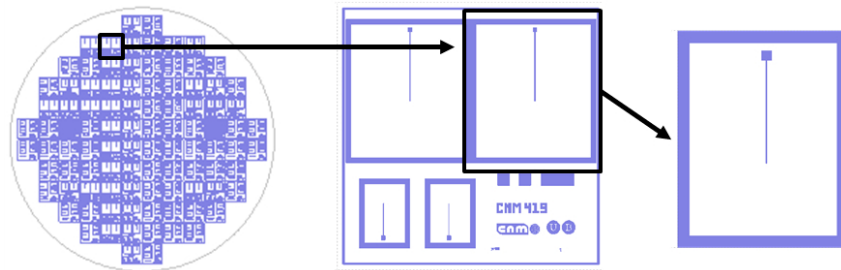


Figure 3.18: Design of the first level of the mask

The second level with dark field is the isolator layer that is necessary to avoid short circuit of the coil tracks. Windows are opened through this insulator layer to enable electrical contact to be made between the Cu coil and the aluminium tracks (figure 3.19).

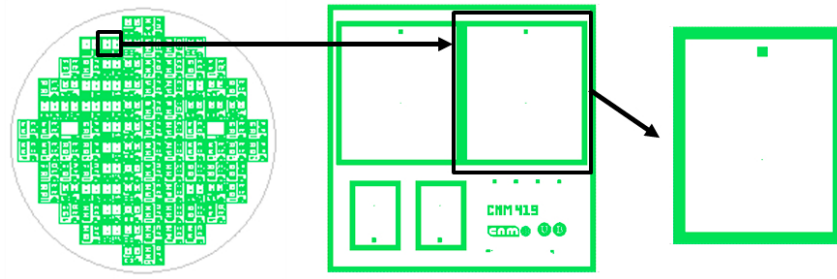


Figure 3.19: Design of the second level of the mask

The third level with dark field corresponds to the thick photoresist lithography to be used as a mould for the electrodeposition step (figure 3.20).

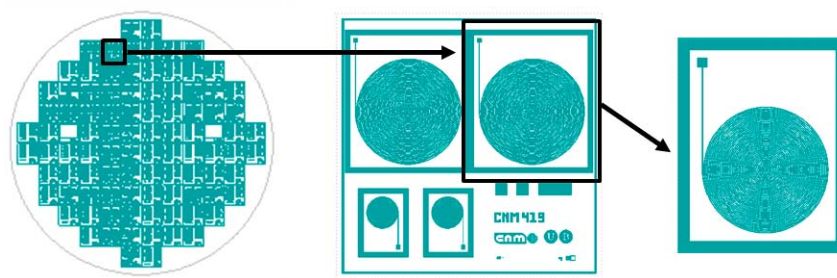


Figure 3.20: Design of the third level of the mask

Each chip of the mask is  $8 \times 8 \text{ mm}^2$  and contains two pairs of coils of different dimensions. The mask includes a guard ring around each coil, and test pads for measurements calibration. The coils contain 25 or 40 tracks, the track width and separation between them are the same and the dimensions go from  $8 \text{ }\mu\text{m}$  to  $20 \text{ }\mu\text{m}$ . An illustration of the mask is shown in figure 3.21.

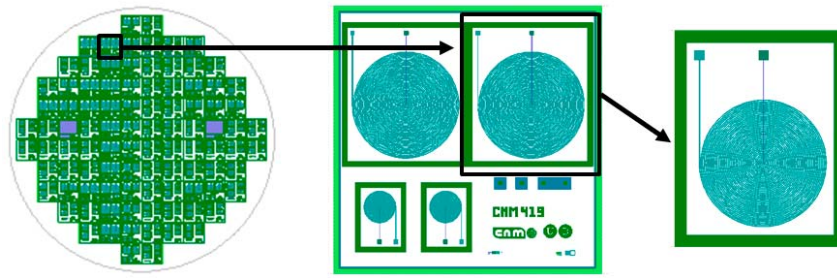


Figure 3.21: Design of the mask for the biosensors

- Microstructure mask: This mask was designed at the Centro Nacional de Microelectrónica (CNM). It consists in a collection of chips of  $5 \times 10 \text{ mm}^2$  divided in 8 elements with bright field on the elements above and dark field at the bottom (figure 3.22). E1 and E5 were groups of 5 equal tranches of 2 mm, but different wide (1 to 100 microns) and separation (1 to 100 microns). E2 and E6 were individual tracks or tranches (1 to 20 microns). E3 and E7 were areas of  $2 \text{ mm} \times 200 \mu\text{m}$  with squares or contacts of different dimensions (1 to 50 microns) and E4 and E8 were checkerboards of  $2 \text{ mm} \times 200 \mu\text{m}$  with different dimensions of the squares (2 to 50 microns). Four types of microstructures can be defined:  $Q^+$  (E3+E4),  $Q^-$  (E7+E8),  $L^+$  (E1+E2) and  $L^-$  (E5+E6).



Figure 3.22: A) Schematic representation of a chip and B) images of the different elements

### 3.5 Simulations

The simulations of the thesis have been performed by Dra. Susanna Martínez from Centro Nacional de Microelectrónica (CNM) and Dr. Christophe Serre.

Simulations were made with ASITIC and were based on a simple model with radial symmetry (2D axis-symmetry), which assumed a coil formed by concentric rings, they have been carried out considering circular spiral coils with 15  $\mu\text{m}$  thick Cu tracks, and a regular track pitch (width = separation) from 8 to 20  $\mu\text{m}$ . The presence of a certain density of magnetic particles in the active area of the device was modelled assuming a continuous layer (10  $\mu\text{m}$  thick in this case) with an effective magnetic permeability ( $\mu_{ef}$ ), given by the volume fraction of magnetic particles on the surface.



## Chapter 4

# Electrodeposition of Copper coils for inductive sensors

### 4.1 Introduction

The possibility of performing in situ field analysis, which permit the detection of toxic species or pathogen agents, such as pesticides or antibiotic in food, is an important requirement in sectors as food processing and pharmaceutical industries, biotechnology, public health and clinical analysis. For that reason recent years have witnessed an increasing interest in biosensor devices presenting not only high sensitivity and specificity but also low cost, easy handling and portability. Immunoassay techniques are based on the biological recognition of the analyte to be detected by a specific antigen or antibody, which is linked to a suitable marker with radioactive, enzymatic or luminescent properties. Then, the analyte coupled to the marker by the immunological reaction is detected using the marker specific properties. These detection techniques provide a high sensitivity and specificity. Several markers have been used during the years,

such as radioactive markers in radioimmunoassay [40] that allow obtaining very high sensitivity but need an expensive, sophisticated and non portable equipment to be used, a part of presenting potential contamination risks. Another kind of markers is enzymatic ones [41] that are cheaper, easy to handle and with good stability compared with radioactive markers. However, they usually present lower sensitivity. Finally, higher sensitivity is reached when using fluorescents markers [41] but complex and expensive equipments are required for their detection.

As an alternative to these techniques, magnetic particles (MP's) have been used as markers because they present high stability, low cost, low toxicity and can be detected in an easy way. Immunomagnetic biosensors based on the use of MP's, as the biological markers for the detection and quantification of biological substances, has been reported [42–45]. In these inductive based devices, sensing is determined by the effects of changes in the inductance of a planar coil due to the presence of the MP's in the sample under analysis [43, 46–48]. The surface of both the MP's and the coil should be functionalised with an antigen specific to the analyte to be detected. Then, the interaction between the analyte and the antigen allows the formation of MP's-antigen-analyte-antigen-coil complex (figure 4.1) from which the amount of analyte can be determined by means of measuring the inductance change of the coil that depends on the amount of MP's bounded.

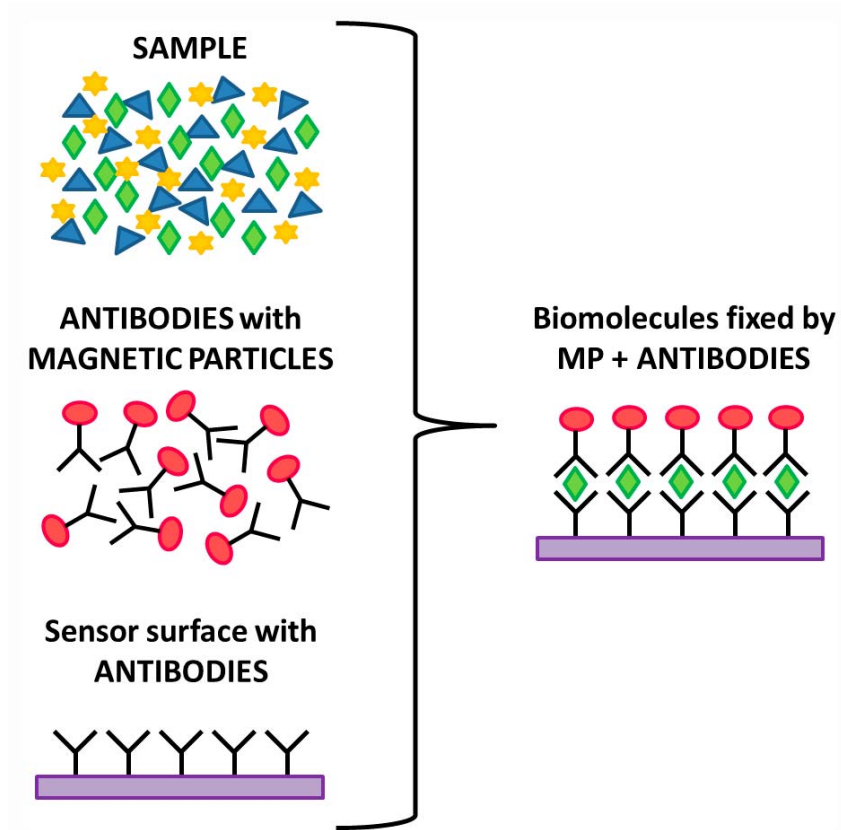


Figure 4.1: Scheme for the detection system using immunoassay techniques and magnetic markers

This type of devices presents high potential for the development of systems with very high sensitivity, low cost and high specificity. Moreover, the fact of not needing a permanent magnetic field to be applied when operating the sensors simplifies the design of these devices and it also permits an easier integration in the whole system. The potential advantages of integrating inductive devices instead of macroscopic solenoids in the Si technology are related to the fabrication cost, yield, and reproducibility of the planar inductive devices. Moreover, the miniaturization of the device dimensions permits smaller volume of samples to be analysed and it will lead to a significant decrease in the cost of the reagents per analysis. In addition, it opens interesting perspectives for the development of

more complex systems such as sensor matrices for simultaneous detection of multiple species.

In previous works, performed in the Electronics department of the *Universitat de Barcelona*, coils formed by concentric rings and two levels of 1.5  $\mu\text{m}$  thick Al metal tracks were fabricated using processes compatible with standard CMOS (Complementary Metal Oxide Semiconductor) technology [49]. However, these coils showed lack of correlation between the inductance changes and the density of MP's when comparing with the simulated values. A conventional method to measure the change in the inductance is measuring the resonance frequency of the coils when applying AC, as resonance occurs at a particular frequency for given values of inductance and capacitance. These Al coils presented very low resonant peak intensity which lead to experimental values with high dispersion and non reproducibility, and it was not possible to characterise the smaller inductive devices because of the presence of parasitic inductive. All these problems were due to a high resistive component in the coil impedance that can compromise the accuracy of the coil inductance measurements. This is a common problem inherent to the planar technology of the Microsystems and an important drawback that severely hinders the performance of these devices. This hinders the measurement of the changes in the inductance by using the common methods based on the measurement of the resonant frequency, since the resistance considerably degrades the resonant peak. In spite of the coils high intrinsic series resistance, the detection of the inductive changes caused by the presence of magnetic particles on the coils surface has been attempted by using differential second order filter circuit topologies working at conditions close to resonance. This circuit

is based on two identical coils connected in parallel, one acts as reference coil and the other as sensing coil and the differences between their signals versus the sensor resonance frequency, related to the inductance, are measured. [42]. Although this method permitted to measure the changes in the coils inductance, the signal still needed to be improved. In order to minimise the problem of the intrinsic high resistance, it was necessary to develop reliable techniques for growing metal layers with thicknesses of several  $\mu\text{m}$  or even beyond 10  $\mu\text{m}$ . An interesting approach for the growth of such layers is the use of electrochemical deposition techniques because electrochemistry is fully compatible with Si Microsystem technologies, being possible to perform the deposition through resist masks. This allows post processing of standard CMOS processed wafers. Electrodeposition has been introduced on different kinds of microstructured substrates for preparing sensors and actuators devices [50–54]. Electrodeposition has been also used in our group to deposit microstructures of different metallic materials and alloys [55–57].

Accordingly, electrochemical deposition of Cu has already been proposed for the development of various advanced inductive devices and microsystems [58, 59]. In principle, Cu is well suited for microsystem applications in Si technology, owing to its low resistivity, moderate cost and ease to grow electrochemically in a well-controlled way. Electrochemical growth of Cu in Si micromachined substrates requires for the use of a surface seed layer. Sputtered Au layers have been reported for these processes [59], with typical layer thickness between 50 and 100 nm. However, the structural analysis of the electrochemically grown layers has shown the existence of a Cu/Au interface region with a high tensile stress, which results in the

presence of a significant stress gradient in the layers. Residual stress and adherence of the layers are parameters that can compromise the viability and lifetime of the devices. They are related to the microstructure of the layers which, in turn, is determined by the electrochemistry processing parameters. Among them, critical issues are the nature of the surface in contact with the electrolyte and the electrolyte composition.

In this framework, the work presented in this chapter reports the design, fabrication and electrical characterisation of enhanced micro inductive devices in relation to biosensing applications, from the first steps of the deposition process to the characterisation of the biosensors with the MP's. Previous to the coils fabrication, it was necessary to find a bath and optimize the electrodeposition conditions and different aspects of the fabrication process:

In this sense, electrolytic baths containing copper(II), sulphuric acid and several additives were studied. As the gap between copper and HER processes is big enough, these baths resulted adequate for the preparation of thick copper deposits. In order to find the bath that lead to the optimum deposit characteristics for the coils fabrication, deposits using different baths with variable amounts of electrolytes and additives were obtained and the morphology, preferential orientation and stress of each one was analysed. For each selected bath, the deposition conditions were chosen from the electrochemical study, and the thickness of the deposits was controlled as a function of the reduction charge. Best deposits were obtained from acidic solutions containing high Cu(II) concentrations and moderated amounts of three additives.

Another aspect to be taken into account was the seed layer. As mentioned before, a seed layer is needed in order to make the substrate (Si/SiO<sub>2</sub>) conductive enough for the electrodeposition process to take place. In some works an Au seed layer was used, but it caused a big stress gradient in the deposits that compromise their lifetime and viability. For that reason, two different seed layers of Ti/Ni and Ti/Cu were proposed in that work. Our interest was focused in analysing the stress and adherence of the deposits in each case to be sure that the deposits would remain attached to the substrate after the different fabrication steps. The best results were obtained for the Si/SiO<sub>2</sub>/Ti/Cu substrates.

Optimization of both the bath and the seed layer cannot be done without corroborating the results when depositing microstructures. For this, square test coils were deposited over photolithographed substrates (Si/SiO<sub>2</sub>/seed layer/resin mask) using the different baths and seed layers. Again the thickness of the tracks can be controlled by adjusting the deposition charge. In this case one more step of the fabrication process was performed. Once the test coils were obtained using the previously optimized bath and conditions, the resin mask and the seed layer were removed. The seed layer must be removed to avoid the short circuit of the coils. Two types of etchings (plasma and chemical) for each seed layer were tested, but better results were observed with the chemical etching, so plasma etching was discarded. The good definition and adherence of the coil tracks were analysed, corroborating the results found when depositing the continuous deposit. In figure 4.2 there is a schematic representation of the fabrication process.

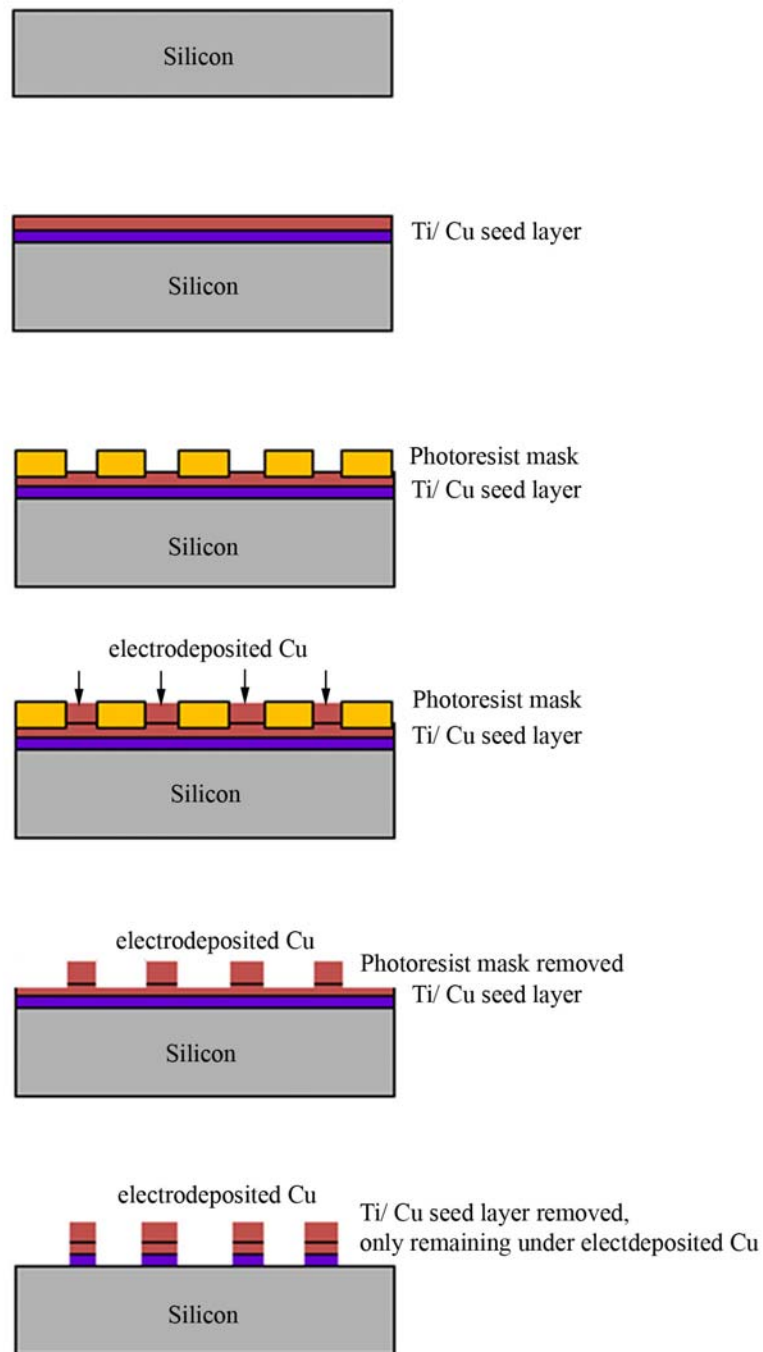


Figure 4.2: Schematic representation of the fabrication process

One of the reasons for using electrodeposited copper to fabricate the biosensors coils was to minimize the drawback of high series resistance inherent to planar technology. In order to check it, the electrical characterisation of the test coils was performed and compared with Al ones.

The devices show electrical series resistance values that are significantly lower than those from planar Al coils fabricated using standard Si technology processes. This made Cu electrodeposition process a good alternative to the materials and techniques previously used for the coils fabrication and opened the possibility of designing and developing advanced inductive biosensors. These results are presented in the paper: “*Optimisation of copper electrodeposition processes for Si technology based inductive microsystems*”. This study was performed using the electrochemical cell of 250 ml, small pieces ( $1 \times 2 \text{ cm}^2$ ) as substrates and the platinum spiral as counter electrode.

The final objective of the work was the implementation of the coils electrodeposition in the fabrication process of a biosensor. Although the previous work was realised with the test coils, the scale up of the electrodeposition process was performed to optimise the different parameters that needed to be changed. First of all, more bath volume was needed, so a new cell with more capacity (up to 2,5 l) was used. It was not possible to de-aerated the solutions by argon bubbling before each experiment and maintain them under argon atmosphere during the process but no interferences were observed. More stirring of the solution was needed to ensure constant contribution of the electroactive species to the electrode during the deposition. A copper-phosphorous alloy was used as counter electrode instead of a platinum spiral to maintain a constant copper concentration in the bath. The phosphorus was necessary to avoid the passivation of the counter electrode which will lead to a change in the control of the process. In figure 4.3 images of the scale up process are shown.

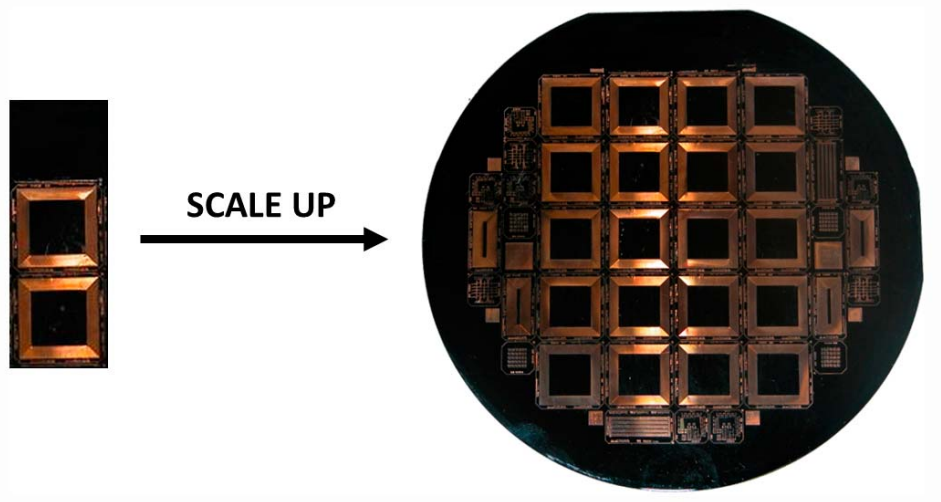


Figure 4.3: Scale up of the electrodeposition process

It was possible to scale the process and obtain micromachined coils fabricated using the optimised electrodeposition conditions that exhibited well-defined tracks, with a good definition of the walls and perfectly follow the photoresin moulds.

In a second step, it was thought that obtaining the coils over flexible, economical and disposable substrates would be interesting for our purpose of fabricating a biosensor to be used in field analysis. The optimized bath and the previous results were a starting point to test the viability of preparing copper coils using plastics as substrates. The selected plastics were: PEEK, PEN, PMMA, PS, Teflon and Kapton. In this case a seed layer was also needed for the electrodeposition process to be performed. The deposition of copper over plastic substrates, analysis of the morphology, structure and stress of the deposits has determined that the PEN is the best candidate in order to manufacture biosensors. The results are presented in “*Implementation of the deposition conditions over plastic substrates*” section.

Finally, a new coil design was proposed based in the simulations of the conditions needed to achieve minimum electrical resistance and maximum sensibility. The highest circuit sensitivity and linearity are achieved by working close to the resonant frequency,  $f_p$ . It had to be taken into account that the shape and position of the resonant peak depends on the electrical parameters of the circuit 4.1.

$$f_p = \left(\frac{f_o}{\sqrt{2}}\right) \left(1 + \sqrt{1 + \frac{1}{2} \left(\frac{R}{f_o \Pi L}\right)^2}\right)^{\frac{1}{2}} \quad (4.1)$$

Where  $f_o = \omega_o/2\Pi$  is the natural frequency of the circuit without taking into account the intrinsic series resistance  $R$  of the coil and  $\omega_o$  is the harmonic frequency  $= (1/LC)^{1/2}$ , where  $L$  is the inductance and  $C$  the capacitance of the coil. The shape of the resonant peak is determined by the  $Q$  factor, a high quality peak leads to narrow and intense resonance peak. The quality factor is determined by 4.2:

$$Q = \left(\frac{L\omega_o}{R}\right) \quad (4.2)$$

So by decreasing the capacitance and resistance the quality factor increases. However, this also implies an increase in  $f_p$ , which can take values out of the range of measurement of common devices. For that reason, simulations of the intrinsic series resistance, the quality factor and the resonance frequencies have been made. According to these simulation results, different coil dimensions were chosen to reach the best compromise between high inductance value, high quality factor and reasonable working frequencies, within the limits defined by the targeted application. The

number of tracks and aspect ratio was optimized for different theoretical track thicknesses.

Using the optimized mask, electrodeposition conditions were adjusted for the new design to prepare coils of around 15 microns-thick, with good edge definition. Round copper coils of good definition were obtained in all cases, when the resin masks were correctly defined. After the preparation of the coils, the resin and the seed layers were removed and the electrical characterisation of the coils was performed. Low electrical resistances measured were in good agreement with the optimum simulated values.

The viability of thick electrodeposited Cu coils for use as biosensors in a configuration of differential second order filter circuit topologies working at conditions close to resonance is analysed [60, 61]. Single second order filter circuit topologies have been applied to measure the microinductive coils inductances, which are incorporated into passive RLC filters made with discrete elements on a Printed Circuit Board (PCB). The resonant frequency and phase of the circuit were then characterised using the Agilent 4294A impedance analyser. Both inductance and resonance frequency values obtained from the prepared coils agreed with the simulation and present a low standard deviation, which is necessary for biosensor designed to work in a differential configuration.

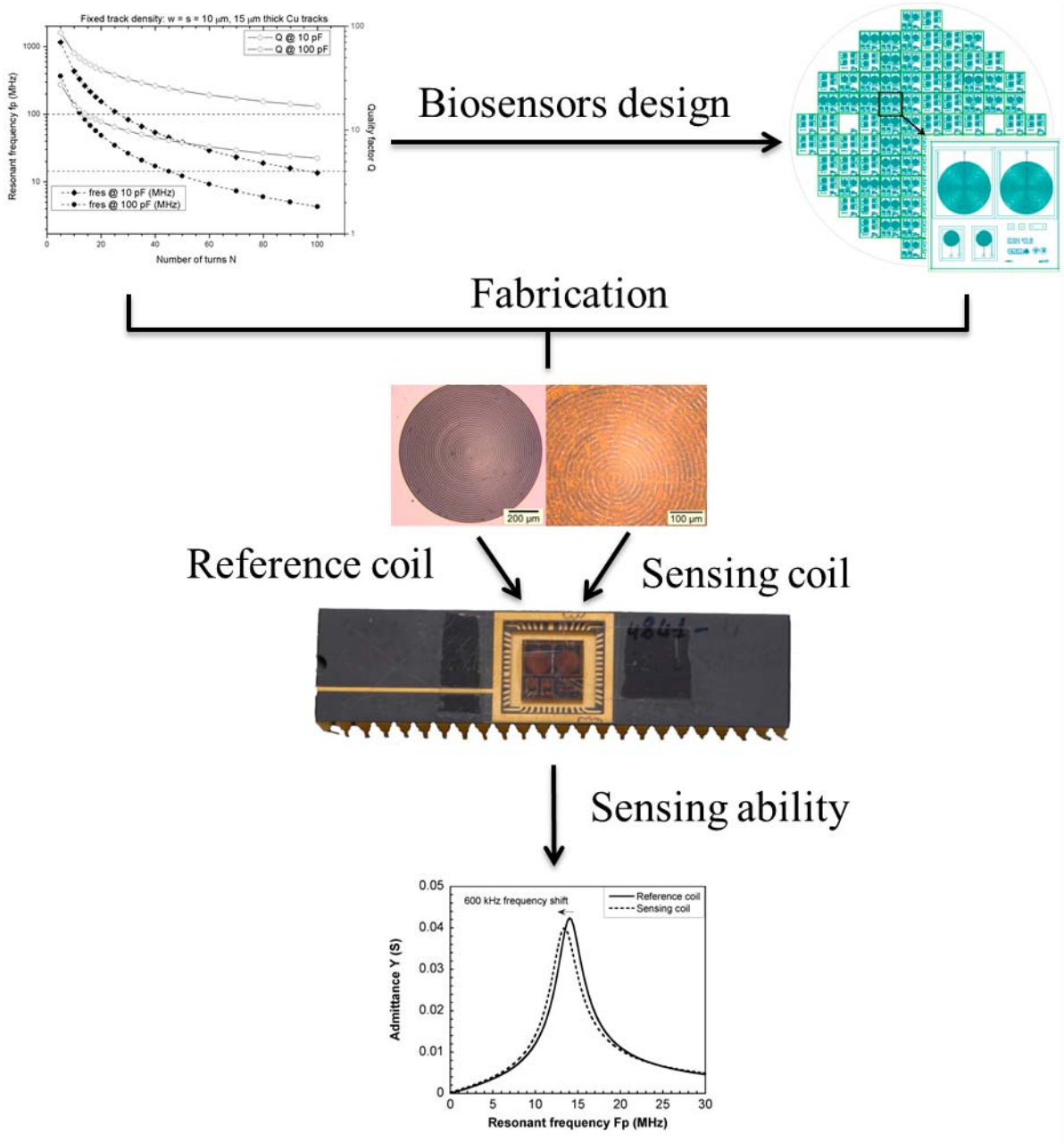


Figure 4.4: Schematic representation of the steps followed to fabricate the new coils

A preliminary characterisation of the device sensing behaviour was performed by using neodymium boron iron powder. The coils were covered with an acrylic-based varnish to insulate them before the characterisation with the powder because it may cause the short circuit of the coils. The results reveal a change in the resonance frequency, permitting the presence

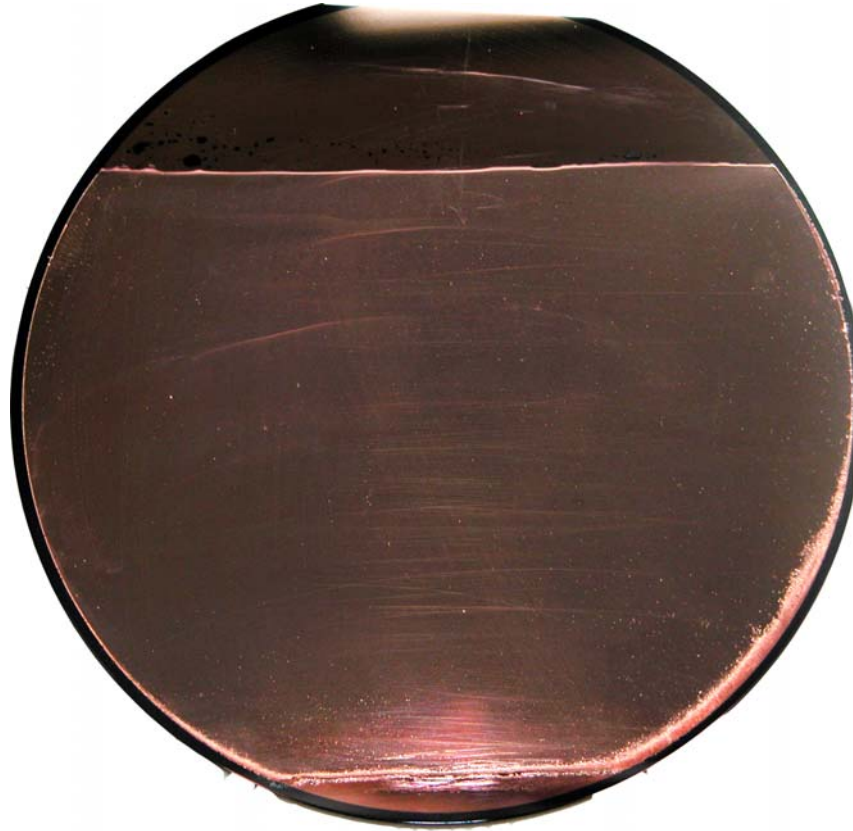
of the magnetic powder to be detected. Extensive additional simulations were performed to study the effects of the coil dimensions and the track density, to improve the design in further work. In figure 4 a schematic representation of the steps followed to fabricate the new coils is shown. The results of this part of the work are presented in the paper “*Design and electrochemical preparation of inductive copper coils for magnetic particles detection*”, where the potential of these microinductive devices for high sensitivity, low cost and high specificity immunomagnetic biosensing applications was demonstrated (figure 4.4).

## 4.2 Results presented in this chapter

- Paper: “*Optimisation of copper electrodeposition processes for Si technology based inductive microsystems*” M. Cortés, E. Gómez, A. Pérez-Rodríguez, C. Serre and E. Vallés, Journal of Electroanalytical Chemistry 619-620 (2008) 176-182
- “*Analysis of the texture and stress of the Cu deposits*”
- “*Implementation of the deposition conditions over plastic substrates*”
- Paper: “*Design and electrochemical preparation of inductive copper coils for magnetic particles detection*” M. Cortés, S. Martínez, C. Serre, E. Gómez, A. Pérez-Rodríguez and E. Vallés, Sensors and Actuators B: Chemical 173 (2012) 737-744



#### 4.2.1 Optimisation of copper electrodeposition processes for Si technology based inductive microsystems





Contents lists available at ScienceDirect

## Journal of Electroanalytical Chemistry

journal homepage: [www.elsevier.com/locate/jelechem](http://www.elsevier.com/locate/jelechem)

# Optimisation of copper electrodeposition processes for Si technology based inductive microsystems

M. Cortés<sup>a</sup>, E. Gómez<sup>a</sup>, A. Pérez-Rodríguez<sup>b</sup>, C. Serre<sup>b</sup>, E. Vallés<sup>a,\*</sup>

<sup>a</sup> *Electrodep, Departament de Química Física and Institut de Nanociència i Nanotecnologia (IN<sup>2</sup>UB), Universitat de Barcelona, Martí i Franquès, 1, 08028 Barcelona, Spain*

<sup>b</sup> *EME/CERMAE, Departament d'Electrònica and Institut de Nanociència i Nanotecnologia (IN<sup>2</sup>UB), Universitat de Barcelona, Martí i Franquès, 1, 08028 Barcelona, Spain*

## ARTICLE INFO

## Article history:

Received 8 February 2008

Received in revised form 9 April 2008

Accepted 9 April 2008

Available online 18 April 2008

## Keywords:

Copper microstructures

Coil devices

Electrodeposition

Stress

XRD

## ABSTRACT

Electrodeposition has been demonstrated as a useful technique for the fabrication of inductive devices formed by thick Cu coils with low stress and good adherence to silicon-based substrates, as required for advanced microsystems compatible with Si technology. Different baths with variable amounts of electrolytes and additives were tested. Stress and microstructural properties of copper deposits were analysed. Best deposits were obtained from acidic solutions containing high Cu(II) concentrations and moderated amounts of three additives. In these conditions, low stress measurements and no preferential orientation of copper were observed, especially on Si/SiO<sub>2</sub>/Ti/Cu substrates. At optimised conditions, several microns thick copper coils of different aspect ratio were prepared, which showed good adherence on the substrate after removing the resin mask and the seed layer. The characterisation of these devices corroborates the interest and suitability of the optimised electrochemical processes for advanced Si technology microsystem applications.

© 2008 Elsevier B.V. All rights reserved.

## 1. Introduction

In the last years, Si technology based inductive microsystems are receiving an increasing interest for different kinds of applications, including microactuators, power microgenerators and biosensors [1–4]. These systems are based on the electromagnetic interaction between a planar coil and a magnetic material. In the case of the microactuators and inertial microgenerators, the design of the device includes a fixed coil and a permanent magnet that is usually mounted onto a mobile microstructure [1–3]. On the other hand, the use of inductive devices for high sensitivity biodetection applications based on the use of magnetic particles as biological labels has also been reported [4]. In all these cases, it clearly appears that the high value of series resistance, inherent to the planar technology of the microsystems, severely hinders the performance of these devices. Therefore, the full exploitation of the potential capabilities of these systems is strongly conditioned to the development of reliable techniques for growing metal layers with thicknesses well above those available with standard Si technology.

This implies the need to grow layers with some microns of thickness, which are much higher than those usually achievable by physical and chemical vapour deposition (PVD, CVD) techniques currently used in Si technology (typically limited to about 1–2 μm).

\* Corresponding author. Tel.: +34 934039238; fax: +34 934021231.

E-mail address: [e.valles@ub.edu](mailto:e.valles@ub.edu) (E. Vallés).

An interesting approach for the growth of such layers is the use of Electrochemical (EC) deposition techniques. EC has several advantages in relation to PVD and CVD processes: a higher deposition rate – allowing a very wide thickness range from values below 0.1 μm up to more than 100 μm –, the easy control of thickness and chemical composition of the layer, and the low cost and high simplicity of the experimental setup. Moreover, EC is fully compatible with Si Microsystem technologies, being possible to perform the deposition through resist masks. This allows post processing of standard CMOS (complementary metal oxide semiconductor) processed wafers. Electrodeposition has been introduced on different kinds of microstructured substrates for preparing sensors and actuators devices [5–9]. Electrodeposition has been used also in our group to deposit microstructures of different metallic materials and alloys [10–12].

EC deposition of Cu has already been proposed for the development of advanced inductive devices and microsystems [13,14]. In principle, Cu is well suited for microsystem applications in Si technology, owing to its low resistivity, low cost and ease to grow electrochemically in a well-controlled way. EC growth of Cu in Si micromachined substrates requires for the use of a surface seed layer. Sputtered Au layers have been reported for these processes [14], with typical layer thickness between 50 and 100 nm. However, the structural analysis of the EC grown layers has shown the existence of a Cu/Au interface region with a high tensile stress, which results in the presence of a significant stress gradient in the layers. Residual stress and adherence of the layers are parameters

that can compromise the viability and lifetime of the devices. They are related to the microstructure of the layers which, in turn, is determined by the EC processing parameters. Among them, critical issues are the nature of the surface in contact with the electrolyte and the electrolyte composition.

In this framework, this work reports a microstructural and stress analysis of Cu layers grown onto different seed surfaces by EC processes. The aim of the work is the optimisation of the electrolytic baths and the electrodeposition conditions for the fabrication of well-defined copper coils compatible with their integration in advanced microsystems such as inertial power microgenerators [15]. For this, conditions leading to low stressed Cu tracks with a good adherence over the substrate after removal of the resin mask and seed layers have been investigated. Finally, the developed processes have been implemented for the fabrication of micro-inductive devices in Si technology, according to the design of an optimised electromagnetic microgenerator reported in [15].

## 2. Experimental

The electrodeposition processes were performed in a conventional three-electrode cell using a microcomputer-controlled potentiostat/galvanostat Autolab with PGSTAT30 equipment and GPES software. Reagents used for the electrolytic bath were  $\text{CuSO}_4 \cdot 5\text{H}_2\text{O}$ ,  $\text{H}_2\text{SO}_4$  and  $\text{NaCl}$  all of analytical grade. Different additives carrier (polyethyleneglycol of high molecular weight, XD7397), brightener (bis-(3-sulphopropyl)-disulphidesodium salt, XD7398) and leveller (polymerized triazine, XD7399) from MacDermid Company were also used. All solutions were freshly prepared with water, which was first doubly distilled and then treated with a Millipore Milli Q system. Solutions were de-aerated by argon bubbling before each experiment and maintained under argon atmosphere during the process. The temperature was maintained at 25 °C.

For the electrochemical study of the deposition processes, a vitreous carbon (Metrohm) electrode of  $0.0314 \text{ cm}^2$  was used as working electrode. It was polished to a mirror finish before each experiment using alumina of different grades (3.75 and  $1.85 \mu\text{m}$ ) and cleaned ultrasonically for 2 min in water treated as described in the previous paragraph. The reference electrode was an  $\text{Ag}/\text{AgCl}/(1 \text{ mol dm}^{-3}) \text{ NaCl}$  electrode mounted in a Luggin capillary containing  $0.5 \text{ mol dm}^{-3} \text{ Na}_2\text{SO}_4$  solution. All potentials are referred to this electrode. The counter electrode was a platinum spiral. The electrochemical study was performed using cyclic voltammetry. Experiments were carried out under quiescent or stirring conditions at  $50 \text{ mV s}^{-1}$ .

Deposits were prepared using potentiostatic and galvanostatic techniques under gentle stirring (60 rpm) conditions. Starting material for the substrates were 100 mm diameter (001) Si wafers, and three kinds of substrates have been used: (a) Si wafers with a Ti (100 nm)/Ni(50 nm) bilayer deposited by sputtering, (b) Si wafers coated with a  $1 \mu\text{m}$  thick  $\text{SiO}_2$  layer and with a Ti (100 nm)/Ni(50 nm) bilayer deposited by sputtering onto the  $\text{SiO}_2$  surface, and (c) Si wafers coated with a  $1 \mu\text{m}$  thick  $\text{SiO}_2$  layer and with a Ti(10 nm)/Cu(100 nm) bilayer evaporated onto the  $\text{SiO}_2$  surface. In these samples, Ti is added to improve the adherence of the EC grown layer, Ni or Cu are used as seed layer and the  $\text{SiO}_2$  layer is required to provide an insulating basement avoiding short circuit of the coil tracks. In all cases, the substrates were cleaned with ethanol and rinsed in water before depositing, for the substrates with a Ti/Ni seed layer a previous wash with acetone was introduced.

Test structures and coils have been fabricated according to the design reported in [7]. In this case, a photolithographic step of AZ4562 photoresist mould (about  $15 \mu\text{m}$  thick) was performed before the EC deposition. The final process steps were the removal of

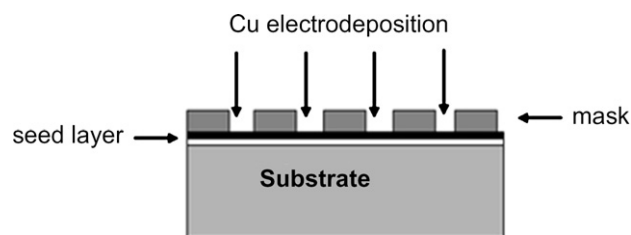


Fig. 1. Schematic representation of the fabrication process of the test microstructures and coils.

the photoresist in acetone and the selective chemical etching of the Ti/seed bilayer between the Cu tracks: nitric acid and a fluorhydric acid + propylenglycol solution were used for Ti/Ni, whereas ammoniacal copper chloride and a fluorhydric acid + propylenglycol solution were used for Ti/Cu. Fig. 1 shows a schematic representation of the process used to obtain these microstructures.

The microstructural analysis of the layers has been performed by X-ray diffraction (XRD)  $2\theta/\theta$  and  $\Psi$ -scan measurements, in order to characterise the existence of preferential orientations in the crystalline grains and their dependence on the EC processing parameters. The average in-plane stress in the layers has been estimated using the  $\sin^2\psi$  method [16]. XRD measurements were performed with a Philips MRD diffractometer with parallel optical geometry using  $\text{CuK}\alpha$  radiation ( $\lambda = 1.5418 \text{ \AA}$ ) and a goniometer that allows control of the sample rotation about the three axes.

The morphology of the deposits was examined with scanning electron microscopy (SEM) using a Hitachi S 2300 microscope. Surface roughness (rms) was measured using a white-light interferometer from Zygo Corporation as a white-light interferometer Fogale-Nanotec ZoomSurf 3D. The test microstructures and coils have also been inspected with the SEM and interferometric equipments. Thickness of deposits were measured using the interferometer.

## 3. Results and discussion

### 3.1. Voltammetric study of the electrodeposition process

The voltammetric study of the EC processes has been performed using baths with 70–200 g/l  $\text{Cu(II)}$ , 70–200 g/l  $\text{H}_2\text{SO}_4$ , 70 mg/l  $\text{NaCl}$

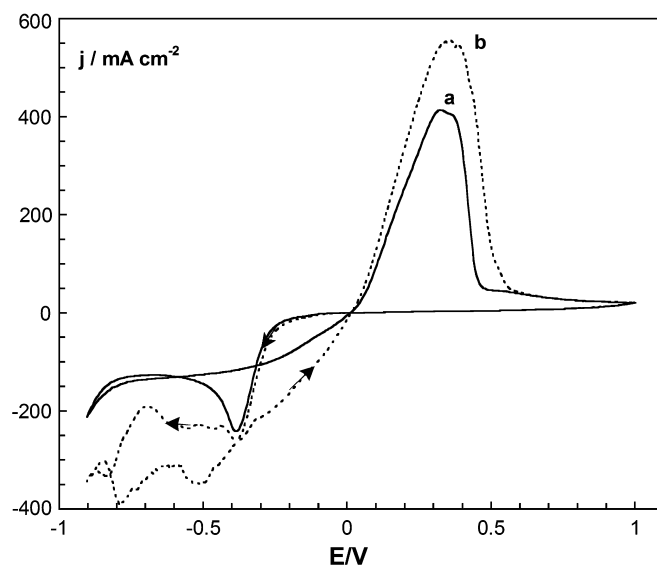
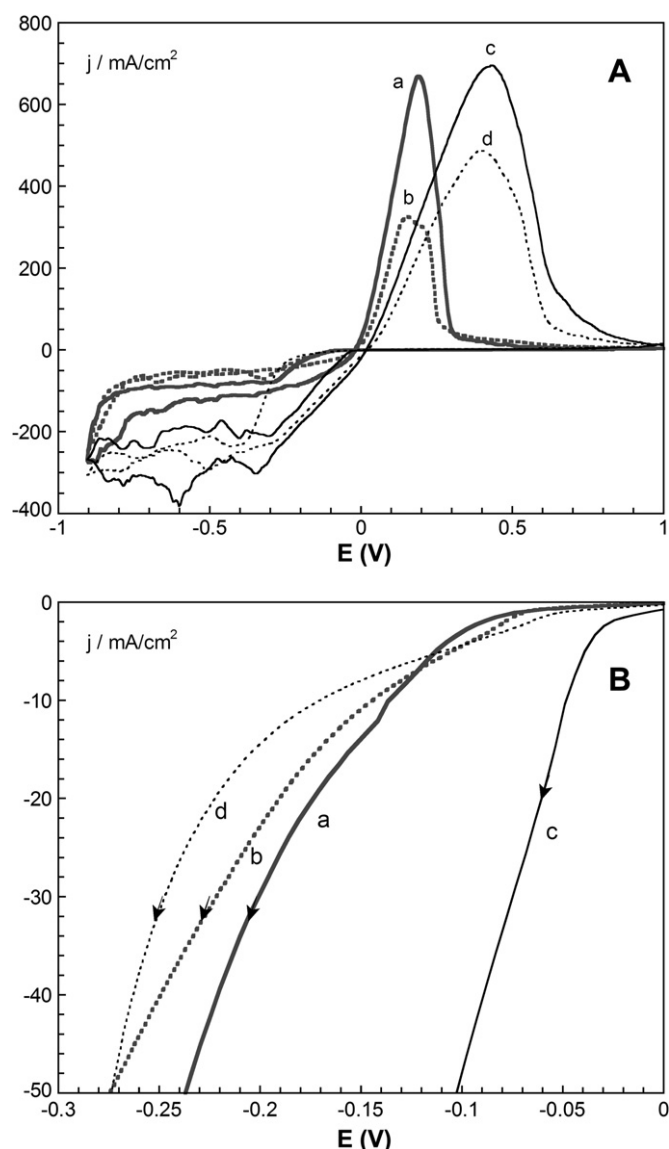


Fig. 2. Cyclic voltammograms of 70 g/l  $\text{H}_2\text{SO}_4$  + 200 g/l  $\text{CuSO}_4$  + 70 mg/l + 10 ml/l carrier + 0.5 ml/l brightener + 0.4 ml/l leveller: (a) quiescent conditions, (b) stirring conditions ( $\omega = 60 \text{ rpm}$ ). Vitreous carbon electrode.



**Fig. 3.** Cyclic voltammograms of baths containing  $u$  g/l  $\text{H}_2\text{SO}_4$  +  $v$  g/l  $\text{CuSO}_4$  +  $w$  mg/l  $\text{NaCl}$  +  $x$  ml/l carrier +  $y$  ml/l brightener +  $z$  ml/l leveller. Stirring conditions ( $\omega = 60$  rpm): (a)  $u = 200$ ,  $v = 70$ ,  $w = 70$ ,  $x = 0$ ,  $y = 0$ ,  $z = 0$ , (b)  $u = 200$ ,  $v = 70$ ,  $w = 70$ ,  $x = 0.67$ ,  $y = 0.13$ ,  $z = 0.13$ , (c)  $u = 70$ ,  $v = 200$ ,  $w = 70$ ,  $x = 0$ ,  $y = 0$ ,  $z = 0$ , (d)  $u = 70$ ,  $v = 200$ ,  $w = 70$ ,  $x = 10$ ,  $y = 0.5$ ,  $z = 0.4$ . Vitreous carbon electrode.

and different amounts of additives (carrier, brightener and leveller). For each substrate tested, the voltammetric scan was started at a potential where no process took place. First, it was scanned to negative potentials and then was reversed to positive ones to study the reduction and the oxidation processes, respectively.

Fig. 2 shows cyclic voltammograms recorded over the vitreous carbon substrate for one of the tested electrolytic baths, using a potential sweep of  $50 \text{ mV s}^{-1}$  and under stationary and stirring conditions (60 rpm). As can be seen in this figure, the diffusion controlled reduction peak corresponding to copper deposition was detected before hydrogen evolution (HER).

A similar voltammetric behaviour has been observed for the different baths tested, although the onset of the copper deposition was logically advanced as the  $\text{Cu(II)}$  concentration increased, as can be seen in Fig. 3. Moreover, the presence of additives in the bath determines a gradual shift (delay) of the onset of the copper deposition, as a consequence of their adsorption on the electrode.

When silicon based substrates were used as working electrodes, the copper deposition was slightly advanced with respect to the

vitreous carbon electrode (Fig. 4), because the metallic nature of the surface coating of these electrodes favours the nucleation process. The onset of the copper deposition process over the Cu seed layer was more positive (180 mV) than over the Ni one, because of the greater affinity of the deposit with respect to the Cu seed layer. No voltammetric differences were observed when the substrate under the seed-layer was varied, therefore we can rule out the influence of the substrate on the process.

When the oxidation charge in the voltammetric curves was compared with the reduction one, high  $Q_{\text{ox}}/Q_{\text{red}}$  ratios (65–85%) were observed, revealing the low interference of hydrogen evolution in the copper deposition process.

### 3.2. Electrochemical deposition of Cu. Morphological analysis

Copper deposits were prepared potentiostatically or galvanostatically under stirred conditions in order to maintain the contribution of electroactive species to the electrode. For each bath and substrate analysed, the deposition potentials were selected according to the shift in the onset of the reduction process observed in the voltammetric curves. In all cases, the morphology of the deposits was analysed at relatively high deposition charges ( $-20/-83 \text{ C cm}^{-2}$ ).

Uniform copper deposits of nodular morphology were obtained from both potentiostatic and galvanostatic methods. The morphology of copper deposits was not dependent on the used seed layer. However, the roughness and grain size of the deposits was drastically dependent on the bath composition, as shown in Fig. 5. Fine grained films of low measured roughness (100 nm) were obtained for high  $\text{Cu(II)}$  concentrations in the presence of additives. At these conditions, the measurement of the thickness of the EC deposited layers with the interferometer gives a growth rate of  $4\text{--}5 \mu\text{m/min}$ .

### 3.3. Structural characterisation and stress analysis

The XRD analysis of all the deposited layers showed the diffraction peaks corresponding to the face cubic centred (fcc) polycrystalline structure of copper, as indicated by the presence of various diffraction lines in the  $\theta\text{--}2\theta$  surveys. No differences were obtained in function of the deposition charge from deposits of deposition charges greater than  $20 \text{ C cm}^{-2}$ . However, the preferential orientation of the crystalline planes of the deposits that were

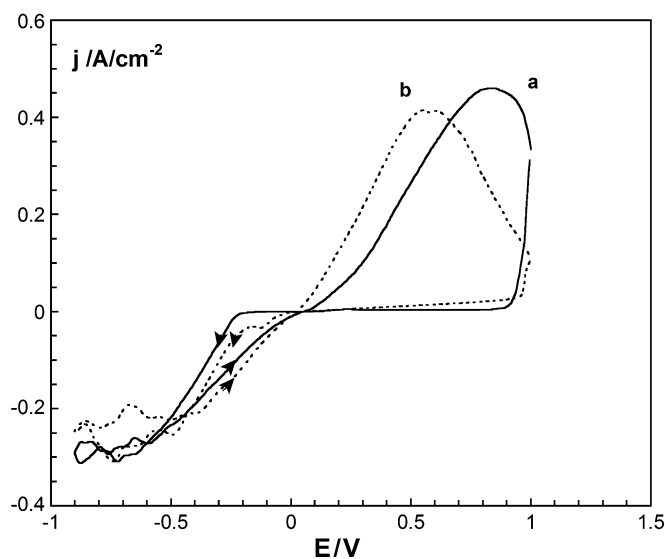


**Fig. 4.** Cyclic voltammograms from the same solution than in Fig. 2.  $\omega = 60$  rpm: (a) silicon/ $\text{SiO}_2$ /Ti/Ni substrate, (b) silicon/ $\text{SiO}_2$ /Ti/Cu substrate.

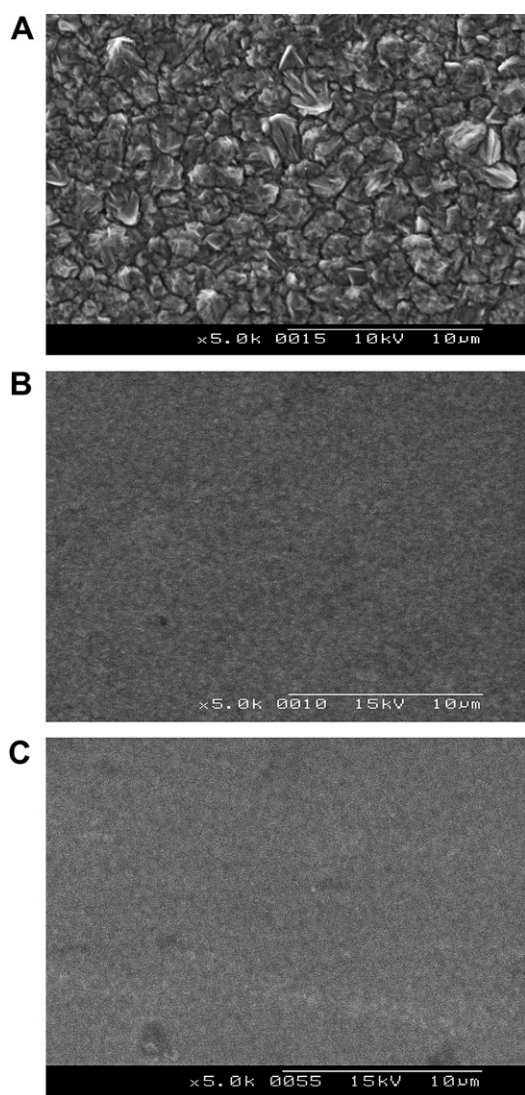


**Fig. 5.** SEM images of copper deposits prepared at 60 rpm from (A) 200 g/l  $\text{H}_2\text{SO}_4$  + 70 g/l  $\text{CuSO}_4$  solution, deposition potential:  $-250$  mV,  $Q = -20$   $\text{C cm}^{-2}$ , Si/SiO<sub>2</sub>/Ti/Ni electrode, (B) 70 g/l  $\text{H}_2\text{SO}_4$  + 200 g/l  $\text{CuSO}_4$  + 10 ml/l carrier + 0.5 ml/l brightener + 0.4 ml/l leveller solution, deposition potential:  $-250$  mV,  $Q = -50$   $\text{C cm}^{-2}$ , Si/SiO<sub>2</sub>/Ti/Cu electrode, (C) 70 g/l  $\text{H}_2\text{SO}_4$  + 200 g/l  $\text{CuSO}_4$  + 10 ml/l carrier + 0.5 ml/l brightener + 0.4 ml/l leveller solution, deposition potential:  $-250$  mV,  $Q = -50$   $\text{C cm}^{-2}$ , Si/SiO<sub>2</sub>/Ti/Ni electrode.

parallel to surface was strongly influenced by the composition of the deposition solution. Fig. 6 shows, for two different copper deposits, the three peaks of higher intensity of the fcc structure of copper. Different ratio between these peaks was observed as a function of the deposition solution. Copper deposits showed a preferential (220) orientation when they were obtained from low Cu(II) (70 g/l) and null or low additives concentrations. This can be clearly seen in Fig. 6A: the intensity ratio between the (220) and the (111) peaks in this figure is around 100%, instead of 40–50% as expected for randomly oriented materials. By increasing the concentration of both Cu(II) and the additives in the bath, the preferential orientation obtained on the deposits was gradually lost. As shown in Fig. 6B, the XRD diffractograms measured from layers grown with high Cu(II) concentrations in the presence of additives show (111), (200) and (220) peaks with the intensity ratios characteristic of fully polycrystalline materials. This point out the absence of preferential orientation of the parallel crystalline planes in the Cu layers grown with these conditions. On the other

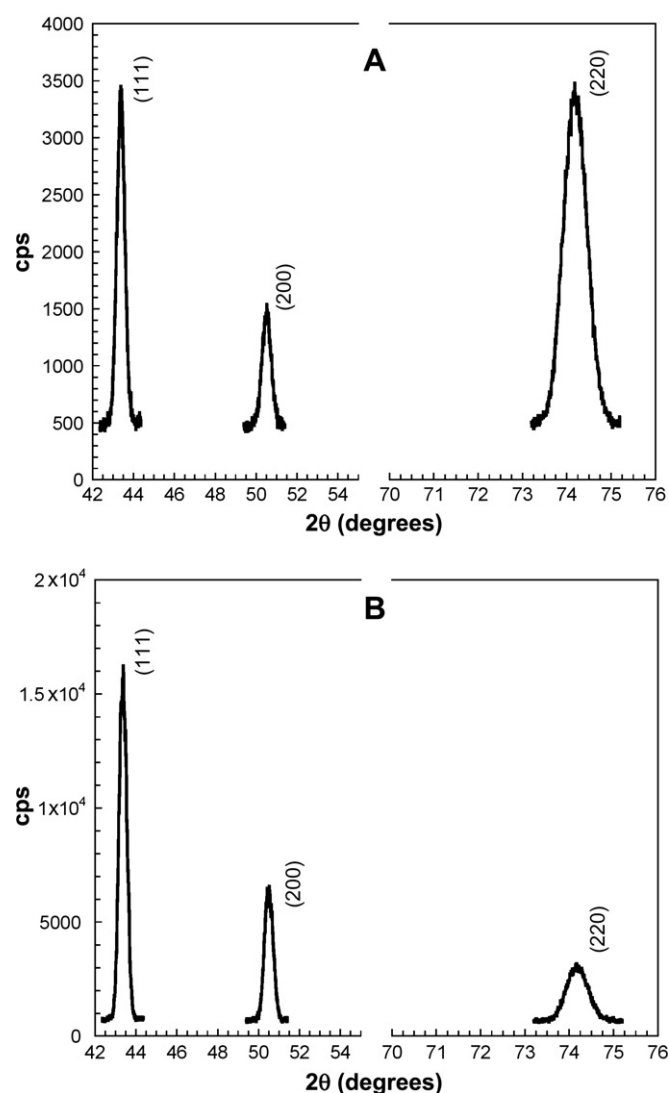


**Fig. 6.** fcc (111), (200) and (220) diffraction peaks of copper deposits prepared potentiostatically over Si/Ti/Ni substrates at 60 rpm: (A) 200 g/l  $\text{H}_2\text{SO}_4$  + 70 g/l  $\text{CuSO}_4$  solution, deposition potential:  $-270$  mV,  $Q = -20$   $\text{C cm}^{-2}$ ; (B) 70 g/l  $\text{H}_2\text{SO}_4$  + 200 g/l  $\text{CuSO}_4$  + 10 ml/l carrier + 0.5 ml/l brightener + 0.4 ml/l leveller solution, deposition potential:  $-250$  mV,  $Q = -57$   $\text{C cm}^{-2}$ .

hand, no differences have been observed for the deposits on Ni or Cu seed layers.

When the stress study was performed with the  $\sin^2\psi$  technique, a correlation between the preferential orientation of the deposits and the stress state of the samples was observed. Copper deposits prepared over Ti/Ni seed bilayers from solutions without additives and low Cu(II) (70 g/l) showed a high compressive stress value (Fig. 7A), with an interface region characterised by a strong stress gradient (several hundreds MPa for lower  $\psi$ , i.e. high penetration depth). Both the existence of such a high stress gradient in the deposit, which is unfavourable for the adherence of the deposits on the substrate, and the presence of a significant compressive residual stress, are well known factors that can seriously compromise the viability of the Microsystems.

A significant reduction of the stress level in the layers has been achieved for the deposits obtained from the most concentrated bath (200 g/l Cu(II)) in presence of additives over the Ni seed layer (Fig. 7B). This low stress value, as well as the absence of significant stress gradients, is expected to improve the adherence of the deposits. Finally, similar measurements performed on the deposits

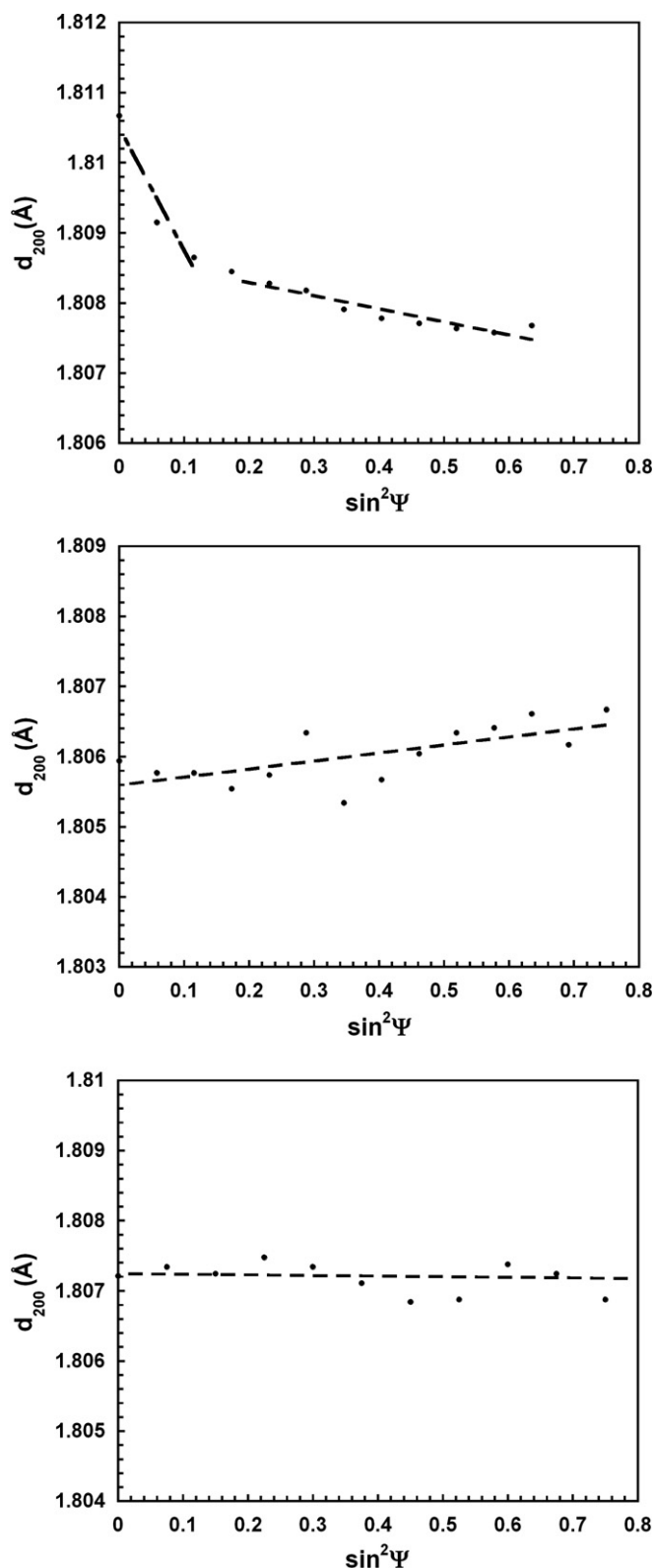


**Fig. 7.** Stress in the plane of copper deposits obtained at 60 rpm from the (200) reflections. (A) 200 g/l  $\text{H}_2\text{SO}_4$  + 70 g/l  $\text{CuSO}_4$  solution, deposition potential:  $-250$  mV,  $Q = -26$  C  $\text{cm}^{-2}$ , Si/Ti/Ni substrate, (B) 70 g/l  $\text{H}_2\text{SO}_4$  + 200 g/l  $\text{CuSO}_4$  + 10 ml/l carrier + 0.5 ml/l brightener + 0.4 ml/l leveller solution, deposition potential:  $-250$  mV,  $Q = -57$  C  $\text{cm}^{-2}$ , Si/Ti/Ni substrate. (C) 70 g/l  $\text{H}_2\text{SO}_4$  + 200 g/l  $\text{CuSO}_4$  + 10 ml/l carrier + 0.5 ml/l brightener + 0.4 ml/l leveller solution, deposition current density:  $-0.1$  A  $\text{cm}^{-2}$ ,  $Q = -50$  C  $\text{cm}^{-2}$ , Si/SiO<sub>2</sub>/Ti/Cu substrate.

made from the same bath, but over the Cu seed layer revealed the growth of almost stress-free Cu layers (Fig. 7C). This can be ex-

plained because the greater affinity between the deposit and the seed layer. In this analysis, no differences have been observed related to the presence of the SiO<sub>2</sub> layer below the Ti/seed bilayer in the substrates.

### 3.4. Cu test microstructures and coils

Thick copper microstructures were prepared by means of the additive process described in Section 2. Fig. 8 shows SEM images of a selected process area of test structures obtained after removal of the photoresist, for Cu deposits performed with different solution compositions. As can be seen in this figure, there is a significant improvement in the spatial resolution and the quality of the structures when layers grown under conditions leading to smaller surface roughness and grain size are used. As previously discussed, this corresponds to deposits performed with high Cu(II) concentrations in the presence of additives, which also allows the growth of non-preferential oriented deposits with a low stress level (Ti seed layer) or stress free (Cu seed layer).

For these bath compositions, the adherence of the microstructures on the substrate was tested after stripping the photoresist away with acetone and removing by selective chemical etching the Ti/seed bilayer. It has been found that the microstructures deposited on Ni seed layers exhibit a low adherence on the substrate after removing the Ti/seed bilayer. Conversely, excellent adherence of the microstructures was observed when a Cu seed layer was used, in correlation with the absence of stresses observed for copper deposits prepared from the optimised bath over Si/SiO<sub>2</sub>/Ti/Cu substrates.

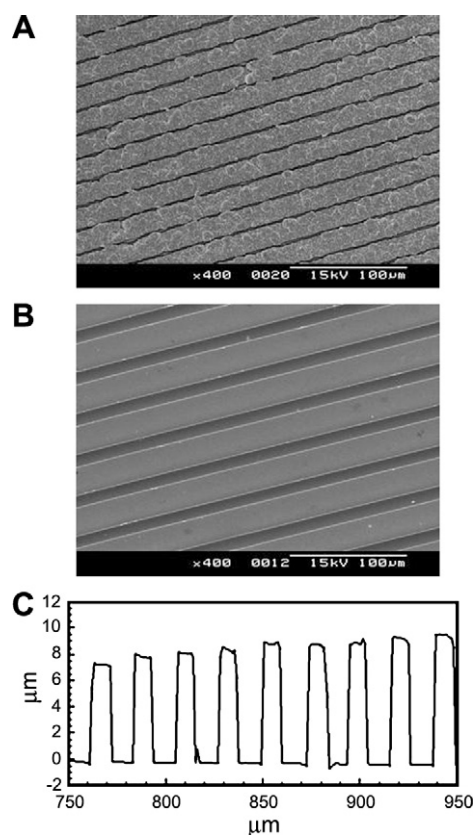


**Fig. 8.** SEM images from copper test structures after removal of the photoresist. (A) 200 g/l  $\text{H}_2\text{SO}_4$  + 70 g/l  $\text{CuSO}_4$ , deposition potential:  $-250$  mV,  $Q = -25$  C, Si/Ti/Ni, (B) 70 g/l  $\text{H}_2\text{SO}_4$  + 200 g/l  $\text{CuSO}_4$  + 10 ml/l carrier + 0.5 ml/l brightener + 0.4 ml/l leveller solution, deposition potential:  $-250$  mV,  $Q = -25$  C Si/Ti/Ni substrate. (C) Interferometry profile of the copper microstructures of part (B).

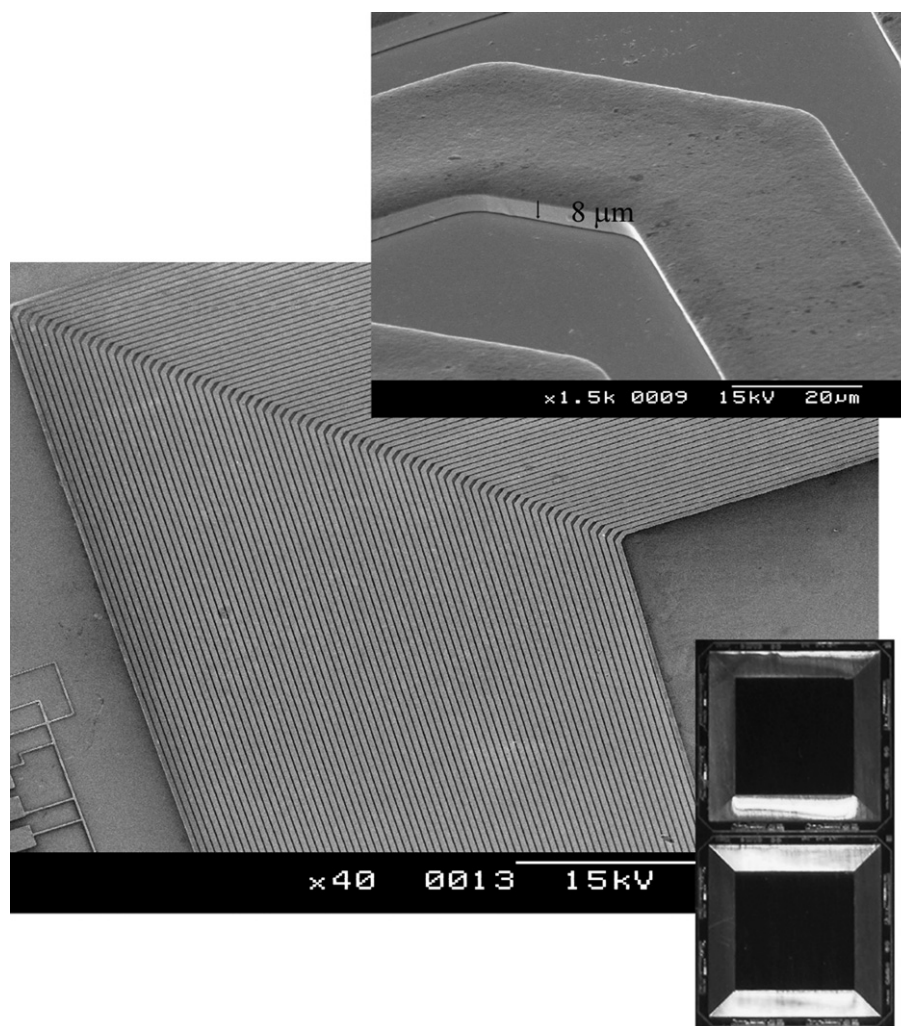


**Fig. 9.** SEM image of a region of an electrodeposited copper coil obtained on a Si/SiO<sub>2</sub>/Ti/Cu substrate after removal of the photoresist and selective etching of the Ti and seed layers between the Cu tracks. Deposition conditions: 70 g/l H<sub>2</sub>SO<sub>4</sub> + 200 g/l CuSO<sub>4</sub> + 10 ml/l carrier + 0.5 ml/l brightener + 0.4 ml/l leveller, intensity: –25 mA, Q = –25 C.

According to these results, micromachined Cu coils were fabricated using thick Cu electrodeposition with the optimised bath on Si/SiO<sub>2</sub>/Ti/Cu substrates. The use of a SiO<sub>2</sub> layer on the silicon substrate will allow the measurement of the electrical resistance of the coils, after removing the seed-layer. The adjustment of the deposition charge allows the control of the thickness of the tracks. These coils have been fabricated according to the design proposed in [15] for optimised inertial power microgenerators. This design corresponds to a square coil with a surface of about 1 cm<sup>2</sup> and a central nucleus of 8 × 8 mm<sup>2</sup>, where a permanent magnet is fixed onto a resonant membrane. Coils with different values of the track width ( $w$ , between 15 μm and 30 μm) and the separation between tracks ( $d$ , between 10 μm and 20 μm) have been fabricated. In these devices, the number of turns in the coil changes between 37 (for the design with the highest values of  $w$  and  $d$ ) and 90 (for the design with the lowest values of  $w$  and  $d$ ).

Fig. 9 shows a SEM image of a detail of a device corresponding to the coil with  $w = 30$  and  $d = 20$ , after removing both the resin mask and the Ti/seed bilayer. In all cases, we have observed a correct filling of the tracks and a good definition of the vertical walls that perfectly follow the photoresist mould. Good adherence on the substrate was also corroborated by means of the adhesion tape test.

The electrical characterisation of the coils fabricated with 15 μm thick Cu tracks gives values of the series resistance between 165 Ω

(coil with 37 turns) and 709 Ω (coil with 90 turns), that are in good agreement with those simulated by ASITIC [17] taking into account the specific resistance of copper and the design of the device. These values are one order of magnitude lower than those previously reported for coils fabricated with the same design with thin Al tracks, using standard Si technology processes [3]. These results open the possibility of using electrodeposition to prepare thick inductive coils with adequate electrical resistance. According to the preliminary characterisation of the microgenerators fabricated with these coils, the improvement in the series resistance of the devices leads to an increase of more than two orders of magnitude of the generated power.

#### 4. Conclusions

By means of electrodeposition processes, thick (several μm's) Cu layers suitable for the fabrication of enhanced microsystems have been prepared. The study performed permitted the optimisation of the electrodeposition conditions, including the composition of the bath and the seed layers. The gap between copper and HER processes is big enough to obtain copper deposits at high efficiency values, allowing controlling the thickness of the deposits as a function of the reduction charge. Electrolytic baths containing copper(II), sulphuric acid and several additives resulted adequate for

the preparation of thick copper deposits. For each selected bath, deposition potentials or current densities can be chosen from the electrochemical study.

Morphology, preferential orientation of crystalline planes and stress of the deposits were strongly dependent on the bath composition. When low Cu(II) and additives concentration were used, a preferential orientation of parallel planes of the surface was obtained, with coarse grained morphology and appreciable stress levels susceptible to compromise the viability of the microsystems. On the contrary, fine grained deposits of metallic shine were obtained from deposition baths containing high Cu(II) concentrations and appreciable amounts of additives. In these conditions, non-oriented deposits with very low residual stress were obtained, especially in the case of deposits performed over a Cu seed layer. An optimum adherence of the deposits on the substrate is also observed in these conditions. Then, the best electrodeposition conditions were obtained using 70 g/l H<sub>2</sub>SO<sub>4</sub> + 200 g/l CuSO<sub>4</sub> + 10 ml/l carrier + 0.5 ml/l brightener + 0.4 ml/l leveller solutions and moderate deposition potentials (around –250 mV) over Ti/Cu seed-layer.

Micromachined coils fabricated using the optimised electrodeposition conditions exhibit well-defined tracks, with a good definition of the walls that perfectly follow the photoresin moulds. The thickness of the tracks can be controlled by adjusting the deposition charge. The devices show electrical series resistance values that are significantly lower than those from planar Al coils fabricated using standard Si technology processes. This makes these devices adequate for the design and development of advanced inductive microsystems with improved performance.

#### Acknowledgements

EME is member of CEMIC (Centre of Microsystems Engineering) of the “Generalitat de Catalunya”. This paper was supported by a Consolider Project number CSD2006-12 from the *Ministerio de Edu-*

*cación y Ciencia* and by the contract MAT 2006-12913-C02-01 from the *Comisión Interministerial de Ciencia y Tecnología (CICYT)*. The authors wish to thank also the *Serveis Científicotècnics (Universitat de Barcelona)* and the *Centre Nacional de Microelectrònica* for the use of their equipment. Also thanks to J. A. Ortega for his help in baths design.

#### References

- [1] D. de Bahilís, C. Murray, M. Duffy, J. Alderman, G. Kelly, S.C.O. Mathuana, *Sensor Actuator* 81 (2000) 285.
- [2] P.D. Mitcheson, T.C. Green, E.M. Yeatman, A.S. Holmes, J. *Microelectromech. Syst.* 13 (2004) 429.
- [3] C. Serre, A. Pérez-Rodríguez, N. Fondevilla, J.R. Morante, J. Montserrat, J. Esteve, *Microsyst. Technol.* 13 (2007) 1655.
- [4] S. Baglio, A. Pérez-Rodríguez, S. Martínez, C. Serre, J.R. Morante, J. Esteve, J. Montserrat, *IEEE Trans. Instrum. Meas.* 56 (2007) 1590.
- [5] T. Osaka, *Electrochim. Acta* 42 (1997) 3015.
- [6] C.R. Neagu, J.G.E. Gardéniers, M. Elwenspoek, J.J. Kelly, *Electrochim. Acta* 42 (1997) 3367.
- [7] L.T. Romankiw, *Electrochim. Acta* 42 (1997) 2985.
- [8] M. Datta, D. Landolt, *Electrochim. Acta* 45 (2000) 2535.
- [9] H.J. Cho, C.H. Ahn, *J. Micromech. Syst.* 11 (2002) 78.
- [10] E. Gómez, E. Pellicer, M. Duch, J. Esteve, E. Vallés, *Electrochim. Acta* 51 (2006) 3214.
- [11] M. Duch, J. Esteve, E. Gómez, R. Pérez-Castillejos, E. Vallés, *J. Micromech. Microeng.* 12 (2002) 400.
- [12] M. Duch, J. Esteve, E. Gómez, R. Pérez-Castillejos, E. Vallés, *J. Electrochem. Soc.* 149 (2002) C201.
- [13] A.L. Coutrot, E. Dufour-Gergam, J.M. Quemper, E. Martincic, J.P. Gilles, J.P. Grandchamp, M. Matlosz, A. Sanchez, L. Darasse, *J. C. Ginefri, Sensor Actuat. A* 99 (2002) 49.
- [14] C. Serre, N. Yaakoubi, S. Martínez, A. Pérez-Rodríguez, J.R. Morante, J. Esteve, J. Montserrat, *Sensor Actuat. A* 123–124 (2005) 633.
- [15] C. Serre, A. Pérez-Rodríguez, N. Fondevilla, E. Martincic, S. Martínez, J.R. Morante, J. Montserrat, J. Esteve, *Microsyst. Technol.* 14 (2008) 653.
- [16] B.D. Cullity, *Elements of X-ray Diffraction*, second ed., Addison-Wesley Publishing Company Inc., 1978 (Chapter 3: Measurement of residual stress).
- [17] A.M. Niknejad, *Analysis, Design and Optimization of Spiral Inductors and Transformers for Si RF ICS*, College of Engineering, University of California, Berkeley, USA, 2000.

#### 4.2.2 Analysis of the texture and stress of the Cu deposits

In figure 4.5 a diffractogram of a Cu deposit prepared potentiostatically (-250 mV) over Si/SiO<sub>2</sub>/Ti/Cu substrate with a deposition charge of -57 C/cm<sup>2</sup> by using the previously optimized solution: 70 g/l H<sub>2</sub>SO<sub>4</sub> + 200 g/l CuSO<sub>4</sub> + 10 ml/l carrier + 0.5 ml/l brightener + 0.4 ml/l leveller and with a stirring of 60 rpm is shown. When comparing the intensity ratio of the different peaks in the diffractogram with the intensity ratio of a powder with an fcc structure, which is supposed to be random orientated, table 4.1, shows that the Cu deposits obtained had a certain preferred (111) orientation of the planes parallel to the surface.

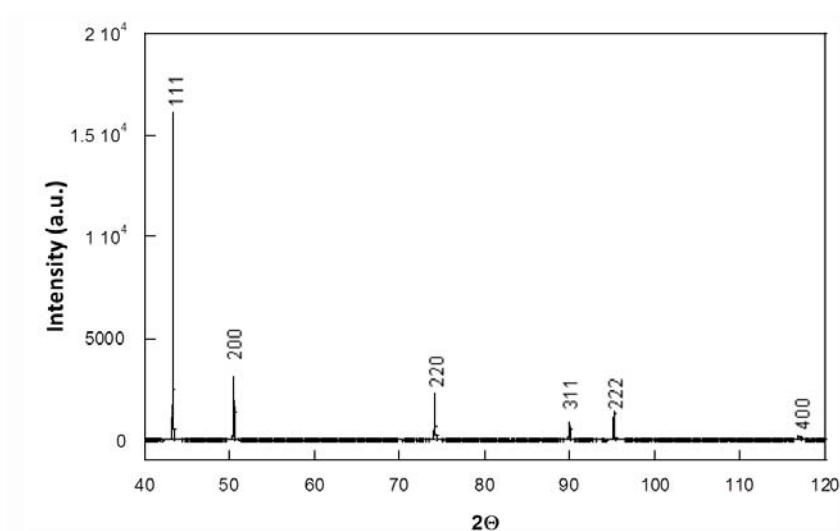


Figure 4.5:  $\theta$ - $2\theta$  diffractogram of a Cu deposit over Si/SiO<sub>2</sub>/Ti/Cu

In a cubic system directions  $[hkl]$  are always perpendicular to the planes  $(hkl)$  with the same Miller index, for that reason we will use both notations indistinctly. In some cases we will refer to a family of planes  $\{hkl\}$  or family of directions  $\langle hkl \rangle$  instead of a specific one because all of them are equivalent in a cubic system.

Table 4.1: Theoretical values of I and  $2\theta$  of an fcc Cu powder and experimental values for the Cu deposit obtained over Si/SiO<sub>2</sub>/Ti/Cu

hkl	$2\theta$ theoretical	I theoretical	$2\theta$ experimental	I experimental
111	43.30	100	43.35	100
200	50.43	46	50.49	23.5
220	74.13	20	74.16	13.1
311	89.93	17	89.97	5.2

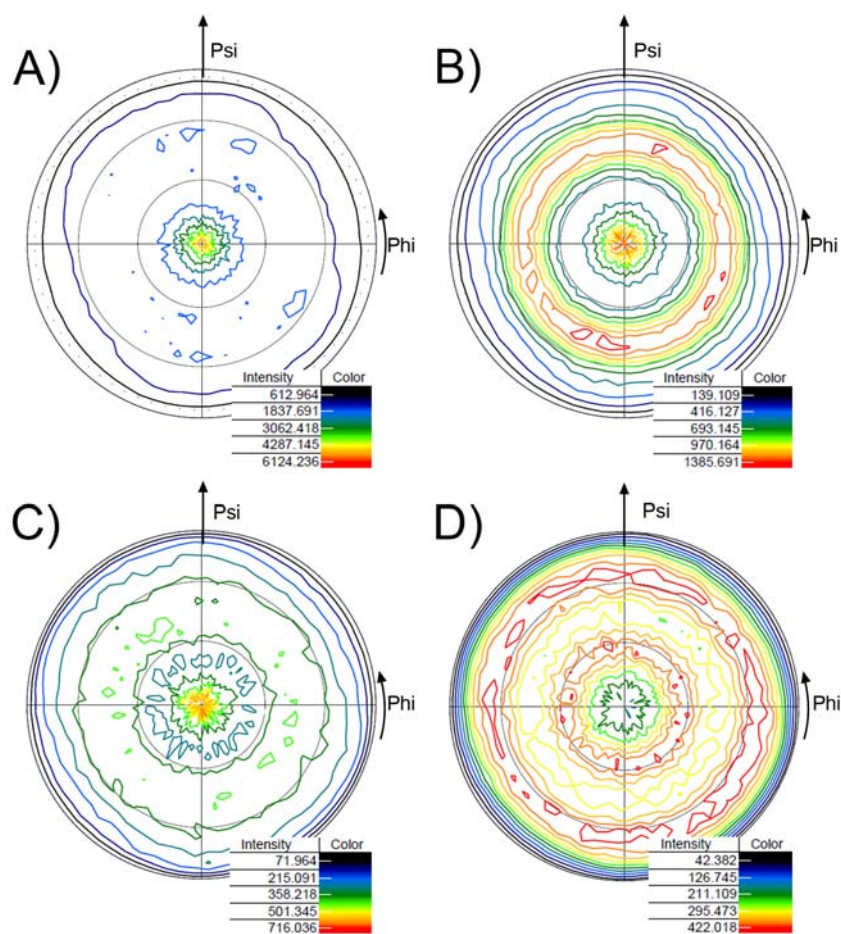


Figure 4.6: Pole figures of copper deposit over Si/SiO<sub>2</sub>/Ti/Cu. Orientations A) 111 B) 200 C) 220 D) 311 (Intensity in arbitrary units)

To study the texture of the deposits, pole figures were obtained. The pole figures consist of a double sweep of  $\psi$  (psi: 0-85°) and  $\varphi$  (phi: 0-360°)

angles fixing  $\theta$ , being  $\theta$  the angle at which the maximum intensity was recorded in the  $\theta/2\theta$  diffractogram for each orientation. Thus, we study the texture of the material, since the intensities of the diffraction pattern of each of the orientations from inside and outside of the plan were recorded and therefore we have information of how are the grains oriented in our material. In Figure 4.6, there are four pole figures with the  $\theta/2\theta$  fixed at the corresponding 111 (A), 200 (B), 220 (C) and 311 (D) reflections. The contour lines observed correspond to the same diffraction intensity values of the specific orientation analysed, which is determined by the  $\theta/2\theta$  fixed.

The poles are interpreted according to angle values in table 4.2 and they are represented in figure 4.7.

Table 4.2: Angles formed by planes in cubic configurations

$(h_1k_1l_1)$	$(h_2k_2l_2)$	Angles between $(h_1k_1l_1)$ and $(h_2k_2l_2)$ planes				
100	100	0.00	90.00			
	110	45.00	90.00			
	111	54.74				
	311	25.24	72.45			
110	110	0.00	60.00	90.00		
	111	35.26	90.00			
	311	31.48	63.76			
111	111	0.00	70.53			
	311	29.50	58.52	79.98		
311	311	0.00	35.10	50.48	62.96	84.78

Figure 4.6A shows that most of the intensity of the reflection 111 is located in the centre of the pole figure, indicating that most of the grains are oriented in the  $\{111\}$  and these are arranged parallel to the surface.

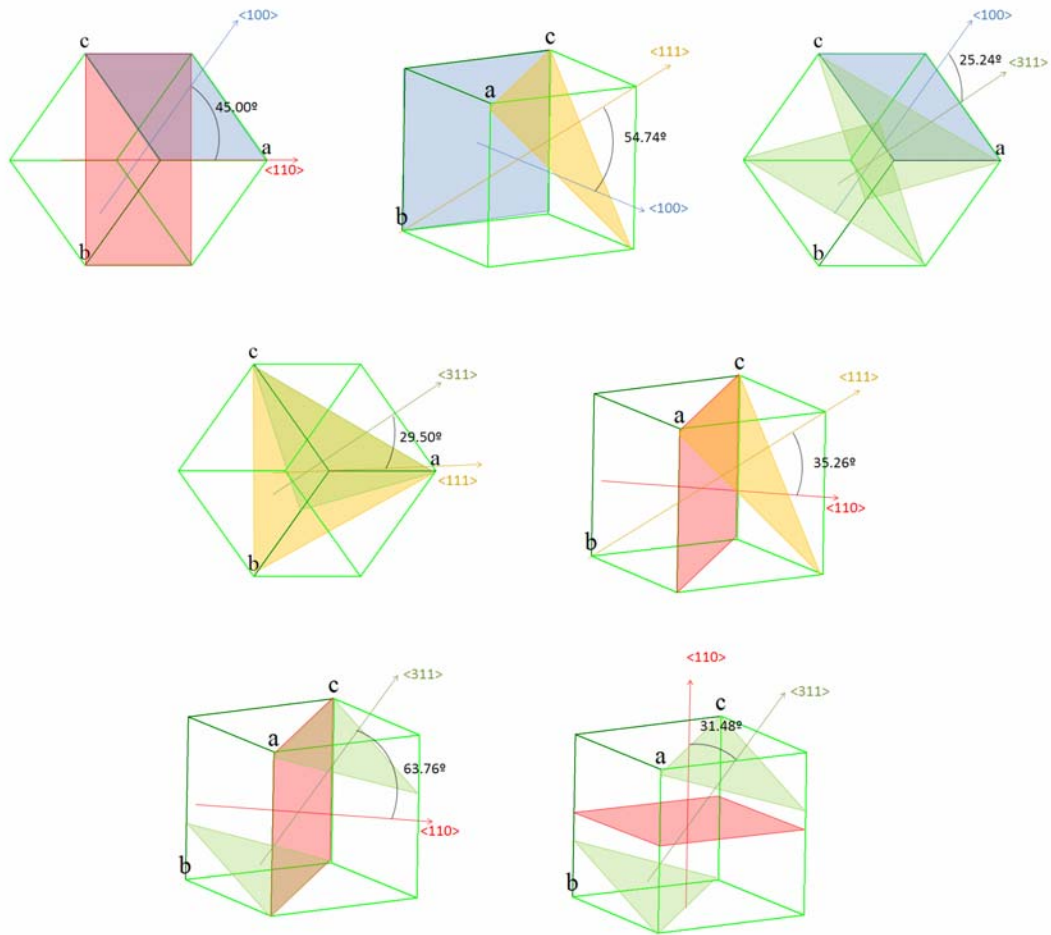


Figure 4.7: Psi ( $\psi$ ) angles between directions in a fcc structure

If the grain distribution was random (not textured) by tilting the sample in the psi angle the amount of grains parallel to the surface at that angle oriented  $\{111\}$  would be the same as in  $\psi=0^\circ$ , so no pole in the centre of the pole figure would be observed. In practice, even when no texture is observed, there is a certain intensity lost because of the angle but it appears as a smooth intensity decrease. In our case the decrease is too steep, so it is not just caused by the intensity dependence with angle (figure 4.8A). The presence of this kind of pole in the centre of the figure indicates a texture out of the plane of the material, because there is a different distribution

of the 111 orientated grains in the different plans analysed, as there is a different distribution of this orientation depending on the Psi angle ( $\psi$ ).

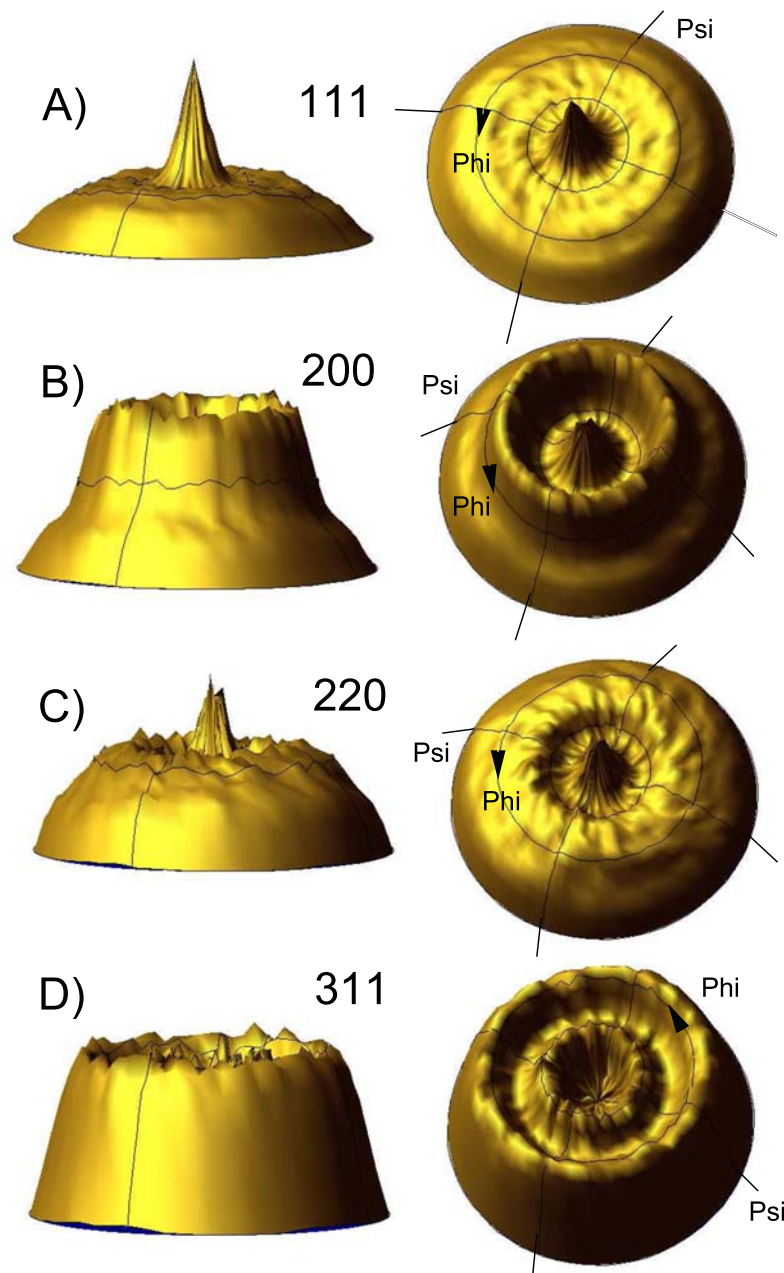


Figure 4.8: 3D Representation of the pole figures of copper deposit over Si/SiO<sub>2</sub>/Ti/Cu. Orientations A) 111 B) 200 C) 220 D) 311

In 4.6B, corresponding to the 200 reflection, certain intensity is observed in the centre of the pole figure, which means there is also a certain amount of grains 200 arranged parallel to the surface, although less than {111}

because the intensity in this case is lower (figure 4.8B). Finally, there are also small populations of grains parallel to the surface oriented  $\{220\}$  and  $\{311\}$ , as can be seen in figures 4.6C and 4.6D where poles in the centre of the figures are detected (figures 4.8C and 4.8D).

In figure 4.8, 3D representations of the pole figures are shown that may help to see the poles. As mentioned before, these results confirm a texture of the material out of plane.

Apart from being textured out of the plane, grains can be textured in the plane which means that there is a certain order of the grains with the same orientation in a plane instead of a random distribution. An example of these two possibilities is shown in figure 4.9.

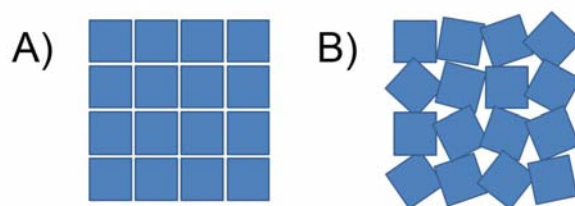


Figure 4.9: Schematic representation of A) textured and B) random orientated  $\{200\}$  grains

In order to study it, the rest of the pole figures were studied (at  $\psi \neq 0$ ). No texture in the plane is detected as the pole figures are isometric and no poles in the figures were observed. In the pole figure of 200 reflection, an increase in the intensity is detected at  $\psi$  ranging from  $45^\circ$  to  $52^\circ$  probably due to 200 reflections caused by grains parallel to the surface arranged  $\{220\}$  ( $\psi=45^\circ$ ) and  $\{111\}$  ( $\psi=54^\circ$ ). That is because in a cubic structure like this if the cub is oriented along the  $[200]$  direction and then tilted  $45^\circ$  then the cub appears oriented in the  $[220]$  direction and when it is tilted

54° the [111] direction is the new orientation. In the pole figure of the 220 reflection an increase in the intensity is detected at  $\psi$  ranging from 35° to 55° corresponding to 220 reflections caused by the grains {111} ( $\psi=35^\circ$ ) and {200} ( $\psi=45^\circ$ ). Finally, in the pole figure of the 311 reflection an increase in the intensity around 30°  $\psi$  is detected, that corresponds to 311 reflections due to the grains {111} ( $\psi 29^\circ$ ) and {220} ( $\psi 31^\circ$ ) parallel to the surface, these grains {220} parallel to the surface also cause an increase in the intensity in the pole figure at 64°  $\psi$ . The angle values between the different directions are in table 2 and their representations are shown in figure 4.9.

Therefore, from this information we can conclude that these copper deposits are textured out of the plane, with the majority of the grains oriented {111} and in a lower proportion grains oriented {200}, {220} and {311}. But they present a random orientation in the plane. In figure 4.10 a schematic representation of the grain distribution is shown.

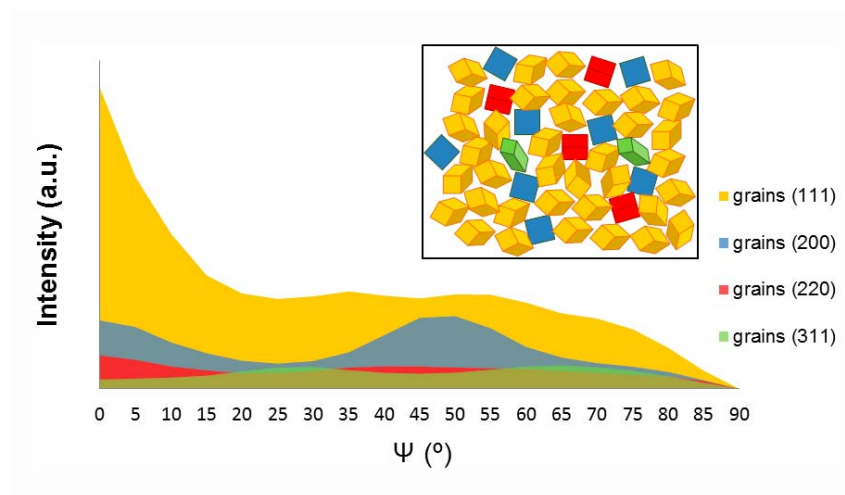


Figure 4.10: Grain distribution along the psi angle. In the inset there is a schematic representation of the grain distribution in plane ( $\psi=0^\circ$ )

The residual stress ( $\sigma$ ) of the deposits was determined by applying the  $\sin^2 \psi$  method. The theory of isotropic elasticity applied here to calculate the stress considers that  $d$  (interplanar spacing) should be linear with  $\sin^2 \psi$  for any  $\varphi$  or  $\psi$ . That is not true in the case of textured materials as in some of our copper deposits, where the elastic constants connecting the measured interplanar spacings (or strains) to the stress will vary with a particular set of planes. For that reason the stress in the copper deposits was performed in the different directions observed in the diffractogram, but the [200] direction was chosen to compare the deposits grown over the different substrates. This direction was selected because it has been reported by Dölle et al. that h00 and hhh reflections are not affected by texture in fcc materials [62]. However, nonlinearity of  $d$  versus  $\sin^2 \psi$  was observed and attributed to reasons that can give additional oscillations such as: Local variations in microstresses, shear stresses and stress gradients. In some cases the first electrodeposited layers present an epitaxial growth where the electrodeposited metal follows a similar structure to that of the underlying substrate. During subsequent growth, the metal growth progressively adopts its own structure with its own cell parameters, leading to a stress gradient within the deposit. To detect this stress it may help to take into account the depth penetration of the X-ray when analysing the results of the stress to know when the effect of the interface is no longer seen. In equation 4.3 it can be seen it is related to the angles  $\theta$  and  $\psi$ :

$$\text{Penetrationdepth} \propto \sin \theta \cos \psi \quad (4.3)$$

The estimated value for Cu at  $\theta=90^\circ$  and  $\psi=0^\circ$  is of  $24.53 \mu\text{m}$  with a

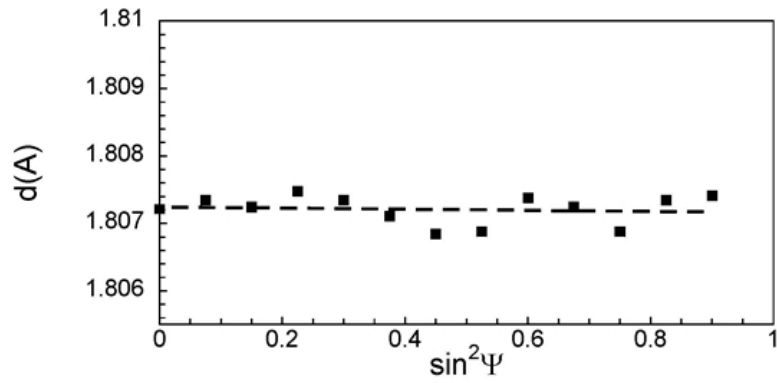


Figure 4.11: Interplanar spacing and stress in the plane value of Cu deposits obtained over Si/SiO<sub>2</sub>/Ti/Cu for [200] direction

90% of absorption. The copper deposits analysed here have a thickness of around 15  $\mu\text{m}$ , that penetration for the 200 reflection is the achieved for angle  $\psi$  values of 35°-40° ( $\sin^2 \psi=0.3-0.4$ ). As no drastic behaviour change is observed around these, stress gradients caused by the interface could be discarded.

In general, the influence of all these effects (including texture) may be present at the same time when measuring the stress, but usually only one is the dominant. As the effect of texture is avoided in the [200] direction and oscillations caused by the other effects are generally small, the classic method ( $\sin^2 \psi$ ) could be used to evaluate the stress. For other orientations it was corroborated that the effect of the texture produces bigger deviations from linearity. Cu deposits over Si/SiO<sub>2</sub>/Ti/Cu show very little stress as can be seen in figure 4.11.



### 4.2.3 Implementation of the deposition conditions over plastic substrates

The aim of this part of the work was the use of sensors consisting of flat inductive coils for the detection of biomolecules coupled to magnetic markers. It had been proposed that to mount these devices it might be interesting to have a flexible, economical and disposable substrate. The previous results were a starting point for preparing copper coils using plastics as substrates. The electrodeposition of adherent copper coils over the plastics is not possible unless a seed layer is added over them.

As the assembly of the biosensor does not require special properties from the plastics, the criteria used for choosing them as substrates to perform the study of copper growth was that they were commercialised in thin films with a maximum thickness of 150  $\mu\text{m}$ .

Different plastics modified with a seed layer to make them conductive were tested:

- PEEK: Polyether ether ketone
- PEN: Polyethylene Naphthalate
- PMMA: Poly(methyl methacrylate)
- PS: Polystyrene
- Teflon: Polytetrafluoroethylene (PTFE)
- Kapton: Polyimide film

A Ti (10 nm)/Cu (100 nm) seed layer was evaporated directly onto the plastic in the cases of: PEEK, PEN, PMMA, PS and Teflon. These modifi-

cations of the plastics were performed in the *Plataforma de Nanotecnologia del Parc Cientfic de Barcelona*.

In the case of Kapton, a RIE (Reactive ion etching) was applied previous to seed layer evaporation in order to roughen the Kapton and favour the adherence of the evaporated layer. Different RIE treatments were tested (Table 4.3).

Table 4.3: RIE performed over Kapton to increase roughness

Sample n°	Gas	Flow (sccm*)	Pressure (mT**)	RF Power (W)	Time (min)	Ti (nm)	Cu (nm)
1	O <sub>2</sub>	50	100	150	8	10	100
2	O <sub>2</sub>	50	100	250	8	10	100
3	O <sub>2</sub>	50	150	400	10	10	10
4	O <sub>2</sub>	50	200	400	15	10	50
5	O <sub>2</sub>	50	100	450	15	10	50
6	Ar	30	100	100	2	10	50
7	CHF <sub>3</sub>	50	100	100	5	10	50
8	O <sub>2</sub>	50	100	100	8	10	50
9	O <sub>2</sub>	50	200	400	5	10	100
10	O <sub>2</sub>	25	100	250	8	10	100

\*Sccm: Standard Cubic Centimeters per Minute

\*\*mT: milliTorr

Although it was possible to obtain a seed layer evaporated on the treated Kapton, the treatment was not effective enough to achieve satisfactory results: as once the electrochemical deposit of copper was formed, the whole seed layer/electrodeposited Cu was detached very easily from the Kapton substrate. That indicates that the adherence of the seed layer to the substrate was not good enough after applying any of the different RIE

treatments tested over the Kapton. For this reason Kapton was discarded.

For the other plastic substrates used, the adhesion of the seed layer proved to be good enough to prepare permanent electrodeposits of Cu over them. From the selected bath, deposits of 6-9  $\mu\text{m}$  thick were prepared over the plastic/Ti/Cu seed layer substrates. In all cases, a fixed density current ( $-83 \text{ mA/cm}^2$ ) was applied maintaining a stirring of 60 rpm of the bath containing: 70 g/l  $\text{H}_2\text{SO}_4$  + 200 g/l  $\text{CuSO}_4$  + 10 ml/l carrier + 0.5 ml/l brightener + 0.4 ml/l leveller. The morphology, structure and stress of these deposits were analysed.

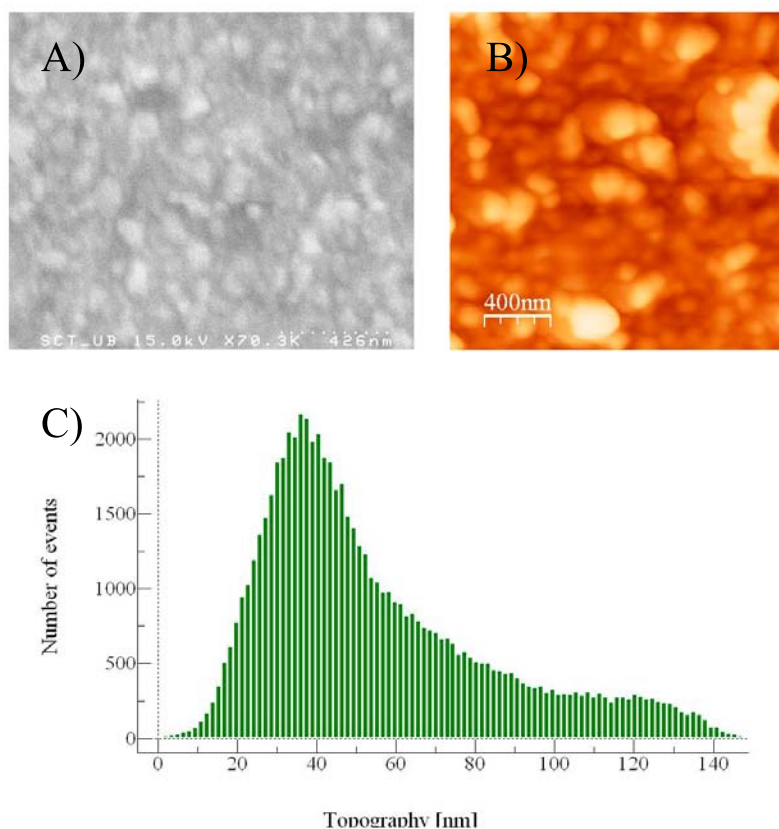


Figure 4.12: Images of A) FESEM and B) and C) distribution of roughness of a  $10 \times 10 \mu\text{M}$  Cu deposit obtained on PMMA/Ti/Cu

The copper deposits obtained were smooth and uniform. In all the cases

FESEM and AFM observation showed a nodular morphology and confirms nanometric size of the grains (Figure 4.12).

Only the deposits obtained over Teflon showed cracks and little uniformity (Figure 4.13), making this plastic unsuitable to manufacture the coils.

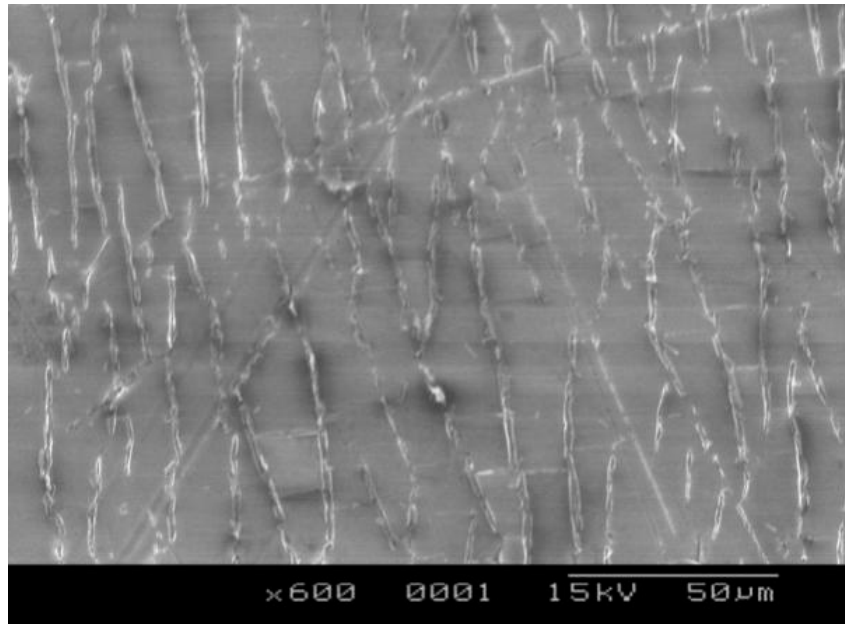


Figure 4.13: SEM image of a copper deposit obtained on Teflon/Ti/Cu

After ageing of the deposits, it was observed that for PS the seed layer/electrodeposited Cu detached from the substrate. The characteristics of deposits obtained over PEEK, PEN, PMMA made them suitable to use them as substrates for preparing the coils.

From the interplanar spacings the stress ( $\sigma$ ) of the deposits was calculated by applying the  $\sin^2 \psi$  method in order to assure the lifetime of the coils. The [200] direction was chosen to study the stress selected because it is not affected by texture in fcc materials [62]. Considerable stress

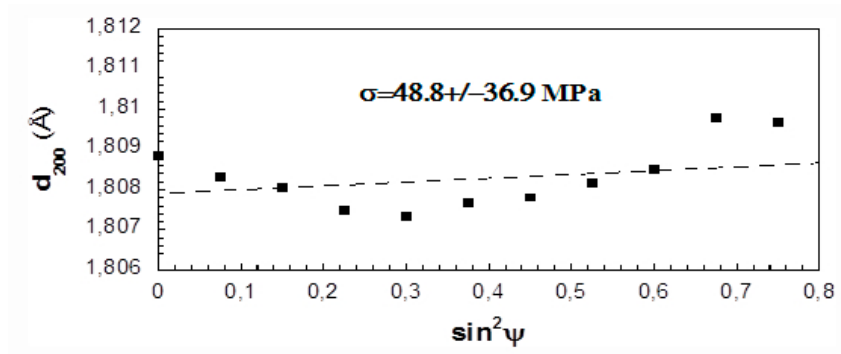


Figure 4.14: Interplanar spacings at various  $\sin^2 \Psi$  for [200] direction of a copper deposit over PEN/Ti/Cu substrate

was found in the Cu deposits over PMMA and PEEK films, determined from the shift and broadening of the diffraction peaks in X-ray diffraction analysis, although the adherence of these deposits over the substrate was confirmed as good. These results indicate that PMMA and PEEK were not optimal substrates for the preparation of Cu coils. On the other hand, in deposits grown over PEN, good adherence and very little tensile stress was observed for the [200] direction. Figure 4.14 shows the interplanar spacings at various tilts of  $\psi$ , represented as  $\sin^2 \psi$ , for the [200] direction of a copper deposit over PEN;

The low stress presented for the Cu deposit obtained over PEN presented it as the best candidate for testing the preparation of coils over a plastic substrate.

Once the optimal plastic substrate was selected, a photolithography of the test square coils was performed on top of the PEN/seed layer substrate in the *Plataforma de Nanotecnologia del Parc Científic de Barcelona*. Cooper electrochemical deposition of the coils was performed using the previous electrodeposition conditions. In Figure 4.15 an image of some coils

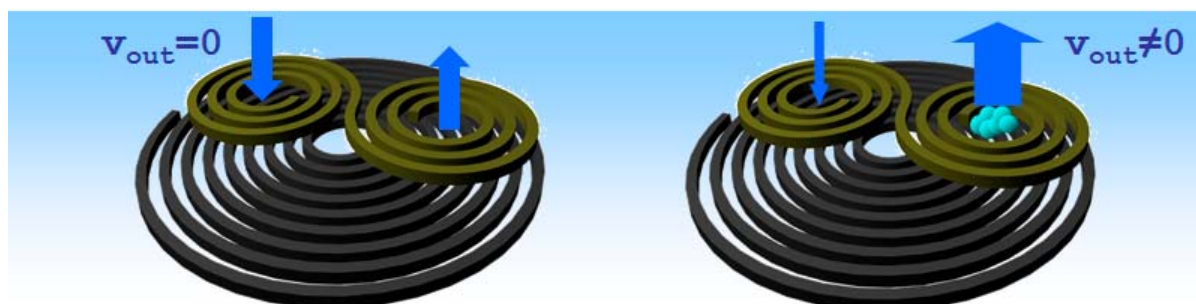
(12  $\mu\text{m}$  thick) obtained over PEN is shown.



Figure 4.15: Image of copper coils obtained over PEN/seed layer substrate

The results obtained demonstrate the possibility of obtaining copper coils over plastic substrates. For PEN, the pieces used for the electrodeposition of the coils had to be small, limiting to a maximum of four coils because of the problems presented by the photolitho: As the plastic did not present a surface sufficiently homogeneous, the heterogeneity is transferred to the photolithography and it presented problems in the revealing process. Once the photolithography process is improved over these kinds of substrates, it opened prospects for implementation of this substrate in future designs of devices for applications in biosensors or inductors where electrodeposited Cu was the conductive element.

#### 4.2.4 Design and electrochemical preparation of inductive copper coils for magnetic particles detection





## Design and electrochemical preparation of inductive copper coils for magnetic particles detection

M. Cortés<sup>a,\*</sup>, S. Martínez<sup>c</sup>, C. Serre<sup>b</sup>, E. Gómez<sup>a</sup>, A. Pérez-Rodríguez<sup>b</sup>, E. Vallés<sup>a</sup>

<sup>a</sup> *Electrodep, Departament de Química Física and Institut de Nanociència i Nanotecnologia (IN<sup>2</sup>UB), Universitat de Barcelona, Martí i Franquès, 1, 08028 Barcelona, Spain*

<sup>b</sup> *EME/CERMAE, Departament d'Electrònica and Institut de Nanociència i Nanotecnologia (IN<sup>2</sup>UB), Universitat de Barcelona, Martí i Franquès, 1, 08028 Barcelona, Spain*

<sup>c</sup> *Institut de Microelectrònica de Barcelona (IMB-CNM), CSIC, Campus Universitat Autònoma de Barcelona, 08193 Barcelona, Spain*

### ARTICLE INFO

#### Article history:

Received 4 October 2011

Received in revised form 3 July 2012

Accepted 23 July 2012

Available online 28 July 2012

#### Keywords:

RLC circuit

Coil devices

Electrodeposition

Inductive sensors

### ABSTRACT

New devices based on inductive planar coils have been designed in a manner that they can be used for the detection of magnetic particles in biodetection applications from the changes induced in coil inductance mounted in simple resonance differential filter circuit configurations. By simulating the conditions needed to achieve minimum electrical resistance and maximum sensibility, the planar coil design has been developed. The number of tracks and aspect ratio has been optimized for different theoretical track thicknesses. Using the optimized mask, electrodeposition was used to prepare coils of around 15- $\mu\text{m}$  thick, with good edge definition and low electrical resistance, matching with the optimum simulated values. The resonant frequency of the fabricated coils measured using an impedance analyzer is identical for each coil type. Preliminary tests of the sensing ability of the coils were performed, revealing a change in the resonant frequency when a magnetic powder is present over the coil.

© 2012 Elsevier B.V. All rights reserved.

### 1. Introduction

Immunomagnetic biosensors based on the use of superparamagnetic particles (MPs) as the biological markers have received a strong interest for the detection and quantification of biological substances [1–3]. This interest is motivated by their potential for the development of systems with very high sensitivity, low cost and high specificity. Among the different sensor strategies, different groups have proposed the use of inductive based devices, where sensing is determined by the effects of changes in the inductance of a coil due to the presence of the MPs in the sample under analysis [1,4–6]. In relation to other magnetic immunoassays, these biosensors are characterized by their very high simplicity, since in this case the application of permanent magnetic fields is not necessary for the sensor operation. This simplifies the design of the device and its integration in the whole system. The integration of inductive devices in Si technology has several potential advantages as compared to macroscopic solenoids. These include features related to the fabrication cost, yield, and reproducibility of the planar inductive devices. In addition, the miniaturization of the device dimensions will lead to a significant decrease of the volume of the sample under analysis, with a consequent expected decrease in the cost of the reagents per analysis. This also opens interesting

perspectives for the development of more complex systems such as sensor matrices for simultaneous detection of multiple species.

However, in all these cases, it clearly appears that the high value of series resistance, inherent to the planar technology of the microsystems, results in low quality factor values. This severely hinders the devices performance by introducing a strong attenuation of the signal at resonance. Therefore, the full exploitation of the potential capabilities of these systems is strongly conditioned to the development of reliable techniques for growing metal layers with thicknesses well above those available with standard Si technology. This resistance can be decreased by increasing the tracks cross section. However, increasing the tracks lateral dimensions would reduce the coils track density, hence presumably the device sensitivity. Therefore, for a given track density, we need to increase the track thickness. For this, the selective growth of thick Cu metal tracks by electrochemical deposition (EC) has been implemented [7] in order to substitute the Al of the standard planar technology used in previous works. These techniques are fully compatible with Si Microsystem Technologies, being possible to perform the deposition through resist masks. This allows post processing of standard CMOS (Complementary Metal Oxide Semiconductor) processed wafers. Accordingly, EC deposition of Cu has already been proposed for the development of various advanced inductive devices and microsystems [8,9]. Cu has been selected because it is well suited for microsystem applications in Si technology, due to its low resistivity, low cost and ease to grow electrochemically in a well-controlled way. Optimization of the electrolytic bath and of the electrodeposition conditions has been performed in a previous work in order to

\* Corresponding author. Tel.: +34 93 403 92 41; fax: +34 93 402 12 31.

E-mail address: [m.cortes@ub.edu](mailto:m.cortes@ub.edu) (M. Cortés).

obtain well-defined copper coils compatible with their integration in advanced microsystems such as inertial power microgenerators [10].

In this framework, this paper describes the design, fabrication and electrical characterization of enhanced micro inductive devices in relation to biosensing applications. The viability of thick EC deposited Cu coils for use as biosensors in a configuration of differential second order filter circuit topologies working at conditions close to resonance [11,12] is analyzed. In previous studies [13] the analysis of conventionally fabricated prototypes of integrated planar Al microcoils has allowed to demonstrate the ability of these very simple circuits for the detection of the inductive changes from the presence of magnetic particles on the coils surface, in spite of their high intrinsic series resistance. In contrast to this earlier study, the present work includes an electrical improvement of the microcoils, obtained by the use of an EC deposition process, for the fabrication of thick Cu tracks within the CMOS process chain. When using copper instead of aluminum the conductivity of the coils was enhanced and then the intrinsic series resistance that hinders these kinds of devices is decreased. For characterization, the fabricated microcoils are incorporated into passive RLC filters made with discrete elements on a Printed Circuit Board (PCB). A first basic electrical characterization allows the validation of the technology, and preliminary tests as sensing devices are presented and discussed.

## 2. Simulations and design

The sensing principle of the inductive biosensors is based on the effects of changes in a coil inductance due to the presence of magnetic particles (MPs) in the active region of the device. In order to detect these inductance variations, the adopted signal conditioning circuit is made of two identical high-pass second-order RLC resonant filters connected in parallel in a differential configuration, as described in [13].

The circuit includes two identical coils, one of which is a reference passive inductance and the other is the sensor inductance. The resistors are the intrinsic coils series resistance, while the capacitors are external discrete components. Each branch of the filter has a quality factor  $Q = (\omega_0 L / R)$ , where  $\omega_0$  is the harmonic frequency  $= (1/LC)^{1/2}$ . Depending on the parameters of the circuit, the transfer function has a resonant peak at a frequency  $f_p$  given by:

$$f_p = \frac{f_0}{\sqrt{2}} \left( 1 + \sqrt{1 + \frac{1}{2} \left( \frac{R}{f_0 \pi L} \right)^2} \right)^{1/2} \quad (1)$$

where  $f_0 = \omega_0 / 2\pi$  is the natural frequency of the circuit without taking into account the intrinsic series resistance  $R$  of the coil.

When both branches of the circuit have the same values of resistance, capacitance, and inductance, the corresponding transfer functions will be identical, which will result in a null differential output. Any change in the inductance value of the sensing coil will cause a change in the transfer function of the corresponding branch, resulting in an unbalanced differential output voltage. The sensitivity of the circuit is determined by the magnitude of the derivative of the transfer function with respect to the inductance, i.e.  $d|H(f)|/dL$  [12]. Accordingly, the highest circuit sensitivity and linearity are achieved by working close to the resonant frequency  $f_p$ . It should be noticed that there is a strong dependence of the shape and position of the resonant peak on the electrical parameters of the circuit. Decreasing the capacitance and resistance enables a higher quality factor, thus leading to a narrower and more intense resonance peak. However, this also implies an increase in  $f_p$ , which can become relatively high with the typical values for planar micro-coils, and can be a potential drawback of this circuit design. For this, the selective

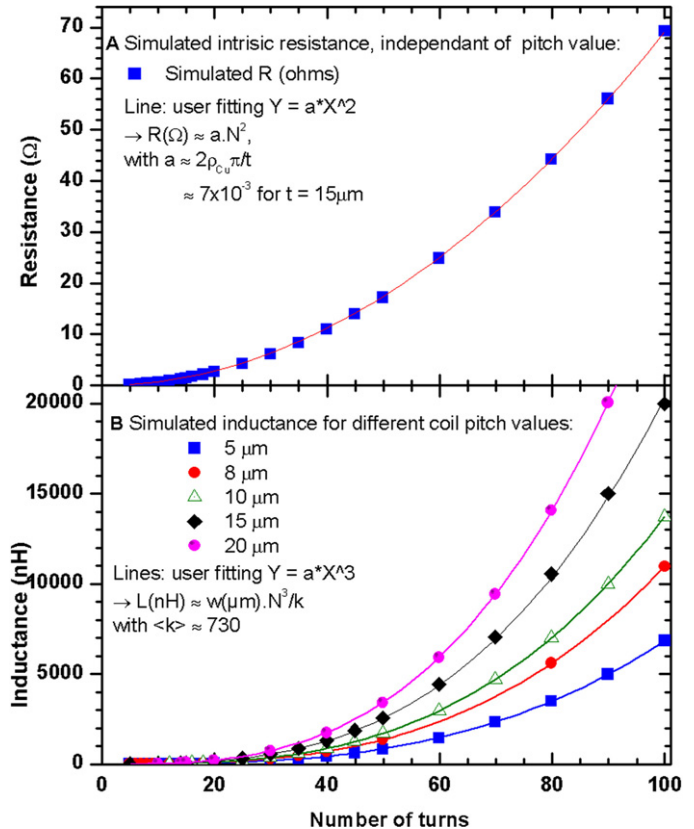


**Fig. 1.** The dependence of coil resistance and inductance on the number of turns and dimensions was simulated: the coil inductance was found to increase with the coil dimensions, whereas the coil resistance remained constant. Increasing the number of turns was found to increase both the coil inductance and resistance. A zoom of the dependence of the coil inductance on the number of turns and dimensions is shown in the inset.

growth of thick Cu metal tracks by electrochemical deposition has been implemented [14] in order to substitute the Al of the standard planar technology.

The resistance values of Al coils are about 16 times higher than the ones calculated for copper coils due to the difference of its resistivity and thickness. In both cases, circular spiral coils with a regular track pitch (width ( $w$ ) = separation ( $s$ )) have been assumed to perform the computations. In these conditions, a simple geometric calculation based on a concentric rings starting from the middle of the coil has been used to calculate the spiral coils series resistance, leading to:

$$R_{\text{coil}} \approx 2\pi \left( \frac{\rho}{t} \right) N^2, \quad (2)$$

where  $N$  is the number of rings,  $\rho$  is the metal resistivity and  $t$  is the track thickness. This gives a good approximation provided that  $N^2 \gg 1$  (Fig. 1a).

Some formulas for calculating planar coils inductance can be found in the literature [16–18]. Although they do not always coincide in exact value, they show a 3rd degree dependency with respect to the number of turns. This  $N^3$  dependency has been corroborated by fitting ASITIC [19] simulated results as shown in Fig. 1b. Since the quality factor  $Q$  varies as  $R^{-1} \times L^{1/2}$ , this means that  $Q$  is proportional to the inverse of the square root of the number of turns  $N^{-1/2}$ . In other words, the effect of increasing the number of turns of a coil is to decrease its quality factor in all cases. Fig. 2 shows the  $Q$  and  $f_p$  simulated for a planar copper coil with 15 μm thick tracks and a width and separation of 10 μm considering external capacitors of 10 and 100 pF. This capacitance range

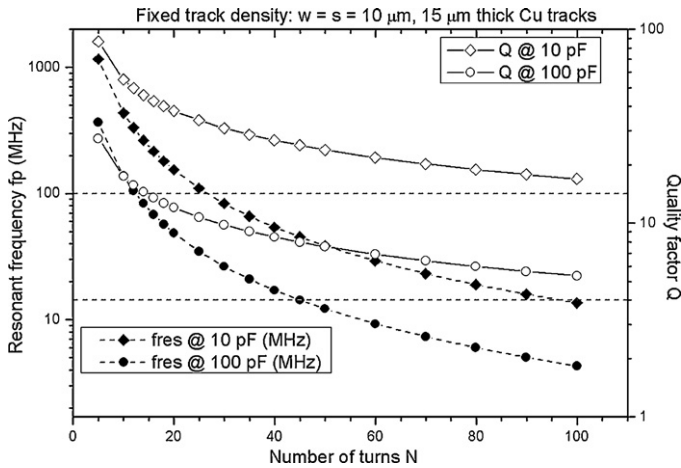


Fig. 2. Simulation of the quality factor ( $Q$ ) and resonant frequency ( $f_p$ ) versus the number of tracks ( $N$ ) of a Cu coil of  $15 \mu\text{m}$ -thickness and  $w = s = 10 \mu\text{m}$ ; external capacitances of 10 or 100 pF were applied.

was chosen because typical parasitic capacitances are usually of the order of a few pF, so it would be difficult to apply external capacitance lower than about 10 pF, which would also imply resonant frequency far too high for practical applications such as those targeted in this work. As for the higher chosen limit, the simulations indicate that by applying values higher than 100 pF, the attenuation and broadening of the resonant frequency peak would be unsuitable for high sensitivity detection applications. The  $15 \mu\text{m}$  pitch coils was selected to perform the measurements because it is the smallest coil that maintains the aspect ratio  $\leq 1$ .

Additionally, in Ref. [20], various planar coils were tested and it was shown that only planar coils with a  $Q$  factor equal or higher than 3.6 were able to detect MPs, although not to quantify them.

Table 1

Values of  $N$  (number of tracks) for the different coil designs.

	$w = s = 5$	$w = s = 8$	$w = s = 10$	$w = s = 15$	$w = s = 20$
$C = 10 \text{ pF}$	35–100	30–100	27–100	25–100	20–100
$C = 100 \text{ pF}$	20–90	15–100	12–100	10–100	10–100

Therefore, according to the above considerations, the design of the coils in the present work was made in order to keep  $Q \geq 4$  and  $f_p < 100 \text{ MHz}$ . In order to reach the best compromise between high inductance values, high quality factors, and relatively low working frequencies, extensive ASITIC simulations have been carried out, considering circular spiral coils with  $15 \mu\text{m}$  thick Cu tracks, and a regular track pitch (width = separation) from 8 to  $20 \mu\text{m}$ . These design constraints are summarized in Fig. 2. This leads to different values of  $N$  for the different coil designs as shown in Table 1.

3. Fabrication

The micromachined coils have been fabricated by combining standard microsystems technology processes, with electroplating post-processes for the fabrication of coils with thick Cu metal tracks by electrochemical (EC) deposition. The mask set designed for this fabrication process has three levels: the first level corresponds to the aluminum track for the center contact with the coil. The second level is the insulator layer that is necessary to avoid short circuit of the coil tracks, it is a  $400 \text{ nm}$  of  $\text{SiO}_2$  grown by plasma-enhanced chemical vapor deposition. Windows are opened through this insulator layer with HF to enable electrical contact to be made between the Cu coil and the aluminum tracks. The third level corresponds to the thick photoresist lithography to be used as a mold for the Cu electrodeposition step. Each chip of the mask contains two pairs of coils of different dimensions. The mask includes a guard ring around each coil, and test pads for measurements calibration. The

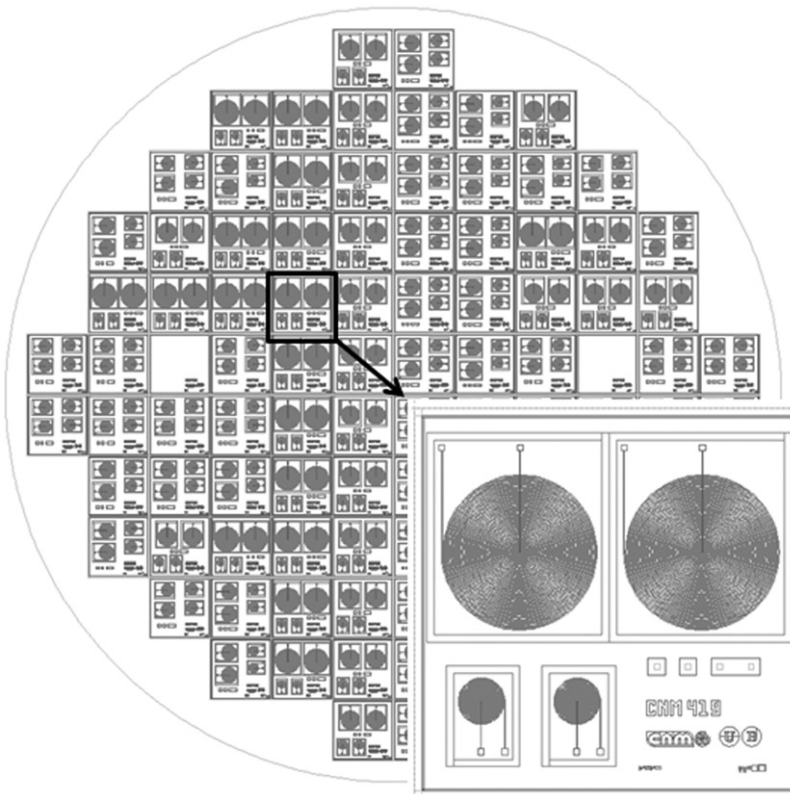
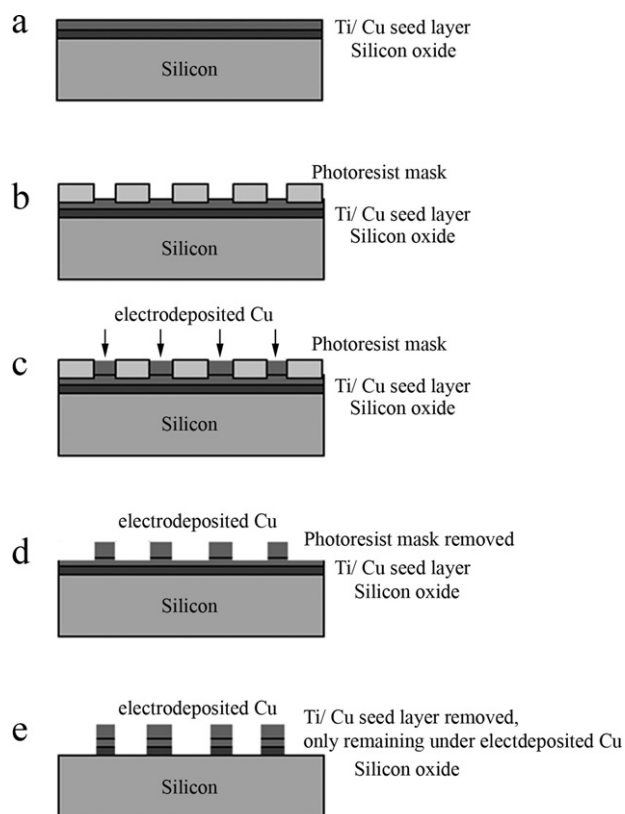


Fig. 3. Three levels photoresist lithography mask showing the five different chips designs with varying coil dimensions (two coils each).



**Fig. 4.** Schematic representation of the five process steps used to obtain the coils: seed layer deposition, photoresist lithography, copper electrodeposition, photoresist removal and seed layer removal.

dimensions of the coils were chosen according to the simulation results previously mentioned. An illustration of the mask is shown in Fig. 3. Fig. 4 shows a schematic representation of the process used to obtain these microstructures.

The key step in this fabrication process is the electrochemical deposition of a thick Cu layer for the coil tracks (Fig. 4c). For this, working electrodes were prepared photolithographically on 100 mm diameter (001) silicon wafers coated with a 1  $\mu\text{m}$  thick  $\text{SiO}_2$  layer and a top Ti (10 nm)/Cu (100 nm) seed layer (Fig. 4a). The photoresist used was AZ4562. The  $\text{SiO}_2$  layer is required to provide an insulating substrate to avoid short circuit of the coil tracks. Ti is added to improve the adherence of the EC grown layer and copper seed layer was used to induce minimum stress in the electrodeposited copper [10]. The seed Ti/Cu layer was deposited by sputtering.

The copper coils were prepared by electrodeposition in a rectangular three-electrode cell using a microcomputer-controlled potentiostat/galvanostat Autolab with PGSTAT30 equipment, GPES software and a booster BSTR10A connected to the equipment. A 70 g/l  $\text{H}_2\text{SO}_4$  + 200 g/l  $\text{CuSO}_4$  + 70 mg/l NaCl + 10 ml/l carrier + 0.5 ml/l brightener + 0.4 ml/l leveler solution was used as the electrolyte.  $\text{CuSO}_4 \cdot 5\text{H}_2\text{O}$ ,  $\text{H}_2\text{SO}_4$  and NaCl reagents were of analytical grade. Carrier (polyethylene glycol of high molecular weight, XD7397), brightener (bis-(3-sulfopropyl)-disulfidesodium salt, XD7398) and leveler (polymerized tiazine, XD7399) were from MacDermid Company. All solutions were prepared with water, which was first doubly distilled and then treated with a Millipore Milli Q system. The temperature was maintained at 25  $^\circ\text{C}$ .

The reference electrode was an Ag/AgCl/(1 mol  $\text{dm}^{-3}$ ) NaCl electrode mounted in a Luggin capillary containing 0.5 mol  $\text{dm}^{-3}$   $\text{Na}_2\text{SO}_4$  solution. All potentials are referred to this electrode. The counter electrode was a copper-phosphorous one. Electrodeposition was performed galvanostatically maintaining a moderate stirring of the solution. The deposition time was adjusted to attain Cu coils of 15  $\mu\text{m}$  of thickness, limited by the thickness of the photoresist mold.

Well adhered, stress free copper was grown over Si/ $\text{SiO}_2$ /Ti/Cu. At the beginning of the deposition process more negative values of potential were recorded as a consequence of the nucleation of the metal (nucleation spike). At longer deposition times, some stabilization of the potential occurs, due to the growth of the deposit

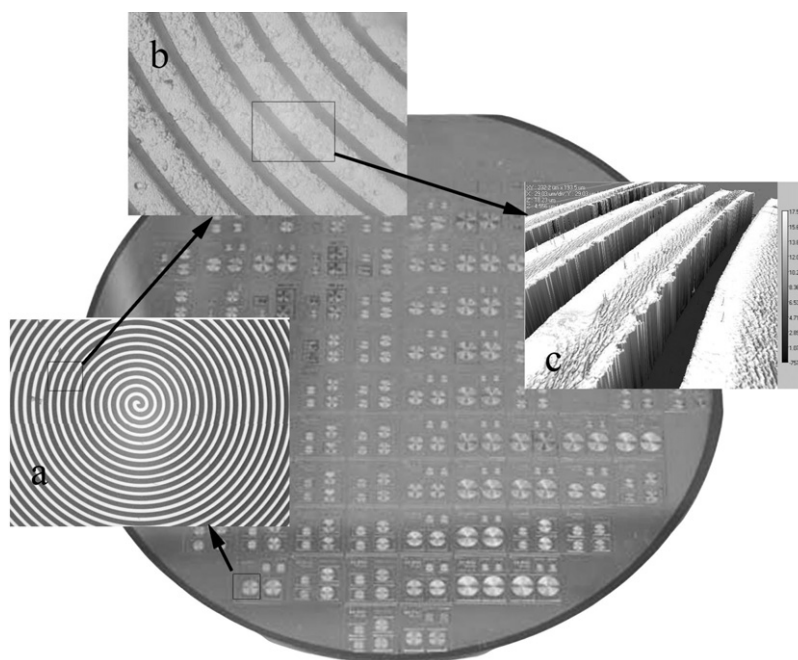


**Fig. 5.** Copper coils of 15  $\mu\text{m}$ -thickness over Si/ $\text{SiO}_2$ /Ti/Cu: images (a)–(c) show the coils after etching the seed-layer. These coils contain all the layers of the fabrication process.

**Table 2**

Average values of electrical resistance and inductance of coils prepared at  $-0.3$  A during 2000s; measured thickness: 15–16  $\mu\text{m}$ .

Coil type	Radius (mm)	Electrical resistance ( $\Omega$ )	Inductance (nH)
20 $\mu\text{m} \times 20 \mu\text{m}$ – 40 tracks	1.60	25.3	1686
15 $\mu\text{m} \times 15 \mu\text{m}$ – 40 tracks	1.20	24.1	1260
12 $\mu\text{m} \times 12 \mu\text{m}$ – 40 tracks	0.96	17.8	935
10 $\mu\text{m} \times 10 \mu\text{m}$ – 40 tracks	0.80	14.4	–
8 $\mu\text{m} \times 8 \mu\text{m}$ – 40 tracks	0.64	15.2	418
20 $\mu\text{m} \times 20 \mu\text{m}$ – 25 tracks	1.00	14.9	455
15 $\mu\text{m} \times 15 \mu\text{m}$ – 25 tracks	0.75	11.4	–
12 $\mu\text{m} \times 12 \mu\text{m}$ – 30 tracks	0.72	13.7	394
10 $\mu\text{m} \times 10 \mu\text{m}$ – 30 tracks	0.60	18.2	351
8 $\mu\text{m} \times 8 \mu\text{m}$ – 30 tracks	0.48	14.7	289

over the initial nucleation layer. However, an absolutely constant potential is not reached because of the changing deposition area. The solution was stirred during the electrodeposition to maintain the contribution of the electroactive species to the electrode and to maintain the deposition uniformity.

The final steps were the removal of the photoresist in acetone (Fig. 4d), followed by the selective chemical etching of the Ti/Cu seed layer between the tracks (Fig. 4e): ammoniacal copper chloride and a fluorhydric acid + propylene glycol solutions were used for this last step.

The coils have been observed with a scanning electron microscope (SEM) using a Hitachi S 2300 microscope. The thickness of the deposited Cu was measured using a white-light interferometer ZoomSurf 3D from Fogale-Nanotec. Under the selected deposition conditions, copper completely filled the tracks defined by the photolithography (Fig. 5). When the photoresist mask was chemically removed from the substrate, well defined copper coils remained (Fig. 5a and b), with the tracks having vertical walls, as illustrated in Fig. 5c.

#### 4. Electrical characterization and preliminary study

After removal of the photoresist mask and seed layer, the wafers were diced. The chips were encapsulated and connected by gold wire bonds for practical electrical characterization. First of all, the series resistance of the coils have been checked by simple measurements with a multimeter. As expected, low resistance values are obtained as shown in Table 2. Also shown in this table are the inductance values measured with an Agilent 4294A impedance analyzer. Both parameters have been found to be in good agreement with those simulated by ASITIC.

In order to characterize their dynamic behavior with respect to the targeted sensing applications, the coils have been connected in a RLC filter configuration with an external capacitor, and the resonant frequency and phase of the circuit were then characterized using the Agilent 4294A impedance analyzer. For these measurements, the test structures included within the chips were used for open and short circuit calibration of the impedance analyzer, providing a thorough compensation of the connections contribution as close as possible to the chip under analysis. As expected according to the designed values of the quality factor  $Q$ , a sharp and intense resonance peak is observed. Moreover, coils with same design parameters exhibit resonant frequencies with a low standard deviation, making them suitable for differential configuration measurement circuits. This can be seen in Table 3, which shows a comparison between frequency values obtained by simulation and experimentally, along with the corresponding standard deviation for the different coil types.

Finally, a preliminary assessment of the sensing ability of the devices has been performed by measuring the RLC filter response to the presence of Neodymium Boron Iron powder (NdBFe). The

**Table 3**

Comparison between frequency values obtained experimentally and by simulation for the different coil types;  $C = 100$  pF.

Coil type	Simulated frequencies (MHz)	Measured frequencies (MHz)	Standard deviation
20 $\mu\text{m} \times 20 \mu\text{m}$ – 40 tracks	12.0	12.6	0.1
15 $\mu\text{m} \times 15 \mu\text{m}$ – 40 tracks	14.0	14.1	0.1
12 $\mu\text{m} \times 12 \mu\text{m}$ – 40 tracks	15.5	15.7	0.1
10 $\mu\text{m} \times 10 \mu\text{m}$ – 40 tracks	17.0	17.1	0.3
8 $\mu\text{m} \times 8 \mu\text{m}$ – 40 tracks	19.0	21.0	2.0
20 $\mu\text{m} \times 20 \mu\text{m}$ – 25 tracks	25.0	27.0	3.0
12 $\mu\text{m} \times 12 \mu\text{m}$ – 30 tracks	27.0	26.0	3.0
10 $\mu\text{m} \times 10 \mu\text{m}$ – 30 tracks	26.0	25.5	0.2
8 $\mu\text{m} \times 8 \mu\text{m}$ – 30 tracks	29.0	28.6	0.2

powder particles were distributed to cover the entire sensing coil surface. As can be seen in Fig. 6a, a displacement of the resonant peak of about 600 kHz to lower frequency values (from  $f_p = 14$  to 13.4 MHz) has been observed using a 15  $\mu\text{m}$  pitch sensing coil. It should be noticed that in this preliminary experiment, this result has been obtained by dropping a huge quantity of particles so that it was not possible to quantify them. However, according to Eq. (1),

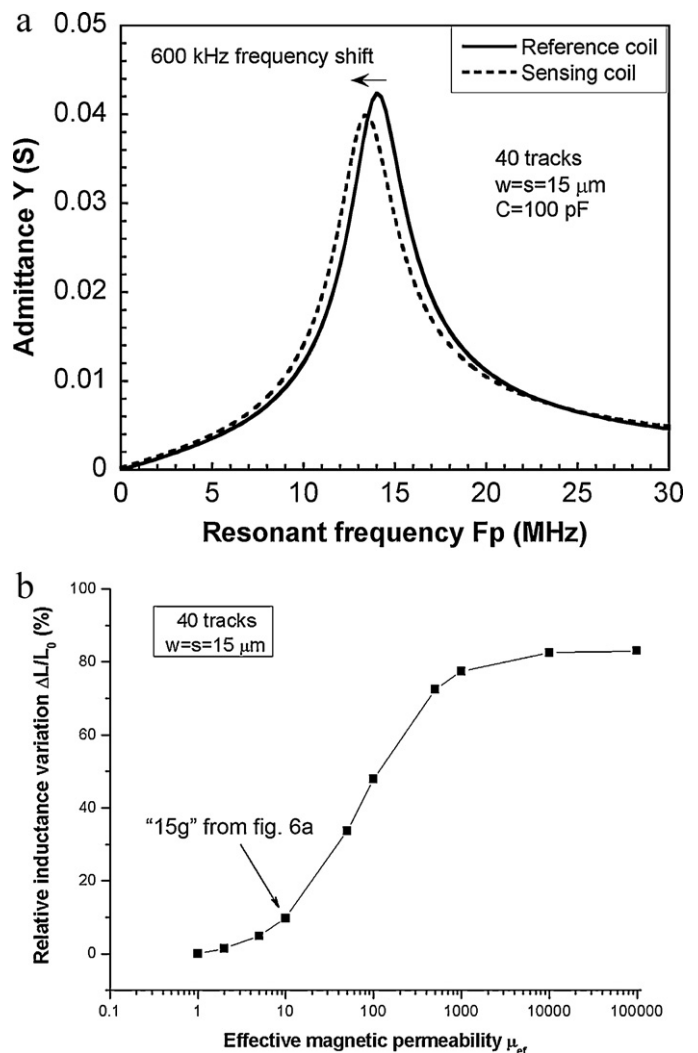


**Fig. 6.** (a) Admittances versus frequency of one pair of 40 track coils, having  $w = s = 15 \mu\text{m}$  and  $C = 100$  pF. The solid line and dashed line indicate the reference coil and the coil with NdBFe on the surface, respectively. (b) Simulated normalized inductance dependence of  $\Delta L = (L - L_0)/L_0$  on magnetic permeability  $\mu_{ef}$  (being  $L_0$  the inductance value at  $\mu_{ef} = 1$ ).

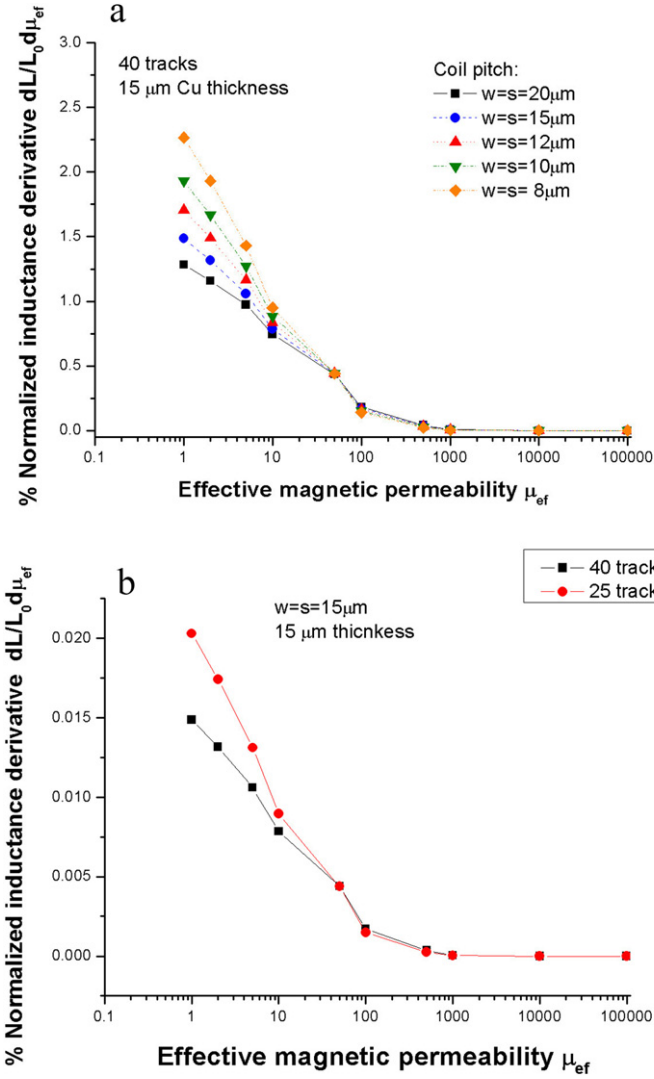


**Fig. 7.** Simulated normalized inductance derivative versus effective magnetic permeability for coils having: (a) 40 tracks of different width and (b) varying number of tracks with a fixed 15  $\mu\text{m}$  width.

this frequency shift corresponds to an inductance increase of about 9%, from  $L_0 = 1304\text{ nH}$  without particles to  $L = 1420\text{ nH}$ . This can be compared with the simulations of Fig. 6b. These simulations have been made by means of finite elements analysis (ANSYS) and are based on a simple model with radial symmetry (2D axis-symmetry) [15], which assumes a coil formed by concentric rings. The presence of a certain density of magnetic particles in the active area of the device is modeled assuming a continuous layer (10  $\mu\text{m}$  thick in this case) with an effective magnetic permeability ( $\mu_{ef}$ ), given by the volume fraction of magnetic particles on the surface. According to this, the inductance increase detected by the device of Fig. 6a would correspond to an increase of the effective permeability from  $\mu_{ef} = 1$  (in air, i.e. without particles) up to  $\mu_{ef} = 10$ . From this figure, it is also worth noting that the dependence of the inductance on the effective permeability can be fitted to an analytical expression of the type

$$L = L_{sat} + \frac{L_0 - L_{sat}}{1 + K\mu_{ef}} \quad (3)$$

where the fitting constant  $K$  depends on each coil, and  $L_0$  and  $L_{sat}$  are the asymptotic inductance values for  $\mu_{ef} \rightarrow 0$  and  $\mu_{ef} \rightarrow \infty$ , respectively. For planar coils such as those analyzed in this work, it has been found in a previous work [15] that  $K \ll 1$ , so that the value of  $L_0$  practically coincides with the value of the inductance

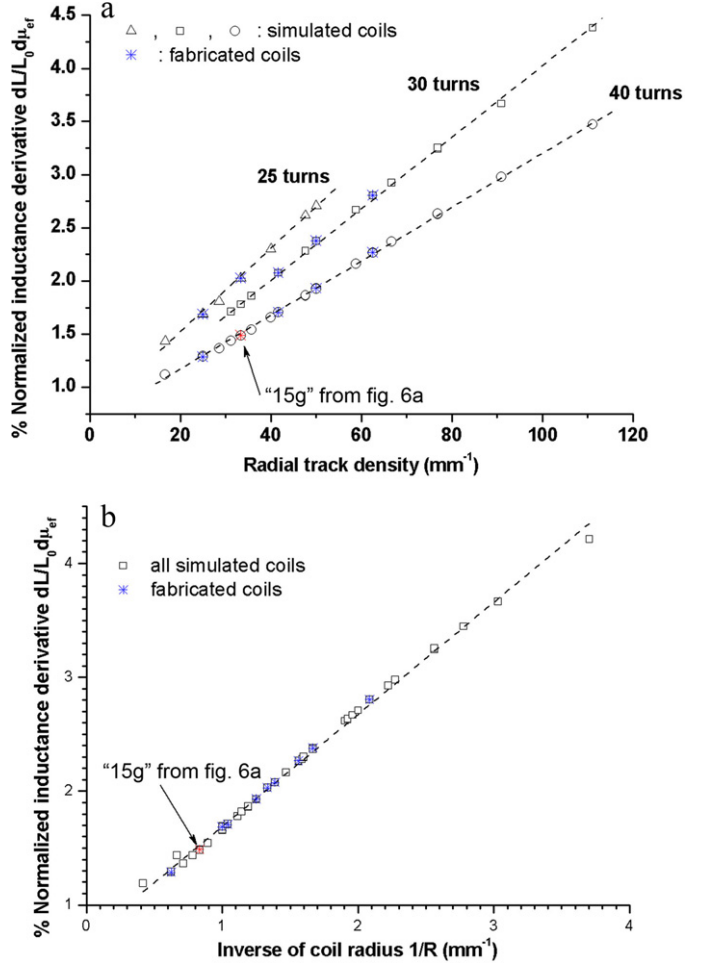


**Fig. 8.** (a) Trends of simulated and fabricated values of sensitivity of inductance change in a coil with respect to radial track density. (b) Trends of simulated and fabricated values of sensitivity of inductance change in a coil with respect to inverse of coil radius.

without particles (i.e. in air,  $\mu_{ef} = 1$ ). The simulations also indicate that, in agreement with [7,21], the maximum inductance increase that can be expected for these devices is of the order of 100%, that is  $L_{sat} \rightarrow 2L_0$ . Within this range of inductance, the sensitivity of the device caused by changes of  $\mu_{ef}$  (related to variations of the magnetic particles density in the active area of the sensing device) is determined by the derivative  $dL/d\mu_{ef}$ , which is represented in Fig. 7a. As can be seen in this figure, the maximum sensitivity occurs at  $\mu_{ef} = 1$ , which indicates that the device should be especially sensitive to small variations of  $\mu_{ef}$  around this value. It also clearly appears that the sensitivity increases as the coil pitch decreases. Furthermore, Fig. 7b shows that for the same pitch value, i.e. for the same track density, the sensitivity is higher for the coil with the smaller number of turns. In order to clarify the effects of the track density, additional simulations have been carried out, by varying the track separation for each one of the fabricated coils, while maintaining their initial track width and number of turns. Fig. 8a shows the coils sensitivity as a function of the radial track density as calculated from this extensive data set, where the radial track density has been calculated as:

$$t_d = \frac{1}{w + s};$$

It appears that coils with the same number of tracks are grouped on a same straight line. Furthermore, if we normalize the radial track density to the number of turns (which is in fact the inverse of the

coil radius), as represented in Fig. 8b, the whole data set gets aligned on a unique common linear curve. According to these results, we can conclude that the sensitivity of the devices depends only on the coil radius, whatever the spatial organization of the windings, which will be determined by the experimental measurement requirements. This includes requirements of inductance values  $L$  and quality factor  $Q$  in order to reach the best compromise for accurate measurements at reasonably low frequencies; provided that the intrinsic coil series resistance can be sufficiently minimized, using thick electrodeposited Cu tracks for instance. Interestingly, the coil labeled “15g” which characterization results are presented in Fig. 6a appears to be one of the less sensitive one among the coils fabricated in this work. Further work is now under progress in order to fully characterize the whole set of fabricated coils with superparamagnetic particles, which will be closer to real working conditions as immunomagnetic biosensors.

## 5. Conclusions

In this paper, an analysis of the viability of using thick Cu EC coils in resonant differential second order filter circuit topologies, for biosensors applications, is presented. Simulations of the intrinsic series resistance, the quality factor and the resonance frequencies have been made. According to these simulation results, different coil dimensions were chosen to reach the best compromise between high inductance value, high quality factor and reasonable working frequencies, within the limits defined by the targeted application. The coils have been fabricated by combining CMOS technology and electrochemical deposition processes. The coils were obtained electrochemically by adjusting the deposition conditions in order to achieve well defined stress free thick Cu tracks with good adhesion and vertical walls. Single second order filter circuit topologies have been applied to the characterization of the microinductive coils. Low series resistance and inductance values, both in good agreement with the simulations, have been measured. The resonance frequency values obtained from the prepared coils agreed with the simulation and present a low standard deviation, which is necessary for biosensor designed to work in a differential configuration. A preliminary characterization of the device sensing behavior has been performed by using neodymium boron iron powder. The results reveal a change in the resonance frequency, permitting the presence of the magnetic powder to be detected. Extensive additional simulations were performed to study the effects of the coil dimensions and the track density, revealing that the sensitivity of the coils depends only on the size of the coil and not on the distribution of the tracks. Finally, it is interesting to notice that the characterization results presented in this work have been obtained with one of the less sensitive coil among the fabricated devices, which corroborate the strong potential of these microinductive devices for high sensitivity, low cost and high specificity immunomagnetic biosensing applications.

## Acknowledgements

EME is member of CEMIC (Centre of Microsystems Engineering) of the “Generalitat de Catalunya”. This paper was supported by a Consolider Project number CSD2006-12 from the *Ministerio de Educación y Ciencia* and by the contract MAT 2006-12913-CO2-01 from the *Comisión Interministerial de Ciencia y Tecnología (CICYT)*. The authors wish to thank also the Centres científics i tecnològics de la Universitat de Barcelona (CCiTUB) and the Centre Nacional de Microelectrònica (CNM) for the use of their equipment. Also thanks to J.A. Ortega for his help in baths design.

## References

- [1] K. Larsson, K. Kriz, D. Kriz, Magnetic transducers in biosensors and bioassays, *Analysis* 27 (1999) 617–621.
- [2] D.L. Graham, H.A. Ferreira, P.P. Freitas, Magnetoresistive-based biosensors and biochips, *Trends in Biotechnology* 22 (2004) 455–462.
- [3] M.A.M. Gijs, Magnetic bead handling on-chip: new opportunities for analytical applications, *Microfluidics and Nanofluidics* 1 (2004) 22–40.
- [4] Ch.B. Kriz, K. Radevik, D. Kriz, Magnetic permeability measurements in bioanalysis and biosensors, *Analytical Chemistry* 68 (1996) 1966–1970.
- [5] Richardson, P. Hawkins, R. Luxton, The use of coated paramagnetic particles as a physical label in a magneto-immunoassay, *Biosensors and Bioelectronics* 16 (2001) 989–993.
- [6] J. Richardson, A. Hill, R. Luxton, P. Hawkins, A novel measuring system for the determination of paramagnetic particle labels for use in magneto-immunoassays, *Biosensors and Bioelectronics* 16 (2001) 1127–1132.
- [7] W.A. Roshen, Effect of finite thickness of magnetic substrate on planar inductors, *IEEE Transactions on Magnetics* 26 (1990) 270–275.
- [8] A.L. Coutrot, E. Dufour-Gergam, J.M. Quemper, E. Martincic, J.P. Gilles, J.P. Grandchamps, M. Matlosz, A. Sanchez, L. Darsse, J.C. Ginefri, Copper micro-moulding process for NMR microinductors realization, *Sensors and Actuators A* 99 (2002) 49–54.
- [9] C. Serre, N. Yaakoubi, S. Martínez, A. Pérez-Rodríguez, J.R. Morante, J. Esteve, J. Montserrat, Electrochemical deposition of Cu and Ni/Cu multilayers in Si Microsystem Technologies, *Sensors and Actuators A* 123–124 (2005) 633–639.
- [10] M. Cortés, E. Gómez, A. Pérez-Rodríguez, C. Serre, E. Vallés, Optimisation of copper electrodeposition processes for Si technology based inductive microsystems, *Journal of Electroanalytical Chemistry* 619–620 (2008) 176–182.
- [11] K. Diaz de Lezama, A. García-Arribas, J.M. Barandiarán, J. Gutiérrez, Comparative study of alternative circuit configurations for inductive sensors, *Sensors and Actuators A* 91 (2001) 226–229.
- [12] S. Baglio, S. Castorina, N. Savalli, Strategies and circuits for micro inductive biosensor conditioning, in: *EuroSensors XVI: Proceedings of the 16th European Conference on Solid-State Transducers*, Prague, 2002, pp. 604–607.
- [13] S. Baglio, A. Pérez-Rodríguez, S. Martínez, C. Serre, J.R. Morante, J. Esteve, J. Montserrat, Microinductive signal conditioning with resonant differential filters: high-sensitivity biodetection applications, *IEEE Transactions on Instrumentation and Measurement* 56 (2007) 1590–1595.
- [14] S. Martínez, N. Yaakoubi, A. Pérez-Rodríguez, C. Serre, P. Gorostiza, J.R. Morante, J. Esteve, Electrochemical deposition of metal layers and structures for Si-based microsystems, *Sensors and Actuators A* 99 (2002) 41–44.
- [15] C. Serre, S. Martínez, A. Pérez-Rodríguez, J.R. Morante, J. Esteve, J. Montserrat, Si technology based microinductive devices for biodetection applications, *Sensors and Actuators A* 132 (2006) 499–505.
- [16] Harold A. Wheeler, Simple inductance formulas for radio coils, in: *Proceedings of the IRE*, 1928, pp. 1398–1400.
- [17] W.G. Hurley, M.C. Duffy, S. O’Reilly, S.C. O’Mathuana, Impedance formulas for planar magnetic structures with spiral windings, *IEEE Transactions on Industrial Electronics* 46 (1999) 271–278.
- [18] M. Thompson, Inductance calculation techniques—Part II: Approximations and handbook methods, *Power Control and Intelligent Motion* (1999).
- [19] A.M. Niknejad, Analysis, Design and Optimization of Spiral Inductors and Transformers for Si RF ICs, College of Engineering, University of California, Berkeley, USA, 2000.
- [20] S. Martínez, N. Yaakoubi, C. Serre, A. Pérez-Rodríguez, J.R. Morante, J. Esteve, R. Pérez-Castillejos, J. Montserrat, High sensitivity detection of biomolecules by microinductive Si technology based devices, in: *Proceedings of the EuroSensors XVII*, 2003, pp. 772–775.
- [21] W.A. Roshen, D.E. Turcotte, Planar inductors on magnetic substrates, *IEEE Transactions on Magnetics* 24 (1988) 3213–3216.

## Biographies

**M. Cortés** obtained her chemistry degree in 2006 and her master in Nanoscience and Nanotechnology in 2008. Since 2007 she joined the Chemist-Physics Department of the University of Barcelona as a research and teaching assistant. Actually Ph.D. student in the Barcelona University (UB) in the research field of electrodeposition of metals and alloys for devices applications.

**S. Martínez** received her diploma in physics in 1999 and her Ph.D. degree in 2004 from the University of Barcelona, Spain. Since 1999 she joined the Electronics Department of the University of Barcelona as a research and teaching assistant. Her principal research interests include signal processing and data acquisition for the characterization of magnetic devices and also simulation, design, fabrication and characterization of high sensitivity magnetic biosensors and micro fuel cells. Actually she has a post-doc position in the Centro Nacional de Microelectrónica (CNM-CSIC).

**C. Serre** was born in Tarbes, France, in 1963. He received the Ph.D. in microelectronics from the University of Grenoble, France, in November 1992. During 1993, he was an assistant professor at the same university and worked on the luminescence of porous silicon at the Laboratory of Physical Spectrometry. He joined the EME (Electronic Materials and Engineering) laboratory of the Department of Applied Physics and Electronics at the University of Barcelona in November 1993 as a

post-doctoral fellow. In February 2002, he was contracted as a researcher (within the Spanish “Ramon y Cajal” programme) in the same laboratory, where he obtained a full professor permanent position in November 2007. His research activities focus on the fabrication and characterization of SiC and SiGeC thin films for micromechanics, as well as micromachining technologies and processes and their application to integrated sensors and actuators.

**E. Gómez** obtained her chemistry degree in 1978 and her doctorate in 1983 from Barcelona University (UB). Since 1989 she holds the position of Professor Titular in the Physical Chemistry Department. Her research interest has been developed on the preparation of micro/nanomaterials using electrochemistry technology, focused at present on the electrodeposition of multifunctional Co-X layers, multilayers and composites.

**A. Pérez-Rodríguez** was born in 1961 in San Cristóbal (Venezuela). In 1984 he received his first degree in Physics from the University of Barcelona. In 1985 he joined the Department of Applied Physics and Electronics of this University as

Associated Lecturer. He received his Ph.D. in Physics in 1987 from this University (with Doctorate Award of the University). Since 1988 he is permanent staff in the Department of Electronics at this University. During 1988/1989 he was Visiting Research Fellow at the University of Surrey (UK). His research projects are related to Si Microsystem Technologies, ion beam processing of nanostructured materials in group IV technologies and advanced characterization and processes for Si based micromachining technologies. He is co-author of 100 papers in the main refereed scientific journals in these fields, as well as more than 200 contributions in Books and Proceedings from international conferences. Actually he is professor of the University of Barcelona.

**E. Vallés** obtained her Ph.D. in chemistry in 1983 from Barcelona University UB. Now she is professor in the department of physical chemistry at the University of Barcelona. Her research fields of interest are: electrochemical coatings (deposits and metallic alloys), preparation (by means electrodeposition) and characterization of thin films with soft or hard-magnetic properties, magnetoresistive films, nanostructured films composites, multilayers.



### 4.3 Conclusions

From the studies performed, the optimised bath developed to prepare uniform fine-grained copper deposits with low stress and good adherence to different substrates was: 70 g/l  $\text{H}_2\text{SO}_4$  + 200 g/l  $\text{CuSO}_4$  + 70 mg/l NaCl + 10 ml/l carrier + 0.5 ml/l brightener + 0.4 ml/l leveller solution. Fine grained deposits were desired to favour the good definition of the deposits into photolithographed microstructures.

Characterisation of the deposits revealed that the optimum seed layer over the silicon/silicon oxide substrate was Ti/Cu because this seed layer favours the good adherence of the copper deposit to the substrate. For that reason Si/SiO<sub>2</sub>/Ti/Cu substrates were used for the coil electrodeposition.

Test coils were electrodeposited with good definition and vertical walls of the tracks, even after removing the resin mask with acetone. It was possible to control the thickness of the tracks by adjusting the deposition charge. In our case tracks of 15  $\mu\text{m}$  were mainly prepared.

In order to avoid the short circuit of the coils, the seed layer was removed after the deposits preparation. Chemical etching (Ti: HF 10%:propylenglycol (1:3), Cu: 0.02 M  $\text{H}_3\text{PO}_4$ , 4.7 M  $\text{NH}_4\text{Cl}$ , 5.7 M  $\text{NH}_4\text{OH}$ ) was the selected from the different methods tested. Although this treatment increases the roughness of the electrodeposited coils when eliminating the seed layer, the tracks still showed good definition and adherence after the etching.

To scale up of the electrodeposition process a cell with more capacity (2,5 l) and more stirring of the solution was needed. Moreover the platinum counter electrode was changed to a copper-phosphorous alloy electrode. Performing all these changes the electrodeposition of a whole wafer was possible. Very little chip thickness variation was measured over the wafer.

In order to find the optimised plastic substrate to obtain the copper coils a Ti/Cu seed layer was evaporated directly onto different plastics. Although it was not possible to obtain the seed layer with a good adherence over Kapton, good results were obtained for PEEK, PEN, PMMA, PS and Teflon. When adherence of the seed layer over the plastic substrates is achieved, copper deposits were obtained. However the best results were obtained over PEN. It was possible to obtain electrodeposited copper coils using PEN as the substrate, which opens the possibility of using it for applications in biosensors or inductors.

New coil design was proposed based in the simulations of the intrinsic series resistance, the quality factor and the resonance frequencies performed. The coils obtained presented the same good results as the test ones.

Single second order filter circuit topologies have been applied to the characterisation of the microinductive coils. Low series resistance, inductance values and resonance frequency values measured agree with the simulations and present a low standard deviation.

A study of the device sensing behaviour performed with neodymium boron iron powder revealed that it was possible to measure a change in the resonance frequency and consequently the presence of the magnetic powder to be detected.

Additional simulations revealed that the sensitivity of the coils depends only on the size of the coil and not on the distribution of the tracks so more sensing behaviour is expected for smaller coils.

These devices demonstrated strong potential for high sensitivity, low cost and high specificity immunomagnetic biosensing applications.



## Chapter 5

# Deposition of CoPt and CoPtP magnetic alloys for MEMS application

### 5.1 Study of the electrodeposition process of the binary CoPt and the ternary CoPtP alloys

Microelectromechanical systems (MEMS) are the integration of mechanical elements, sensors, actuators, and electronics on a substrate, commonly silicon, through microfabrication technology. Some of the commercial applications of MEMS include: inkjet printers, accelerometers in cars, accelerometers in consumer electronics devices such as game controllers, cell phones and a number of digital cameras, MEMS microphones in portable devices, car tire pressure sensors, disposable blood pressure sensors, optical switching, Bio-MEMS applications, fluid acceleration such as for micro-cooling.

In figure 5.1 a schematic representation of an actuator MEMS to be

used in microfluidics is shown.

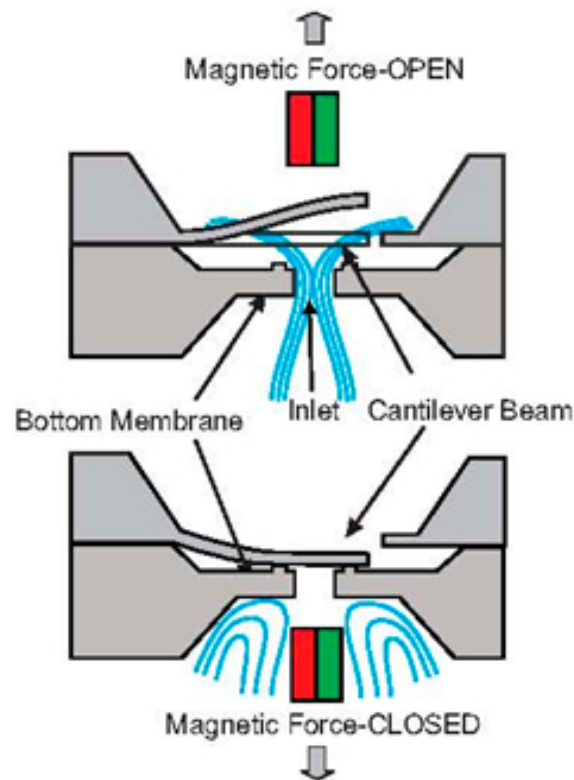


Figure 5.1: Schematic representation of a microelectromechanical system (MEMS) used to control a fluid circulation applying a magnetic field

An actuator is a device that uses a force for moving or controlling a mechanism or system in order to generate an effect on an automated process. It can be operated by different sources of energy: electric current, hydraulic fluid pressure, pneumatic pressure or magnetic fields. In order to use magnetic fields to operate another mechanism or system, magnets must be used (figure 5.2). However, placing a magnet in a microactuator is not easy. For that reason, recently there has been a growing interest in the miniaturization of hard magnetic materials and in their direct integration in MEMS because this fact would enable the efficiency of these devices.

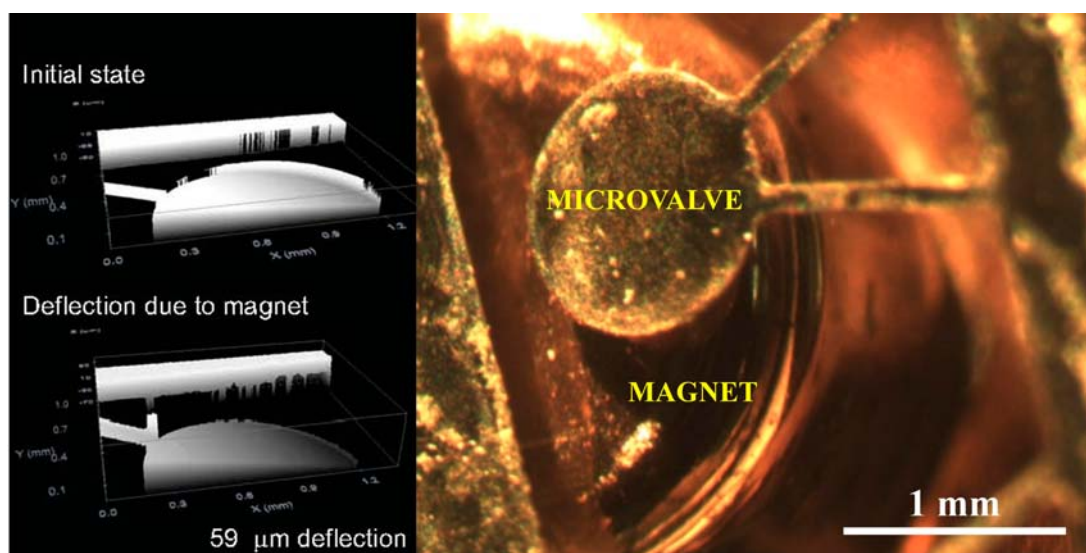


Figure 5.2: Microactuator deflection of a Si/Ti/Ni/electrodeposited CoNi microvalve caused by a magnet

Electrochemical methods can be used in order to prepare magnetic materials compatible with MEMS processing. Additionally to the known advantages, electrodeposition is fully compatible with microfabrication processes and has been used to prepare several micron-thick deposits of metals, alloys, and compounds on various substrates.

Although most of the magnetic microactuators developed by different researchers use soft magnetic materials [63–65], hard magnetic materials are also desirable in some applications (micro-sized motors, minipumps, microactuators) [54, 66]. The preparation of hard magnetic deposits by different techniques for MEMS magnetic actuators has recently been studied [67–74]. Different Co alloys have been prepared by electrodeposition for this purpose [18]. The incorporation of ferromagnetic particles into a CoNi alloy matrix by means of electrodeposition has been studied as a way of preparing hard magnetic films [30]. Direct electrodeposition of hard magnetic films over the silicon/seed-layer substrate has also been tested. The

most common hard magnetic materials are CoPt, FePt, and rare earths as  $\text{Nd}_2\text{Fe}_{14}\text{B}$  or  $\text{SmCo}_5$  [75–77], however the codeposition of rare earth magnetic thin films implies the use of organic solvents and the application of high negative potentials. Co-based alloys, such as CoNiP [21, 67, 74], CoP [18], CoPt [78–80], or CoPtP [18, 81–83], have been electrodeposited, resulting in low coercivity films. Hard magnetic properties in fact require anisotropic, often ordered, crystal structures; a subsequent annealing step after deposition is usually applied to obtain a change in the crystalline phase that gives the desired hard magnetic response.

The aim of the present section is to study the electrodeposition process of the CoPt and CoPtP systems in order to control the preparation of binary and ternary films over silicon/seed-layer substrates with modulate magnetic properties.

In this sense, solutions containing  $\text{CoCl}_2$ ,  $\text{Na}_2\text{PtCl}_6$  and sodium hypophosphite in boric acid and  $\text{NH}_4\text{Cl}$  were selected. The reduction processes of each metal as well as the blank solution were studied separately over vitreous carbon. Platinum reduction process took part at more positive potentials than cobalt one. The baths used resulted adequate for the codeposition of both metals of the alloy as the gap between their reduction processes was small. Moreover, when depositing both metals simultaneously the onset of cobalt reduction was advanced, due to an easier nucleation of cobalt over previous deposited platinum.

The same effect was observed when moderate quantities of hypophosphite were present in the bath, which reveals that the possible P incorporation in the initial stages of the deposition catalyses Co reduction. P

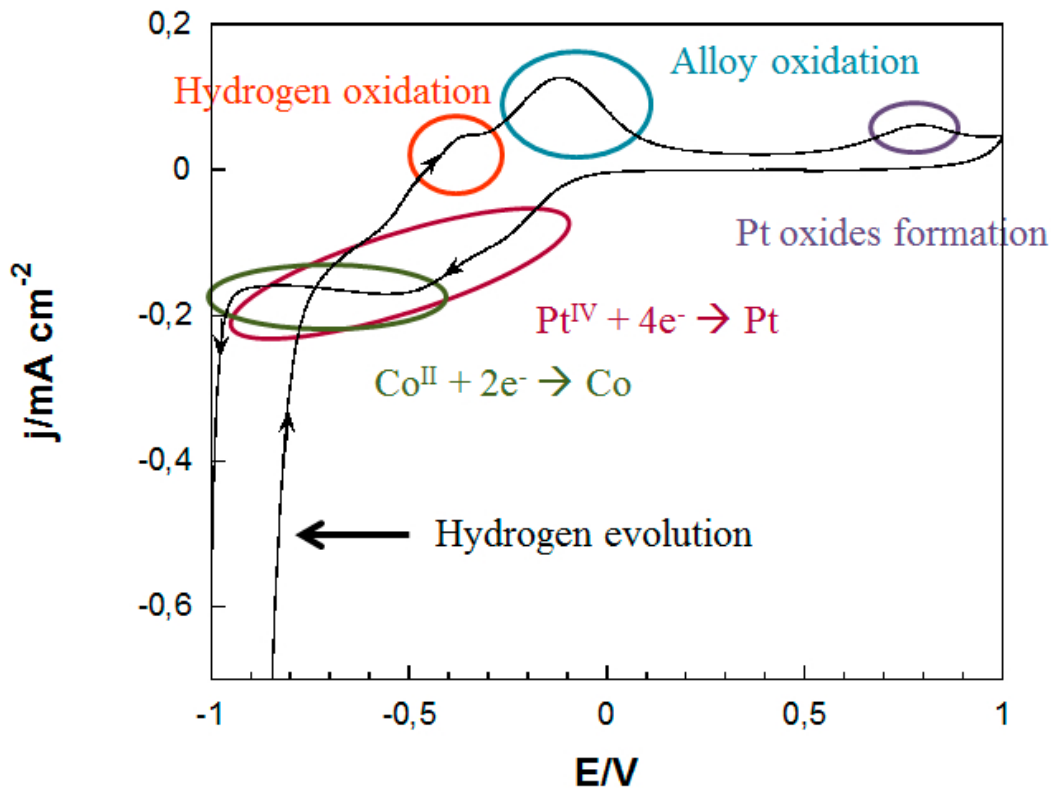


Figure 5.3: Cyclic voltammograms of a bath containing 1 M  $\text{NH}_4\text{Cl}$  + 30 g/l  $\text{H}_3\text{BO}_3$  +  $10^{-2}$  M  $\text{NaH}_2\text{PO}_2$  +  $2.5 \cdot 10^{-3}$  M  $\text{CoCl}_2$  +  $10^{-3}$  M  $\text{Na}_2\text{PtCl}_6$ , over vitreous carbon

was incorporated in the alloy because it was caught whilst deposition took place. Because of the presence of platinum in the alloy significant hydrogen evolution was observed. However this process was far enough from the codeposition of both metals in order to be able to obtain the alloy (figure 5.3).

Studies of the deposition of the alloy over Si/Ti/Ni substrate were performed. CoPtP deposits with low P content (0.5-6 wt. % P) and different wt. % of Pt were obtained potentiostatically over these substrates as well as a few CoPt deposits. The influence of the deposition bath and the deposition conditions (bath composition, pH, temperature, charge and deposition potentials) on the composition structure and coercivity of the

magnetic films were analysed.

The platinum content in the alloy depended on the amount of P present. The differences in the platinum amount revealed significant changes in the structure of the deposits and consequently in their coercivity. CoPt and CoPtP deposits with different magnetic properties from soft to hard were obtained. The annealing effect was also studied but not significant differences were observed before and after the thermal treatment, probably because not enough temperature was applied. The results of this part of the work are presented in the paper: “*Ternary CoPtP electrodeposition process: Structural and magnetic properties of the deposits*”.

In a second work, the effect of the P incorporation in the deposit was widely studied (figure 5.4). Both galvanostatic and potentiostatic techniques were used to obtain platinum-rich CoPt films in order to obtain hard magnetic films deposited on silicon/seed-layer substrates without the need for subsequent annealing of the deposited films. High Pt percentages were desired for enhancing the magnetic anisotropy of the cobalt phase. Different deposition conditions were characterised in order to obtain films with a composition and structure optimized for maximum coercivity, maximum permeability, and good corrosion resistance, desirable properties for use in magnetic microdevices.

The influence of the P incorporation in the magnetic, structural, morphological, and corrosion-resistance properties of the CoPt electrodeposits, as well as the analysis of the changes in the deposition process and in the deposition rate was performed. The efficiency of the process in both cases was calculated by comparing the theoretical and the experimental charge.

In order to calculate the experimental one, the dimensions of the deposit and their density were used. The results revealed there was a significant dependence of the efficiency with the substrate. The density could be estimated from the crystalline phase and the position of the peaks shown by X-ray diffractograms.

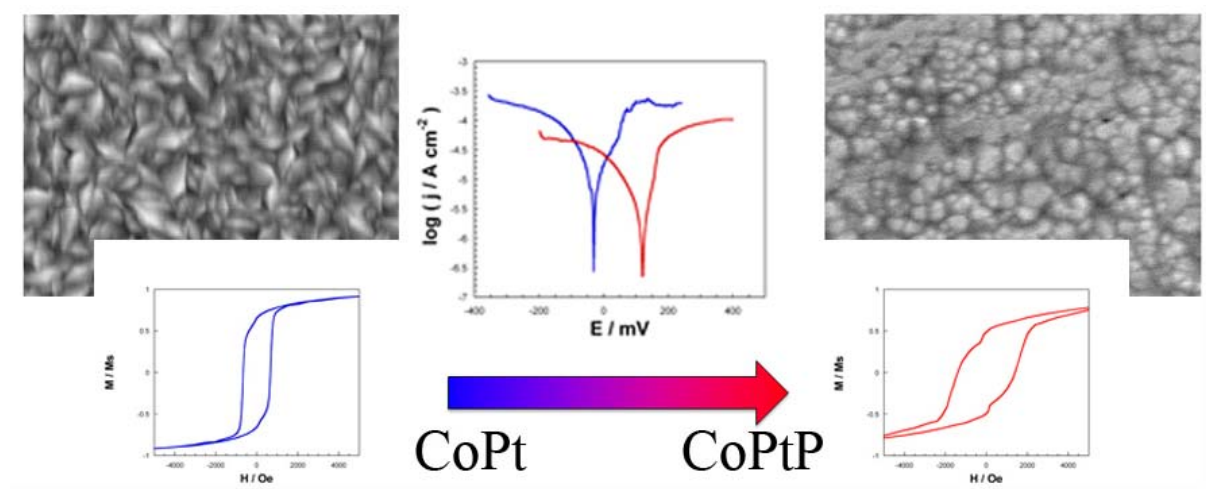


Figure 5.4: Schematic representation of the effect of the P in the morphology, magnetic properties and corrosion resistance of the alloy

These studies showed the possibility of preparing magnets that can be directly integrated on devices involving silicon substrates. The results of this part of the work are presented in the paper: “*Magnetic properties of nanocrystalline CoPt electrodeposited films. Influence of P incorporation*”

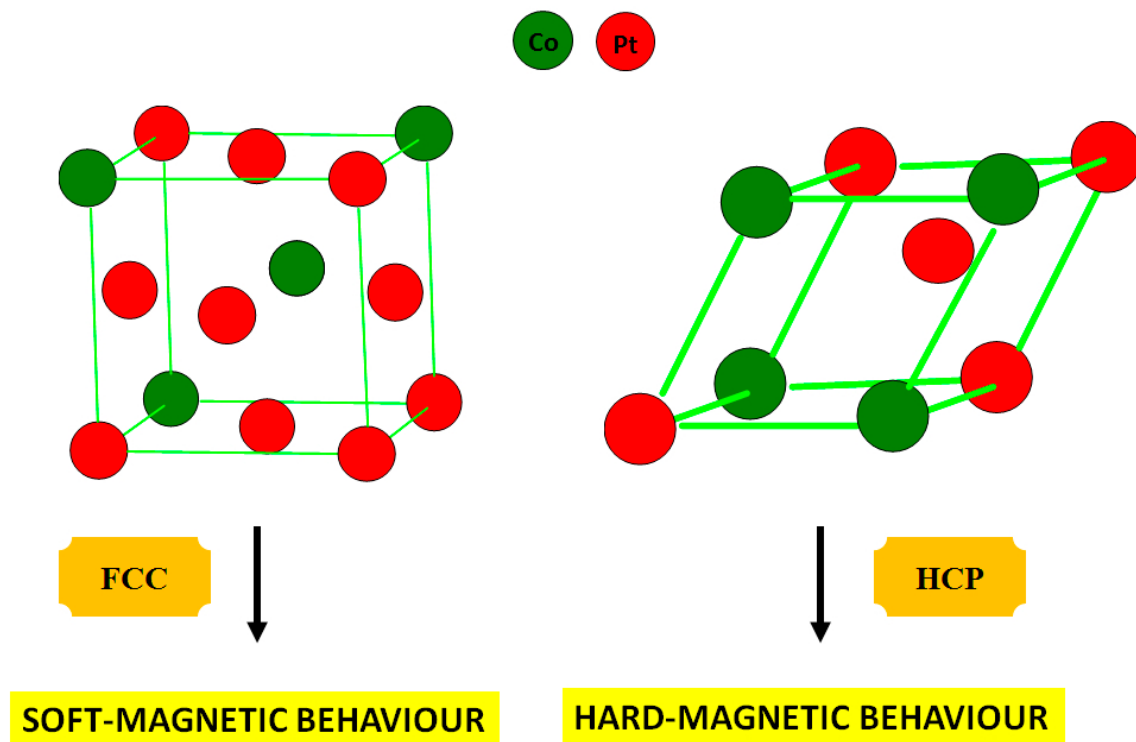


## 5.2 Results of the preparation of thin films CoPt and CoPtP

- Paper: “*Ternary CoPtP electrodeposition process: Structural and magnetic properties of the deposits*” M. Cortés, S. Matencio, E. Gómez and E. Vallés, Journal of Electroanalytical Chemistry 627 (2009) 69-75
- Paper: “*Magnetic properties of nanocrystalline CoPt electrodeposited films. Influence of P incorporation*” Meritxell Cortés, Elvira Gòmez, Elisa Vallés, Journal of Solid State Electrochemistry 14(12) (2010) 2225-2233



5.2.1 Ternary CoPtP electrodeposition process: Structural and magnetic properties of the deposits





## Ternary CoPtP electrodeposition process: Structural and magnetic properties of the deposits

M. Cortés, S. Matencio, E. Gómez, E. Vallés \*

*Electrodep, Departament de Química Física and Institut de Nanociència i Nanotecnologia (IN<sup>2</sup>UB), Universitat de Barcelona, Martí i Franquès 1, E-08028 Barcelona, Spain*

### ARTICLE INFO

#### Article history:

Received 13 November 2008  
Received in revised form 19 December 2008  
Accepted 22 December 2008  
Available online 29 December 2008

#### Keywords:

Magnetic films  
Electrodeposition  
Cobalt–platinum–phosphorous alloy  
Coercivity

### ABSTRACT

Ternary CoPtP electrodeposition process in an acid bath has been studied and CoPtP films have been electrodeposited over silicon/seed-layer. The influence of bath composition, temperature and pH on ternary electrodeposition process, deposits composition, structure and magnetic properties has been studied. Homogeneous and bright ternary deposits have been obtained with magnetic properties from soft magnetic to hard magnetic. A clear enlargement of films coercivity was obtained when platinum percentage in the deposits was around 30–40 wt%. Susceptibility of the CoPtP films has increased after annealing of the samples. Deposits show hexagonal structure with gradual Pt incorporation in the Co crystalline lattice.

© 2008 Elsevier B.V. All rights reserved.

### 1. Introduction

There has recently been a growing interest in the miniaturization of hard magnetic materials and in their integration in micromechanical systems (MEMS) because this fact would enable the efficiency of these devices. The integration of soft magnetic materials with micro-fabrication processes has indeed been successfully achieved.

Nowadays, the electrodeposition of cobalt alloys films is of particular interest because these films show magnetic properties that are useful in different applications. Some of these films can be incorporated in magnetic recording media and in micro-electromechanical systems (MEMS) such as actuators and sensors where films of permanent magnets are required. Most of the magnetic microactuators developed include electrodeposited films of binary and ternary cobalt alloys as CoNiB, CoNiP, CoNiZnP, CoNiReP, CoNiFe, CoNiMo, CoMo, CoB, CoFeB, and CoFeCr [1–7].

Recently, the possibility of preparing hard magnetic films by electrodeposition is being analysed in order to prepare permanent magnets in the microscale to be used in micro-devices. Hard magnetic properties in fact required anisotropic, often ordered, crystal structures and closely controlled microstructures, down to the deep sub-micron scale. Electroplating is an attractive technique because of the simple experimental setup. It is easy scalable for high mass-production and it allows a fast deposition rate as well as preparing directly patterned samples over silicon-based substrates. Different Co alloys have been prepared by electrodeposition for this purpose [8] and even electrodeposition through lithographi-

cally defined masks is sometimes used [9]. Some CoPt and CoPtP alloys seem to be promising candidates due to their good hard magnetic properties [10–16]. Although some authors describe how CoPt films with optimum hard magnetic properties can be prepared by electrodeposition, few studies deal with the electrochemical behaviour of the binary or ternary electrodeposition process [17].

The aim of the present work is to study the electrodeposition process of the CoPtP system in order to control the preparation of ternary films over silicon/seed-layer substrates with modulate magnetic properties. The influence of the deposition bath and the deposition conditions (bath composition, temperature, pH) on the composition, structure and coercivity of the magnetic films were analysed. Some CoPtP deposits with different magnetic properties from soft to hard were obtained. A dependency of the coercivity with the composition of deposits was observed. The annealing effect was also studied.

### 2. Experimental

Electrochemical study and deposits preparation have been performed in a conventional three-electrode cell with control of the temperature. Solutions contained  $\text{CoCl}_2$ ,  $\text{Na}_2\text{PtCl}_6$  and sodium hypophosphite in boric acid and  $\text{NH}_4\text{Cl}$ , all of analytical grade. Solutions were freshly prepared with water which was first doubly distilled and then treated with a Millipore Milli Q system. The solution pH was adjusted with HCl or NaOH solutions. Solutions were de-aerated by argon bubbling before each experiment and maintained under argon atmosphere during it.

\* Corresponding author. Tel.: +34 403 92 38; fax: +34 402 12 31.  
E-mail address: [e.valles@ub.edu](mailto:e.valles@ub.edu) (E. Vallés).

Electrodeposition has been carried out using a microcomputer-controlled potentiostat/galvanostat Autolab with PGSTAT30 equipment and GPES software. Vitreous carbon rods (Metrohm) and silicon/Ti(1000 Å)/Ni(500 Å) substrates supplied by IMB-CNM-CSIC (Centro Nacional de Microelectrónica) have been used for electrochemical study. Deposits were prepared over the silicon/seed-layer substrates. Vitreous carbon electrode was polished to a mirror finish using alumina of different grades (3.75 and 1.87  $\mu\text{m}$ ) and cleaned ultrasonically for 2 min in water. The silicon-based substrates were cleaned with acetone, ethanol and rinsed in water before deposition. The reference electrode was an Ag/AgCl/1 mol dm<sup>-3</sup> NaCl electrode. All potentials were referred to this electrode. The counter electrode was a platinum spiral.

Voltammetric experiments were carried out at 50 mV s<sup>-1</sup>, scanning initially from 500 mV towards negative potentials. A single cycle was run in cyclic voltammetric experiments.

Leica Stereoscan S-360 scanning electron microscope was used to analyse deposits composition. Quanta 200 FEI, XTE 325/D8395 scanning electron microscope and AFM Nanoscope Extended Multimode were used for morphology observation.

Structure of deposits were studied by means of a Philips MRD diffractometer with parallel optical geometry using Cu K $\alpha$  radiation ( $\lambda = 1.5418 \text{ \AA}$ ) and a texture goniometer that allows control of the sample rotation about the three axes.

Magnetic properties were characterized by means of a SQUID magnetometer at room temperature.

Roughness (rms) and thickness of the coatings were measured using a white-light interferometer from Zygo Corporation.

### 3. Results and discussion

#### 3.1. Voltammetric study of the electrodeposition process

The influence of the different parameters in the electrodeposition process was analysed by recording voltammetric curves. Voltammetric study was performed mainly in vitreous carbon electrode because this electrode allows to detect the oxidation processes of the studied systems in a wide potential range without oxidation of the own electrode. Fig. 1 shows the voltammograms of a blank solution B ( $\text{NH}_4\text{Cl} + \text{H}_3\text{BO}_3 + \text{NaH}_2\text{PO}_2$ ) (curve a), B +  $\text{CoCl}_2$  (curve b) and B +  $\text{PtCl}_6^{2-}$  (curve c) over vitreous carbon electrode. When Co(II) was present in the solution a cobalt reduction current around  $-1.0 \text{ V}$  was detected during the negative going sweep (curve b) and a ratio between oxidation respect to reduction charge ( $Q_{\text{ox}}/Q_{\text{red}}$ ) around 22% was obtained. Some oxidation current was detected due to the oxidation of both molecular hydrogen retained over the electrode and electrodeposited cobalt. In the case of  $\text{PtCl}_6^{2-}$ , platinum reduction current and proton reduction over the platinum was observed [18] from around  $0.0 \text{ V}$ , previous to the massive hydrogen evolution (curve c). Very low  $Q_{\text{ox}}/Q_{\text{red}}$  value (around 8%) was obtained, as it was expected for platinum deposition.

In the solutions containing both  $\text{CoCl}_2$  and  $\text{Na}_2\text{PtCl}_6$ , the current related to platinum reduction was slightly decreased whereas the onset of simultaneous cobalt reduction was advanced, due to an easier nucleation of cobalt over previous deposited platinum (Fig. 2). Three oxidation peaks were detected in the anodic scan: One detected around  $-0.35 \text{ V}$  that disappeared when the anodic scan was recorded in stirring conditions, which revealed that this peak corresponded to the oxidation of molecular hydrogen retained over the electrode [18–20]. The second oxidation peak, around  $-100 \text{ mV}$ , was assigned to some cobalt or alloy oxidation whereas oxidation current around  $0.8 \text{ V}$  was due to platinum oxides formation [21,22]. Intermediate  $Q_{\text{ox}}/Q_{\text{red}}$  values between those corresponding to Co–P and Pt–P systems in voltammetric experi-

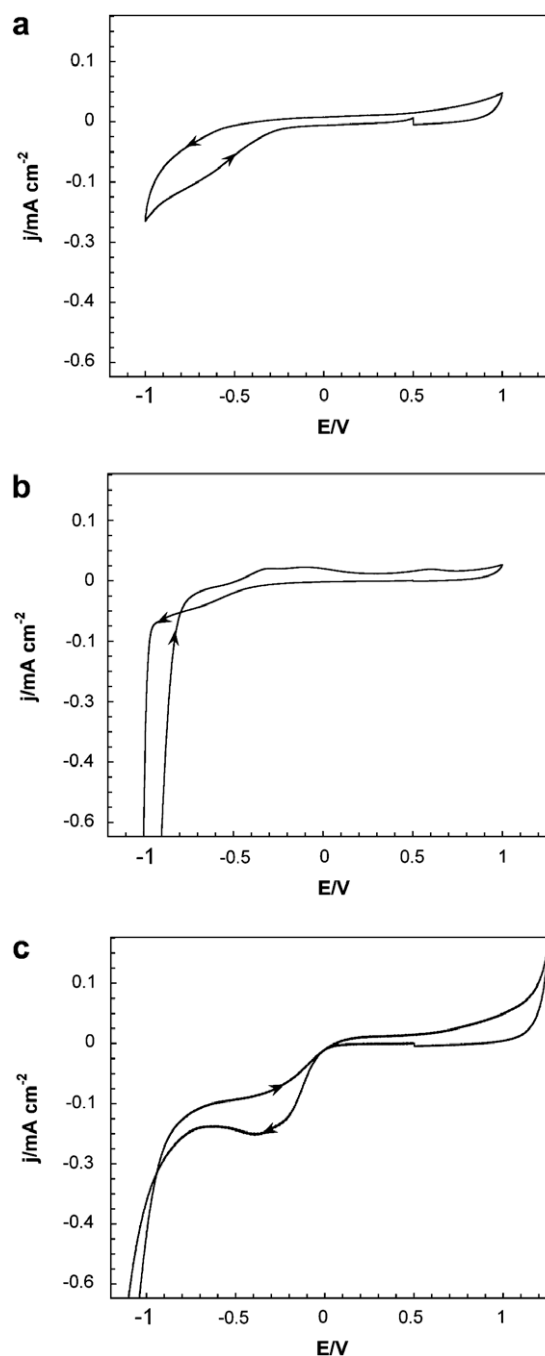
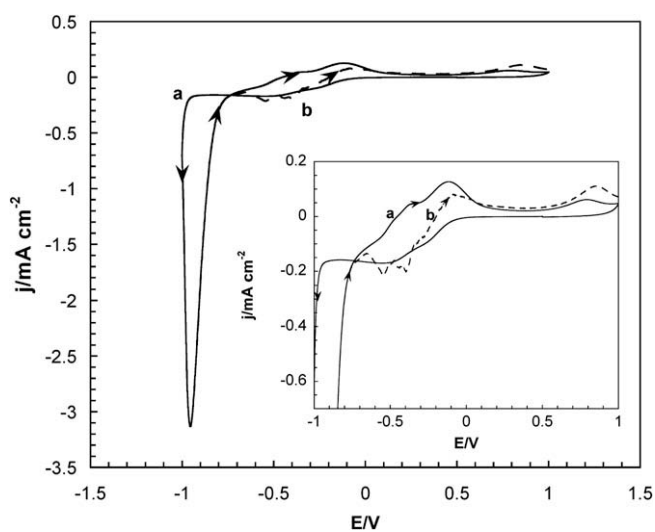


Fig. 1. Cyclic voltammograms of (a) blank solution B (1 M  $\text{NH}_4\text{Cl} + 30 \text{ g/l H}_3\text{BO}_3 + 5 \times 10^{-2} \text{ M NaH}_2\text{PO}_2$ ), (b) B +  $2.5 \times 10^{-3} \text{ M CoCl}_2$  solution, and (c) B +  $1.01 \times 10^{-3} \text{ M PtCl}_6^{2-}$  solution.  $T = 25 \text{ }^\circ\text{C}$ , pH 4.5. Quiescent conditions. Vitreous carbon electrode.

ments with similar cathodic limits were obtained. No difference in the voltammetric responses was observed between pH 4.5 and pH 5.5. Similar voltammetric curves were recorded at different bath temperatures, although by increasing the temperature the deposition process was advanced and the reduction current increased.  $Q_{\text{ox}}/Q_{\text{red}}$  values decreased slightly with an increase in the temperature or a decrease of the solution pH.

When Si/seed-layer substrate was used, a significant reduction current was detected from  $-0.7 \text{ V}$  due to simultaneous alloy deposition and hydrogen evolution (Fig. 3). Oxidation scan showed the two first peaks previously detected. Anodic limit was shortened in the voltammetric experiments performed with Silicon/Ti/Ni substrates due to the seed-layer oxidation.



**Fig. 2.** Cyclic voltammograms of a bath containing 1 M  $\text{NH}_4\text{Cl}$  + 30 g/l  $\text{H}_3\text{BO}_3$  +  $1 \times 10^{-2}$  M  $\text{NaH}_2\text{PO}_2$  +  $2.5 \times 10^{-3}$  M  $\text{CoCl}_2$  +  $1 \times 10^{-3}$  M  $\text{PtCl}_6^{2-}$ . (a) The continuous line shows quiescent conditions and (b) the dotted line shows stirring conditions in the oxidation scan ( $\omega = 300$  rpm).  $T = 25$  °C, pH 4.5. Vitreous carbon electrode.

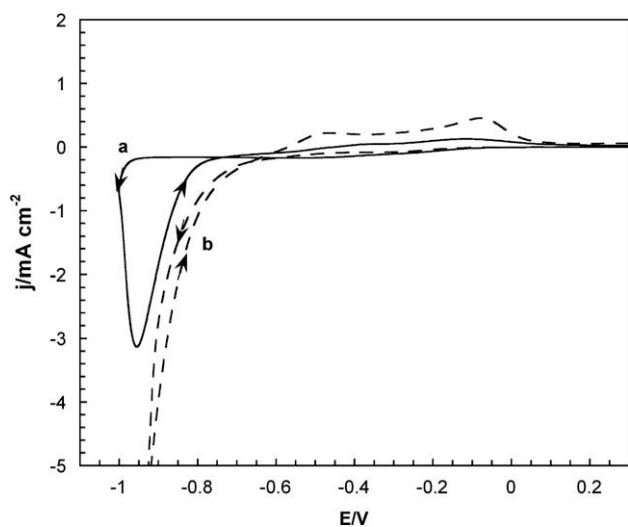


**Fig. 3.** Cyclic voltammograms of the same bath than in Fig. 2. (a) Vitreous carbon electrode and (b) Si/Ti(100 nm)/Ni(50 nm) electrode.  $T = 25$  °C, pH 4.5. Quiescent conditions.

Fig. 4A shows the effect of changing the  $\text{PtCl}_6^{2-}$  concentration of the bath on the voltammetric curves. Platinum reduction current previous to the onset of the simultaneous Co reduction was logically greater for higher  $\text{PtCl}_6^{2-}$  concentrations. On the other hand, a decrease in the oxidation current was observed as this current was the result of the sum of both oxidation and reduction current of two different processes that took place simultaneously. In the same way, an increase of the Co(II) content in the solution led to an advance of the simultaneous Co deposition (Fig. 4B). For moderate quantities of hypophosphite in the bath, an increase of the concentration implies a slight advance of the onset of the simultaneous cobalt deposition (Fig. 5), which reveals that the possible P incorporation in the initial stages of the deposition catalyses Co reduction.

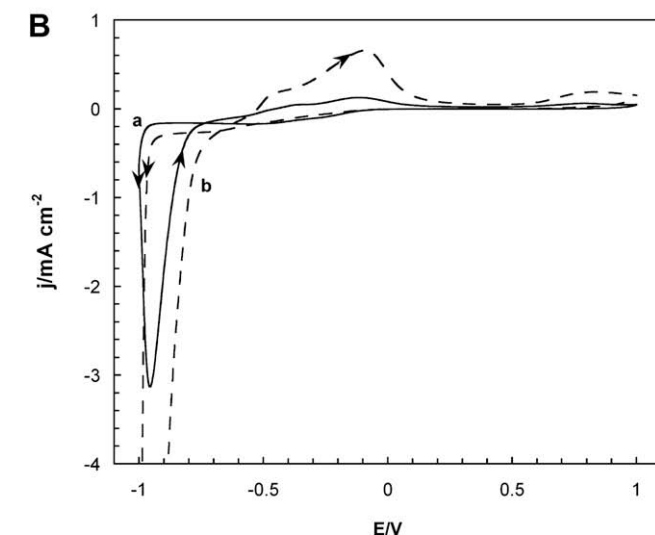
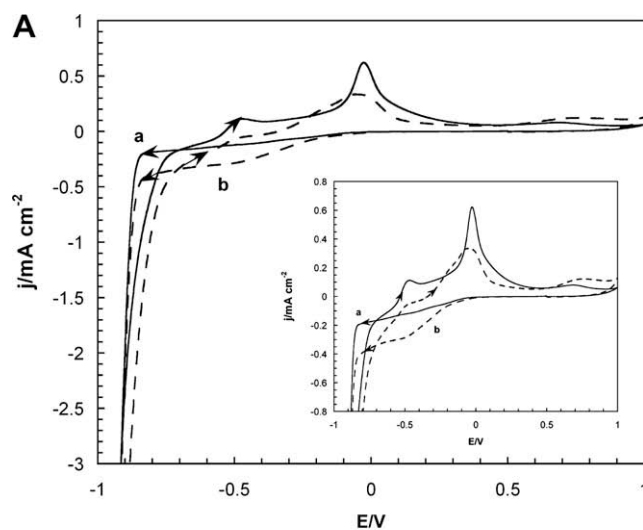


**Fig. 4.** Cyclic voltammograms in quiescent conditions over vitreous carbon electrode of: (A) 1 M  $\text{NH}_4\text{Cl}$  + 30 g/l  $\text{H}_3\text{BO}_3$  +  $1 \times 10^{-2}$  M  $\text{NaH}_2\text{PO}_2$  +  $2.5 \times 10^{-3}$  M  $\text{CoCl}_2$  solution + (a)  $0.6 \times 10^{-3}$  M  $\text{PtCl}_6^{2-}$  and (b)  $1.5 \times 10^{-3}$  M  $\text{PtCl}_6^{2-}$ .  $T = 40$  °C, pH 5.5. (B) 1 M  $\text{NH}_4\text{Cl}$  + 30 g/l  $\text{H}_3\text{BO}_3$  +  $1 \times 10^{-2}$  M  $\text{NaH}_2\text{PO}_2$  +  $1 \times 10^{-3}$  M  $\text{PtCl}_6^{2-}$  solution + (a)  $2.5 \times 10^{-3}$  M  $\text{CoCl}_2$  and (b)  $5 \times 10^{-3}$  M  $\text{CoCl}_2$ .  $T = 25$  °C, pH 4.5.

### 3.2. Deposits preparation and characterization

From the previous voltammetric study, Pt and Co codeposition seems to be possible from the tested bath by applying enough negative potential. The induced incorporation of P in the deposits will be determined by compositional analysis. Moderate concentration of  $\text{PtCl}_6^{2-}$  was used because of the low solubility of the platinum salt. Moderate stirring of solution (60–300 rpm) during the electro-deposition was maintained.

Deposits were potentiostatically prepared over silicon/seed-layer substrates. The influence of the bath composition, pH and temperature on the deposits' composition was analysed (Table 1). Moderate pH values were selected in order to avoid excessive hydrogen evolution and platinum oxides precipitation.

Ternary CoPtP deposits were obtained with variable composition as a function of the solution composition. Low P percentages were observed in all the cases.

The analysis of the results revealed a moderated influence of pH, deposition charge and deposition potentials over deposits' composition (Table 1). However, the enhancement of the Co depo-

sition process in the presence of hypophosphite, detected in the voltammetric experiments, is corroborated by the analysis of the deposits. When hypophosphite is not present in the solution, deposits with high Pt percentages were obtained, whereas in the presence of hypophosphite Pt percentage decreased and Co one increased, although the P percentage remains low. The higher Pt percentages were attained when P percentages in the deposits were very low.

### 3.3. Morphology, structure and magnetic properties of CoPtP deposits

Ternary 100–300 nm thick CoPtP deposits were grey shiny and show low roughness (lower than 20 nm). Thin deposits were obtained as a consequence of the significant hydrogen evolution dur-

ing the electrodeposition process. AFM images show a nodular morphology with some elongated crystals (Fig. 6). No differences in composition were observed in the different zones of the deposits. SEM observation of the deposits revealed the presence of some voids due to hydrogen evolution.

X-ray diffractograms of prepared CoPtP coatings were recorded. In order to favour the identification of the peaks, the diffractograms were compared with those obtained for the own substrate (Si/Ti/Ni). Besides some peaks corresponding to the substrate, several defined diffraction peaks were observed, revealing the polycrystalline nature of the coatings (Fig. 7A). A shift in the coating's

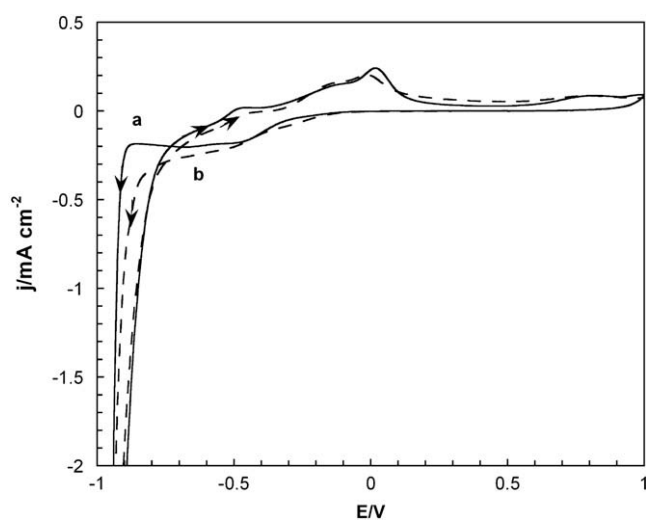


**Fig. 5.** Cyclic voltammograms of 1 M  $\text{NH}_4\text{Cl}$  + 30 g/l  $\text{H}_3\text{BO}_3$  +  $1 \times 10^{-2}$  M  $\text{NaH}_2\text{PO}_2$  +  $2.5 \times 10^{-3}$  M  $\text{CoCl}_2$  +  $1.5 \times 10^{-3}$  M  $\text{PtCl}_6^{2-}$  solution + (a)  $1 \times 10^{-2}$  M  $\text{NaH}_2\text{PO}_2$  and (b)  $2 \times 10^{-2}$  M  $\text{NaH}_2\text{PO}_2$ .  $T = 25^\circ\text{C}$ , pH 5.5. Quiescent conditions. Vitreous carbon electrode.

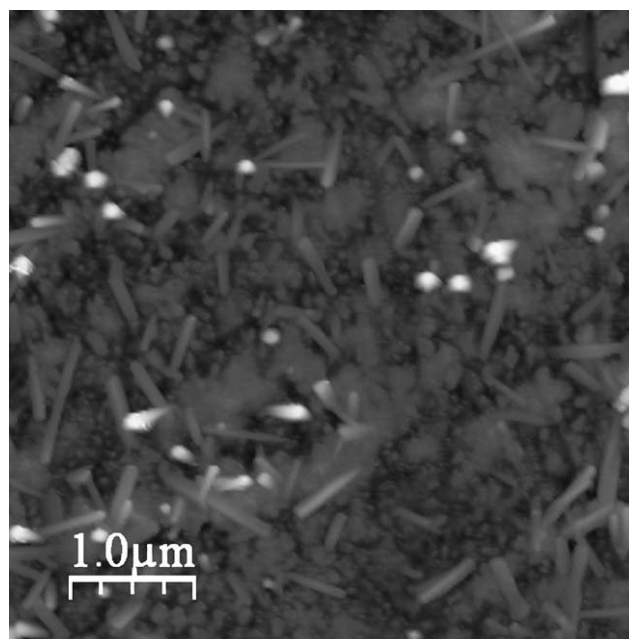


**Fig. 6.** AFM image of a region of a ternary CoPtP deposit (59.1 wt% Co, 40.4 wt% Pt, and 0.5 wt% P) obtained on a Si/Ti/Ni substrate.

**Table 1**  
Composition of some deposits prepared as a function of deposition conditions.

[CoCl <sub>2</sub> ]/M	[Na <sub>2</sub> PtCl <sub>6</sub> ]/M	[NaH <sub>2</sub> PO <sub>2</sub> ]/M	pH	T/°C	-E/mV	Q/C cm <sup>-2</sup>	% Co	% Pt	% P
$5 \times 10^{-3}$	$10^{-3}$	$10^{-2}$	4.5	25	950	10	71.7	25.1	3.3
					1050	20	74.2	21.4	4.4
					1100	20	73.2	22.8	4.1
$2.5 \times 10^{-3}$	$10^{-3}$	$10^{-2}$	4.5	16	950	10	65.1	33.3	1.6
					925	20	67.5	30.1	2.4
					950	10	66.7	30.8	2.5
			55	950	20	68.9	28.3	2.8	
				975	20	69.2	28.3	2.5	
				850	26.7	67.5	31.2	1.3	
			5.5	950	26.7	67.3	30.7	2.0	
				859	26.7	65.6	33.5	0.9	
				900	26.7	62.5	36.5	1.0	
$2.5 \times 10^{-3}$	$10^{-3}$	$5 \times 10^{-2}$	4.5	25	925	20	80.7	13.3	6.0
					950	10	78.2	15.5	6.3
					950	20	79.1	15.3	5.7
			40	975	20	78.5	15.5	6.0	
				950	20	62.6	35.6	1.8	
				900	20	59.1	40.6	0.3	
$2.5 \times 10^{-3}$	$1.5 \times 10^{-3}$	$10^{-2}$	5.5	40	950	20	59.1	40.4	0.5
					850	20	68.8	29.3	1.9
					900	20	67.5	30.3	2.2
$2.5 \times 10^{-3}$	$1.5 \times 10^{-3}$	$2 \times 10^{-2}$	4.5	40	900	20	64.5	33.6	1.9
					950	10	88.2	-	11.8
					950	10	-	100	-
$2.5 \times 10^{-3}$	$10^{-3}$	$5 \times 10^{-2}$	4.5	25	950	10	-	100	-
					950	10	-	100	-
					950	10	40.3	59.7	-

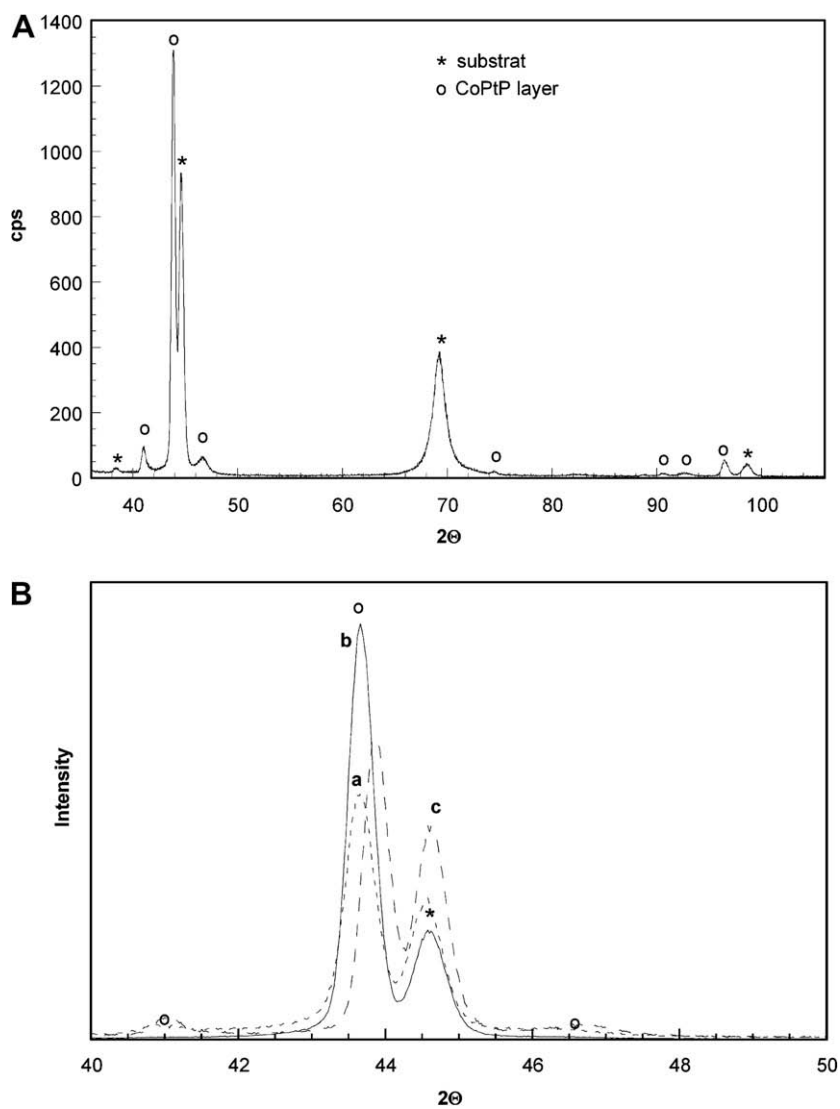


**Fig. 7.** (A) X-ray diffractogram of a CoPtP deposit (64.5 wt% Co, 34.6 wt% Pt, and 0.9 wt% P) obtained on a Si/Ti/Ni substrate. (B) X-ray diffractograms of CoPtP deposits obtained on a Si/Ti/Ni substrate. (a) 55.3 wt% Co, 43.8 wt% Pt, and 0.9 wt% P. (b) 59.1 wt% Co, 40.4 wt% Pt, and 0.5 wt% P. (c) 64.5 wt% Co, 34.6 wt% Pt, and 0.9 wt% P.

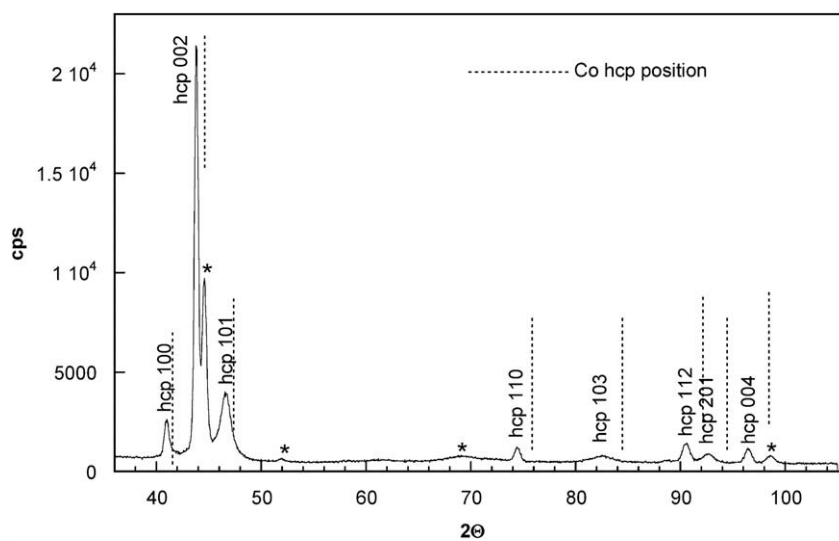


**Fig. 8.** X-ray diffractogram resulting from the sum of  $\theta - 2\theta$  scans at different values of the angle  $\psi$ . CoPtP deposit (64.5 wt% Co, 34.6 wt% Pt, and 0.9 wt% P) obtained on a Si/Ti/Ni substrate.

peaks was observed as a function of the deposits composition (Fig. 7B). Different  $\theta - 2\theta$  scans at different values of the angle  $\psi$  were recorded. The samples were decoupled to prevent the signal from silicon and all diffractograms were added up to enhance the peaks. From these diffractograms (Fig. 8) the identification of all the peaks corresponding to the deposit has been possible. The coating's peaks corresponded to a cobalt hcp structure with the position of the peaks shifted to lower  $\theta$  values respect to pure cobalt ones, due to the incorporation of platinum in the crystalline cell. Taking into account the  $2\theta$  position of the peaks, the cell parameters of the hexagonal phase ( $a, c$ ) and the cell volumes ( $V$ ) have been determined using the DICVOL04 indexation program [23]. Table 2 shows the adjusted parameters for different electrodeposited films. A gradual increase (with linear dependence) in the  $a$  and  $c$  parameters of the hexagonal phase and the cell volume with the increase of platinum percentage was obtained. This dependence corroborates that CoPtP films prepared from the electrolytic bath tested corresponded to an hcp cobalt phase distorted by the Pt incorporation, following solid solution behavior.

Pure CoPt samples led to similar X-ray diffractograms. However, the non presence of P in the coatings led to more Pt rich deposits. Then, the positions of the peaks corresponding to the hcp phase were more shifted to low  $\theta$  values, as consequence of higher Pt incorporation (Fig. 9). A drastic increase of cell volume of the hexagonal phase was observed for CoPt films with 60 wt% Pt (Table 2). No CoPt intermediate compounds were obtained for the binary CoPt or ternary CoPtP films prepared in the bath tested.

Binary CoP deposits prepared with appreciable P percentage (around 12 wt%) from the same bath without platinum compound did not show diffraction peaks different to those of the substrate, revealing perhaps amorphous nature of the films.

**Table 2**

Adjusted cell parameters ( $a, c$ ) and cell volume ( $V$ ) of the hexagonal phase for deposits of different composition.

wt% Co	wt% Pt	wt% P	$a/\text{\AA}$	$c/\text{\AA}$	$V/\text{\AA}^3$
64.9	34.1	1.0	2.543	4.129	23.13
64.5	34.6	0.9	2.545	4.130	23.17
59.1	40.4	0.5	2.550	4.142	23.38
58.5	40.8	0.7	2.557	4.154	23.53
40.3	59.7	–	2.599	4.223	24.70

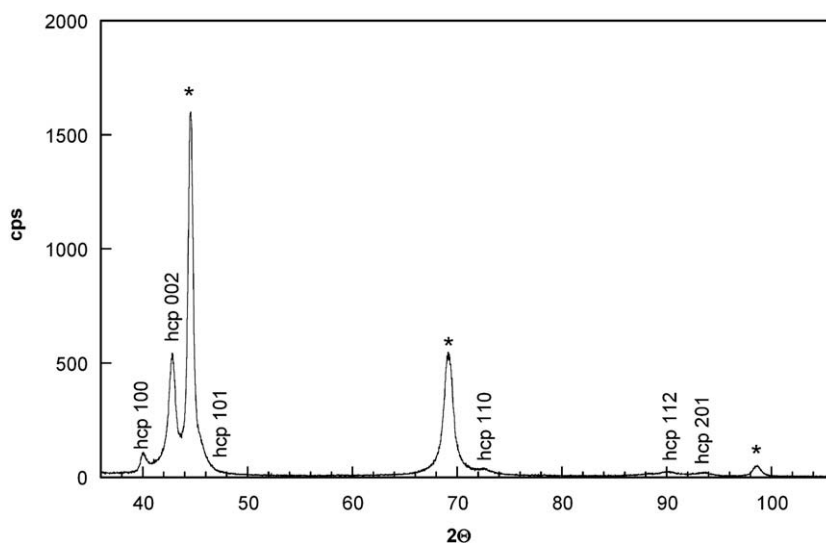


**Fig. 9.** X-ray diffractogram of a binary CoPt deposit (40.3 wt% Co, 59.7 wt% Pt) obtained on a Si/Ti/Ni substrate.

Magnetic characterization of the CoPtP deposits were performed by recording magnetization-magnetic field curves. Some binary deposits (CoP and CoPt) were also analysed. Magnetic response depends on deposits' composition. Fig. 10 reveals the drastic increase on the films coercivity with Pt incorporation; the higher the platinum percentage, the higher the hard magnetic response. A decrease on the susceptibility of the films ( $M-H$  slope) was simultaneously observed.

The maximum coercivity values were obtained for binary CoPt films or ternary CoPtP ones with high Pt percentages and low P incorporation (Fig. 11A). Coercivity values up to 1100–1200 Oe were attained directly by electrodeposition, without annealing of the samples. Ternary CoPtP deposits prepared presented lower  $M-H$  slopes than CoPt ones. The annealing of the samples at 400 °C during 90 min did not cause variation in the magnetization curves of CoPt whereas an increase of the magnetic susceptibility was observed for CoPtP samples (Fig. 11B). It can be seen that the incorporation of low percentages of P in the deposits led to

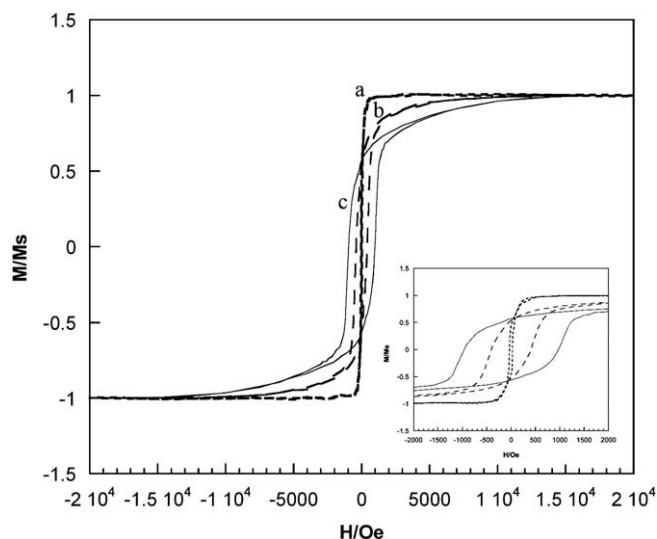


**Fig. 10.** Normalized room-temperature magnetization curves taken with the applied field parallel for deposits obtained on a Si/Ti/Ni substrate: (a) binary CoPt deposit (88.2 wt% Co, 11.8 wt% P), (b) ternary CoPtP (71.7 wt% Co, 25.1 wt% Pt, 3.3 wt% P) and (c) ternary CoPtP (67.5 wt% Co, 30.1 wt% Pt, and 2.4 wt% P).

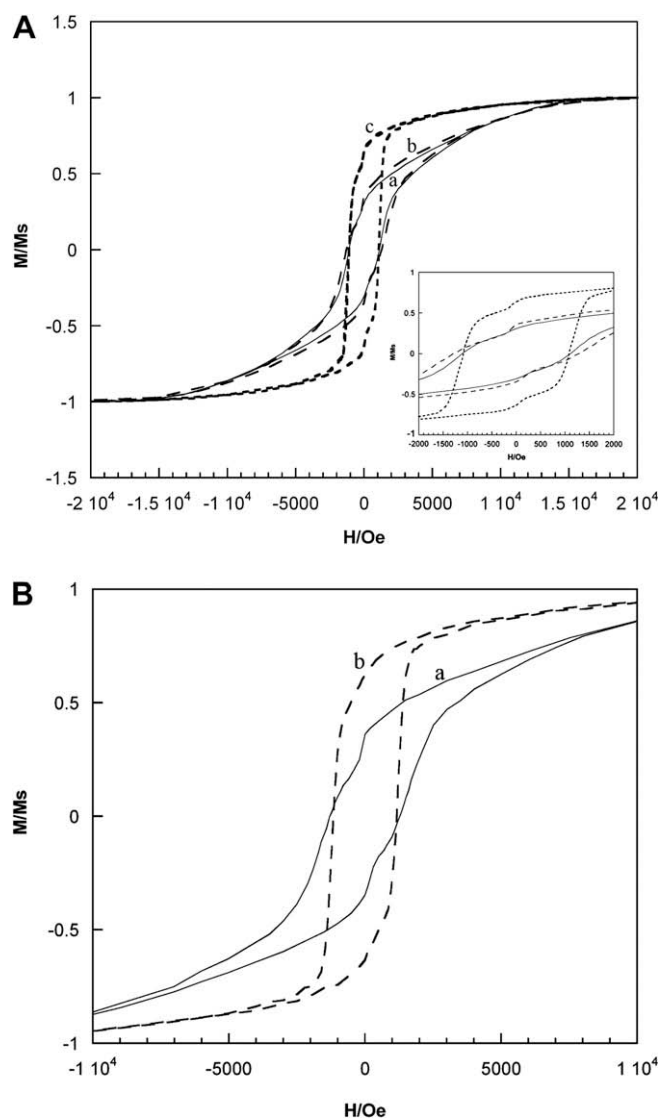


**Fig. 11.** Normalized room-temperature magnetization curves taken with the applied field parallel for: (A) CoPtP deposits obtained on a Si/Ti/Ni substrate. (a) 67.5 wt% Co, 30.3 wt% Pt, and 2.2 wt% P. (b) 59.1 wt% Co, 40.4 wt% Pt, and 0.5 wt% P. (c) CoPt deposit (40.3 wt% Co, 59.7 wt% Pt). (B) The same ternary deposit than Fig. 11A. (a) Without annealing treatment and (b) with an annealing treatment of 400 °C during 90 min.

films with similar coercivity as pure CoPt ones but with lower Pt percentages in the deposits.

#### 4. Conclusions

The electrochemical study of the electrodeposition process led to the detection of the potentials useful for deposits preparation,

the significant hydrogen evolution during the electrodeposition and the enhancement of the cobalt deposition in the presence of hypophosphite. The incorporation of P in the CoPt electrodeposit led to a decrease of the Pt percentage in the deposits.

Fine-grained ternary CoPtP deposits with variable percentages of composition depending on electrodeposition conditions have been obtained. P incorporation in the deposits implied a decrease of the Pt percentage. A maximum value of platinum of around 40 wt% was obtained in presence of hypophosphite. Pt was gradually incorporated in the crystalline lattice of the hcp Co phase, leading to an increase in the crystalline cell parameters.

CoPt or CoPtP films with high Pt percentages present high values of coercivity without annealing of the samples, that fact opens the possibility of preparing magnets that can be directly integrate on devices involving silicon substrates.

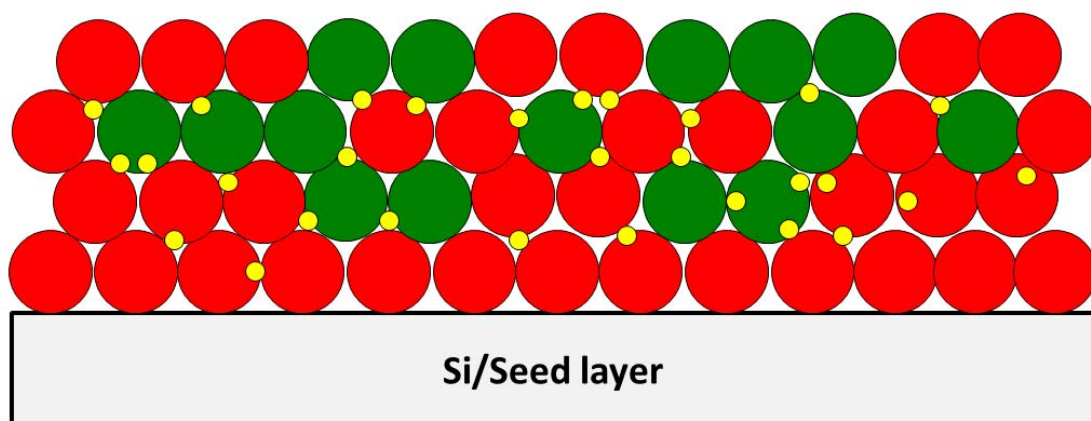
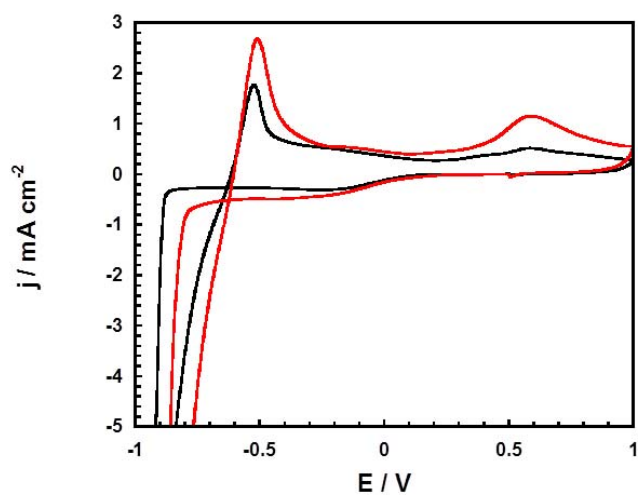
#### Acknowledgments

The authors wish to thank the Serveis Científicotècnics (Universitat de Barcelona) and the Servei de Magnetoquímica (Universitat de Barcelona) for the use of their equipment. This paper was supported by contract MAT2006-12913-C02-01 from the *Comisión Interministerial de Ciencia y Tecnología (CICYT)*.

#### References

- [1] M. Onoda, K. Shimizu, T. Tsuchiya, T. Wanabe, J. Magn. Magn. Mater. 126 (1993) 595.
- [2] T. Osaka, Electrochim. Acta 42 (1997) 3015.
- [3] T. Osaka, T. Sawaguchi, F. Mizutani, T. Yokoshima, M. Takai, Y. Okinaka, J. Electrochem. Soc. 146 (1999) 3295.
- [4] I. Tabakovic, V. Inturi, S. Riemer, J. Electrochem. Soc. 149 (2002) C18.
- [5] F. Lallemand, D. Comte, L. Ricq, P. Renaux, J. Pagetti, C. Dieppedale, P. Gaud, Appl. Surf. Sci. 225 (2004) 59.
- [6] E. Pellicer, E. Gómez, E. Vallés, Surf. Coat. Technol. 201 (2006) 2351.
- [7] E. Gómez, E. Pellicer, M. Duch, J. Esteve, E. Vallés, Electrochim. Acta 51 (2006) 3214.
- [8] N.V. Myung, D.Y. Park, M. Schwartz, K. Nobe, H. Yang, C.-K. Yang, J.W. Judy, Proc. Electrochem. Soc. PV 2000-29 (2000).
- [9] I. Zana, G. Zangari, J.-W. Park, M.G. Allen, J. Magn. Magn. Mater. 272–276 (2004) e1775.
- [10] P.L. Cavallotti, M. Bestetti, S. Franz, Electrochim. Acta 48 (2003) 3013.
- [11] L. Vieux-Rochaz, C. Dieppedale, B. Desloges, D. Gamet, C. Barragatti, H. Rostaing, J. Meunier-Carus, J. Micromech. Microeng. 16 (2006) 219.
- [12] N. Yasui, A. Imada, T. Den, Appl. Phys. Lett. 83 (2003) 3347.
- [13] K.H. Lee, S.W. Kang, G.H. Kim, W.Y. Jeung, J. Magn. Magn. Mater. 272–276 (2004) e925–e926.
- [14] S. Kulkarni, S. Roy, J. Appl. Phys. 101 (2007) 09K524.
- [15] H.D. Park, K.H. Lee, G.H. Kim, W.Y. Jeung, J. Appl. Phys. 99 (2006) 08N305-1.
- [16] O. Berh, Yu. Rosenberg, Y. Shacham-Diamand, E. Gileadi, Microelectron. Eng. 84 (2007) 2444.
- [17] P.L. Cavallotti, N. Lecis, H. Fauser, A. Zielonka, J.P. Celis, G. Wouters, J. Machado da Silva, J.M. Brochado Oliveira, M.A. Sà, Surf. Coat. Technol. 105 (1998) 232.
- [18] E. Gómez, R. Pollina, E. Vallés, J. Electroanal. Chem. 386 (1995) 45.
- [19] P. Garrido, E. Gómez, E. Vallés, J. Electroanal. Chem. 441 (1998) 147.
- [20] E. Pellicer, E. Gómez, E. Vallés, Surf. Coat. Technol. 201 (2006) 2351.
- [21] H. Angerstein-Kozłowska, B.E. Conway, W.B.A. Sharp, J. Electroanal. Chem. 43 (1973) 9.
- [22] J. Clavilier, D. Armand, J. Electroanal. Chem. 199 (1986) 187.
- [23] A. Boulitf, D. Louër, J. Appl. Cryst. 37 (2004) 724.

## 5.2.2 Magnetic properties of nanocrystalline CoPt electrodeposited films. Influence of P incorporation



# Magnetic properties of nanocrystalline CoPt electrodeposited films. Influence of P incorporation

Meritxell Cortés · Elvira Gómez · Elisa Vallés

Received: 18 January 2010 / Revised: 15 March 2010 / Accepted: 16 March 2010 / Published online: 14 April 2010  
© Springer-Verlag 2010

**Abstract** Platinum-rich CoPt films have been electrodeposited with the aim of preparing hard magnetic films on silicon-based substrates without the need for subsequent annealing. Electrodeposition conditions have permitted the crystalline structure of the films to be controlled. Pt percentages of up to 60–65 wt.% have been attained while maintaining the hexagonal Co phase, leading to CoPt films with moderate coercivity and good corrosion resistance. However, when low deposition potentials were used, CoPt films with higher Pt percentages were obtained, but in this case, the films exhibited an fcc structure, having lower coercivity and less corrosion resistance. The presence of hypophosphite in the solution limited the platinum percentage in the deposited CoPtP films, but an hexagonal close-packed (hcp) structure was always observed in this case. The incorporation of P into the deposits led to increases in both the coercivity of the films and the corrosion resistance of the coatings, with respect to pure CoPt. The highest coercivity was obtained for hcp CoPtP deposits with 40 wt.% of Pt.

**Keywords** Electrodeposition · Magnetic films · Cobalt–platinum–phosphorous alloy · X-ray diffraction · Corrosion resistance

## Introduction

Microelectromechanical systems (MEMS) are the integration of mechanical elements, sensors, actuators, and electronics on a substrate, commonly silicon, through microfabrication technology. Recently, there has been growing interest in how magnetic materials could be incorporated into MEMS devices for sensors or actuator applications. Electrochemical methods can be used in order to prepare magnetic materials compatible with MEMS processing. Electrodeposition has several advantages over other techniques, including the low cost and simplicity of the experimental setup, not requiring high temperatures or vacuum conditions. Moreover, it permits easy control of the growth process, film thickness, and chemical composition of the layer. Additionally, electrochemistry is fully compatible with microfabrication processes and has been used to prepare several micron-thick deposits of metals, alloys, and compounds on various substrates.

In our laboratory, soft magnetic layers of CoNi have been prepared by electrodeposition over silicon/seed layer substrates and incorporated as mobile elements in microvalves [1]. Although most of the magnetic microactuators developed by different researchers use soft magnetic materials [2–4], hard magnetic materials are also desirable in some applications (microsized motors, minipumps, microactuators) [5, 6]. The preparation of hard magnetic deposits by different techniques for MEMS magnetic actuators has recently been studied [7–14]. In this paper, we investigate how electrochemical deposition of microscale permanent magnets can be achieved for implementation in microactuators devices. The incorporation of ferromagnetic particles into a CoNi alloy matrix by means of electrodeposition has been studied as a way of preparing

M. Cortés · E. Gómez · E. Vallés (✉)  
Electrodep, Departament de Química Física and Institut de  
Nanociència i Nanotecnologia (IN2UB),  
Universitat de Barcelona,  
Martí i Franquès 1,  
08028 Barcelona, Spain  
e-mail: e.valles@ub.edu

hard magnetic films [15]. Another possibility is the direct electrodeposition of hard magnetic films over the silicon/seed-layer substrate. The most common hard magnetic materials are CoPt, FePt, and rare earths as  $\text{Nd}_2\text{Fe}_{14}\text{B}$  or  $\text{SmCo}_5$  [16–18], although the codeposition of rare earth magnetic thin films implies the use of organic solvents and the application of high negative potentials. Co-based alloys, such as CoNiP [7, 14, 19], CoP [20], CoPt [21–23], or CoPtP [20, 24–26], have been electrodeposited, resulting in high coercivity films. In these studies, a subsequent annealing step after following deposition is usually necessary in order to obtain the desired hard magnetic response. In our previous work, solutions for simultaneous deposition of Co, Pt, and P were tested [27].

Here, we report the preparation of platinum-rich CoPt films in order to obtain hard magnetic films deposited on silicon/seed-layer substrates without the need for subsequent annealing of the deposited films. High Pt percentages were desired for enhancing the magnetic anisotropy of the cobalt phase. Different deposition conditions will be characterized in order to obtain films with a composition and structure optimized for maximum coercivity, maximum permeability, and good corrosion resistance, desirable properties for use in magnetic microdevices. The influence of the P incorporation in the magnetic, structural, morphological, and corrosion-resistant properties of the CoPt electrodeposits, as well as the analysis of the changes in the deposition process and in the deposition rate, will be performed.

## Experimental

Solutions containing  $\text{CoCl}_2$ ,  $\text{Na}_2\text{PtCl}_6$ , boric acid, and  $\text{NH}_4\text{Cl}$ , all of analytical grade, were used to perform the CoPt electrodeposition in a three-electrode cell with control of the temperature. A solution containing  $2.5 \times 10^{-3} \text{ M CoCl}_2 + 1.2 \times 10^{-3} \text{ M Na}_2\text{PtCl}_6 + 1 \text{ M NH}_4\text{Cl} + 30 \text{ g dm}^{-3} \text{ H}_3\text{BO}_3$  was mainly used, although for some experiments the  $[\text{Na}_2\text{PtCl}_6]/[\text{CoCl}_2]$  was decreased. Solutions were deaerated by argon bubbling before each experiment and then maintained under argon atmosphere. Sodium hypophosphite ( $10^{-2} \text{ M NaH}_2\text{PO}_2$ ) was used to induce phosphorous incorporation into some deposits. The pH of the solutions was adjusted to 4.5 to simultaneously avoid the precipitation of platinum oxides and the excessive evolution of hydrogen. Different temperatures (25 °C, 40 °C) have been tested. Stirring of the solution (60, 1,100 rpm) was maintained during the electrodeposition to assure a constant composition throughout the deposits.

A microcomputer-controlled potentiostat/galvanostat Autolab with PGSTAT30 equipment and GPES software was used for deposits preparation over silicon/Ti (1,000 Å)/

Ni (500 Å) substrates (supplied by IMB-CNM.CSIC). These substrates were cleaned with acetone and ethanol and rinsed in water before deposition. The reference electrode was an Ag/AgCl/1-mol  $\text{dm}^{-3}$  NaCl electrode. All potentials were referred to this electrode. The counter electrode was a platinum spiral.

Corrosion test was carried out at 25 °C in a 5% NaCl (p.a.) solution. The films on 0.3-cm<sup>2</sup> silicon-based substrates were immersed in NaCl media for 3 h in order to determine the steady-state potential ( $E_{\text{ss}}$ ). Immediately afterward, a linear potentiodynamic sweep between  $\pm 300 \text{ mV}/E_{\text{ss}}$  was performed at  $0.1 \text{ mV s}^{-1}$  to find out corrosion potential ( $E_{\text{corr}}$ ) and corrosion current density ( $j_{\text{corr}}$ ). Nonstirring conditions were used during both polarization and potentiodynamic scan.

Leica Stereoscan S-360 and Hitachi H-4100FE scanning electron microscopes (SEM) were used to analyze deposits composition and for morphology observation, respectively. Structure of deposits were studied by means of a Philips MRD diffractometer with parallel optical geometry using Cu  $K\alpha$  radiation ( $\lambda=0.1542 \text{ nm}$ ) and a texture goniometer that allows control of the sample rotation about the three axes.

Magnetic properties were characterized by means of a SQUID magnetometer at room temperature. Thicknesses of the coatings were measured using a Zygo NEW VIEW 100 white-light interferometer.

## Results and discussion

### Deposits preparation

Films were prepared potentiostatically or galvanostatically. Figure 1 shows representative transients corresponding to the electrodeposition. Potentiostatic curves obtained under stirring conditions showed (Fig. 1a, b) monotonic growth of the current density with time. Similar deposition rate was obtained at fixed potential in the presence or in absence of the hypophosphite in solution (in the range 500–700 nm/h). However, clear differences in the Pt percentage of the films were observed: Pt percentage decreased from 59.6 wt.% from free-hypophosphite bath to 38.7 wt.% Pt in the solution containing hypophosphite, and a 3.3 wt.% in P was detected.

When the galvanostatic technique was used, very negative potential values were attained to induce nucleation of the metals (nucleation spike). Subsequent stabilization of the potential occurred at longer deposition times, corresponding to the growth of the deposit over the initial nuclei formed. By comparing the  $E-t$  transients recorded at the same current density ( $-4 \text{ mA cm}^{-2}$ ; Fig. 1c), less negative stabilization potentials were observed for CoPt

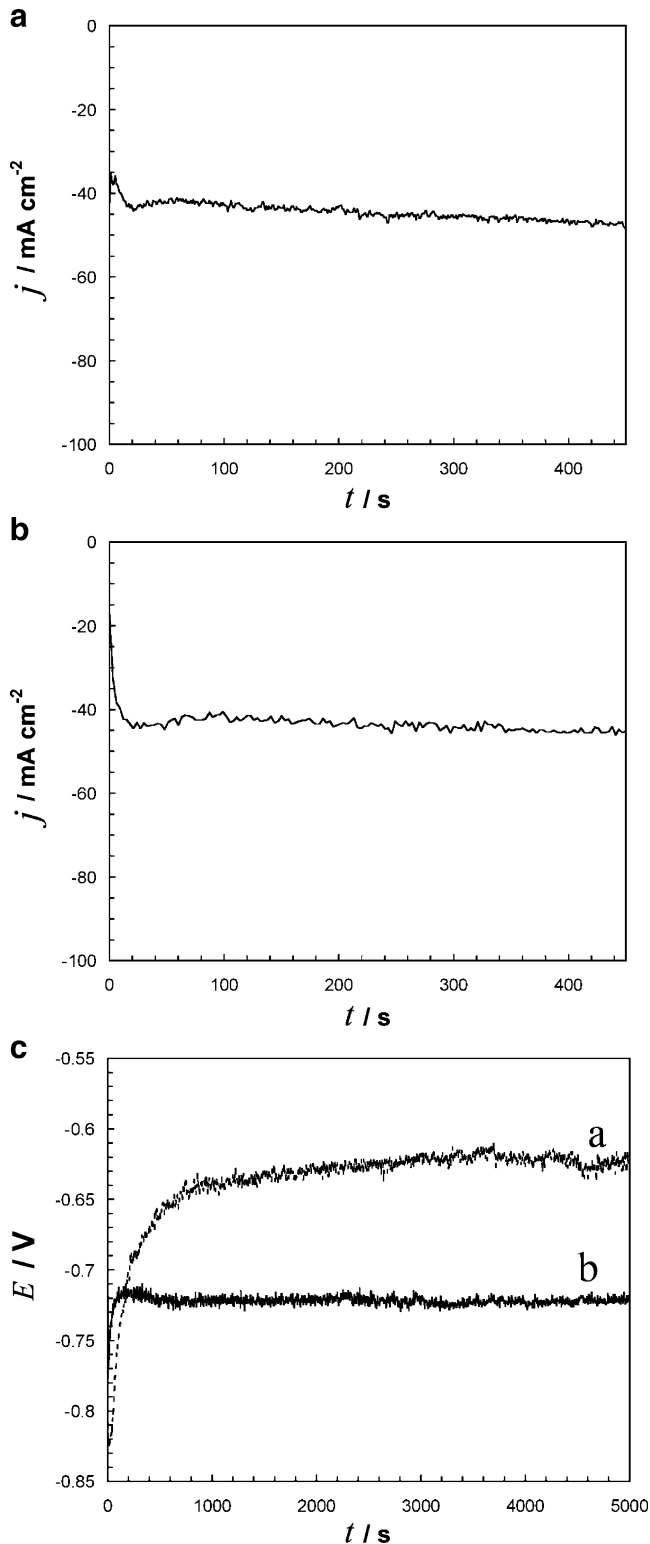


**Fig. 1** Potentiostatic curves at  $-950$  mV of a bath containing  $2.5 \times 10^{-3}$  M  $\text{CoCl}_2 + 1.2 \times 10^{-3}$  M  $\text{Na}_2\text{PtCl}_6 + 1$  M  $\text{NH}_4\text{Cl} + 30$  g dm<sup>-3</sup>  $\text{H}_3\text{BO}_3$ . **a** Without hypophosphite, **b** with  $10^{-2}$  M  $\text{NaH}_2\text{PO}_2$ . **c** Galvanostatic curves at  $-4$  mA cm<sup>-2</sup> of **a** the same solution as **a**, **b** the same solution than **b**.  $T=40$  °C.  $\omega=60$  rpm

deposition (Fig. 1c, curve a) leading to platinum-rich CoPt deposits (77.4 wt.% Pt). For the same applied current density, more negative potentials were necessary to maintain the electrodeposition in the presence of phosphorous compound (Fig. 1c, curve b), and as a consequence, more cobalt-rich deposits were obtained (56 wt.% Co, 3 wt.% P). In the absence of hypophosphite, wide nucleation spike was obtained due to the significant simultaneous hydrogen evolution during platinum formation, which makes slow the nucleation process. Several authors have detected the capability of adsorption of hypophosphite anion over several metals as Ni, Co, Pd, and Pt [28–31]. Then, in the presence of hypophosphite, its adsorption over the first nuclei shifts both electrodeposition process and hydrogen evolution to more negative potentials. Then, growth of the deposit takes place at more negative potentials, and cobalt percentage in the deposits increased.

#### CoPt films

The CoPt films prepared were rich in platinum (Table 1). At one fixed deposition potential, composition has low temperature dependence, so 40 °C was selected as preparation temperature in order to attain higher deposition rates. For high deposition charge, it was possible to maintain a nearly constant composition, avoiding the decrease of the Pt percentage by providing a vigorous stirring to the solution (1,100 rpm) which permitted the removal of the evolved hydrogen present. After increasing the Co/Pt ratio, high cobalt content was detected in the deposits.

Deposits with nanometric thickness ( $<1$   $\mu\text{m}$ ) containing 60–65 wt.% Pt were very smooth and reflective. Morphological analysis made by FE-SEM showed that they were formed by polyhedral fine grains (Fig. 2a). More compact and uniform deposits with smaller grain sizes were obtained for CoPt deposits by increasing the deposition charge, attaining micrometric thickness of the films (Fig. 2b), probably as a consequence of that the higher stirring rate used in these conditions favor both electroactive species approach and simultaneous hydrogen detachment. The observed morphology is characteristic of cobalt deposits showing hexagonal close-packed (hcp) structure [32]. The X-ray diffractograms of these CoPt deposits showed, next to some peaks corresponding to the substrate (\*), diffraction peaks assigned to an hcp phase (Fig. 3a). However, the high incorporation of Pt in the deposits led to an hcp structure very distorted respect to that corresponding to pure hcp Co. The diffraction peak positions corresponding to the hcp phase shifted to lower  $2\theta$  values, indicating that platinum incorporation leads to greater lattice spacing with respect to the pure hcp cobalt phase. Using the DICVOL04 indexation program [33], the cell parameters of the hexagonal phase

**Table 1** Composition of CoPt deposits prepared in different conditions

Sample	$-E$ (mV)	$-j$ (mA cm $^{-2}$ )	Stirring (rpm)	$-Q$ (C cm $^{-2}$ )	$T$ (°C)	wt.% Co	wt.% Pt
A1 <sup>a</sup>	950		60	20	40	40.4	59.6
A2 <sup>a</sup>	950		60	20	25	35.1	64.9
A3 <sup>a</sup>	950		60	30	40	37.4	62.6
A4 <sup>a</sup>	950		1,100	190	40	41.4	58.6
A5 <sup>a</sup>	950		1,100	276	40	39.6	60.4
A6 <sup>a</sup>		4	60	20	40	22.6	77.4
A7 <sup>a</sup>		4	60	67	40	20.6	79.4
B1 <sup>b</sup>	950		60	20	40	60.9	39.1

<sup>a</sup>  $2.5 \times 10^{-3}$  M CoCl $_2$  +  $1.2 \times 10^{-3}$  M Na $_2$ PtCl $_6$  + 1 M NH $_4$ Cl + 30 g dm $^{-3}$  H $_3$ BO $_3$  solution

<sup>b</sup>  $5 \times 10^{-3}$  M CoCl $_2$  +  $1 \times 10^{-3}$  M Na $_2$ PtCl $_6$  + 1 M NH $_4$ Cl + 30 g dm $^{-3}$  H $_3$ BO $_3$  solution

were within the range of  $a=0.260$ – $0.261$  nm and  $c=0.422$ – $0.424$  nm corresponding to a cell volume ( $V$ ) of  $0.0247$ – $0.0250$  nm $^3$ . From the broadening of the peaks, one can estimate the crystalline size domains using the Debye–Scherrer formula [34]. From the full width at half maximum values of the diffraction peaks corresponding to the 100 and 002 reflections and taking into account the instrumental linewidth, the estimated value of the crystalline domains was in the range of 20–25 nm, as corresponds to a nanocrystalline material.

These deposits showed coercivity values around 700 Oe and a high value of the  $M/H$  slope, revealing high

permeability of the films (Fig. 3b). The incorporation of significant proportion of Pt in the hcp phase of Co led to a drastic increase of the coercivity of the films with respect to pure Co films [35] due to the high anisotropy induced. Higher Pt percentages in the deposits (>70 wt.%) were obtained applying low current densities ( $-4$  mA cm $^{-2}$ ) as corresponds to the low stabilization potential attained ( $-600$  mV). These platinum-rich layers showed nodular morphology (Fig. 4a) with around 100 nm of grain size. No polyhedral morphology was observed and a drastic decrease of the coercivity value was observed (Fig. 4b), probably as a consequence of a structural changes, no longer being the hexagonal phase. Actually, the XRD of these deposits showed that close to the peaks corresponding to the substrate, wide peaks assigned to the layer, revealing the nanometric size of the crystalline domains in the CoPt electrodeposits. An fcc phase was observed instead of an hexagonal one, as a consequence of the increase on Pt percentage (Fig. 4c), justifying the drastic different magnetic behavior of the coatings. For the fcc phase, the cell parameter estimated for CoPt deposits of 77 wt.% Pt was  $a=0.380$  nm and the cell volume ( $V$ ) was  $0.0549$  nm $^3$ . A significant decrease of the crystalline domains was detected from the CoPt hcp to CoPt fcc phase due to Scherrer estimation led to a 7-nm value.

Corrosion experiments were carried out in order to evaluate whether the corrosion resistance was sensitive to the structure and morphology of the prepared CoPt deposits. Figure 5 shows the potentiodynamic polarization curves corresponding to different CoPt deposits. This figure indicates that hcp CoPt samples (B1, curve a and A1, curve b) show better corrosion resistance than the fcc CoPt (sample A6, curve c) because the corrosion potential values ( $E_{\text{corr}}$ ) were more positive for CoPt deposits of hcp structure than for that presenting fcc structure. Moreover, for hcp CoPt coatings, the corrosion potential moved positively with increasing Pt content in the deposits (sample B1 39.1 wt.% Pt, sample A1 59.6 wt.% Pt). Higher  $j_{\text{corr}}$  was obtained for deposits with the fcc structure, corresponding to a higher corrosion rate (Table 2). A clear relation between composition, morphology, crystalline structure,

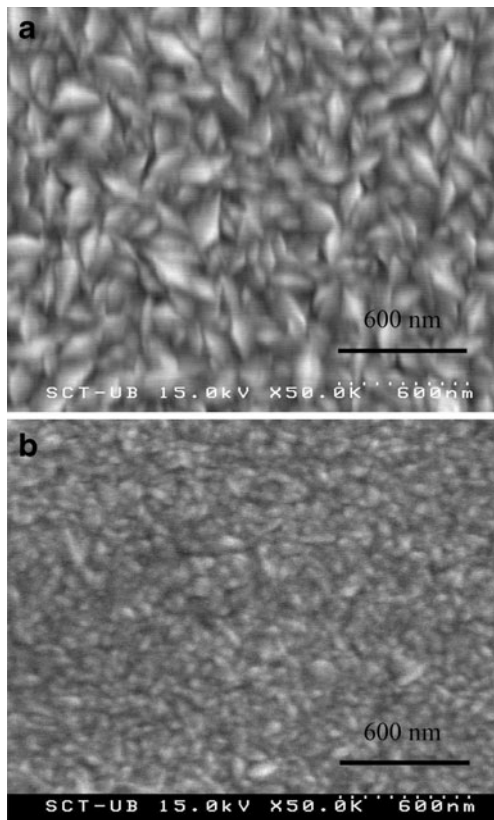
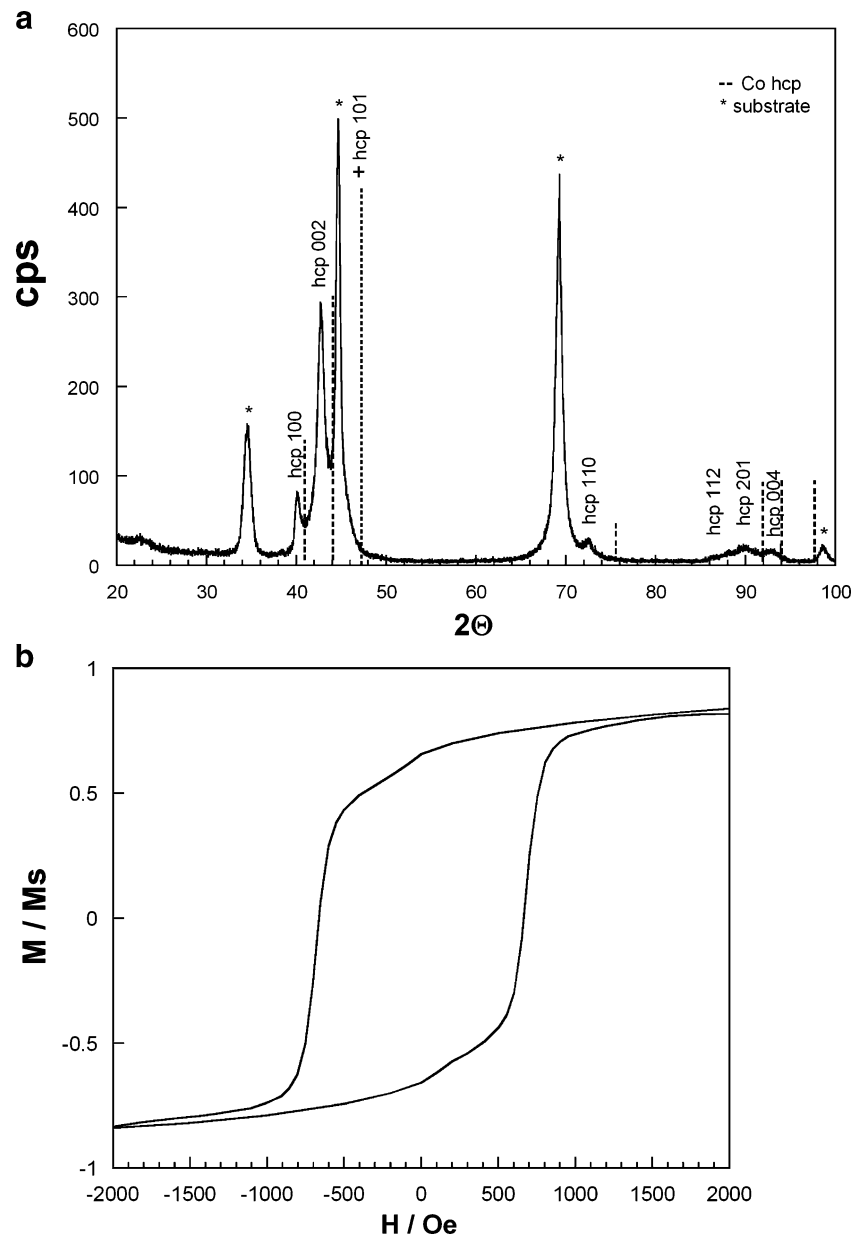


**Fig. 2** FE-SEM images of CoPt deposits obtained from the solution of Fig. 1 at  $-950$  mV. **a** Sample A3, thickness 180 nm, **b** sample A5, thickness 1.5  $\mu$ m

**Fig. 3** **a** X-ray diffractogram of a CoPt deposit of 150 nm (sample A1), **b** normalized room temperature magnetization curve taken with the applied field parallel for a CoPt deposit of 150 nm (sample A2)



magnetic behavior, and corrosion resistance was observed for the CoPt prepared electrodeposits from the selected solution. CoPt hexagonal films showing polyhedral morphology presented more accused hard magnetic behavior and better corrosion resistance.

#### Influence of P in CoPt deposits

For the deposits prepared from the solution containing hypophosphite, P was moderately incorporated while Pt percentage decreased (Table 3). A limit in the Pt percentage in the ternary deposits was observed in the presence of hypophosphite because no more of 45 wt.% was obtained, while 60–65 wt.% was obtained from the same solution but in the absence of hypophosphite. For the ternary CoPtP

deposition, it was difficult to maintain the deposits composition for high deposition charges, even under vigorous stirring conditions of the solution. A decrease of P incorporation was observed by increasing significantly deposition charge. Moreover, a higher increase of the deposition charge led to a decrease in Pt percentage in the deposits (Table 3). In the presence of hypophosphite, the polyhedral morphology of the films was lost, although deposits were rich in cobalt, probably as a consequence of the P incorporation into the deposits. Rounded grains of nanometric size (60–100 nm; Fig. 6a) were observed. Nodular morphology was maintained by increasing deposition charge (Fig. 6b).

Deposits prepared galvanostatically present different morphology as a function of the current density applied as

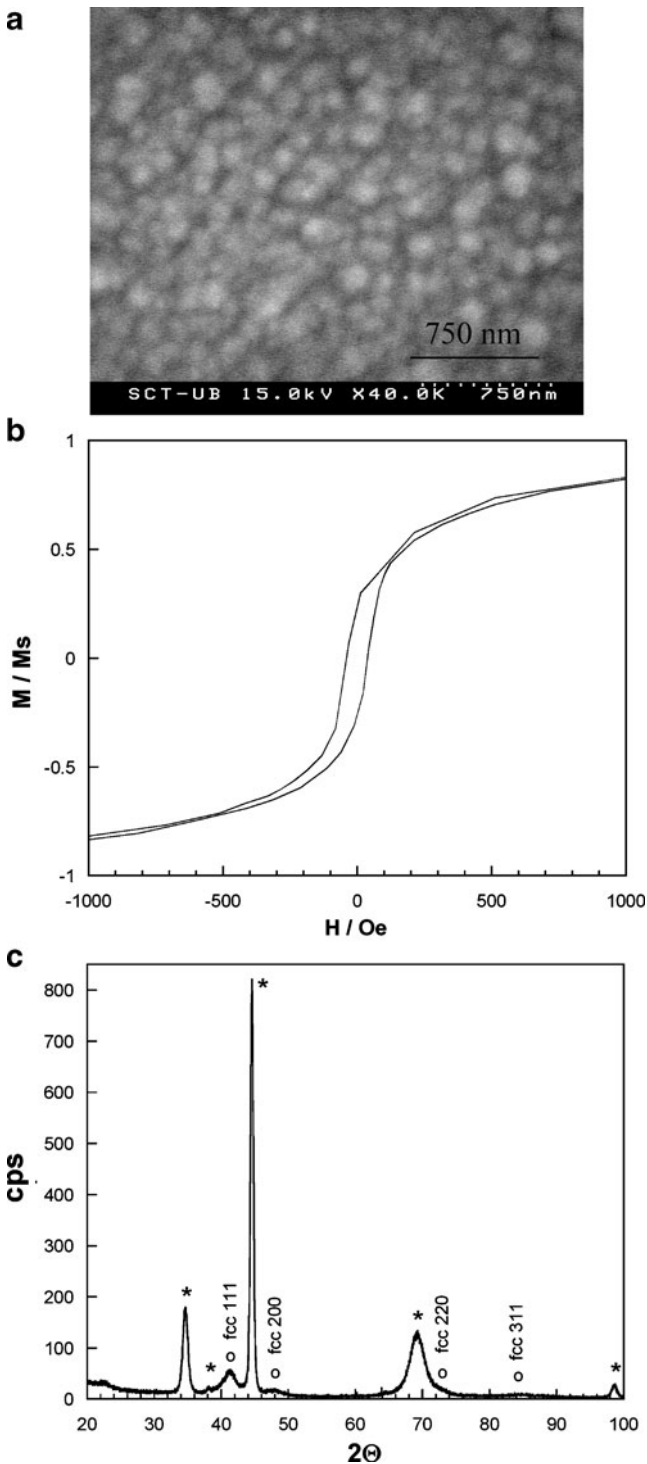


**Fig. 4** **a** FE-SEM image of a CoPt deposit of 155 nm (sample A6), **b** normalized room temperature magnetization curve taken with the applied field parallel, and **c** X-ray diffractogram of the same deposit

it led to different stabilization potential ( $-690$  mV at  $-4$  mA  $\text{cm}^{-2}$  (Fig. 6c, d) and  $-900$  mV at  $-25$  mA  $\text{cm}^{-2}$  (Fig. 6e)): Low current densities led to coral-like no uniform deposits whereas more compact deposits were

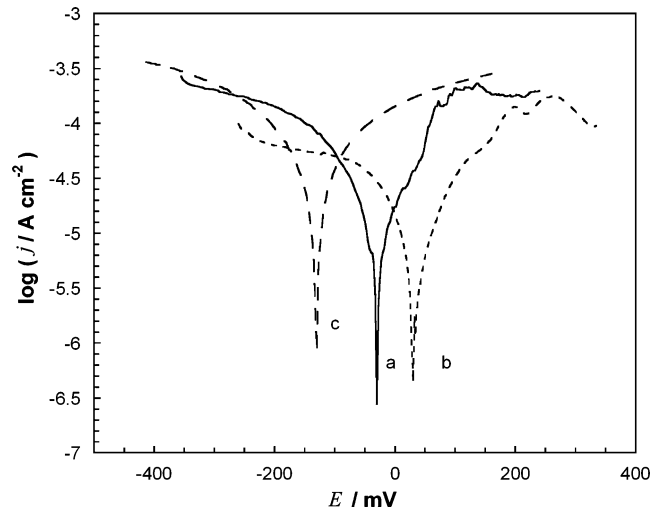


**Fig. 5** Potentiodynamic polarization curves in logarithmic scale corresponding to CoPt deposits of around 120–150 nm. **a** Sample B1, hcp phase; **b** sample A1, hcp phase; **c** sample A6, fcc phase

obtained by increasing current densities. In this case, cracked films were obtained that evolved to more compact and less cracked ones by increasing their thickness (Fig. 6f).

High coercivity values were obtained (Fig. 7a) for deposits containing P. Hard magnetic properties can be enhanced due to the segregation of P at grain boundaries, forming defects sites capable to behave as pinning sites against domain wall motion [36]. CoPtP deposits showed hcp structure (Fig. 7b) with Pt incorporation into the cobalt lattice, independently of the deposition technique used (potentiostatic or galvanostatic). Cell parameters for CoPtP deposits with 40 wt.% Pt were  $a=0.255$  nm,  $c=0.418$  nm, and  $V=0.0235$  nm<sup>3</sup>, lower than those obtained for pure-CoPt films as a consequence of the lower Pt incorporation. Then, high coercivities of the CoPt films containing phosphorous can be originated by the combination of the high magnetic anisotropy of the hexagonal phase and the presence of nonmagnetic precipitates that hinder domain wall motion. CoPtP deposits showing Pt percentages around 40 wt.% and some P incorporation showed the maximum coercivity (1,300–1,400 Oe), but lower permeability than pure CoPt deposits. The comparison of the magnetic properties of the films prepared at different deposition charges revealed similar magnetic behavior,

**Table 2** Corrosion potentials ( $E_{\text{corr}}$ ) and corrosion current densities ( $j_{\text{corr}}$ ) of CoPt deposits

Crystalline structure	Co (wt.%)	Pt (wt.%)	$E_{\text{corr}}$ (mV)	$j_{\text{corr}}$ ( $\mu\text{A cm}^{-2}$ )
hcp	60.9	39.1	-31	0.40
hcp	40.4	59.6	30	0.46
fcc	22.6	77.4	-130	0.68

**Table 3** Composition of CoPtP deposits prepared at 40 °C in different conditions from  $2.5 \times 10^{-3}$  M  $\text{CoCl}_2 + 1.2 \times 10^{-3}$  M  $\text{Na}_2\text{PtCl}_6 + 1$  M  $\text{NH}_4\text{Cl} + 30$  g  $\text{dm}^{-3}$   $\text{H}_3\text{BO}_3 + 10^{-2}$  M  $\text{NaH}_2\text{PO}_2$  solution

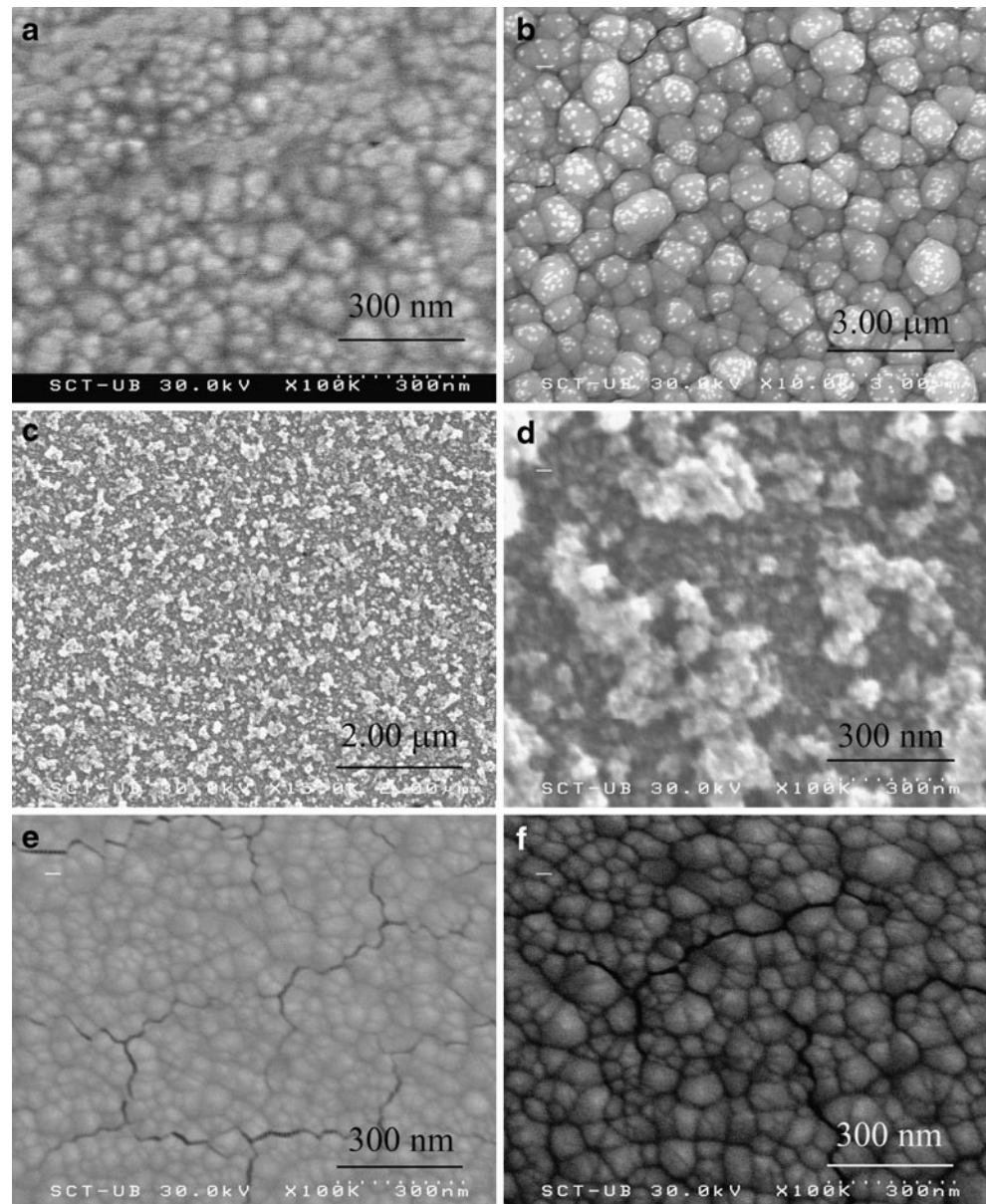
Samples	$-E$ (mV)	$-j$ ( $\text{mA cm}^{-2}$ )	Stirring (rpm)	$-Q$ ( $\text{C cm}^{-2}$ )	wt.% Co	wt.% Pt	wt.% P
C1	950		60	20	58.0	38.7	3.3
C2	950		1,100	170	58.3	41.3	0.4
C3	950		1,100	290	74.5	25.4	0.1
C4		4	60	20	55.8	40.8	3.4
C5		25	60	20	52.0	45.2	2.8
C6		25	60	40	55.1	44.6	0.3

although at high deposition charges, the decrease of both platinum and phosphorous percentages may decrease the coercivity and increase the susceptibility of the deposit.

Corrosion resistance of CoPtP was analyzed and compared with that corresponding to CoPt deposits of similar Pt

percentage and same structural phase (hcp; Fig. 8). Even in the presence of low P percentages in the deposits, a shift of the corrosion potential to more positive values was observed for CoPtP films respect to CoPt ones (120 mV for CoPtP and  $-31$  mV for CoPt); the corrosion current

**Fig. 6** FE-SEM images of different CoPtP deposits obtained from a  $2.5 \times 10^{-3}$  M  $\text{CoCl}_2 + 1.2 \times 10^{-3}$  M  $\text{Na}_2\text{PtCl}_6 + 1$  M  $\text{NH}_4\text{Cl} + 30$  g  $\text{dm}^{-3}$   $\text{H}_3\text{BO}_3 + 10^{-2}$  M  $\text{NaH}_2\text{PO}_2$  solution. **a** Sample C1, thickness 130 nm. **b** Sample C2, thickness 1.0  $\mu\text{m}$ . **c, d** Sample C4, thickness 145 nm. **e** Sample C5, thickness 120 nm. **f** Sample C6, thickness 306 nm



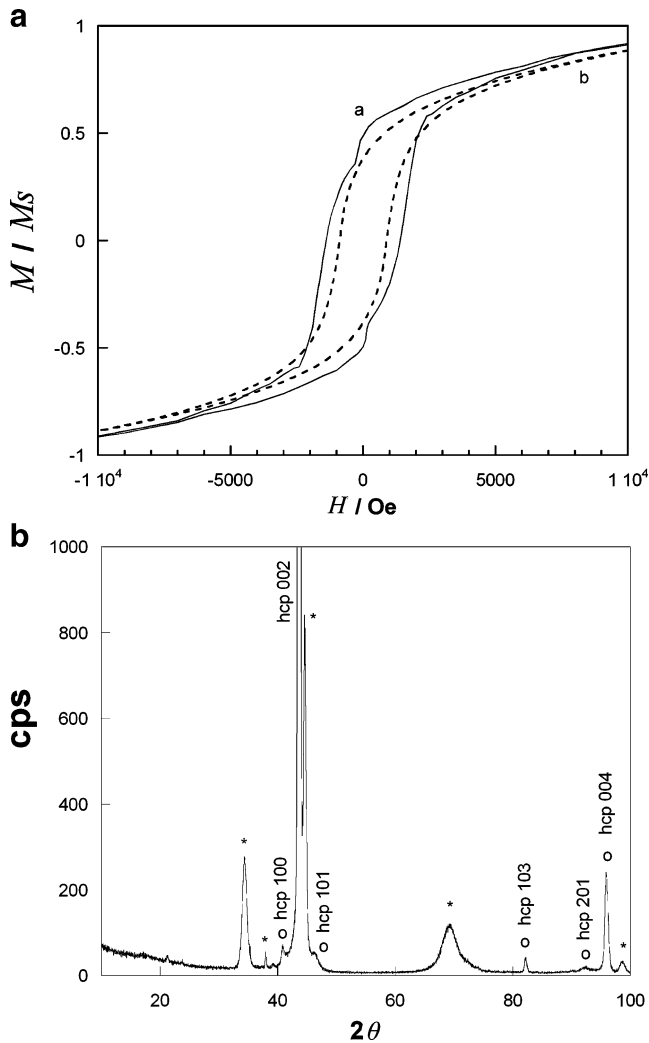


**Fig. 7** **a** Normalized room temperature magnetization curves taken with the applied field parallel of CoPtP deposits. *a* Sample C1, thickness 130 nm; *b* sample C3, thickness 1.4  $\mu\text{m}$ . **b** X-ray diffractogram of the deposit of sample C1

densities are lower for CoPtP ( $0.17 \mu\text{A cm}^{-2}$ ) than for CoPt ( $0.40 \mu\text{A cm}^{-2}$ ). The presence of P makes nobler the alloy respect to pure CoPt in a similar way that the phosphorous inclusion in some nanocrystalline metals as Ni or Co improves their corrosion resistance, even for low P percentages [37, 38]. The possible segregation of P in the grain boundaries or the enrichment of P on the surface seems to minimize the corrosion process of the alloy. Then, the incorporation of P in the deposits led to films with higher coercivity and better corrosion resistance properties.

## Conclusions

It was possible to electrodeposit CoPt and CoPtP films of different thickness over silicon/seed layer. The presence of hypophosphite in the bath did not affect the deposition rate

of the deposits. However, differences in the nucleation process were observed that entailed differences in the deposits compositions, limiting the Pt percentage in the deposits obtained from the bath containing hypophosphite. For CoPt deposits, it was possible to maintain a constant composition for different deposition charges, whereas for CoPtP deposits, the P and Pt percentages decrease by increasing deposition charge.

For pure-CoPt deposits, it was possible to control the films properties (morphology, crystalline structure, magnetic behavior, and corrosion resistance) as a function of the applied potential/current density and, as a consequence, of the films composition. Low deposition potentials (around  $-600 \text{ mV}$ ) led to CoPt films with a Pt percentage around 75 wt.%, nodular morphology, fcc structure, and low coercivity. More negative deposition potentials (around  $-950 \text{ mV}$ ) allowed obtaining CoPt films with Pt percentage up to 65 wt.%, polyhedral fine grains, Co hcp structure distorted due to Pt incorporation, higher coercivity, tending to hard magnetic behavior, and better corrosion resistance. Nanocrystalline domains were present in both cases.

The presence of hypophosphite in the chloride bath induced the incorporation of low P percentages in the CoPt deposits but modified the magnetic and corrosion resistance properties of the films. Since the hypophosphite presence in the electrolytic bath tested limited the Pt incorporation, the more anisotropic hcp structure of the films was maintained and the formation of a Pt-rich fcc structure that presented worse hard magnetic and corrosion resistance properties was avoided. However, the presence of hypophosphite in the bath led to a change in the morphology of the deposits that evolved from polyhedral to nodular ones, although they were nanocrystalline in both cases. Hard magnetic behavior

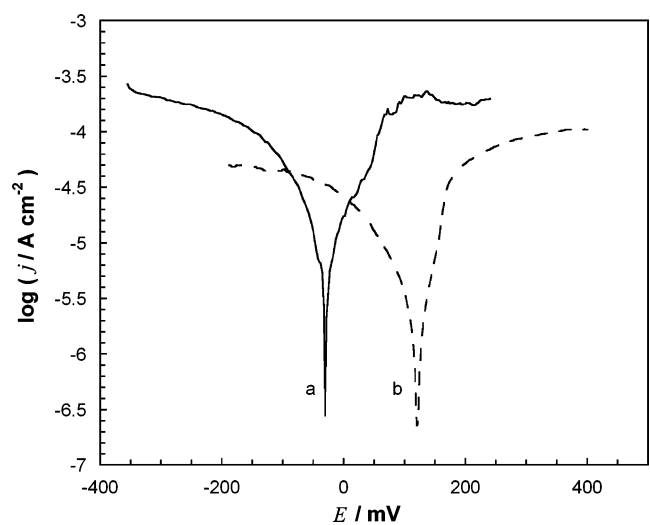


**Fig. 8** Potentiodynamic polarization curves in logarithmic scale corresponding to *a* sample B1, thickness 140 nm, *b* sample C5, thickness 110 nm

and corrosion resistance were enhanced probably as a consequence of P segregation between the magnetic grains. The maximum coercivity value (1,400 Oe) was obtained from CoPtP deposits with Pt percentages of 40 wt.%. This entails profits because better coercivity values were obtained from CoPtP films with 40 wt.% than CoPt films with high Pt percentages (60 wt.%), being more economic the preparation process. The P incorporation also improves the corrosion resistance of the deposit. So these deposits are promising layers to be incorporated in magnetic MEMS devices.

**Acknowledgments** The authors wish to thank the Serveis Científicotècnics (Universitat de Barcelona) and the Servei de Magnetoquímica (Universitat de Barcelona) for the use of their equipment. This paper was supported by contract MAT2006-12913-C02-01 from the Comisión Interministerial de Ciencia y Tecnología (CICYT).

## References

- Casals-Terré J, Duch M, Plaza JA, Esteve J, Pérez-Castillejos R, Vallés E, Gómez E (2008) *Sens Actuators, A, Phys* 147:600
- Osaka T, Sawaguchi T, Mizutani F, Yokoshima T, Takai M, Okinaka Y (1999) *J Electrochem Soc* 146:3295
- Tabakovic I, Inturi V, Riemer S (2002) *J Electrochem Soc* 149: C18
- Lallemand F, Comte D, Ricq L, Renaux P, Pagetti J, Dieppedale C, Gaud P (2004) *Appl Surf Sci* 225:59
- Chin TS (2000) *J Magn Magn Mater* 209:75
- Cho HJ, Ahn CH (2002) *J Microelectromechanical Syst* 11:78
- Park DY, Myung NV, Schwartz M, Nobe K (2002) *Electrochim Acta* 47:2893
- Myung NV, Park DY, Yoo BY, Sumodjo PTA (2003) *J Magn Magn Mater* 265:189
- Niarchos D (2003) *Sens Actuators A Phys* 109:166
- Guan S, Nelson BJ (2005) *Sens Actuators A Phys* 118:307
- Guan S, Nelson BJ (2005) *J Magn Magn Mater* 292:49
- Su Y, Wang H, Ding G, Cui F, Zhang W, Chen W (2005) *IEEE Trans Magn* 41:4380
- Pigazo F, Palomares FL, Cebollada F, González JM (2008) *J Magn Magn Mater* 320:1966
- Lew KS, Rajab M, Thanikaikarasan S, Kim T, Kim YD, Mahalingam T (2008) *Mater Chem Phys* 112:249
- Pané S, Gómez E, Vallés E (2007) *Electrochem Commun* 9:1755
- Xu QY, Kageyama Y, Suzuki T (2005) *J Appl Phys* 97:10K308
- Chen XY, Jiang ZhL, Zhang L, Chen Y, Bai FM, Chen HM, Zhu J (2003) *Mater Sci Forum* 426:2381
- Liu Y, Dallimore MP, McCormick PG, Alonso T (1992) *Appl Phys Lett* 60:3186
- Pattanaik G, Kirkwood DM, Xu X, Zangari G (2007) *Electrochim Acta* 52:2755
- Myung NY, Park DY, Schwartz M, Nobe K, Yang H, Yang CK, Judy JW (2000) *Magnetic materials, processes and devices*. In: Krongelb S, Romankiw LT, Ahn CH, Chang JW, Schwarzacher W (eds) *The electrochemical society proceedings series*. Electrochemical Society, Pennington
- Zuzek-Rozman K, Krause A, Leistner K, Fähler S, Schultz L, Schlorb H (2007) *J Magn Magn Mater* 314:116
- Cavallotti PL, Bestetti M, Franz S (2003) *Electrochim Acta* 48:3013
- Zana I, Zangari G, Park JW, Allen MG (2004) *J Magn Magn Mater* 272–276:e1775
- Lee KH, Kang SW, Kim GH, Jeung WY (2004) *J Magn Magn Mater* 272–276:e925
- Park HD, Lee KH, Kim GH, Jeung WY (2006) *J Appl Phys* 99:08N305
- Vieux-Rochaz L, Dieppedale C, Desloges B, Gamet D, Barragatti C, Rostaing H, Meunier-Carus J (2006) *J Micromech Microeng* 16:219
- Cortés M, Matencio S, Gómez E, Vallés E (2009) *J Electroanal Chem* 627:69
- Oliveira MC, do Rego AMB (2006) *J Alloys Compd* 425:64
- Dulal SMSI, Kim TH, Shin CB, Kim CK (2008) *J Alloys Compd* 461:382
- Cheonga WJ, Luana BL, Shoesmitha DW (2004) *Appl Surf Sci* 229:282
- Homma T, Komatsu I, Tamaki A, Nakai H, Osaka T (2001) *Electrochim Acta* 47:47
- Gómez E, Vallés E (2002) *J Appl Electrochem* 32:693
- Boultif A, Louër D (2004) *J Appl Crystallogr* 37:724
- Cullity BD (1978) *Elements of X-ray diffraction*, 2nd edn. Addison-Wesley, Boston
- García-Torres J, Gómez E, Vallés E (2009) *J Appl Electrochem* 39:233
- Homma T, Sezai Y, Osaka T, Maeda Y, Donnet DM (1997) *J Magn Magn Mater* 173:314
- Burchardt T, Hansen V, Valand T (2001) *Electrochim Acta* 46:2761
- Jung H, Alfantazi A (2006) *Electrochim Acta* 51:1806

### 5.3 Electrodeposition of CoPt micro/nanostructures. Modulation of the magnetic properties

In the last years the study of nanostructured magnetic systems has attracted considerable interest due to their physical and chemical properties and their technological applications. They might be used as media for high density magnetic recording [84] or incorporated in microdevices [85]. One of the main points in the study of such systems is how the magnetic properties change as a function of their shape and size. Clearly, for the development of magnetic devices based on arrays of those nanostructures, not only the nanostructures magnetic properties should be studied but also knowledge of the magnetic behaviour of these structures when forming the array is of fundamental importance.

The most widely studied systems are nanoparticles and nanowires arrangements. Different techniques have been used for the arrays manufacturing [86–96]. One of these techniques has been electrodeposition [97–102]. Electrochemical methods can be used to prepare permanent magnets in the nanoscale for use in micro-devices [103–106].

In the previous section of this chapter two alloys were studied. Considering the advantages and disadvantages of both systems, the rest of the work was performed with the CoPt alloy since it presented faster response to the magnetic applied field and higher magnetic energy product and only a little bit lower corrosion resistance and lower coercivity than CoPtP. Moreover this last disadvantage could be compensated by preparing films of higher Pt percentages and it was a simpler system. The CoPt alloy electrodeposition from a bath containing:  $2.5 \cdot 10^{-3}$  M  $\text{CoCl}_2$  +  $1.2 \cdot 10^{-3}$  M  $\text{Na}_2\text{PtCl}_6$

+ 1M  $\text{NH}_4\text{Cl}$  + 30 g  $\text{dm}^{-3}$   $\text{H}_3\text{BO}_3$  at pH 4.5 was demonstrated and the dependence of the magnetic properties with composition was studied. Deposits with an hcp structure and a high platinum percentage showed the largest coercivity.

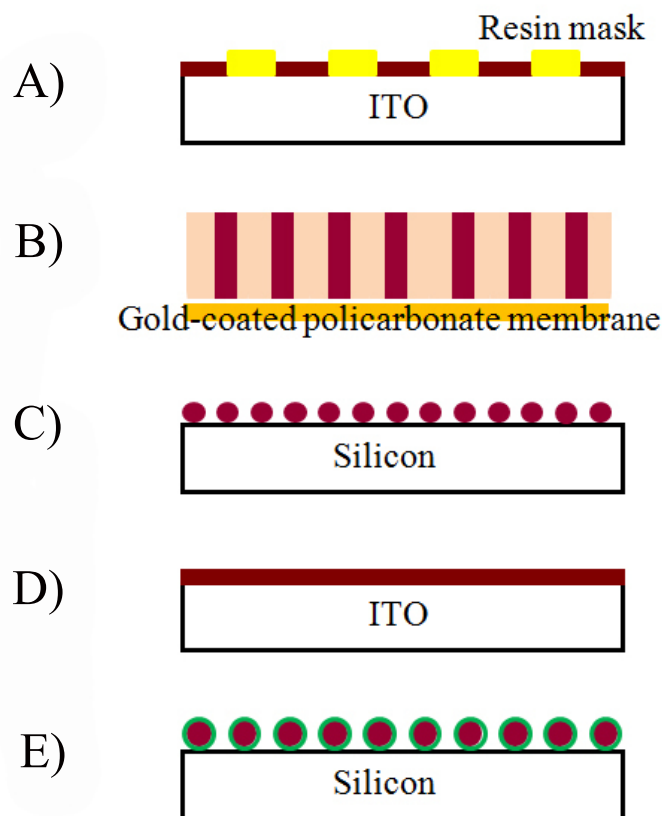


Figure 5.5: Schematic representation of the micro/nanostructures obtained

In this section preparation of micro/nanostructures of platinum-rich CoPt alloy is contemplated in order to modulate their magnetic properties as a function of the shape and size of the deposits. The difficulty of preparation of well-defined structures is always dependent on the dimensions of the pattern (if used) and the characteristics of the used electrolytic

bath [107]. In the literature, baths containing citrate were found to enhance the coercivity [79], for that reason in some cases it was added to the previously mentioned bath, but not remarkable differences were detected in our case. For each kind of structure, a selection of the best non-magnetic electrodes was used to enable simultaneous electrodeposition of the alloy and the measurement of their magnetic properties. Lithographically defined masks, polycarbonate and alumina templates were used in some cases because they permitted the control of both the separation between the nanostructures and their aspect-ratio.

The micro/nanostructures prepared were:

- Squared and lined patterned microstructures of some microns (figure 5.5A)
- Nanowires of different length and width and with different separation between them (figure 5.5B)
- Submicro-particles (figure 5.5C)
- Thin films (figure 5.5D)
- Core-shell submicroparticles (figure 5.5E)

Glass/ITO was the selected substrate for the thin films fabrication because it does not interfere with the magnetic measurements. As it was not very conductive substrate high reduction potentials were applied in order to induce significant nuclei formation. The low conductivity of the substrate permitted to obtain thin films instead of thick ones as the deposition rate was small enough.

A 1.2- $\mu\text{m}$ -thick photolithographed mask over ITO substrate was used to obtain squared and lined patterned microstructures. Although in some cases the presence of a resin difficulties the deposition process, in this case similar potentials to that of thin films preparation were applied because the defined patterns in the mask were big enough to allow the arrival of the electroactive species.

Nanowires were obtained by using both polycarbonate and alumina templates sputtered with Au. Although the movement of the electroactive species into the porous channels is usually difficult, in our case, the presence of the conductive gold seed layer and the size of the porous make the onset of the deposition process easy. The onset of the deposition process occurred at less negative potentials than that of glass/ITO substrates. Due to the commercial alumina membrane presented higher hydrophobicity a more negative potential was necessary in these membranes to attain a similar reduction current than in polycarbonate ones in order to favour the flow of ions through the membrane to reach the gold.

Finally both graphite and silicon electrodes were used for submicroparticles preparation. The silicon substrate was immersed in a 5 (wt/v) % HF solution for 60 s to remove the native silicon oxide prior to electrodeposition took place. In both cases high potentials were applied because of the low conductivity of these substrates. Less negative potentials were used for graphite than for silicon ones. However, these potentials were not as negative as in the case of ITO ones because here a low nucleation rate is desired to obtain the particles.

In all cases, morphology, composition and crystalline phase were studied.

The final objective of this work is the implementation of these structures in MEMS. Due to the small size of the structures and the high proportion of atoms in the surface these structures might be susceptible of being oxidized, for that reason corrosion resistance tests were performed revealing good resistance to oxidation in all the cases. Magnetic properties were analysed and compared (figure 5.6, 5.7 and 5.8).

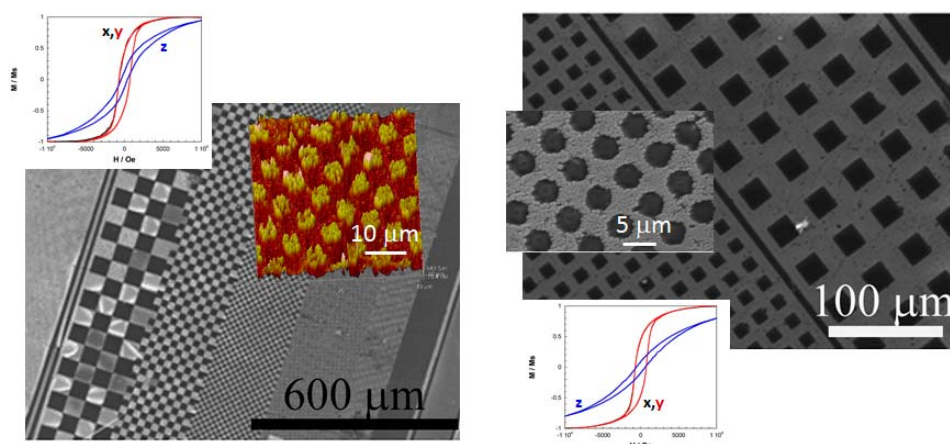


Figure 5.6: Analysis of the magnetic properties of different patterned microstructures in different applied field configurations

The results of this part are presented in the papers: “*Magnetic CoPt (60-70 wt % Pt) microstructures fabricated by the electrochemical method*”, “*Electrochemical growth of CoPt nanowires of different aspect ratio and their magnetic properties*”, “*Electrochemical preparation and characterisation of CoPt magnetic particles*” and “*CoPt nanoscale structures with different geometry prepared by electrodeposition for modulation of their magnetic properties*”.

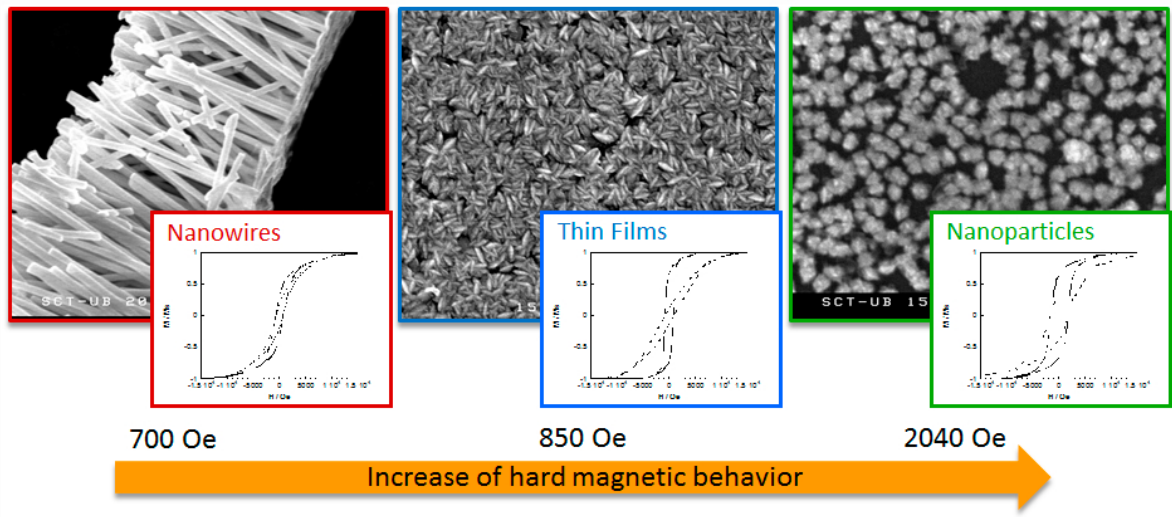


Figure 5.7: Comparison of the magnetic properties of different nanostructures

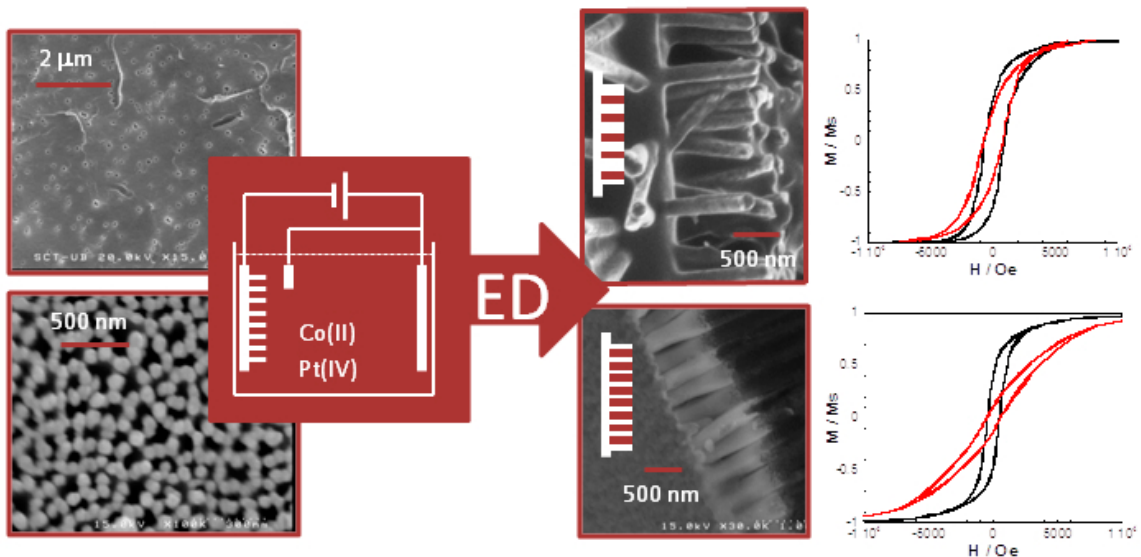


Figure 5.8: Differences in the magnetic properties of the nanowire arrays depending on the distances between nearby nanowires

Finally, core-shell type particles in which the central material is surrounded by a different material are another interesting system. The external material could exert either as protective material [108–111] or to promote novel properties [112–115]. In particular, core-shell nanoparticles

with magnetic core have been extensively prepared from different techniques in order to take advantage of the change of the properties of the ferromagnetic material when its size diminishes. Protective character of the shell is especially important when the ferromagnetic core is unstable toward oxidation in air, which easily occurs when their size becomes small. However, in some occasions core-shell particles with intermediate dimensions (hundreds of nanometers) are of interest because they show magnetic properties greatly different with respect to either nanoparticles or bulk configurations for the same material system [116,117]. For example, when systems in which soft and hard magnetic materials are positioned in contact, these particles can be used in exchange-spring systems, which are based on the exchange coupled of soft and hard ferromagnetic phases. These systems can combine the high magnetization of soft phase with the coercivity of hard phase to attain a high energy product to obtain a maximum magnetic energy product [118–121]. A system is recognized as an exchange spring magnet when both phases are coupled to each other [119,120]. The study of these kinds of systems combining soft and hard ferromagnets has not improved significantly because of the lack of effective fabrication methods. It is desirable to work with moderate particle size of soft and hard phases, which guarantees a high remanence and sufficient high coercivity [119].

In this line core-shell type particles (figure 5.5 E), with a core of CoPt alloy in intermediate dimensions (100-500 nm) (semi-hard magnetic response) and a shell of CoNi (soft-magnetic alloy) of controllable thickness were prepared using electrochemical methods. The shell deposit was prepared using a 0.2 M  $\text{CoCl}_2$  + 0.9 M  $\text{NiCl}_2$  + 30 g  $\text{dm}^{-3}$   $\text{H}_3\text{BO}_3$  + 0.7 g  $\text{dm}^{-3}$  saccharine, pH = 3, solution over silicon substrate. The lower con-

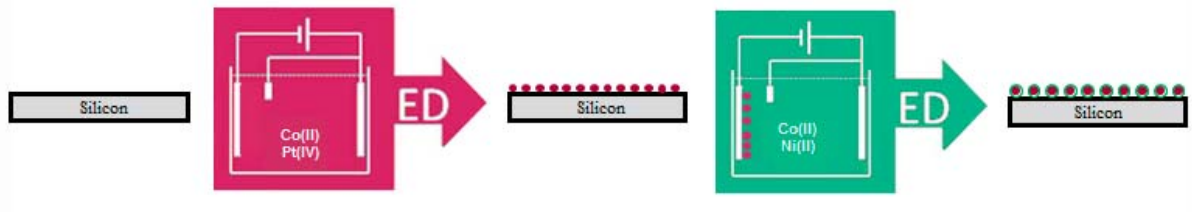


Figure 5.9: Differences in the magnetic properties of the nanowire arrays depending on the distances between nearby nanowires

ductivity of this substrate, with respect to metallic or carbon substrates, can favour, at low deposition charges, a lower nucleation rate and hence, the formation of particles rather than continuous layers and it permitted recovering the alloy core particles (CoPt) with the second alloy (CoNi) avoiding its deposition onto the substrate (figure 5.9). The analysis of the variation of the magnetic properties of the global structure as a function of the shell thickness was performed. The non-magnetic behaviour of the substrate permitted the detection of the magnetic response of the particles prepared over it.

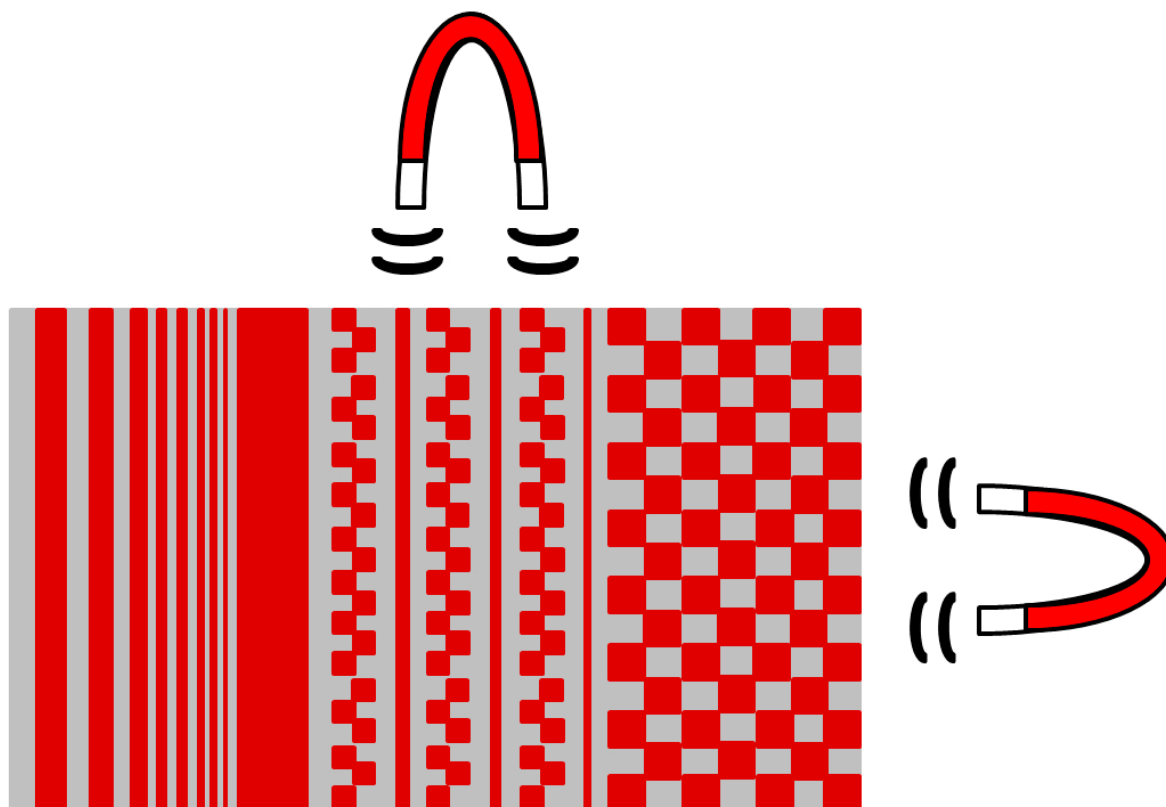
The results of this part of the work are presented in the paper: “*Electrochemical preparation and magnetic properties of submicrometric core-shell CoPt-CoNi particles*”.

## 5.4 Results of the micro/nanostructures preparation

- Paper: “*Magnetic CoPt (60-70 wt % Pt) microstructures fabricated by the electrochemical method*” M. Cortés, E. Gómez and E. Vallés, J. Micromech. Microeng. 22 (2012) 1-7
- Paper: “*Electrochemical growth of CoPt nanowires of different aspect ratio and their magnetic properties*” M. Cortés, E. Gómez, E. Vallés. Journal of Electroanalytical Chemistry, In Press
- Paper: “*Electrochemical preparation and characterisation of CoPt magnetic particles*” M. Cortés, E. Gómez, E. Vallés, Electrochemistry Communications 12 (2010) 132-136
- Paper: “*CoPt nanoscale structures with different geometry prepared by electrodeposition for modulation of their magnetic properties*” M. Cortés, A. Serrà, E. Gómez, E. Vallés, Electrochimica Acta 56 (2011) 8232-8238
- Paper: “*Electrochemical preparation and magnetic properties of sub-micrometric core-shell CoPt-CoNi particles*” M. Cortés, E. Gómez, E. Vallés, Journal of Electroanalytical Chemistry 650 (2010) 36-40



5.4.1 Magnetic CoPt (60-70 wt % Pt) microstructures fabricated by the electrochemical method



# Magnetic CoPt (60–70 wt% Pt) microstructures fabricated by the electrochemical method

M Cortés, E Gómez and E Vallés<sup>1</sup>

Electrodep, Departament de Química Física and Institut de Nanociència i Nanotecnologia (IN<sup>2</sup>UB), Universitat de Barcelona, Martí i Franquès 1, 08028 Barcelona, Spain

E-mail: [e.valles@ub.edu](mailto:e.valles@ub.edu)

Received 27 January 2012, in final form 18 March 2012

Published 16 April 2012

Online at [stacks.iop.org/JMM/22/055016](http://stacks.iop.org/JMM/22/055016)

## Abstract

CoPt microstructures, in the form of both discontinuous layers and patterned arrays, of 60–70 wt% Pt and nanometric thickness have been grown by electrodeposition through a resist mask prepared directly onto a glass/ITO substrate. This substrate was selected because its conductive ITO layer permits the electrodeposition process but does not show magnetic response. The lack of magnetic response of the substrate enables the magnetic properties of the microstructures deposited over it to be measured directly. Test microstructures of the different aspect ratio were successfully prepared, which confirms the suitability of the used bath; a good definition of both has been attained in spite of the significant hydrogen co-evolution. The deposition conditions have been adjusted to obtain a highly distorted hcp crystalline structure. Differences in the magnetic behaviour of the microstructures were observed depending on the orientations of the magnetic field applied. This work demonstrates the capability of the electrodeposition method to grow well-defined nanometric thick microstructures of hcp magnetic CoPt alloy with modulable magnetic properties as a function of the orientation of the applied magnetic field, microstructures which could be directly incorporated in magnetic microelectromechanical systems.

(Some figures may appear in colour only in the online journal)

## 1. Introduction

It is known that both soft- and hard-magnetic materials are required in the development of microelectromechanical systems (MEMS), of which soft magnetic materials have been widely studied and successfully integrated into them. Usually, Cobalt alloys have been tested to be used in these magnetic microactuators [1–7]. Now, the interest is focused on the incorporation of hard-magnetic materials into the MEMS. This objective presents two challenges: the direct growth of the material in the device and its miniaturization. The interest in developing magnetic micro/nanostructures is focused on both their specific properties and potential applications.

The electrodeposition has been demonstrated as a good alternative to prepare micro/nano permanent magnets to be

used in micro-devices [8–10], taking advantage of the fact that it can be applied under very different kinds of substrates as templates or photolithographical substrates [11, 12]. In general, electrochemical methods are easily applied and permit the control of both the growth and the chemical composition of the deposit.

CoPt alloys have been studied due to their potential applications in MEMS, as a specific field into the general interest for sensing and actuating devices [13]. Promising results were obtained with electrodeposition processes in the aqueous solution over different substrates [14–16]. In previous works performed in our laboratory, the incorporation of a high proportion of Pt in the hcp lattice of Co has been tested by means of electrodeposition [17] with the objective of inducing the maximum magnetic anisotropy: for Co percentages lower than 30 wt%, a distorted Pt–fcc phase, showing soft magnetic behaviour, is obtained. If the Co content is increased, a change

<sup>1</sup> Author to whom any correspondence should be addressed.

in the crystalline structure occurs, leading to the formation of a distorted Co-hcp phase. An alloy composition of 30–40 wt% of Co is desired to induce the formation of a very anisotropic hcp structure.

CoPt microstructures can also be of special interest due to their possible different properties with that of the bulk material. The electrodeposition through lithographically defined masks has been extensively used to define metallic structures of different shapes. The difficulty of preparation of well-defined structures is always dependent on the dimensions of the pattern and the characteristics of the used electrolytic bath [18]. The aim of this work is to test the quality of the growth of Pt-rich CoPt microstructures of different shapes and aspect ratios by means of the electrodeposition method, using patterned resin masks, and the analysis of their magnetic properties. The electrodeposition conditions will be adjusted to obtain a desired composition of 30–40 wt% of Co in order to obtain a very distorted hcp phase, to enhance the crystalline magnetic anisotropy and, then, to obtain a significant value of coercivity. This material can be an alternative, without annealing of the samples, to the electrodeposition of the more anisotropic CoPt tetragonal phase [19, 20] obtained usually after annealing of the samples. The final proposal is the direct growth of hard magnetic CoPt microstructures in MEMS devices without the need of post-annealing of the alloy.

## 2. Materials and methods

Electrochemical study and sample preparation have been performed in a conventional three-electrode cell with control of temperature (30 °C) from a solution containing  $2.5 \times 10^{-3}$  M  $\text{CoCl}_2 + 1.2 \times 10^{-3}$  M  $\text{Na}_2\text{PtCl}_6 + 0.5 \times 10^{-2}$  M sodium citrate + 1 M  $\text{NH}_4\text{Cl} + 30 \text{ g dm}^{-3}$   $\text{H}_3\text{BO}_3$  (the pH of the solution was adjusted at 4.5 with NaOH solutions). All the reagents were of analytical grade. The solution was freshly prepared with water which was first doubly distilled and then treated with a Millipore Milli Q system. The solution was de-aerated by argon bubbling before each experiment and maintained under argon atmosphere during the experiment.

A microcomputer-controlled potentiostat/galvanostat Autolab with PGSTAT30 equipment and GPES software was used for deposit preparation. Glass/ITO/resin photolithographed substrates supplied by IMB-CNM.CSIC (Centro Nacional de Microelectrónica) were used for the deposit preparation. The resin mask was applied on the glass/ITO (layer of indium tin oxide of 25 nm, sputtered on glass). A 1.2 mm-thick HiPR 6512 photoresist (Fujifilm) layer was spun and heated at 100 °C for 20 min to remove moisture. The photoresist was irradiated and soft baked at 110 °C for 30 min. Finally, it was developed and hard baked at 115 °C for 20 min.

To determine the range of resolution of the deposited alloy structures, different patterns have been designed on the mask. Figure 1 shows the main elements of the mask used, which consists in a collection of chips of  $5 \times 10$  mm divided in elements with field course on the elements (+) and dark field in the elements (–).  $L_+$  and  $L_-$  include groups of five equal tranches of 2 mm, but of different widths (1–100  $\mu\text{m}$ ) and gaps (1–100  $\mu\text{m}$ ).  $Q_+$  and  $Q_-$  include areas of  $2 \text{ mm} \times 200 \mu\text{m}$  with

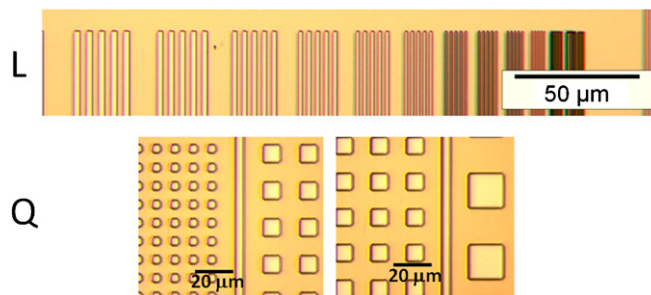


**Figure 1.** Example of the elements ( $L$ ,  $Q$  configurations) in the test mask.

squares or contacts of different dimensions (1–50  $\mu\text{m}$ ) and checkerboards of  $2 \text{ mm} \times 200 \mu\text{m}$  with different dimensions of the squares (2–50  $\mu\text{m}$ ).

The reference electrode was an  $\text{Ag/AgCl}/1 \text{ mol dm}^{-3}$   $\text{NaCl}$  electrode. All potentials were referred to this electrode. The counter electrode was a platinum spiral. Stirring of the solution (100 rpm) was maintained during the electrodeposition to ensure a constant composition throughout the samples.

After the formation of the microstructures by electrodeposition, the resin mask was removed with acetone. Samples were observed using an Olympus PMG 3 optical (OM), a Leica Stereoscan S-360 scanning electron microscopy (SEM) and an extended multimode<sup>®</sup> 8 with a Nanoscope V controller (Bruker, Germany). AFM images were recorded in the peak force tapping mode with triangular silicon cantilevers (nominal radius of 8 nm and spring constant  $0.5 \text{ N m}^{-1}$ ) at a scan rate of 1 Hz. Elemental composition was determined with an x-ray analyser incorporated in Leica Stereoscan S-360 equipment. Thicknesses of the thin films were measured using Leica DCM 3D Confocal and Interferometer. The crystalline structure of the deposits was studied by means of a Philips MRD diffractometer with parallel optical geometry using radiation  $\text{Cu K}_\alpha$  ( $\lambda = 1.5418 \text{ \AA}$ ) and a texture goniometer that allows control of the sample rotation about the three axes.

Magnetic properties were characterized by means of a SQUID magnetometer at room temperature in helium atmosphere. Measurements were carried out at 27 °C K by applying the magnetic field in different directions with respect to the plane of the substrate. The substrate allows us to measure directly the magnetic properties of the samples prepared because it does not affect the magnetic response of the CoPt alloy.

## 3. Results and discussion

The voltammetric study in stationary conditions was performed over the glass/ITO/resin mask substrates in order to analyse the different redox processes during the cyclic scan and to determine the optimum working potential range to electrodeposit the CoPt alloy. As can be seen in the cyclic voltammogram recorded in figure 2, the first reduction current from  $-0.2 \text{ V}$  corresponding to platinum deposition, followed by the simultaneous Co deposition from  $-0.8 \text{ V}$  were detected. Simultaneous proton reduction occurred, as expected for

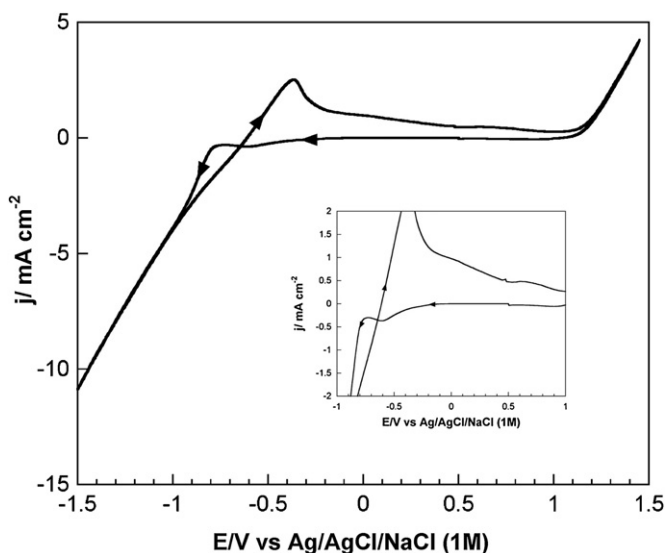


**Figure 2.** Cyclic voltammetry at  $0.05 \text{ V s}^{-1}$ .  $\omega = 0 \text{ rpm}$ . Initial potential:  $0.5 \text{ V}$ . An expanded view of the voltammogram is shown as an inset.

**Table 1.** Composition of the microstructures as a function of the deposition potential ( $E$ ) at similar deposition charge ( $Q \approx -5.5 \text{ C}$ ).

$E \text{ (V)}$	Pt wt%	Co wt%
-1.15	64	36
-1.20	71	29
-1.25	64	36
-1.30	63	37
-1.325	64	36
-1.35	61	39
-1.375	65	35
-1.40	67	33

platinum alloys, as corroborated in the anodic scan by the peak at  $-0.4 \text{ V}$  assigned to the oxidation of molecular hydrogen retained over the electrode: this oxidation peak at  $-0.4 \text{ V}$  disappears when the recording of the voltammetric curve is made while stirring the solution, because stirring favours the detachment of the molecular hydrogen of the electrode. Next to that peak, an oxidation band corresponding to the alloy oxidation was detected from  $-0.4$  to  $0.1 \text{ V}$ , followed by the formation of superficial platinum oxides (band centred at  $0.6 \text{ V}$ ).

From the voltammetric experiments, the potentials where simultaneous platinum and cobalt deposition took place were selected. As CoPt electrodeposition is a slow process over the glass/ITO electrode, due to its semiconductor nature, high potentials were needed to obtain deposits with enough Co content. Deposits were prepared using a range from  $-1.15$  to  $-1.4 \text{ V}$ . Deposit formation was performed under stirring. Under the selected deposition conditions, CoPt deposits of 61–71 wt% of Pt ( $\text{Co}_2\text{Pt}_{1-1.5}$ ) were obtained with no significant variation in the composition (table 1) as has been observed previously for CoPt and CoPtP deposition [17]; the stirring of the solution during the electrodeposition, which keeps the contribution of the electroactive species (Co(II), and platinate anion) to the electrode, infers that the variation of potential in

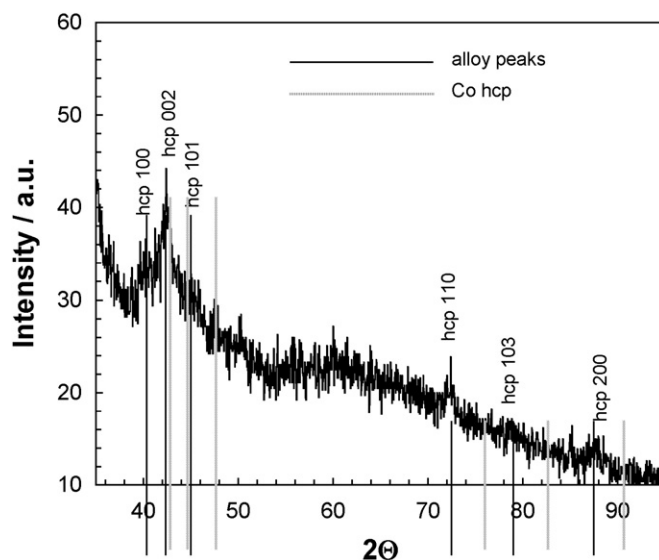


**Figure 3.** XRD pattern of a set of microstructures of 36 wt% of Co prepared at  $-1250 \text{ mV}$ ,  $310 \text{ nm}$  thick.

this range does not affect in a different way the two deposition rates, because they are diffusion-controlled processes.

The crystalline structure of the CoPt microstructures was analysed. X-ray diffraction indicates (figure 3) that the microstructures of the CoPt alloy were crystalline and they correspond to a Co hcp phase structure, as was observed in previous papers for deposited CoPt films [17, 21], in which, for bigger samples, the assignment of the phase and their characterization has been easier. In this paper, the small size of the microstructures led to less defined x-ray diffractograms but sufficient to detect and assign the hcp distorted phase. A significant shift of the diffraction peaks of the alloy to lower angles reveals the high incorporation of the platinum in the cobalt crystalline lattice as corresponds to cell parameters higher than those corresponding to pure hcp Co.

After CoPt alloy electrodeposition, the resin mask was removed in acetone. In figure 4, some SEM images of structures with different dimensions prepared over the photolithographed glass/ITO substrate are shown. In these images, clear zones correspond to granular CoPt deposits which presented a metallic grey colour. The alloy completely filled the structures defined by the photolithography (A). Well adherent structures with a good definition were obtained in both tested cases: when the deposit fills the gaps left by the mask ((A) and (C)) or when it defines them ((B) and (D)). Structures of any dimension can be deposited, only limited by the resolution of the resin mask that can be produced: figures 4(E) and 5 show that the mask does not define correctly the lowest squares (observed as circles in the pictures) but it can be observed that deposit follows the shapes defined by the mask.

By adjusting the deposition time, microstructures with thicknesses in the range of  $100\text{--}400 \text{ nm}$  were obtained. These values were measured by interferometry (figure 6). Well-defined vertical walls were observed. Samples obtained at less negative potentials exhibited better definition, since increasingly negative potentials favoured the simultaneous hydrogen evolution.

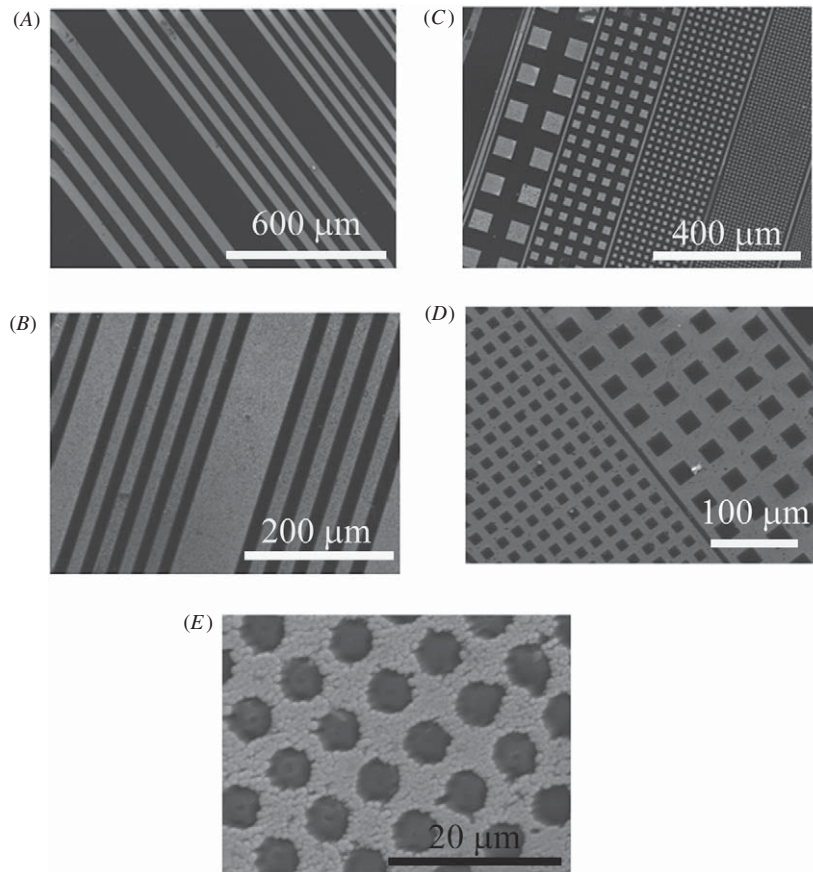


**Figure 4.** SEM images of (A) field course tracks ( $L_+$ ), (B) dark field tracks ( $L_-$ ), (C) field course squares ( $Q_+$ ), (D) dark field squares ( $Q_-$ ) and (E) zoom of a zone of D. Microstructures of 36 wt% of Co prepared at  $-1.15$  V, 230 nm thick.

In order to study the magnetic response of the different arrays defined by the photolithography, the samples were cut into four parts:  $Q_+$ ,  $Q_-$ ,  $L_+$  and  $L_-$ . For each one, the magnetic field was applied in three different configurations:  $x$ ,  $y$  and  $z$  (figure 7) to analyse their possible influence in the magnetic response of the microstructures. One specific magnetic layer can show different magnetic properties as a function of its crystalline structure, shape and dimensions, thickness of the films and orientation of the applied magnetic field. For thin films, the magnetic anisotropy depends on the contribution of bulk, surface and shape anisotropies [22].

Here, we compare samples of equal crystalline structure, composition and thickness but different geometric shape, using different test microstructures. The interest in measuring the magnetic properties of different shape and aspect ratio microstructures is to test what kind of microstructures can be more adequate for their incorporation in specific magnetic MEMS. Knowledge of the magnetic response as a function of the patterning of the structures and the direction of the magnetic field applied can be interesting before the design of the MEMS.

In all cases, the samples were more easily saturated when the magnetic field was applied in the plane of the film than perpendicular to it (magnetic anisotropy of the structures) (figures 8, 9), which can be a consequence of the intrinsic strong uniaxial anisotropy expected for an hcp structure and possible shape anisotropy [23]. The square

structure arrays ( $Q_+$ ,  $Q_-$ ) do not present differences in the magnetic magnetization-magnetic field ( $M-H$ ) curves for the  $x$ ,  $y$  configurations whereas there is a clear difference for the  $z$  configuration (figure 8). Both square structures, in field course ( $Q_+$ ) and in dark field ( $Q_-$ ) presented semihard-magnetic response with coercivity ( $H_c$ ) values of 720 Oe. Moreover, higher magnetic anisotropy between the parallel ( $x$ ,  $y$ ) and the perpendicular ( $z$ ) configuration was observed for the  $Q_-$  structure (figure 8(A)) than for  $Q_+$  structure (figure 8(B)), which reveals a contribution of the shape anisotropy to the magnetic anisotropy of the samples. As  $Q_-$  configuration looks more similar to a 2D layer than  $Q_+$  one, more accused 2D shape anisotropy was expected to these discontinuous layers with respect to the patterned arrays.

The magnetic response between the line structure arrays in both field course ( $L_+$ ) and dark field ( $L_-$ ) is similar (figure 9). Coercivity is maintained at 720 Oe. For the  $L$  configurations (line structure arrays) also the  $x$ - $y$  plane is an easy axis for the magnetization of the samples, and the identical hysteresis curve was obtained in  $x$  and  $y$  configurations: the micrometric size of the majority of the structures probably does not allow us to detect differences by applying the magnetic field in the two directions of the  $x$ - $y$  plane: clear changes in the shape anisotropy were observed sometimes only when structures change to nanometric size [24]. The difference between the magnetic anisotropy of the  $L$  (figure 9(A)) and  $L_+$  (figure 9(B)) structures is lower than that observed between

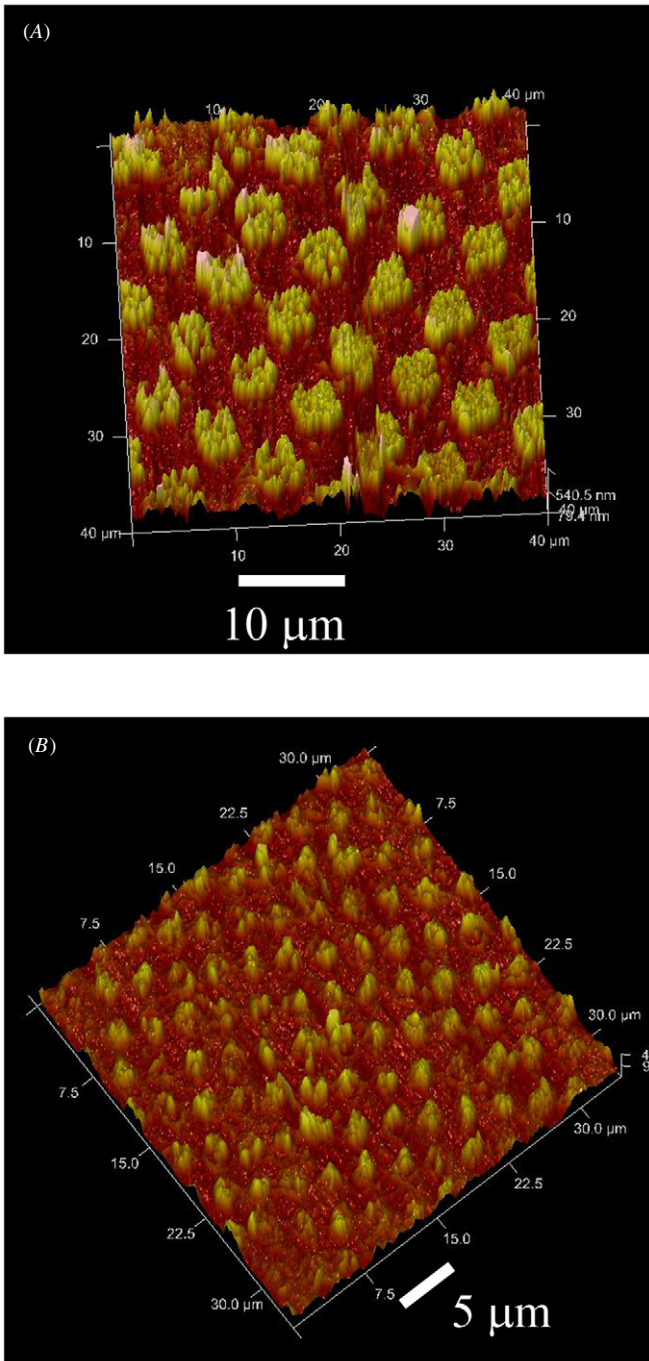


**Figure 5.** AFM images of different square microstructures ( $Q_+$ ) of (A) CoPt squares of  $5 \mu\text{m} \times 5 \mu\text{m}$  and (B) CoPt squares of  $2.5 \mu\text{m} \times 2.5 \mu\text{m}$ .

$Q_-$  and  $Q_+$  ones, probably due to not very different shape anisotropy between  $L_-$  and  $L_+$  configurations.

The analysis of the magnetic properties of the microstructures shows (table 2) that the response in the  $x$ - $y$  plane to the application of the magnetic field is similar in the four configurations (similar values of remanence ( $M_r$ ), coercivity ( $H_c$ ) and magnetic  $M$ - $H$  slope, which reveals low interaction between the neighbouring structures because there is a micrometric separation between them. The anisotropy

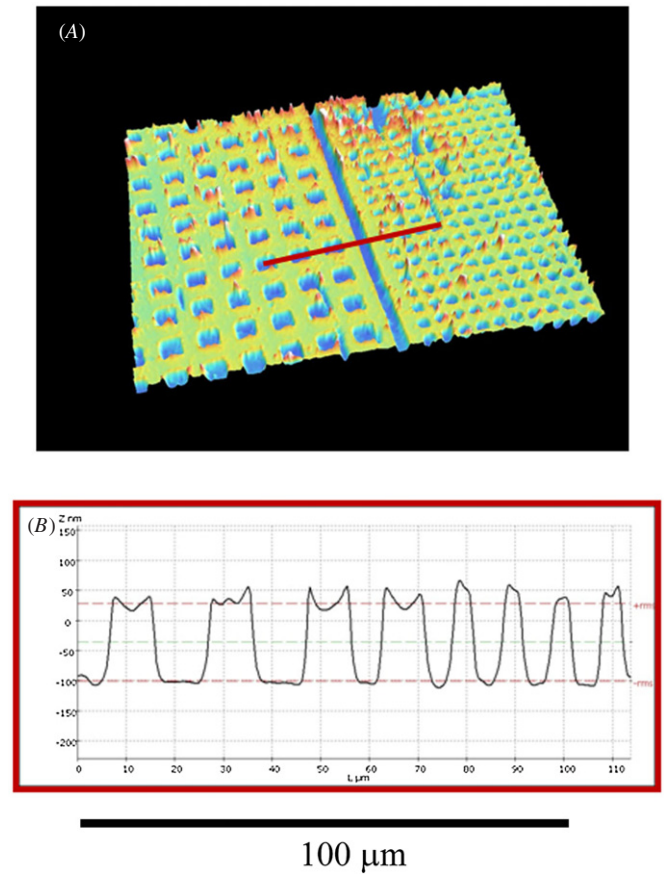


**Figure 6.** Interferometric image and profile of a dark field square ( $Q_-$ ) microstructures of 29 wt% of Co prepared at  $-1.2 \text{ V}$ , 130 nm thick.

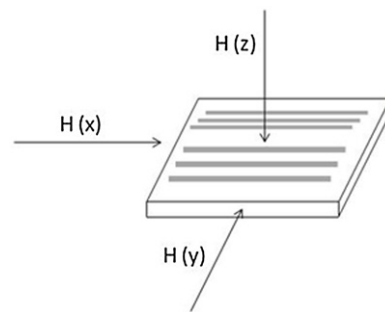


**Figure 7.** Schematic representation of the magnetic field applied in configurations:  $x$ ,  $y$  and  $z$ .

constant ( $K_{an}$ ) was estimated for these deposits using the following expression [25]:

$$H_{s\parallel} + H_{s\perp} = 4\pi M_s + 2K_{an}/M_s \quad (1)$$

where  $H_{s\parallel}$  and  $H_{s\perp}$  are the magnetic fields at which the saturation is attained in the parallel or perpendicular configurations, respectively, and  $M_s$  is the magnetization of saturation. The values of  $H_s$  (table 2) have been measured, with an imprecision of about 100 Oe, from the magnetic hysteresis curves in the  $+20\,000$  to  $-20\,000$  Oe range. The magnetization of the saturation value was determined from the hysteresis curves of CoPt films of known weight and the same composition than the microstructures, recorded after detaching

**Table 2.** Magnetic properties of the different CoPt microstructures by applying the magnetic field in the  $x$ ,  $y$  and  $z$  directions with respect to the sample.  $M_r/M_s$  normalized remanence,  $M-H$  slope of the magnetization curve at  $M = 0$ ,  $H_s$ : magnetic field at which saturation is attained,  $K_{an}$ : magnetic anisotropy constant.

	$Q_+$			$Q_-$			$L_+$			$L_-$		
	$x$	$y$	$z$									
$M_r/M_s$	0.44	0.44	0.13	0.45	0.45	0.10	0.49	0.49	0.08	0.44	0.44	0.07
$M-H$ (cgs)	0.008	0.008	0.005	0.008	0.008	0.0015	0.010	0.010	0.0035	0.010	0.010	0.0035
$H_s$ (Oe)	5500	5500	12 000	6000	6000	17 500	5500	5500	12 500	6500	6500	15 000
$K_{an}$ (J cm $^{-3}$ )	0.30			0.53			0.32			0.46		

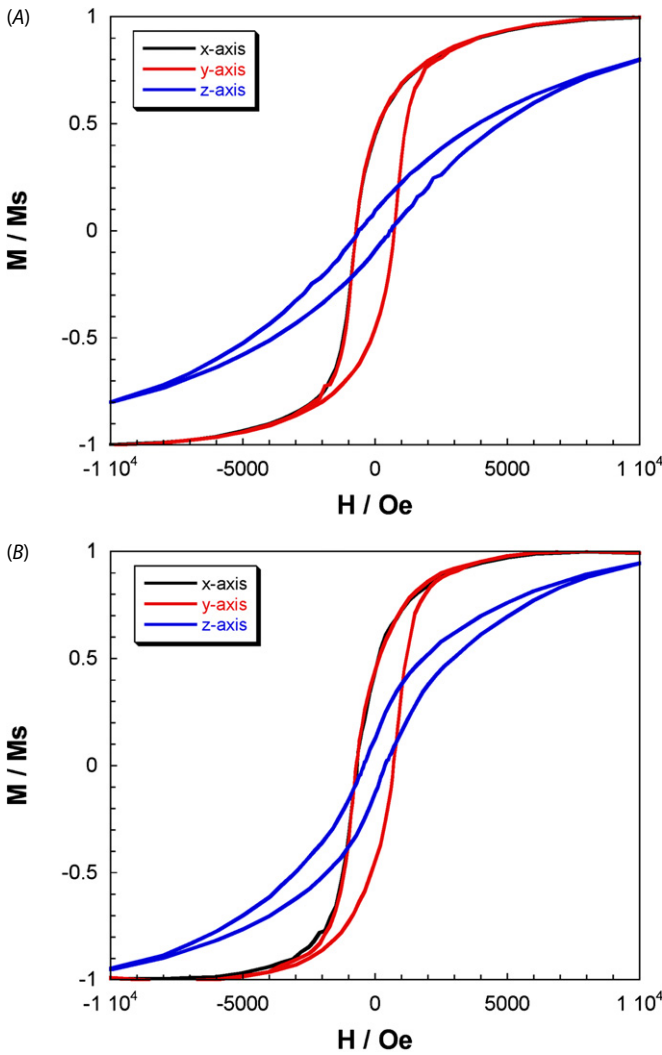


**Figure 8.** Normalized room-temperature magnetization curves taken in the in the three configurations of (A) dark field square ( $Q_-$ ) and (B) field course square ( $Q_+$ ) microstructures of 36 wt% of Co prepared at  $-1150$  mV, 230 nm thick.

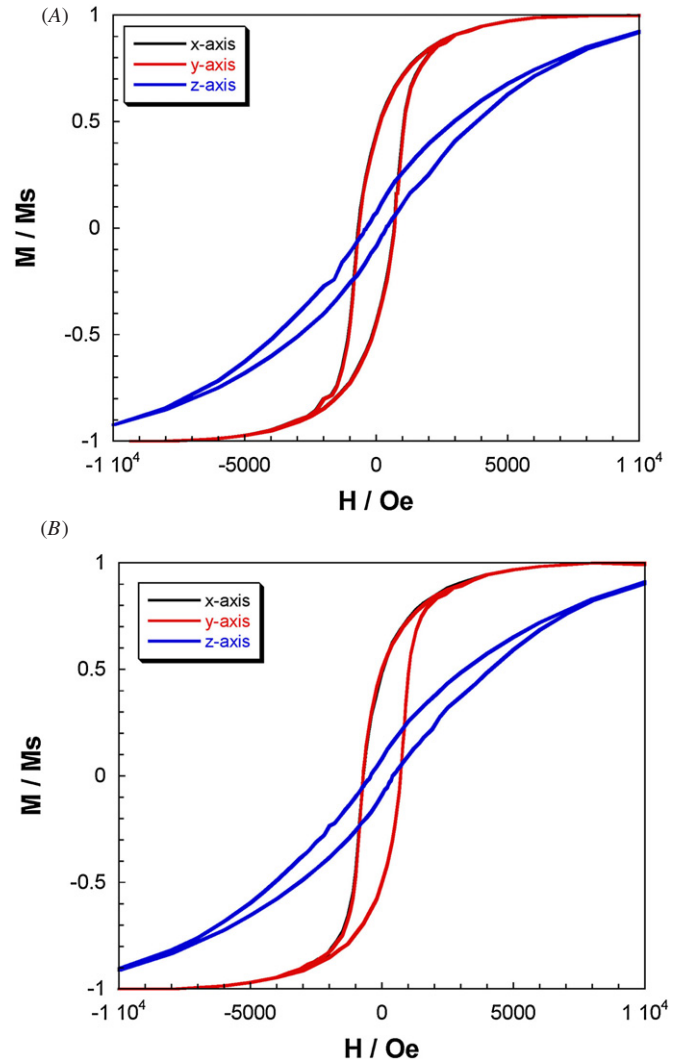


**Figure 9.** Normalized room-temperature magnetization curves taken in the in the three configurations of (A) dark field track ( $L_-$ ) and (B) field course track ( $L_+$ ) microstructures of 36 wt% of Co prepared at  $-1.15$  V, 230 nm thick.

the films from the substrate; the average value obtained was  $45.6 \text{ emu g}^{-1}$ . From these values, the anisotropy constants for the four configurations are shown in table 2. The values of the  $M-H$  slope and the  $K_{an}$  of the samples (table 2) were different when the magnetic field was applied perpendicularly to the sample. The  $K_{an}$  varies in the following sense:  $Q_- > L_- > L_+ > Q_+$ , which demonstrates the gradual decrease of the shape

anisotropy. Then, the different configurations are differently affected by the orientation of the magnetic field applied.

#### 4. Conclusions

Well-defined nanometric-thick CoPt magnetic microstructures have been obtained over patterned glass/ITO substrates via electrodeposition in a CoPt electrolytic bath. Good adhesion

of the deposited layer to the substrate was observed after removing the resin mask, in spite of the smooth substrate used.

The microstructure of the deposits was found to be defined by the patterned resin mask; the CoPt alloy completely fills the exposed region of the patterned substrate for the electrodeposition conditions tested here. CoPt shaped microstructure arrays or discontinuous layers can be prepared. A wide range of deposition potentials can be applied to obtain CoPt microstructures with high Pt percentage and thereby a much distorted hcp structure, which enhances the magnetic coercivity. The magnetic response of the substrate–microstructure system can be modulated by the orientation of the applied magnetic field.

## Acknowledgments

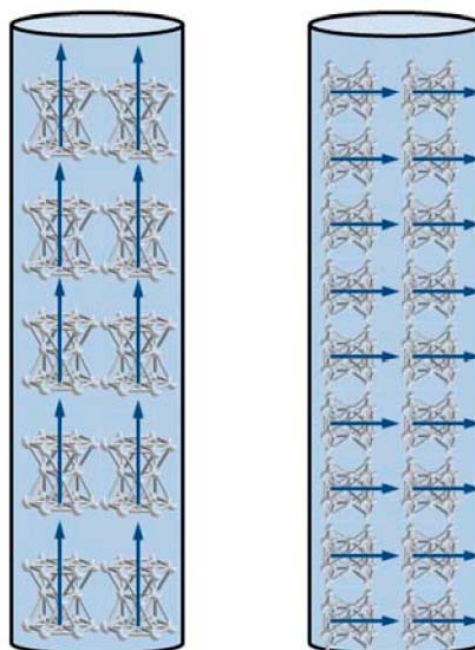
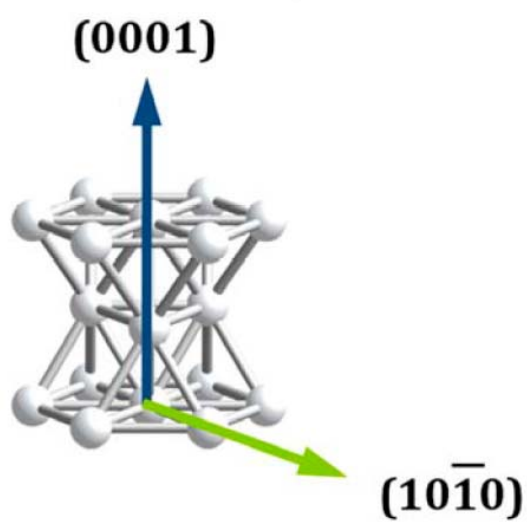
This paper was supported by contract CTQ2010-20726 (subprogram BQU) from the Comisión Interministerial de Ciencia y Tecnología (CICYT). The authors wish to thank the Centres Científics i Tecnològics de la Universitat de Barcelona (CCiTUB) for the use of their equipment. The substrates have been prepared in the Clean Room of the IMB-CNM (CSIC), supported by the IMB-CNM (CSIC)NGG-214 (2011) project. MC would also like to thank the Departament d'Innovació, Universitats i Empresa of the Generalitat de Catalunya and Fons Social Europeu for their financial support.

## References

- [1] Onoda M, Shimizu K, Tsuchiya T and Wanabe T 1993 Preparation of amorphous/crystalloid soft magnetic multilayer nickel–cobalt–boron alloy films by electrodeposition *J. Magn. Magn. Mater.* **126** 595–8
- [2] Osaka T 1997 Electrochemical formation and microstructure in thin films for high functional devices *Electrochim. Acta* **42** 3015–22
- [3] Osaka T, Sawaguchi T, Mizutani F, Yokoshima T, Takai M and Okinaka Y 1999 Effects of saccharin and thiourea on sulfur inclusion and coercivity of electroplated soft magnetic CoNiFe film *J. Electrochem. Soc.* **146** 3295–9
- [4] Tabakovic I, Inturi V and Riemer S 2002 Composition, structure, stress, and coercivity of electrodeposited soft magnetic CoNiFe films thickness and substrate dependence *J. Electrochem. Soc.* **149** C18–22
- [5] Lallemand F, Comte D, Ricq L, Renaux P, Pagetti J, Dieppedale C and Gaud P 2004 Effects of organic additives on electroplated soft magnetic CoFeCr films *Appl. Surf. Sci.* **225** 59–71
- [6] Pellicer E, Gómez E and Vallés E 2006 Use of the reverse pulse plating method to improve the properties of cobalt–molybdenum electrodeposits *Surf. Coat. Technol.* **201** 2351–7
- [7] Gómez E, Pellicer E, Duch M, Esteve J and Vallés E 2006 Molybdenum alloy electrodeposits for magnetic actuation *Electrochim. Acta* **51** 3214–22
- [8] Zana I, Zangari G, Park J W and Allen M G 2004 Electrodeposited Co–Pt micron-size magnets with strong perpendicular magnetic anisotropy for MEMS applications *J. Magn. Magn. Mater.* **272** e1775–6
- [9] Myung N V, Park D Y, Schwartz M, Nobe K, Yang H, Yang C K and Judy J W Electrodeposited hard magnetic thin films for mems applications *Proc. Electrochem. Soc.* PV 2000–29
- [10] Pattanaik G, Kirkwood D M, Xu X and Zangari G 2007 Electrodeposition of hard magnetic films and microstructures *Electrochim. Acta* **52** 2755–64
- [11] Cojocar P, Magagnin L, Gomez E, Vallés E, Liu F, Carraro C and Maboudian R 2010 Magnetic micromechanical structures based on CoNi electrodeposited alloys *J. Micromech. Microeng.* **20** 125017
- [12] Vieux-Rochaz L, Dieppedale C, Desloges B, Gamet D, Barragatti C, Rostaing H and Meunier-Carus J 2006 Electrodeposition of hard magnetic CoPtP materials and integration into magnetic MEMS *J. Micromech. Microeng.* **16** 219–24
- [13] Nespoli A, Besseghini S, Pittaccio S, Villa E and Viscuso S 2010 The high potential of shape memory alloys in developing miniature mechanical devices: a review on shape memory alloy miniactuators *Sensors Actuators A* **158** 149–60
- [14] Cavallotti PL, Bestetti M and Franz S 2003 Microelectrodeposition of Co–Pt alloys for micromagnetic applications *Electrochim. Acta* **48** 3013–20
- [15] Wang N and Arnold D P 2008 Thick electroplated Co-rich CoPt micromagnet arrays for magnetic MEMS *IEEE Trans. Magn.* **44** 3969–72
- [16] Gibbs M R J 2007 Materials optimization for magnetic MEMS *IEEE Trans. Magn.* **43** 2666–71
- [17] Cortés M, Gómez E and Vallés E 2010 Magnetic properties of nanocrystalline CoPt electrodeposited films. Influence of P incorporation *J. Solid State Electron.* **14** 2225–33
- [18] Romankiw L T, Croll I and Hatzakis M 1970 Batch-fabricated thin-film magnetic recording heads *IEEE Trans. Magn.* **3** 597–601
- [19] Cavallotti P L, Bestetti M and Franz S 2003 Microelectrodeposition of Co/Pt alloys for micromagnetic applications *Electrochim. Acta* **48** 3013–20
- [20] Fujita N, Maeda S, Yoshida S, Takase M, Nakano M and Fukunaga H 2004 Preparation of Co–Pt alloy film magnets by electrodeposition *J. Magn. Magn. Mater.* **272** e1895–7
- [21] Cortés M, Serrà A, Gómez E and Vallés E 2011 CoPt nanoscale structures with different geometry prepared by electrodeposition for modulation of their magnetic properties *Electrochim. Acta* **56** 8232–8
- [22] Hubert A and Schäfer R 1998 *Magnetic Domains: The Analysis Of Magnetic Microstructures* (Berlin: Springer) 297–321
- [23] Klavunde K J ed 2001 *Nanoscale Materials In Chemistry* (New York: Wiley)
- [24] Henry Y, Oumadjela K, Piroux L, Dubois S, George J-M and Duvail J-L 2001 Magnetic anisotropy and domain patterns in electrodeposited cobalt nanowires *Eur. Phys. J. B* **20** 35–54
- [25] Xiao J Q, Chien C L and Gavrin A 1996 Observation of perpendicular anisotropy in granular magnetic solids *J. Appl. Phys.* **79** 5309–11

5.4.2 Electrochemical growth of CoPt nanowires of different aspect ratio and their magnetic properties

**Magnetization easy axis**



# Electrochemical growth of CoPt nanowires of different aspect ratio and their magnetic properties

M. Cortés, E. Gómez, and E. Vallés\*

*Electrodep, Departament de Química Física and Institut de Nanociència i Nanotecnologia (IN<sup>2</sup> UB),  
Universitat de Barcelona, Martí i Franquès 1, 08028 Barcelona, Spain.*

The electrodeposition process of the CoPt system into two types of gold-coated polycarbonate and alumina membranes have been studied to test the possibility of electrochemical growth of CoPt nanowires with different length and aspect ratio but fixed composition showing hcp phase with maximum Pt incorporation. The evolution of the nanowires as a function of the deposition time was analysed; nanowires from 250 nm to 8  $\mu\text{m}$  have been prepared. During the initial stages of the deposition, the formation of nanotubes in the membranes of higher porous diameter was observed, subsequently forming nanowires after continued deposition. With around 60 wt. % of Pt the CoPt nanowires show distorted hcp cobalt phase and preferred orientation conditioned by the pore diameter of the membrane. When using polycarbonate membranes, nanowires with an aspect ratio of 0.025 or lower showed clear magnetic anisotropy and the membrane magnetizes easily by applying a parallel magnetic field (magnetic field perpendicular to the nanowires axis). When the length of the nanowires was reduced, magnetic anisotropy decreased. Coercivity remains in the range between 500-1000 Oe. When using an alumina template, the arrays showed similar coercivity, however, a higher magnetic anisotropy was observed with respect to those of similar length in a polycarbonate membrane, probably as a consequence of the elevated density of the arrays that permits higher interaction between the wires.

## I. INTRODUCTION

The preparation of ferromagnetic arrays is a recent and attractive topic of study due to their different properties when compared to the corresponding bulk material, which allows their potential use for a great number of applications related to their specific magnetic properties<sup>1-4</sup>. In this field, the preparation of CoPt arrays has been the object of interest for its potential applications in recording media<sup>5</sup> or incorporation in microdevices<sup>6</sup>. The magnetic properties of the system depend not only on its composition and crystalline structure but also on its shape. Electrodeposition of particles directly over a substrate<sup>7</sup> has been a method of preparing CoPt arrays of nanostructures but in this case the control of separation and size of the particles is not trivial. The use of membranes could permit the control of both the separation between the nanostructures and their aspect-ratio, defining nanowires of different length and width. CoPt nanowires has been previously prepared by electrodeposition, usually exhibiting an fcc structure; after annealing at high temperature to induce face centred tetragonal L10 ordered phase formation, their magnetic properties have been analysed<sup>6,8-13</sup>, having a large magnetocrystalline anisotropy. In these studies, nanowires of fixed length were prepared. Few studies analyse the influence of the length of the CoPt fcc nanowires<sup>14,15</sup>. Our objective is to analyse the possibility of directly growing CoPt nanowires of hcp structure, which are more anisotropic than the fcc, with different aspect ratios. In a previous work, CoPt hcp films of different composition have been prepared by electrochemical deposition from a chloride bath<sup>16</sup>; elevated percentages of Pt in the deposits, as long as the hcp cobalt phase is maintained, led to semi hard magnetic behaviour. The aim of the present paper is to

test the possibility of nanowire grown by means of electrodeposition with constant composition but having different aspect ratios over two types of membranes: polycarbonate and alumina. These membranes present different pore density, which will permit to study the effect of the distance between the nanowires in the magnetic properties of the array. The electrodeposition process in both types of membranes will be studied. The magnetic properties of the nanowire arrays will be tested and compared. The final objective is the preparation of miniaturized structures which could be integrated in microdevices<sup>14,17-19</sup>, growing the nanostructures directly without subsequent annealing of the samples.

## II. EXPERIMENTAL

Nanowires were prepared from a  $2.5 \cdot 10^{-3}$  M  $\text{CoCl}_2$  +  $1.2 \cdot 10^{-3}$  M  $\text{Na}_2\text{PtCl}_6$  +  $0.5 \cdot 10^{-2}$  M sodium citrate + 1M  $\text{NH}_4\text{Cl}$  +  $30 \text{ g dm}^{-3}$   $\text{H}_3\text{BO}_3$ , pH=4.5, solution prepared from reagents of analytical grade and distilled water treated with a Millipore Milli Q system. A three-electrode electrolytic cell with horizontal working electrode arrangement was used. The membranes were placed at the bottom of the cell. A microcomputer-controlled potentiostat/galvanostat Autolab with PG-STAT30 equipment and GPES software was used to perform the electrochemical experiments. Two kinds of membranes were used to prepare the nanowires: polycarbonate membranes with 20  $\mu\text{m}$ -thick channels (from Millipore) and nominal pore diameters of 200 nm and 100 nm and 500 nm of average separation between them (Figure 1A) and alumina membranes (from Whatman) of 60  $\mu\text{m}$  of thickness, nominal 100 nm of porous, 80 nm of average separation between them (Figure 1B).

Both polycarbonate and alumina membranes were coated with a 100 nm-thick gold layer by vacuum evaporation to make them conductive. Prior to the electrodeposition the membranes were kept in distilled water for several hours to make the pores hydrophilic for uniform filling of the pores; after, the distilled water was replaced with the electrolyte solution for depositing the nanowires.

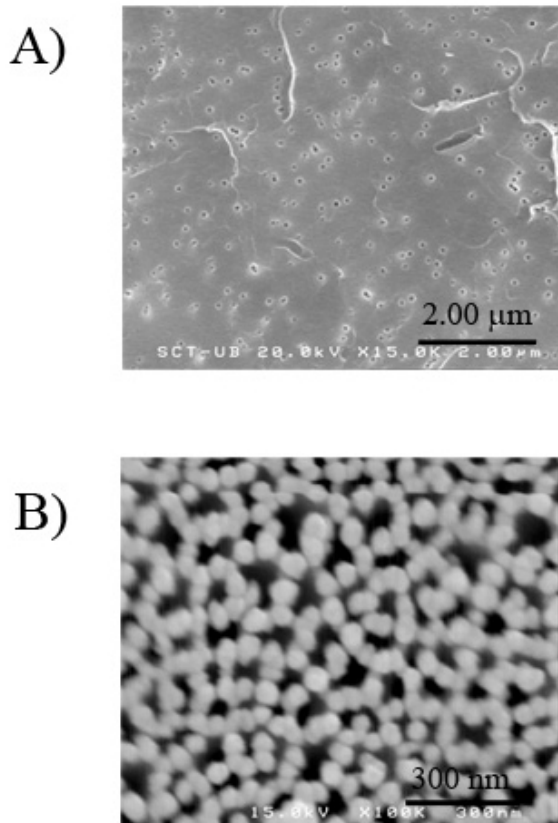


FIG. 1: FE-SEM images of A) polycarbonate and B) alumina membranes of a nominal diameter of porous ( $\varnothing$ ) of 100 nm

The reference electrode was an Ag/AgCl/1 mol dm<sup>-3</sup> NaCl electrode. The counter electrode was a platinum spiral. The solution was stirred with argon current near the membrane to ensure a constant composition throughout the nanowires. Elemental composition was determined with an X-ray analyser incorporated in Leica Stereoscan S-360 system. A hitachi H-4100FE-SEM (field emission scanning electron microscope) was used for the observation of the samples. Both FEI Strata FIB201 and JEOL 2100 TEM (Transmission Electron Microscopy) were used for the study of the shorter nanowires. The structure of the deposits was studied by means of a Philips MRD diffractometer with parallel optical geometry using Cu K $\alpha$  radiation ( $\lambda = 1.5418$  Å) and a texture goniometer that allows control of the

sample rotation about the three axes. A SQUID magnetometer at room temperature in helium atmosphere was used to magnetic characterisation.

### III. RESULTS AND DISCUSSION

The voltammetric study of the CoPt system was performed to find the optimum range of working potentials to allow the electrodeposition in the two types of membranes. Figure 2 shows the voltammetric curves obtained over polycarbonate (dashed line) and alumina template (solid line) coated with gold layer. Similar voltammetric behaviour was observed for both membranes. The voltammetric profile corresponding to the deposition process showed the platinum reduction current (at around -0.3 V) followed by the alloy deposition. When alloy oxidation occurred, simultaneous oxidation of the seed layer was favoured (anodic peak), as was observed after the scan although oxidation process is more difficult in alumina membranes. For the polycarbonate membrane/gold layer substrate, the onset of the deposition process occurred at less negative potentials than over alumina membrane, due to it is more hydrophilic than the commercial alumina template used, so less negative potential was necessary in order to attain a similar reduction current. However, the I/E slope of the CoPt reduction process is similar in both cases once the codeposition has started.

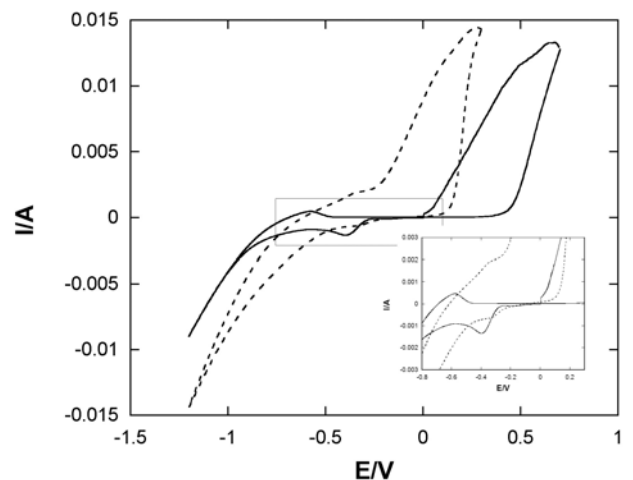


FIG. 2: Cyclic voltammograms of the working bath over polycarbonate membrane (dashed line) and alumina membrane (solid line) of  $\varnothing = 100$  nm. In the inset a zoom of the centre of the figure

Potentiostatic deposition was used for nanowire preparation. Potentials leading to deposits containing a significant amount of platinum were selected. Simultaneous hydrogen evolution was observed during the alloy de-

position. Figure 3A shows the potentiostatic curves of the deposition by applying a fixed potential but different times in polycarbonate membranes with the same porous diameter ( $\varnothing = 200$  nm).

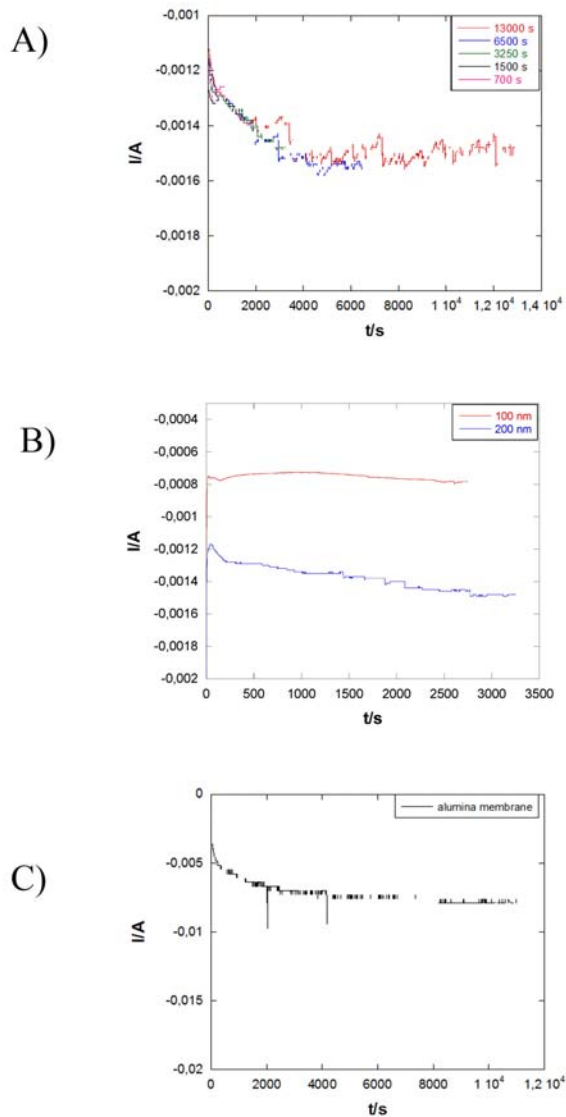


FIG. 3: Potentiostatic curves of A) depositions at  $-800$  mV and different times over polycarbonate membranes with  $\varnothing = 200$  nm, B) depositions at  $-800$  mV over polycarbonate membranes with different diameter of the porous ( $\varnothing = 100$  and  $200$  nm) and C) deposition at  $-1000$  mV over an alumina membrane with  $\varnothing = 100$  nm

Good reproducibility of the I-t transients at the different times is observed, which demonstrates that the membranes presented a similar porosity, which implies equal effective area in contact with the solution. The observed oscillations were a consequence of the stirring with argon

and the hydrogen evolution inner the porous channels. The shape of the potentiostatic curves recorded showed that a stationary value of current was attained, which revealed that the stirring of the solution during the deposition with argon bubbling near the membranes was enough to maintain a stationary regime of the electroactive species through the channels to reach the gold layer and permitted a constant growth of the nanowires. Figure 3B shows the comparison between the I-t responses over polycarbonate membranes with different pore diameter. The different intensities recorded in each case reflect the different effective areas. The slope of the I-t transients is higher in the membranes of  $200$  nm of diameter, which reveals higher growth rate respect to that in the membranes of  $100$  nm of pore diameter. The decrease in the diameter of the channels can difficult the transport of the electroactive species and their incorporation to the growing nanowire.

When alumina membranes were used, although similar deposition curves and growth regime were observed, a more negative potential was necessary to attain a similar reduction current and I/t tendency (Figure 3C). As mentioned before, this fact can be explained by the higher hydrophobicity of the commercial alumina membrane caused by a thermal processing performed on them. If the material is more hydrophobic a higher potential is needed to favour the flow of ions through the membrane to reach the gold.

The gradual formation of the nanowires at fixed deposition potential was analysed by FE-SEM. For better observation, the polycarbonate membranes were treated with a saturated  $I^2/I^-$  solution to remove the gold layer and after they were totally or partially dissolved with chloroform. The section of some alumina templates with nanowires into them were directly observed after cutting the membranes in two. To observe the shorter nanowires, the alumina was removed with  $1M$  NaOH solution. Figure 4 shows different images of the structures formed on the different membranes. CoPt nanotubes were initially formed in the membranes during the first stages of the deposition as can be observed in some pictures (Figures 4A, 4G). More compact and better defined nanowires were observed for deposits of similar length but lower diameter of pores (Figure 4C) because the channels with smaller pores are more easily filled. Solid nanowires grow as the deposition time increases (Figure 4E). Figures 4B and 4F show how the material is incorporated into the nanowires trough the channels of the polycarbonate (B) or alumina (F) templates. Figure 4D clearly shows the separation of the nanowires in the polycarbonate membranes of  $100$  nm of diameter whereas Figures 4G and 4F shows the closeness of the nanowires in the alumina membranes.

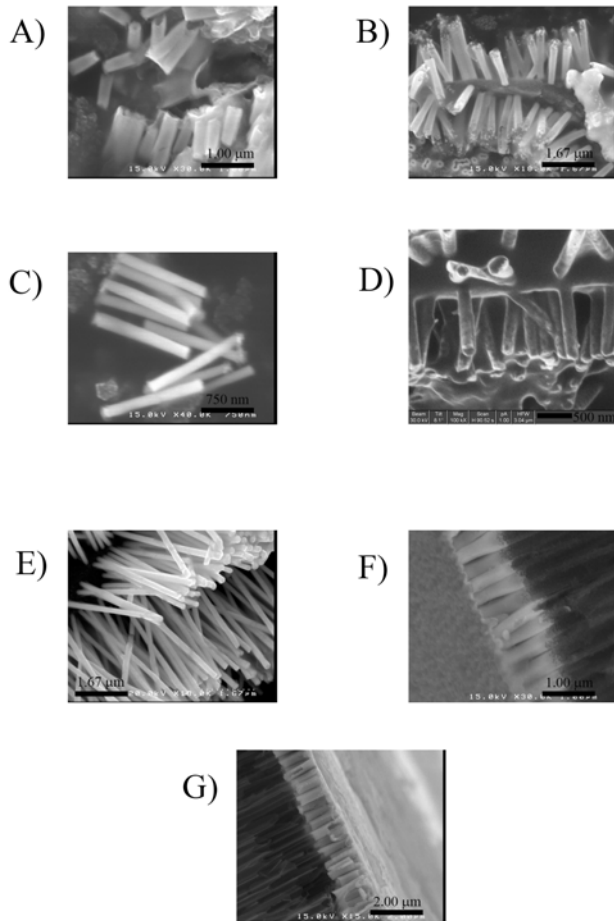


FIG. 4: FE-SEM images of some representative nanowires of different lengths obtained using polycarbonate membranes A)  $0.7 \mu\text{m} \varnothing = 200 \text{ nm}$ , (B)  $1.1 \mu\text{m} \varnothing = 200 \text{ nm}$ , (C)  $1 \mu\text{m} \varnothing = 100 \text{ nm}$ , (D) FIB image of nanowires of  $1 \mu\text{m} \varnothing = 100 \text{ nm}$ , FE-SEM images of nanowires obtained using polycarbonate membranes (E)  $4 \mu\text{m} \varnothing = 100 \text{ nm}$  and using alumina membranes (F)  $1 \mu\text{m} \varnothing = 100 \text{ nm}$ , (G)  $1 \mu\text{m} \varnothing = 100 \text{ nm}$

Some of the shorter nanowires were also observed for TEM, after removing the membranes (Figure 5). From these images, we show that the electrolytic bath selected allows the formation of CoPt wires of different length and aspect ratio as a function of the deposition time and the selection of the membrane. The length of the prepared nanowires was only limited by the thickness of the membranes. However, higher growth rate (around  $25 \text{ nm/min}$ ) was obtained for the CoPt nanowires deposited into polycarbonate membranes with respect to that measured for the alumina membranes (around  $14 \text{ nm/min}$ ), when comparing applied potentials selected to attain the same composition of the CoPt alloy.

The analysis of the different nanowires revealed a platinum percentage of 55-65 wt. % attained by the conditions applied and using both kinds of membranes. Previous studies with the same bath showed that an hcp struc-

ture corresponded to deposits with these compositions<sup>16</sup>. This structure was corroborated by XRD diffraction (Figure 6).

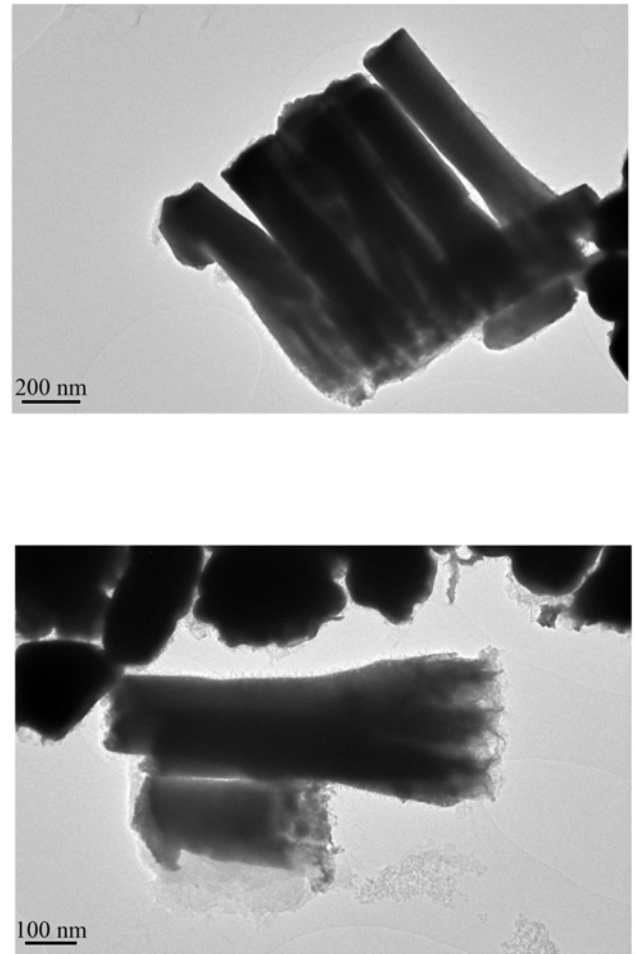


FIG. 5: TEM images of nanowires obtained using alumina templates of nominal  $\varnothing = 100 \text{ nm}$ .

When the channel pores were of  $200 \text{ nm}$  diameter, a 002 preferred orientation of the CoPt nanowires was observed, but a preferred 100 orientation was induced by decreasing the diameter of the channels. The increase of the pore diameter ( $200 \text{ nm}$  diameter) favour the preferred orientation observed electrodepositing CoPt films of similar composition<sup>20</sup> because the growth is less limited by the channel walls. However, lower pore diameter induced the orientation of the crystals in the direction perpendicular to the axis of the nanowire. The diameter of the pores, and the difficulty of the solution entering into the channels, and, then, the different growth rate observed, controls the texture of the nanowires. The difficulty of the hydrogen formed during the deposition escaping, again related to the pore diameter, and also influences the texture of the nanowires. The grain size

was similar for the nanowires in both types of membranes and it was estimated to be around 35 nm by means of Scherrer equation<sup>21</sup>.

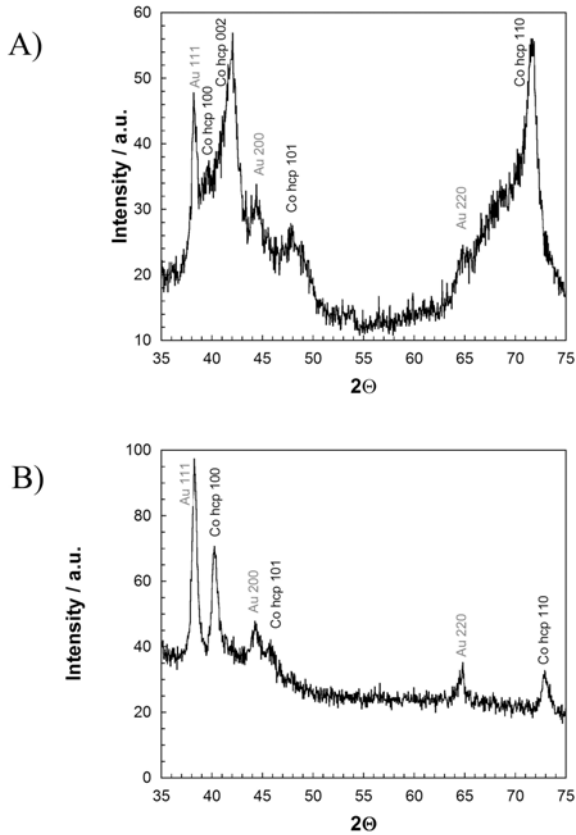


FIG. 6: X-ray diffractogram of nanowires obtained using polycarbonate templates of A) 12  $\mu\text{m}$ ,  $\varnothing = 200$  nm and B) 8  $\mu\text{m}$ ,  $\varnothing = 100$  nm

The magnetic properties of the nanowires were analysed as a function of their aspect ratio. Nanowires of 100 nm diameter, but different length, were prepared and analysed (Figure 7, Table I) due to their higher compactness from the earlier stages of formation and the higher anisotropy expected. Figure 7A presents the hysteresis loops (magnetization-magnetic field applied) of the deposited nanowires into polycarbonate membranes with different lengths with both an external field parallel ( $\parallel$ ) and perpendicular ( $\perp$ ) to the membranes. The longer nanowires (8 and 4 microns length) were easily magnetized by applying the magnetic field parallel to the membranes (magnetic field perpendicular to the axis of the nanowire).

Although the shape anisotropy aligns the magnetization along the nanowire axis, as the nanowires of 100 nm of pore diameter presented a 100 crystalline orientation, the magnetocrystalline anisotropy tends to align the

TABLE I: Differences between the saturation field ( $H_s(\parallel)$ - $H_s(\perp)$ ) and remanence relation ( $M_r(\parallel)/M_r(\perp)$ ) for nanowires of 100 nm of diameter and different lengths, by applying the magnetic field parallel ( $\parallel$ ) to the membrane (perpendicular to the axis of the nanowires) or perpendicular ( $\perp$ ) to the membrane (parallel to the axis of the nanowires)

Membrane	E mV	Lenght $\mu\text{m}$	$H_s(\parallel)$ - $H_s(\perp)$ Oe	$M_r(\parallel)/M_r(\perp)$
Polycarbonate	-800	8	6200	2.6
		4	2800	2.5
		1	1500	1.1
		0.19	1500	1.3
Alumina	-1000	1	7500	3.6
		0.7	6000	2.0

magnetic moments in the perpendicular direction. This means that crystal anisotropy of the CoPt hcp structure favours an orientation of the magnetization perpendicular to the direction favoured by shape anisotropy (axis of the nanowires). In this case, as crystal anisotropy is higher than shape anisotropy, the easy magnetization is in the direction parallel to the membrane, as occurs in thin films of pure Co with hcp phase<sup>22</sup>. This behaviour is similar to that observed also for Cobalt nanowires with diameters from around 100 nm, characterised by a strong perpendicular-to-axis crystal anisotropy that counterbalances shape anisotropy<sup>23</sup>.

When the length of the nanowires decreases, lowering their aspect ratio, the difference between the hysteresis curves in the parallel or perpendicular configurations decreases. This fact is contrary to the expected behaviour, since the contribution of the shape anisotropy is lower, and then, the predominance of the magnetocrystalline anisotropy should be higher, which leads to more difference between the parallel and perpendicular curves. As this difference is not observed, a change in the preferred orientation of the shorter nanowires is expected.

When nanowires were electrodeposited into alumina membranes of the same pore diameter (100 nm), the nanowires magnetized also easily perpendicularly to the magnetic field. However, comparing nanowires of similar diameter and length (around 1  $\mu\text{m}$ ) but prepared in the two different membranes, polycarbonate or alumina, it was observed that more pronounced magnetic anisotropy was present in the nanowire arrays in alumina templates (Figure 7B), in which the nanowires were more close to each other. The space between the pores in the alumina template is lower than 80 nm and a higher interaction between the nearly nanowires is expected. In the simile of the nanowire acting as a dipole, the magnetic field produced by one nanowire could be described by equation 1, where the magnetic field drastically decreases with the distance ( $\vec{r}$ ).

$$\vec{B} = \left( \frac{\mu_0}{4\pi} \vec{\nabla} \times \left( \frac{\vec{m} \times \vec{r}}{r^3} \right) \right) \quad (1)$$

Where  $\vec{m}$  is the dipole magnetic moment and  $\mu_0$  the permeability of free space.

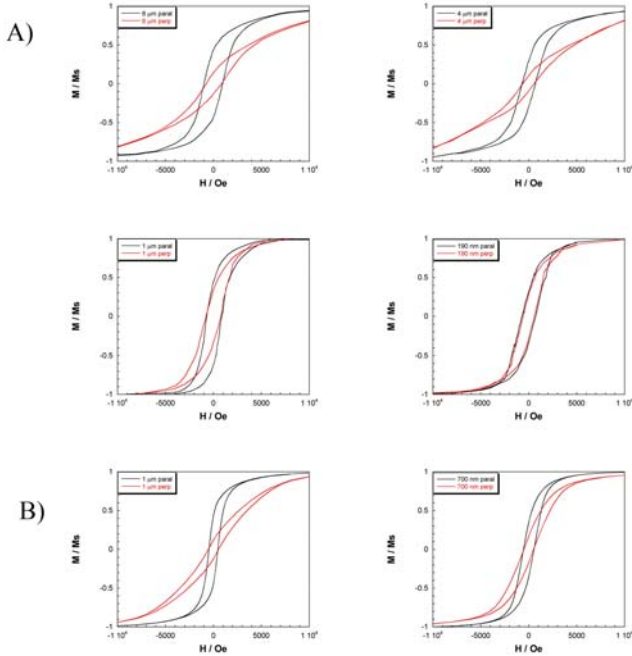


FIG. 7: Normalized room temperature magnetization curves taken with the applied field parallel and perpendicular to the membrane of  $\varnothing = 100$  nm nanowires of different lengths obtained using A) polycarbonate membranes and B) alumina membranes

The shorter distance between the wires in the alumina template can favour exchange coupling and enhance the magnetization in the array when the field is applied parallel to the membrane. A magnetostatic dipole interaction field between the wires will favour the magnetic

easy axis perpendicular to the nanowire axis. Coercivity of the samples was in the 500-1000 Oe range. These values are similar to those obtained for CoPt thin films of hcp structure and similar composition<sup>16</sup>. The nanowires diameter probably is not low enough to enhance the coercivity drastically with respect to CoPt films of a similar composition and structure. The diameter of the nanowires seems to facilitate the formation of magnetic multi-domain structures, so no single-domain behaviour occurs.

#### IV. CONCLUSIONS

Electrodeposition in the selected chloride-citrate bath allows the preparation of CoPt nanowires with different aspect ratios, allowing the modulation of both the preferred orientation of the hcp cobalt phase and the magnetic anisotropy of the wires. The nanowire growth evolution is observed. Similar compositions (55-65 wt. % Pt) were obtained in both alumina and polycarbonate templates for nanowires of varying lengths. The preferred orientation of the alloy depends on the diameter of the channel pores. The magnetocrystalline character of the CoPt hcp phase formed lead to arrays of nanowires with easy magnetization in the direction perpendicular to the axis of the wire. This effect is more pronounced when alumina templates are used, due to the increased interaction between nearby nanowires.

#### V. ACKNOWLEDGMENTS

This article was supported by contract CTQ2010-20726 (subprogram BQU) from the Comisin Interministerial de Ciència y Tecnología (CICYT). The authors wish to thank the Centres Científics i Tecnològics de la Universitat de Barcelona (CCiTUB) for the use of their equipment. M. C. would also like to thank the Departament dInnovació, Universitats i Empresa of the Generalitat de Catalunya and Fons Social Europeu for their financial support.

\* Electronic address: e.valles@ub.edu

<sup>1</sup> G. M. McClelland, M. W. Hart, C. T. Rettner, M. E. Best, K. R. Carter, B. D. Terris, *Appl. Phys. Lett.* **2002**, *81*, 1483-1485.

<sup>2</sup> M. Sun, G. Zangari, M. Shamsuzzoha, R. M. Metzger, *Appl. Phys. Lett.* **2001**, *78*, 2964-2966.

<sup>3</sup> M. Albrecht, C. T. Rettner, A. Moser, M. E. Best, B. D. Terris, *Appl. Phys. Lett.* **2002**, *81*, 2875-2877.

<sup>4</sup> T. M. Liakopoulos, W. Zhang, C. Ahn, *IEEE Trans. Magn.* **1996**, *32*, 5154-5156.

<sup>5</sup> N. Yasui, A. Imada, T. Den, *Appl. Phys. Lett.* **2003**, *83*, 3347-3349.

<sup>6</sup> Y. Dahmane, L. Cagnon, J. Voiron, S. Pairis, M. Bacia, L. Ortega, N. Benbrahim, A. Kadri, *J. Phys. D* **2006**, *39*, 4523-4528.

<sup>7</sup> M. Cortes, E. Gomez, E. Valles, *Electrochem. Commun.* **2010**, *12*, 132-136.

<sup>8</sup> H. Khurshid, Y. H. Huang, M. J. Bonder, G. C. Hadjipanayis, *J. Magn. Magn. Mat.* **2009**, *321*, 277-280.

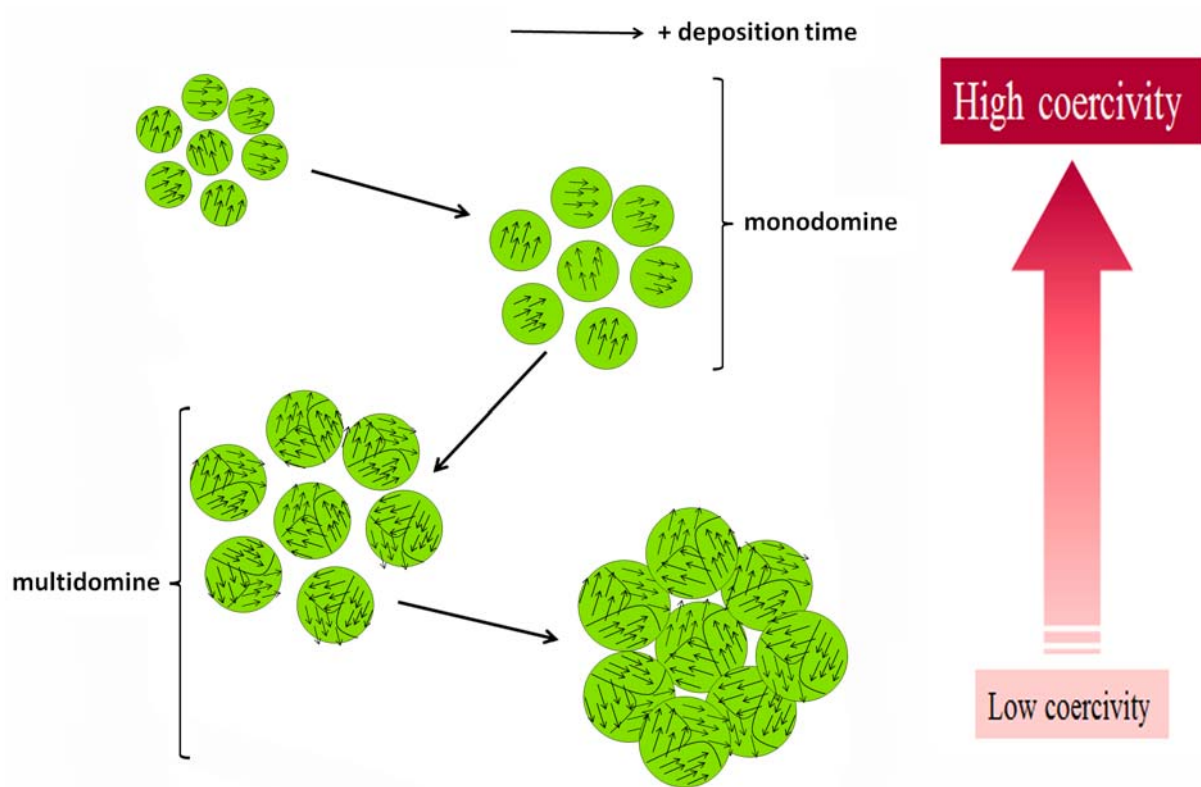
<sup>9</sup> Y. H. Huang, H. Okomura, G. C. Hadjipanayis, D. Weller, *J. Appl. Phys.* **2002**, *91*, 6869-6871.

<sup>10</sup> W. Chen, Z. Li, G. B. Ji, S. L. Tang, M. Lu, Y. W. Du, *Solid State Commun.* **2005**, *133*, 235-239.

<sup>11</sup> J. H. Min, H.-L. Liu, J. H. Lee, J.-H. Wu, J.-S. Ju, Y. K.

- Kim, *IEEE Trans. Magn.* **2009**, *45*, 3471–3474.
- <sup>12</sup> L. Cagnon, Y. Dahmane, J. Voiron, S. Pairis, M. Bacia, L. Ortega, N. Benbrahim, A. Kadri, *J. Magn. Magn. Mat.* **2007**, *310*, 2428–2430.
- <sup>13</sup> F. N. Byrne, L. M. A. Monzon, P. Stamenov, M. Venkatesan, J. M. D. Coey, *Appl. Phys. Lett.* **2011**, *98*, 252507(1–3).
- <sup>14</sup> S. Shamaila, R. Sharif, S. Riaz, M. K. ur Rahman, X. F. Han, *Appl. Phys. A.* **2008**, *92*, 687–691.
- <sup>15</sup> S. Shamaila, R. Sharif, S. Riaz, M. Ma, M. K. ur Rahman, X. F. Han, *J. Magn. Magn. Mat.* **2008**, *320*, 1803–1809.
- <sup>16</sup> M. Cortes, E. Gomez, E. Valles, *J Solid State Electrochem.* **2010**, *14*, 2225–2233.
- <sup>17</sup> S. Z. Chu, S. Inoue, K. Wada, K. Kurashima, *Electrochim. Acta.* **2005**, *51*, 820–826.
- <sup>18</sup> A. I. Gapin, X. R. Ye, L. H. Chen, D. Hong, S. Jin, *IEEE Trans. Magn.* **2007**, *43*, 2151–2153.
- <sup>19</sup> N. B. Chaure, F. M. F. Rhen, J. Hilton, J. M. D. Coey, *Electrochem Commun.* **2007**, *9*, 155–158.
- <sup>20</sup> M. Cortes, A. Serra, E. Gomez, E. Valles, *Electrochimica Acta* **2011**, *56*, 8232–8238.
- <sup>21</sup> B. D. Cullity, *Elements of X-Ray Diffraction*, Addison-Wesley Publishing Company Inc, Massachusetts (USA), **1956**.
- <sup>22</sup> U. Ebels, P. Wigen, K. Ounadleja, *Europhys. Lett.* **1999**, *46*, 94–100.
- <sup>23</sup> Y. Henry, K. Ounadljela, L. Piraux, S. Dubois, J. M. George, J. L. Duvail, *Eur. Phys. J. B.* **2001**, *20*, 35–54.

### 5.4.3 Electrochemical preparation and characterisation of CoPt magnetic particles





## Electrochemical preparation and characterisation of CoPt magnetic particles

M. Cortés, E. Gómez, E. Vallés\*

*Electrodep, Departament de Química Física and Institut de Nanociència i Nanotecnologia (IN<sup>2</sup>UB), Universitat de Barcelona, Martí i Franquès 1, 08028 Barcelona, Spain*

### ARTICLE INFO

#### Article history:

Received 13 October 2009

Received in revised form 3 November 2009

Accepted 3 November 2009

Available online 10 November 2009

#### Keywords:

Magnetic properties

Electrodeposition

Cobalt–platinum alloy

Particles

Coercivity

### ABSTRACT

CoPt particles of different size and modulate magnetic properties have been prepared by electrodeposition. Particles of growing size from 50 nm until continuous deposits have been obtained and their composition, crystalline structure and magnetic properties have been analyzed. The prepared CoPt particles from 50 nm to 250 nm showed ferromagnetic behaviour so did the continuous deposits. However, drastic changes in magnetism have been detected related to the size of the particles: the smallest particles presented lower coercivity which increases with increasing size, with a maximum value for particles of 150–250 nm diameter. The coercivity decreased when continuous deposits were attained due to the disordered growing and the loss of the surface anisotropy.

© 2009 Elsevier B.V. All rights reserved.

### 1. Introduction

Recently, a significant effort has been employed in the modulation of magnetic properties of different systems for application in microelectromechanical-systems (MEMS), in which both soft- and hard-magnetic materials are required. Electrodeposition has been demonstrated to be a useful technique to prepare hard-magnetic materials such as composites [1,2] or alloys [3,4] that can be grown over the device. One of the alloys studied for this purpose is CoPt [5,6] after annealing at high temperature to obtain the crystalline phase showing high-magnetic properties, although it is possible to obtain a phase showing high coercivity values without such annealing [7].

In a previous work the dependence of the magnetic properties with composition was studied for CoPt films [8]. Deposits with an hcp structure and a high percentage of platinum showed the largest coercivity. To enhance the coercivity, the aim of the present work is to explore the production of CoPt particles of submicron size using electrodeposition techniques, in order to study the influence of the size and composition of the particles on their magnetic properties. Although nanoscale (3–5 nm) CoPt particles prepared in a water-in-oil microemulsion show superparamagnetic behaviour [9], submicron particles are expected to have different magnetic behaviour depending on the size. This is due to the different contributions to magnetic anisotropy which depend upon size [10], as well as the fact that coercivity is related to the motion of domain walls and the number of domains depends on the particle

size [11]. Particles will be grown upon graphite substrates; this electrode was chosen instead of metallic one to induce lower nuclei density. The variation of both composition and coercivity of the CoPt particles with the deposition conditions will be studied. The crystalline structure of the particles will be analysed, due to its relation to magnetic properties.

### 2. Experimental

CoPt deposits were prepared potentiostatically at 40 °C and different deposition times using a  $2.5 \times 10^{-3}$  M  $\text{CoCl}_2 + 1.2 \times 10^{-3}$  M  $\text{Na}_2\text{PtCl}_6 + 1$  M  $\text{NH}_4\text{Cl} + 30$  g  $\text{dm}^{-3}$   $\text{H}_3\text{BO}_3$ , pH 4.5 solution. Solutions were stirred at 60 rpm using a magnetic stirrer. Solutions were freshly prepared with distilled water treated with a Millipore Milli Q system. Solutions were de-aerated by argon bubbling before each experiment and maintained under argon atmosphere during it.

Electrodeposition has been carried out using a potentiostat/galvanostat Autolab PGSTAT30 with GPES software in a three-electrode cell under temperature controlled conditions. Graphite electrodes were polished using alumina of 1.87  $\mu\text{m}$  and cleaned ultrasonically for 2 min in water. The reference electrode was an  $\text{Ag}/\text{AgCl}/1$  mol  $\text{dm}^{-3}$   $\text{NaCl}$  electrode. The counter electrode was a platinum spiral.

Leica Stereoscan S-360 and Hitachi H-4100FE scanning electron microscopes were used to analyse deposits composition and for morphology observation, respectively.

Structure of deposits was studied by means of a Philips MRD diffractometer with parallel optical geometry using  $\text{Cu K}\alpha$  radiation ( $\lambda = 1.5418$  Å).

\* Corresponding author. Tel.: +34 403 92 38; fax: +34 402 12 31.  
E-mail address: [e.valles@ub.edu](mailto:e.valles@ub.edu) (E. Vallés).

Magnetic properties were characterized by means of a SQUID magnetometer at room-temperature. Deposits were detached from the substrate and placed into a capsule for magnetic characterisation.

### 3. Results and discussion

The study of the CoPt system was performed to find the range of potentials to work with. In the cyclic voltammetry the potential was first scanned to negatives potentials (Fig. 1). A reduction current was detected from 0.15 V; this reduction process was assigned to platinum deposition and was supported by the pure Pt obtained from deposition in this potential range. From potentials of  $-0.9$  V simultaneous codeposition of cobalt and platinum took place. Three oxidation peaks were detected in the positive scan: The peak at  $-0.5$  V corresponded to the oxidation of molecular hydrogen retained over the electrode. This was a consequence of the simultaneous hydrogen evolution during the electrodeposition; this was confirmed by the disappearance of this peak for the stirred voltammogram. The oxidation peak detected at  $-0.25$  V appeared when CoPt was formed and it corresponds to cobalt or alloy oxidation. The peak at positive potentials (0.6 V) was detected also for pure platinum oxidation and it corresponds to the superficial platinum oxide formation [12].

#### 3.1. Preparation and characterisation of the CoPt particles as a function of the deposition time

The potential range to induce simultaneous platinum and cobalt deposition was selected from voltammetric experiments. Particles were obtained potentiostatically using short deposition times. Different potentials were chosen in the range ( $-950$ ,  $-1150$  mV) to induce different deposits compositions. The  $j-t$  transients recorded show distortions due to hydrogen bubble detachment during the deposition (Fig. 2).

The observation of the samples (FE-SEM) at short times reveals the formation of nanoscale size particles that evolved into coalesced crystals (Fig. 2). Rounded nuclei/crystallites were initially formed, these structured with time. As the deposition time was increased, the particles increase in size until a continuous deposit was reached. After this, the grain size increased with the deposition time. At short deposition times, CoPt particles were richer in platinum due to the initial platinum formation. The Pt percentage

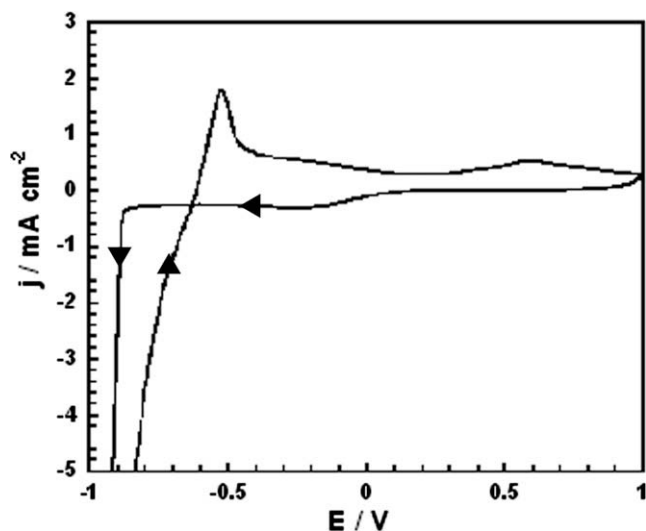


Fig. 1. Cyclic voltammetry at  $50 \text{ mV s}^{-1}$ ,  $\omega = 0 \text{ rpm}$ . Initial potential: 0.5 V.

of the particles was slightly decreased by increasing the deposition time. For moderate deposition times deposit composition was practically constant.

All samples prepared (CoPt particles and continuous deposits (55–72 wt.% Pt)) had a crystalline Co-hcp phase distorted by the Pt incorporation. Fig. 3A shows a representative diffractogram of one of the samples, similar diffraction patterns were measured for other samples (not shown). The diffraction peak positions shifted to lower  $\theta$  values with respect to pure cobalt ones, being the shift more significant by increasing Pt percentage.

Magnetic response of the CoPt particles depended on both the size of the particles and their composition, although ferromagnetic behaviour was observed in all cases (Fig. 3B). Low coercivity ( $H_c$ ) values (150 Oe, curve a) were measured for the smallest particles (40–50 nm at  $-1050$  mV). By increasing deposition time, particles grow with a corresponding increase in the hard-magnetic response (curve b), until a maximum value of  $H_c$  (1800 Oe, curve c) was reached before the particle coalescence (curve d).  $H_c$  drastically decreased when continuous deposits were formed but no further  $H_c$  variation was observed when the grain size increased in the stage of continuous film deposition.

The variation in  $H_c$  observed is not justified by the particles composition, as increases while decreasing the platinum content [8]. That fact can be explained for the different contributions (bulk, surface and shape anisotropy) to the effective magnetic anisotropy for unit volume of the material ( $K_{\text{eff}}$ ) [11]. Surface anisotropy is significant when the magnetic system is formed of particles due to the high surface area. Consequently, higher coercivity was observed for the CoPt particles than for continuous deposits. Increasing the particle size caused an increase in the  $K_{\text{eff}}V$  product due to the greater volume ( $V$ ) of the system. This result indicates that most of the obtained particles are mono-domain, rather than wall-domain formation which would favour a decrease in  $H_c$  [11,13]. A decrease in  $H_c$  is not observed in our case until after the formation of continuous deposits. After a critical particle radius, a magnetic system evolves from mono-domain into multi-domain [13] and  $H_c$  of the material decreases. The critical radius of the CoPt system is expected to be higher than that of the corresponding pure hcp Co (34 nm) and similar to other hard-magnetic systems, such as NdFeB (100 nm) [14]. This could explain why the CoPt electrodeposited particles were mono-domain, resulting in a maximum  $H_c$  value.

When deposition was performed at  $-1050$  mV, the maximum  $H_c$  values were obtained for CoPt 150–190 nm size particles.  $H_c$  values up to 1800 Oe were attained directly by electrodeposition of the particles, without annealing of the samples.

After the formation of continuous deposits a decrease on the coercivity of the films was observed (Fig. 3B, curve d) due to the decrease of surface anisotropy and the increase of disorder. Moreover, constricted loops were observed, which could reveal a double contribution in magnetism probably as a consequence of a double orientation of the grains.

#### 3.2. Influence of the applied potential in the magnetic properties of the CoPt particles

Fig. 4 shows two deposits prepared at different deposition potential and fixed time. Smaller particles were obtained, as expected, even for higher deposition charge, at more negative deposition potentials because nucleation was energetically favoured. The control of deposition times and potentials led to control the size of the particles. A decrease in the Pt percentage was observed by applying more negative potentials.

For all the potentials tested, hard-magnetic behaviour of the particles was observed (Fig. 4). The specific  $H_c$  value was dependent on particles composition, but mainly on the particles size. A decrease of the Pt percentage in the particles led to a decrease in

Sample	t / s	wt. % Pt	wt. % Co	morphology
A	5	--	--	40-56 nm
B	20	68.6	31.4	64-105 nm
C	100	60.2	39.8	150-192 nm
D	500	57.7	42.3	Coalescence
E	1000	55.9	44.1	Coalescence

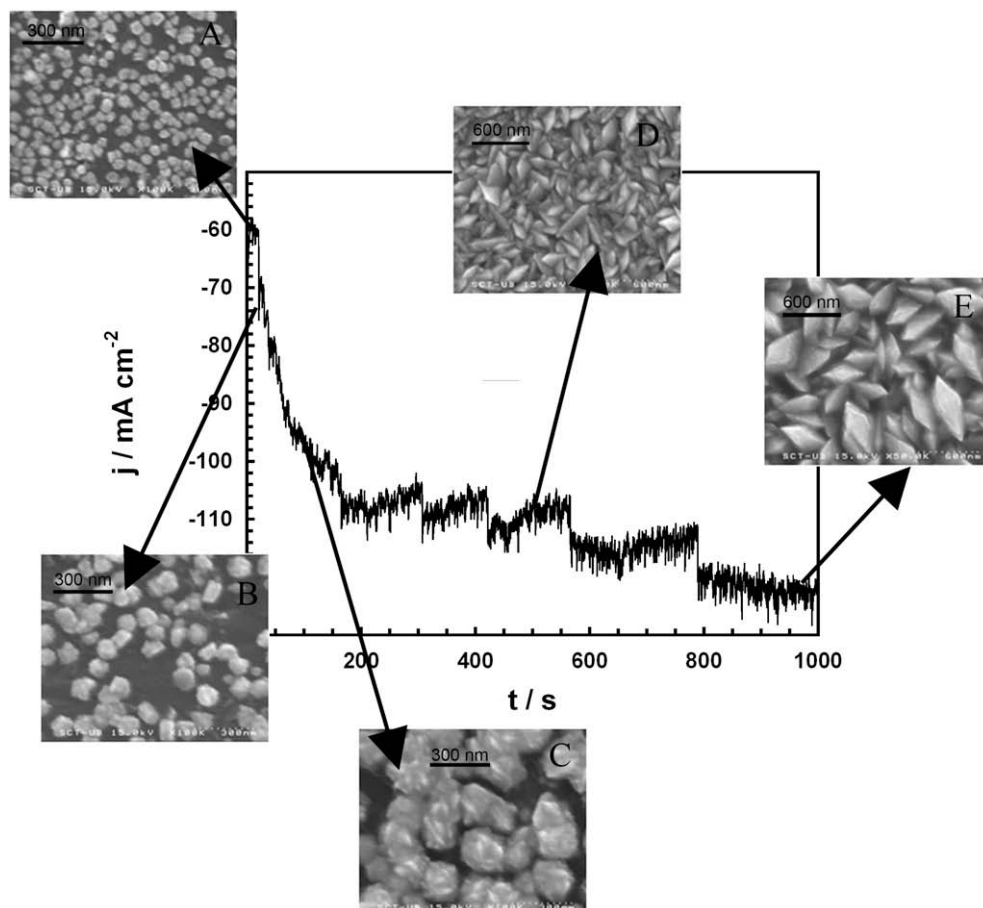


Fig. 2.  $j-t$  transient at  $-1050$  mV,  $\omega = 60$  rpm and FE-SEM images and compositions of CoPt deposits obtained at different deposition times.

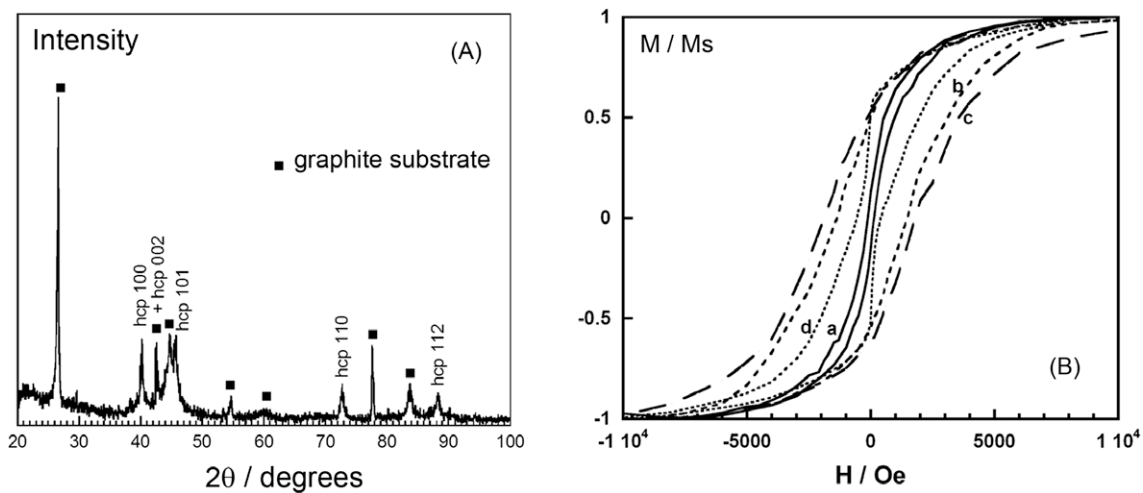


Fig. 3. (A) X-ray diffractogram of a CoPt deposit, sample D. (B) Normalized room-temperature magnetization curves of CoPt deposits, samples (a) A (b) B (c) C (d) D and E.

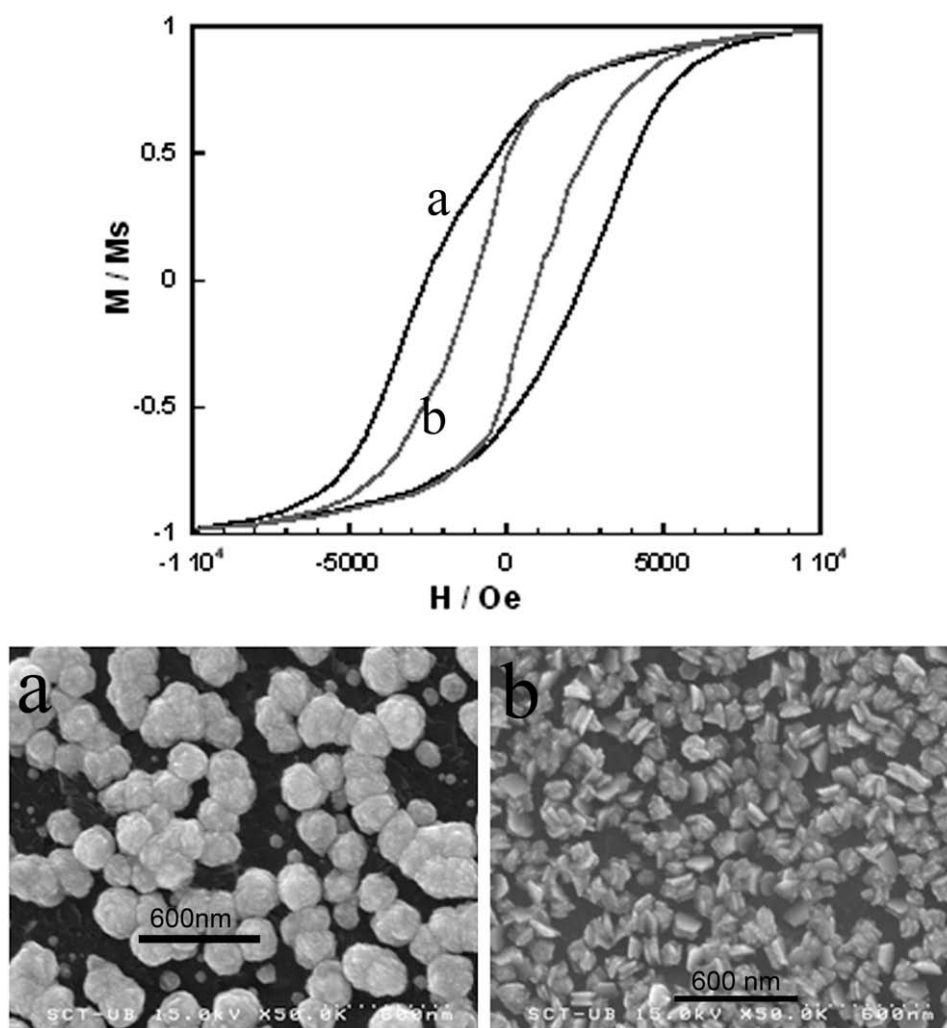


Fig. 4. Normalized room-temperature magnetization curves and FE-SEM images of CoPt particles obtained at 50 s at (a)  $-950$  mV, 71% wt. Pt, (b)  $-1150$  mV, 63% wt. Pt.

the coercivity. An increase in the particles size induced more hard-magnetic behaviour. All the obtained particles were thought to be mono-domain particles due to the fact that by increasing the size the coercivity value increases. No domain-walls were formed since if a domain wall was formed the magnetic energy decreases [13].

Particles of 71% wt. of Pt, electrodeposited at moderate potential ( $-950$  mV) and 150–250 nm size show the maximum hard-magnetic behaviour (2500 Oe of  $H_c$ ).

#### 4. Conclusions

The electrodeposition method allowed us to obtain submicron CoPt particles and modulate the size and the magnetic properties as a function of the deposition potential. Using this method we also obtain continuous deposits. The deposits composition varied with time in the first stages of the process as a consequence of the initial Pt deposition over which simultaneous Co deposition occurred; Pt percentage in the deposits slightly decreased with time to attain a constant value. Both CoPt particles and continuous deposits with 55–70% wt Pt prepared showed a hexagonal cobalt face distorted by the presence of Pt.

Magnetic behaviour depended on the size of the CoPt particles as well as of their composition. However, the most significant factor is the particles size, because it has been found that the size of

the particles has a dramatic influence in the coercivity values of the material (150–2500 Oe). By controlling the size of the particles electrochemically magnetic properties can be modulated. The bigger the particles the higher the coercivity value as long as the particles are mono-domain. It has been possible to prepare CoPt particles with significantly more hard-magnetic properties than the corresponding continuous deposits. Particles of 150–250 nm, hexagonal structure and a high wt percentage in Pt showed the higher coercivity.

#### Acknowledgments

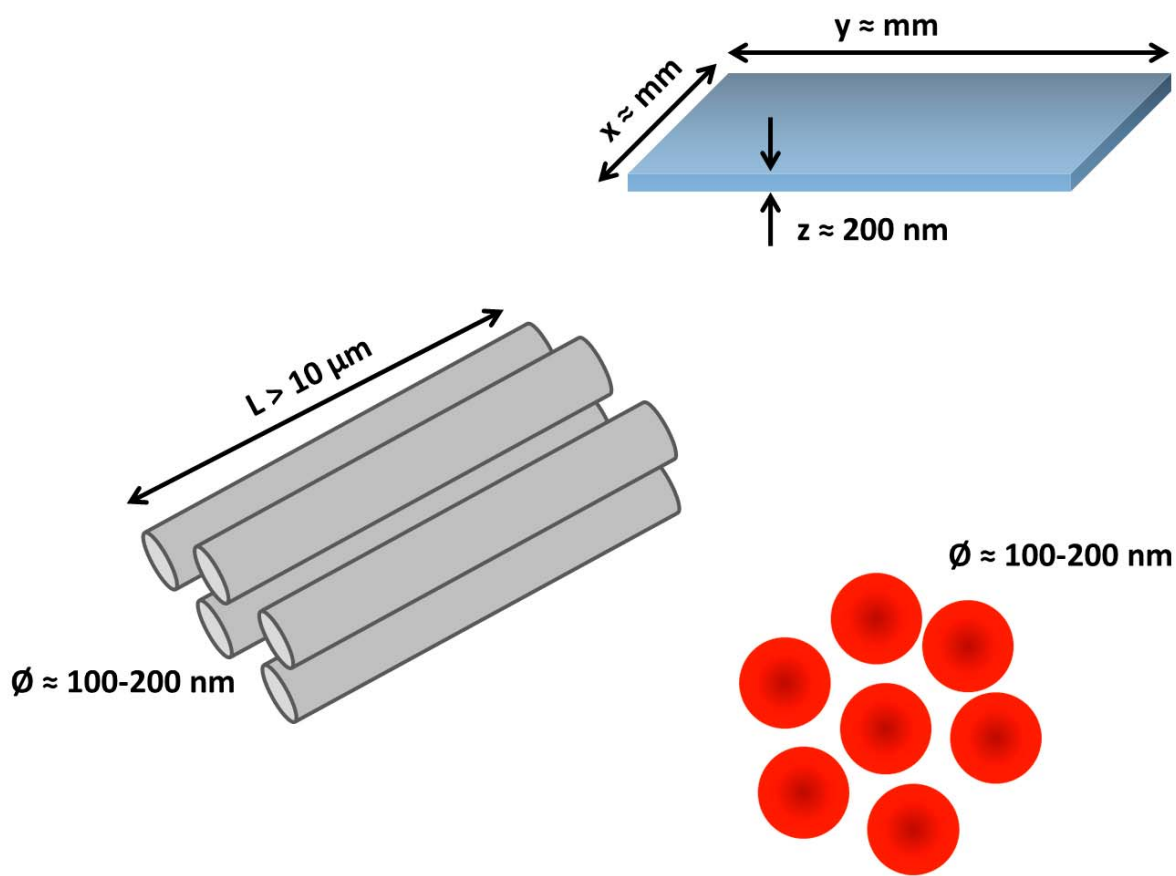
The authors wish to thank the Serveis Científicotècnics (Universitat de Barcelona) for the use of their equipment. This paper was supported by contract MAT2006-12913-C02-01 from the *Comisión Interministerial de Ciencia y Tecnología (CICYT)*.

#### References

- [1] S. Guan, B.J. Nelson, K. Vilmers, J. Electrochem. Soc. 151 (2004) C545–C549.
- [2] S. Pané, E. Gómez, E. Vallés, Electrochem. Commun. 9 (2007) 1755–1760.
- [3] I. Zana, G. Zangari, J.-W. Park, M.G. Allen, J. Magn. Magn. Mater. 272–276 (2004) e1775.
- [4] L. Vieux-Rochaz, C. Dieppedale, B. Desloges, D. Gamet, C. Barragatti, H. Rostaing, J. Meunier-Carus, J. Micromech. Microeng. 16 (2006) 219–224.
- [5] P.L. Cavallotti, M. Bestetti, S. Franz, Electrochim. Acta 48 (2003) 3013–3020.
- [6] N. Fujita, S. Maeda, S. Yoshida, M. Takase, M. Nakano, H. Fukunaga, J. Magn. Magn. Mater. 272 (2004) e1895.

- [7] G. Pattanaik, G. Zangari, *J. Electrochem. Soc.* 153 (2006) C6.
- [8] M. Cortés, S. Matencio, E. Gómez, E. Vallés, *J. Electroanal. Chem.* 627 (2009) 69.
- [9] J. Solla-Gullón, E. Gómez, E. Vallés, A. Aldaz, J.M. Feliu, *J. Nanopart. Res.*, doi: 10.1007/s11051-009-9680-4.
- [10] N.A. Spalding, *Ferroelectrics and ferromagnets*, in: *Physics of Ferroelectrics*, Springer-Verlag GmbH, Heidelberg 2007.
- [11] R.A. McCurrie, *Ferromagnetic Materials, Structure and Properties*, Academic Press Inc., San Diego, 1994.
- [12] J. Clavilier, D. Armand, *J. Electroanal. Chem.* 199 (1986) 187.
- [13] C. Tannous, J. Gieraltowski, *The Stoner-Wohlfarth Model of Ferromagnetism: Static properties*, arXiv:physics/0607117v3 [physics.class-ph], 2008.
- [14] R. Skomski, *J. Phys.: Condens. Matter* 15 (2003) R841.

5.4.4 CoPt nanoscale structures with different geometry prepared by electrodeposition for modulation of their magnetic properties





# CoPt nanoscale structures with different geometry prepared by electrodeposition for modulation of their magnetic properties

M. Cortés, A. Serrà, E. Gómez<sup>1</sup>, E. Vallés<sup>\*,1</sup>

*Electrodep, Departament de Química Física and Institut de Nanociència i Nanotecnologia (IN<sup>2</sup>UB), Universitat de Barcelona, Martí i Franquès 1, 08028 Barcelona, Spain*

## ARTICLE INFO

### Article history:

Received 14 April 2011

Received in revised form 21 June 2011

Accepted 22 June 2011

Available online 30 June 2011

### Keywords:

Electrodeposition

Nanoparticles

Nanowires

CoPt

Magnetic properties

## ABSTRACT

Different nanoscale structures of CoPt have been prepared by electrodeposition. Nonmagnetic materials were used in all cases, so that the substrates did not interfere in the magnetic properties of the deposits. Thin films of 200–300 nm-thick were obtained on glass/ITO substrates; nanoparticles of 150 nm of diameter were obtained over silicon; nanowires of 100–200 nm of diameter and 14  $\mu\text{m}$  length were obtained by using polycarbonate membranes sputtered with Au. All deposited geometries had a fixed composition (68–71 wt.% Pt) and crystalline structure typical of Co-hcp, distorted due to platinum incorporation. A study of the magnetic properties of the different geometries was performed. Dramatic changes in magnetism have been detected, related to the shape of the nanostructures: nanowires presented the lowest coercivity (330–700 Oe), thin films had a coercivity value of 850 Oe, while nanoparticles had the highest coercivity (2040 Oe). These coercivity variations were caused by different anisotropy contributions, depending on the geometry. The corrosion resistance test has been performed to determine the viability of the prepared nanostructures, nanostructures with higher exposed surface area had increase tendency to oxidation.

© 2011 Elsevier Ltd. All rights reserved.

## 1. Introduction

The miniaturisation of hard magnetic materials has recently attracted interest for their integration in micromechanical systems (MEMS). For this application, both soft and hard-magnetic materials are required, of which soft magnetic materials have already been successfully integrated with micro-fabrication processes. The hard-magnetic materials can be also applied in actuators and sensors as permanent magnets. Electrochemical methods can be used to prepare permanent magnets in the nanoscale for use in micro-devices [1–4] because electrodeposition allows very different type of deposits over several substrates to be obtained, even over templates or photolithographically prepared substrates [5–11]. Additionally, electrochemistry permits an easy control of the growth process, and chemical composition of the deposit.

Some binary and ternary cobalt alloys have been tested to be used in magnetic microactuators [12–18]. CoPt alloys show great potential for this purpose, including applications in magnetic recording media, micro-electromechanical systems (MEMS) as magneto-optical properties [19–25]. CoPt deposition has been demonstrated by several electrodeposition methods, such as

galvanostatic control or alternating-current, although electrodeposition of CoPt is hindered by the significant hydrogen evolution. The CoPt structure obtained by electrodeposition is mainly Fcc, which exhibits a soft ferromagnetic behaviour; subsequent thermal treatments are necessary to obtain crystalline structures with high magnetocrystalline anisotropy and hard-magnetic behaviour. In previous works, films of CoPt of different composition were obtained in our laboratory [26]. Deposits containing high proportion of Pt but maintaining an hcp structure showed relatively high coercivity without annealing the samples. Also, CoPt particles were prepared [27] showing variable magnetic properties as a function of their size, although measuring the magnetic response of the particles over the graphite substrate was difficult.

Following these previous results, the aim of this paper is to analyse the possibility of controlling the electrodeposition parameters for preparing platinum-rich CoPt alloys with fixed composition in the form of different nanoscale structures (nanometric thin films, particles and nanowires), modulating their magnetic properties as a function of the geometry of the deposits. An alloy composition of 60–70 wt.% of Pt is desired to induce the formation of a very anisotropic hcp structure. The final objective will be to induce better hard-magnetic behaviour as a function of the shape, without the need for sample annealing. For each kind of structure, a selection of better non-magnetic electrodes will be used to enable simultaneous electrodeposition of the alloy and the measurement of their magnetic properties.

\* Corresponding author. Tel.: +34 403 92 38; fax: +34 402 12 31.

E-mail address: [e.valles@ub.edu](mailto:e.valles@ub.edu) (E. Vallés).

<sup>1</sup> ISE member.

## 2. Experimental

The electrochemical study and sample preparation has been performed using a solution containing  $2.5 \times 10^{-3}$  M  $\text{CoCl}_2 + 1.2 \times 10^{-3}$  M  $\text{Na}_2\text{PtCl}_6 + 0.5 \times 10^{-2}$  M sodium citrate + 1 M  $\text{NH}_4\text{Cl} + 30 \text{ g dm}^{-3}$   $\text{H}_3\text{BO}_3$  (the pH of the solution was adjusted at 4.5 with NaOH solutions). All the reagents were of analytical grade. The solution was freshly prepared with water which was first doubly distilled and then treated with a Millipore Milli Q system. The solution was de-aerated by argon bubbling before each experiment and maintained under argon atmosphere during it. Electrodeposition was mainly performed in a three-electrode cell with control of the temperature and vertical arrangement of the working electrode, while for the nanowires a cell with horizontal working electrode arrangement was used.

A microcomputer-controlled potentiostat/galvanostat Autolab with PGSTAT30 equipment and GPES software was used for the preparation of deposits. Different substrates were used to obtain the different structures of CoPt. Doped silicon pieces (p-B Sitronix 11523-13012 with a resistivity of  $0.008\text{--}0.012 \Omega \text{ cm}$ ) of  $0.6 \text{ cm} \times 0.3 \text{ cm}$  were used as working electrodes to obtain the sub-micrometer particles. The silicon substrate was etched with a 5% (p/v) HF solution for 60 s to remove the native silicon oxide prior to be immersed in the electrodeposition solution.

20  $\mu\text{m}$ -thick polycarbonate membranes with pore diameters of 200 nm and 100 nm were used to grow the nanowires. Vacuum evaporation was used to coat the membranes with around a 100 nm-thick gold layer, enabling conductivity. Prior to the electrodeposition the porous template was kept in distilled water for several hours to make the pores hydrophilic for uniform filling of the pores. After that, the distilled water was replaced with the prepared electrolyte bath for depositing the nanowires. This additional step was crucial for obtaining homogeneous growth over the entire membrane. The gold-coated membranes were placed in contact with the solution, at the bottom of the cell. Finally, glass substrates covered with ITO (Indium Tin Oxide) (25 nm thick) were used to obtain the thin films. The reference electrode was an  $\text{Ag}/\text{AgCl}/1 \text{ mol dm}^{-3}$  NaCl electrode. The counter electrode was a platinum spiral. The solution was stirred during the electrodeposition to assure a constant composition throughout the samples. Without stirring, dissolution during the deposit preparation corresponded to a decrease of the platinum composition, resulting in obtaining non-uniform properties as a function of the deposit thickness. All substrates used allowed the magnetic properties of the prepared deposits to be measured directly, because they do not affect the magnetic response of the CoPt alloy.

Elemental composition was determined with an X-ray analyser incorporated in Leica Stereoscan S-360 equipment. Both Hitachi H-4100FE (field emission scanning electron microscope) and JEOL 2100 Transmission Electron Microscopy (TEM) were used for the observation of the samples. Thicknesses of the thin films were measured using Leica DCM 3D Confocal and Interferometer.

The structure of the deposits was studied by means of a Philips MRD diffractometer with parallel optical geometry using  $\text{Cu K}\alpha$  radiation ( $\lambda = 1.5418 \text{ \AA}$ ) as well as JEOL JEM 2100 TEM in the case of the nanowires. Magnetic properties were characterized using a SQUID magnetometer at room temperature in helium atmosphere.

Corrosion tests were carried out at  $25^\circ\text{C}$  in a 5% NaCl (p.a.) solution. The samples were immersed in NaCl media for 3 h in order to determine the steady-state potential ( $E_{\text{ss}}$ ). Immediately afterwards, a linear potentiodynamic sweep from  $E_{\text{ss}} - 300$  to  $+300 \text{ mV}$  was performed at  $0.1 \text{ mV s}^{-1}$  to evaluate corrosion potential ( $E_{\text{corr}}$ ) and current density corrosion ( $j_{\text{corr}}$ ). No stirring was performed during both the polarisation and potentiodynamic scan.

## 3. Results and discussion

The substrates selected to obtain the different geometries of the CoPt deposits were suitable for studying the magnetic properties of the deposited alloy, without interfering in the magnetic measurements. Glass/ITO was selected to prepare the nanometric thin films; this substrate is not very conductive, so a high applied negative potential is needed to perform the CoPt electrodeposition. However, once the deposition took place, an elevated nucleation rate was observed, so it was possible to obtain thin films. Although the nucleation rate was not high enough to have an excess of growth of the deposit and to obtain thick deposits instead of thin ones. The activated silicon substrate was used to prepare the particles because nucleation on this substrate is not favoured and the first nuclei formed grown leading to particles; no layers were formed within moderate deposition times. Finally, polycarbonate membranes sputtered with gold were chosen as templates for nanowires due to the conductivity of gold permits the deposition into the porous channels.

The voltammetric study of the CoPt system was performed to find the optimum range of working potentials over each substrate (Fig. 1). Fig. 1a shows the voltammetric curve obtained over glass/ITO substrate. A first reduction current was detected from  $-0.2 \text{ V}$ , assigned to the initial platinum reduction; from around  $-0.9 \text{ V}$ , an increase of the reduction current was detected, assigned to the simultaneous deposition of platinum and cobalt and hydrogen evolution. The oxidation peak detected at  $-0.5 \text{ V}$  disappears when the solution is stirred and therefore corresponds to the oxidation of the molecular hydrogen retained on the electrode. The following oxidation current corresponds to alloy oxidation (band at  $-0.4$  to  $0 \text{ V}$ ) and platinum oxidation ( $0.6 \text{ V}$ ).

Similar voltammetric behaviour was observed over the activate silicon substrate (Fig. 1b), although lower current corresponding to initial platinum deposition, prior to CoPt deposition, was detected. The voltammetric profile, corresponding to the deposition process over the polycarbonate membrane coated with gold layer, showed also the platinum reduction current followed by the alloy deposition (Fig. 1c). When alloy oxidation occurred, simultaneous oxidation of the seed layer was favoured (anodic peak), as was observed after the scan. More reduction current density was obtained with respect to those obtained from the other substrates, taking into account the geometrical area of the pores, which reveals the higher real surface area in the channel pores after depositing the gold layer.

For all the substrates used, a minimum value of potential will be necessary to induce CoPt deposition, avoiding pure-platinum deposition. The onset of the CoPt deposition process and the  $j/E$  slope corresponding to the reduction process varied as a function of the nature of the conducting layer over each substrate. For the polycarbonate membrane/gold layer substrate, the onset of the deposition process occurred at less negative potentials than that of glass/ITO or activated silicon substrates. The  $j/E$  slope of the CoPt reduction process followed the trend: silicon > polycarbonate membrane/gold layer > glass/ITO. Although the movement of the electroactive species into the porous channels is usually difficult, in our case, the presence of the conductive gold seed layer and the size of the porous make the onset of the deposition process easy. In previous studies we have determined that the alloy composition can be modulated from the overpotential applied. Increasing the overpotential causes an increase in the cobalt percentage and by controlling the applied potential deposits ranging from nearly pure platinum to high cobalt percentage can be attained. To prepare the structures, potentiostatic deposition was selected and the potentials were chosen to attain a fixed alloy composition in all the cases. Compositions in the range 60–70 wt.% Pt were desired to obtain CoPt alloys with high incorporation of Pt in the cobalt crys-

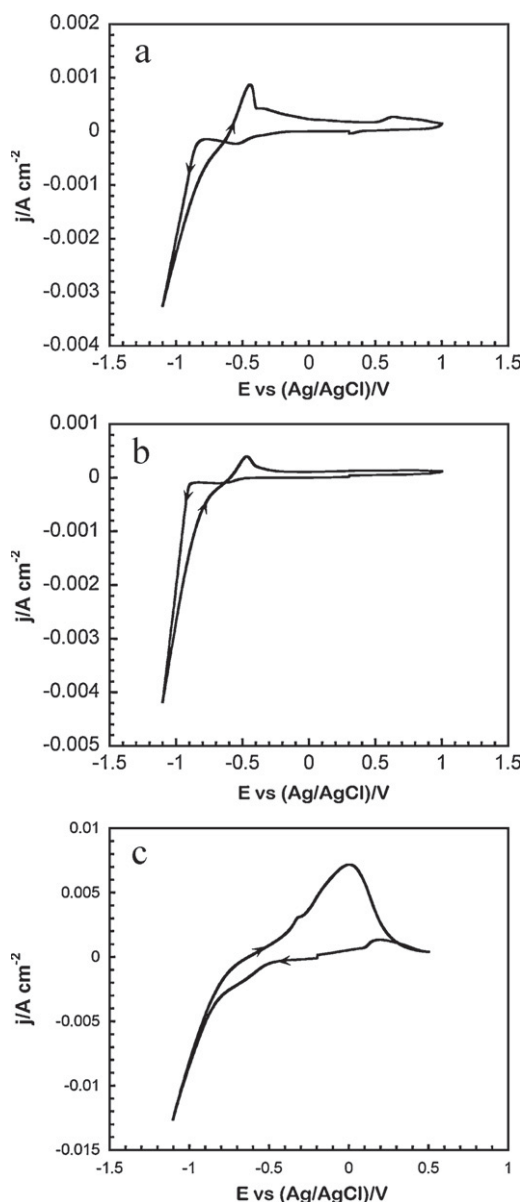


Fig. 1. Cyclic voltammograms of the working bath ( $2.5 \times 10^{-3}$  M  $\text{CoCl}_2 + 1.2 \times 10^{-3}$  M  $\text{Na}_2\text{PtCl}_6 + 0.5 \times 10^{-2}$  M citrate + 1 M  $\text{NH}_4\text{Cl} + 30 \text{ g dm}^{-3}$   $\text{H}_3\text{BO}_3$ ) over (a) ITO, (b) Si and (c) polycarbonate membrane of  $\theta = 200$  nm.

talline phase, with the maximum coercivity. Higher than 75 wt.% of platinum leads to a change in the crystalline structure and a drastic change in the magnetic properties [26].

In the glass/ITO substrate, the low  $j/E$  slope recorded in the voltammetric curve revealed the low incorporation of Co with the applied potential; very negative potentials ( $-1300$  mV) will be necessary to attain the same cobalt percentages.

### 3.1. Preparation and characterisation of CoPt thin films

CoPt thin films were deposited over glass/ITO substrates at  $-1300$  mV, to induce significant nuclei formation, using a deposition time of 300 s to assure coalescence of the crystallites and subsequent film formation. Less deposition time will lead to an inhomogeneous layer and with longer deposition times the thin film will evolve to deposits with properties tending to bulk ones. Smooth and reflective deposits of 230 nm-thick (Fig. 2b) with a Pt percentage of around 68 wt.% were obtained. FE-SEM observation

shows polyhedral fine grains (Fig. 2a). A representative diffractogram of one of the samples is shown in Fig. 2c. The XRD pattern reveals that all the samples present a Co-hcp structure significantly distorted for the high Pt incorporation, although some small peaks corresponding to cobalt oxide are also observed. These deposits showed coercivity values around 850 Oe at room temperature. Similar coercivity was obtained for Pattanaik et al. when the magnetic field was applied parallel to the film [28]. However, in their case higher coercivity was observed when applying the field perpendicular to the sample because of the lower thickness of the deposits and the Ru/Cu underlayer used for the hcp deposit orientation. Very different values of the saturation fields can be observed by applying the field parallel or perpendicular to the sample, revealing the magnetic anisotropy of the films (Fig. 2d). Shape anisotropy is expected for the samples of nanometric thickness and millimetric  $x$ - $y$  dimensions. The magnetization easy axis was the parallel to the applied field.

### 3.2. Preparation and characterisation of CoPt particles

Particles were obtained at  $-1050$  mV over silicon substrate with a deposition time of 40 s. Particles prepared had a platinum percentage of 71 wt.% that is in the desired composition range. The deposition time was adjusted in order to obtain nanoscale size particles (around 150 nm of diameter) (Fig. 3a). The particles were polycrystalline with a Co-hcp phase distorted by the Pt incorporation, the diffraction peak positions shifted to lower  $\theta$  values with respect to pure cobalt ones (Fig. 3b). Some peaks according to some cobalt oxides were also observed.

Normalized magnetization curves were taken with the field applied parallel to the samples at different temperatures. No superparamagnetic behaviour was observed as a consequence of the size of the particles. On the contrary, high coercivity was obtained for the particles over the substrate, even at room temperature. High coercivity is caused by different contributions to the effective magnetic anisotropy ( $K_{\text{eff}}$ ) of the CoPt particles: from the bulk, surface and shape. In this case, the main effect is caused by the surface anisotropy of the particles, due to their high relative surface area [29]. The particle size is likely to be smaller than the critical radius of the CoPt system, which is anticipated to be greater than pure hcp Co (34 nm) and more similar to other hard-magnetic systems, such as NdFeB (100 nm) [30]. The presence of mono-domains may also explain the high  $H_c$  of electrodeposited CoPt particles. Although cobalt oxide is antiferromagnetic, its presence should not affect the magnetic properties of the particles in the concentration evidenced by XRD. A slight increase in the coercivity value ( $H_c$ ) was obtained by decreasing the temperature (Fig. 3c) from 2040 Oe at 300 K to 2700 Oe at 5 K, which is similar to the results obtained from Ouchi et al. [31] although patterned substrates were not required. This result which is consistent with the expected behaviour; a higher magnetic field is required to switch magnetic domains when the thermal energy is decreased.

### 3.3. Preparation and characterization of CoPt nanowires

The possibility of growing CoPt nanowires of the desired composition was tested using polycarbonate membranes with 100 and 200 nm diameter pores. Long deposition times were selected to test the electrodeposition of long well defined nanowires. By applying a potential of  $-800$  mV several microns long nanowires were obtained in both type of membranes. As it can be observed in a cross-sectional view of the electrodeposited membrane (Fig. 4a), nanowires were well grown and parallel to one another throughout the entire membrane, up to 14  $\mu\text{m}$  length. Both types of nanowires contained 68 wt.% of Pt, which demonstrates that using the electrodeposition method from the selected bath and conditions allows

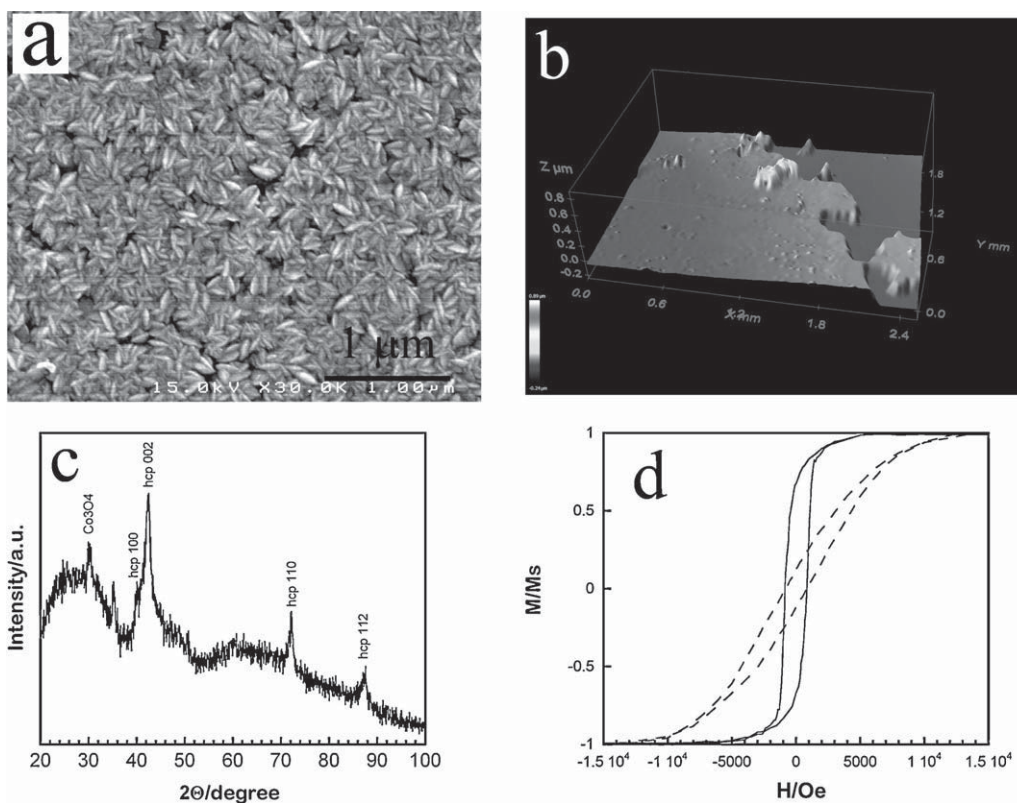


**Fig. 2.** (a) SEM micrograph, (b) interferometer image, (c) XRD pattern and (d) normalized magnetic curves with the field applied parallel (solid line) and perpendicular (dashed line) of a CoPt deposit over ITO,  $t = 300$  s, 68 wt.% Pt.

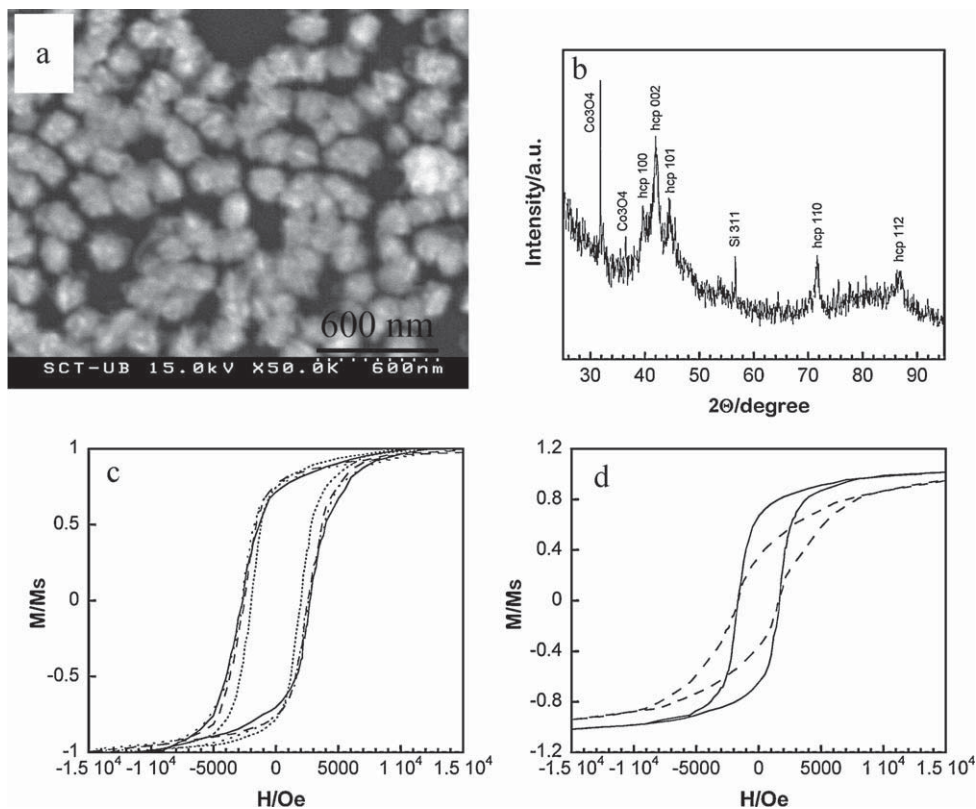


**Fig. 3.** (a) SEM micrograph, (b) XRD pattern and (c) normalized magnetic curves at 300 K (solid line), 50 K (dashed line), 5 K (plotted line) (d) normalized magnetic curves at room temperature with the field applied parallel (solid line), perpendicular (dashed line) of CoPt particles, 71 wt.% Pt.

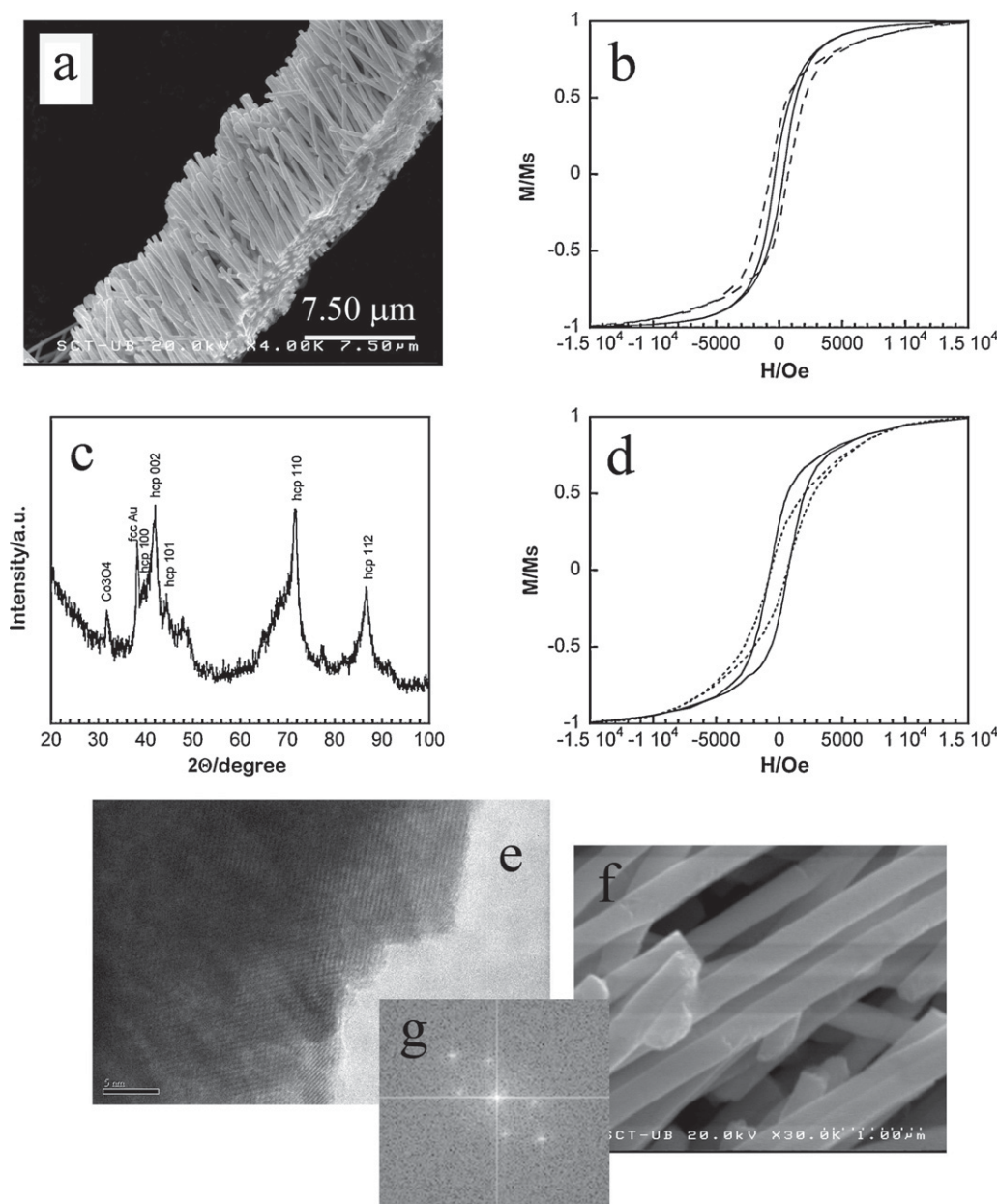


**Fig. 4.** (a) SEM micrograph of CoPt nanowires,  $\varnothing=200$  nm, 68 wt.% Pt. (b) Normalized magnetic curves with the field applied perpendicular to the nanowire axis of CoPt nanowires,  $\varnothing=200$  nm, 68 wt.% Pt (solid line), deposition time 26,000 s, CoPt nanowires,  $\varnothing=100$  nm, 67 wt.% Pt (dashed line), deposition time 22,000 s. (c) XRD pattern of CoPt nanowires,  $\varnothing=200$  nm, 68 wt.% Pt (d) normalized magnetic curves of CoPt nanowires,  $\varnothing=200$  nm, 68 wt.% Pt with the field applied perpendicular to the nanowire axis (solid line), parallel to the nanowire axis (dashed line). Deposition time 26,000 s, (e) FFT image and FE-SEM micrograph of CoPt nanowires,  $\varnothing=200$  nm, 68 wt.% Pt, removed from the template.

the preparation of CoPt nanowires with modulated composition. A representative XRD pattern for both diameter-thick nanowires is shown in Fig. 4c. As it is expected, nanowires of this composition correspond to an hcp-cobalt crystalline structure distorted by the platinum incorporation as in the other geometrical structures previously obtained in this work. In this case a peak corresponding to cobalt oxide is present in the diffractogram as well as an fcc-Au peak. The nanowire structure was also studied by means of TEM after removing them from the template. First, the gold layer was removed using a saturated  $I_2/I^-$  solution and then polycarbonate membrane was dissolved with chloroform. Fig. 4f shows a detail of the released nanowires from which the TEM observation was performed. The HRTEM micrographs always show different sets of fringe patterns in the nanowires, from which the crystalline structure can be deduced. Fig. 4e is a representative lattice image from

one edge of a nanowire. The fast Fourier transform (FFT) pattern taken from a representative region of the sample is represented (Fig. 4g). The FFT patterns were positioned in regions exhibiting significant contrast differences. Each of the diffraction spots was indexed. The FFT image let to identify specific lattice fringes. On one hand,  $d$ -spacings of 2.23 Å, 2.11 Å and 2.00 Å were measured, which match perfectly with the (100), (002) and (101) orientations of a distorted Co-hcp structure, respectively. Moreover,  $d$ -spacing of 4.67 Å  $Co_3O_4$ -fcc (111), 2.86 Å  $Co_3O_4$ -fcc (220) and 2.44 Å  $Co_3O_4$ -fcc (311) were also present. These results confirm those obtained by XRD.

Fig. 4b and d shows the normalized hysteresis loops of nanowires of  $\varnothing=200$  nm and  $\varnothing=100$  nm arrays with the magnetic field applied parallel and perpendicular to the nanowire axis. In both cases the easy magnetization axis is perpendicular to the long

wire axis, however for the nanowires with  $\varnothing = 200$  nm the difference is not so significant. When the membrane is removed and the nanowires are released the same hysteresis loop is obtained, which is expected because the average separation between the nanowires in the polymer membranes is higher than 500 nm. This distance between the nanowires is high enough to not produce any inter-wire magnetostatic interaction. Although the shape anisotropy tends to force the magnetization to be along the nanowire axis, the magnetocrystalline anisotropy could align the magnetic moments in the perpendicular direction as it has been detected for other systems as a function of the porous diameter [32]. That fact has occurred here due to there is no a clear preferred orientation in the (002) direction that in the conditions where XRD was performed would mean that the easy axis of crystal anisotropy lied parallel to the cylinder axis. That corresponds to a crystalline orientation where there is a high percentage of the crystals with the (002) direction aligned perpendicular to the nanowire axis and hence magnetocrystalline anisotropy tends to align the magnetic moments in this direction. When the easy magnetization axis of the magnetocrystalline anisotropy is not in the same direction as that of the shape anisotropy, their competition will weaken anisotropy and hence differences in longitudinal and perpendicular M–H loops will be small. Shape anisotropy contributes less as the nanowire diameter increases because of the nanowire length/diameter ratio decreases, so in the  $\varnothing = 200$  nm nanowires the difference is less important. Some differences can be observed in the coercivity depending on the diameter (Fig. 4b). When the applied field is perpendicular to the axis of the nanowires, the coercivity ( $H_c$ ) of the nanowires with  $\varnothing = 100$  nm (around 700 Oe) is higher than the  $H_c$  values for the 200 nm diameter ones (around 330 Oe).

#### 3.4. Comparison of the different nanostructures

Although hydrogen evolution may differ as a consequence of the different geometry of the samples, electrodeposition has permitted the preparation of the CoPt alloy of the same composition in all the cases by adjusting both substrate and applied deposition potentials. However several differences were observed in their properties. Independent of the substrate used, hexagonal cobalt phase was detected in which the crystalline cell was distorted by the presence of the significant platinum percentage in the deposits. The (002) reflection decreased in the trend particles–films–nanowires, whereas the (110) reflection increases in the same trend, which reveals that the geometry of the deposits modulates the preferred orientation of the deposits.

In X-ray diffractograms, the peaks corresponding to cobalt oxides are also different in each microstructure. Continuous films reveal less oxide peaks whereas submicrometric particles present detected greater oxidation, as is usual when the dimension of the metallic structures is reduced. Electrochemical corrosion experiments were performed to corroborate this behaviour. Fig. 5 shows the potentiodynamic curves corresponding to two CoPt samples: CoPt films 300 nm thick and CoPt particles of 100–150 nm of diameter immersed in a NaCl 5% solution. A positive corrosion potential was observed for the CoPt films, revealing the expected behaviour for a Pt-containing alloy. A more negative value was detected for the CoPt nanometric particles revealing more accused tendency to the oxidation. Moreover, the particles presented higher  $j_{\text{corr}}$  ( $35.44 \mu\text{A cm}^{-2}$ ) than films ( $9.33 \mu\text{A cm}^{-2}$ ), corresponding to a higher corrosion rate.

Significant differences between the magnetic behaviour of different samples were observed. Although the thin films presented the highest shape anisotropy, evidenced by the highest difference between the saturation fields measured when applying the external magnetic field parallel or perpendicular (Fig. 2d), the highest coercivity was present in the nanoparticles, and consequently the

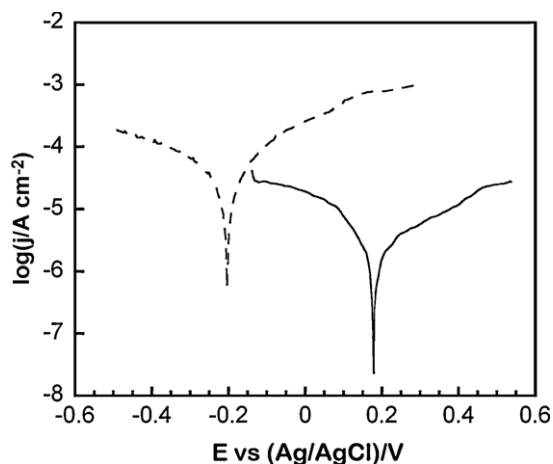


Fig. 5. Potentiodynamic polarization curves in logarithmic scale corresponding to CoPt 300 nm-thick films (solid line) and  $\varnothing = 100$ –150 nm particles (dashed line).

highest global anisotropy, even when some cobalt oxides were detected. That fact can be explained as a consequence of the different contributions in the anisotropy constant. For the nanoparticles, shape anisotropy was not expected and as can be observed in Fig. 3d, the saturation field difference observed when applying the field parallel or perpendicular was not too accused. As the nanoparticles were obtained electrochemically on top of a substrate, they are not perfectly round, causing a small amount of this type of anisotropy. Another effect which might contribute to the shape anisotropy is the attachment of the nanoparticles to substrate, so that interactions between them were different when applying parallel or perpendicular fields. As both thin films and nanoparticles exhibit the same crystal structure, hcp, the high global anisotropy observed here was attributed to the surface anisotropy. In the case of nanowires, a higher anisotropy was expected a priori (Fig. 4d), although the relatively high nanowire porous diameter reduces the expected anisotropy. The main reason for the observed anisotropy in these structures was the synergy of both shape and magnetocrystalline anisotropy effects. While shape anisotropy always tends to align the magnetic moments along the nanowire's axis, magnetocrystalline anisotropy can contribute either positively or negatively, depending on the orientation of the easy magnetization axis of the crystalline structure. For example, the small anisotropy observed in the case where the easy axis was oriented perpendicular to the wire axis is expected.

#### 4. Conclusions

Electrodeposition has been demonstrated as a useful method to obtain different CoPt structures with modulated geometry, defining particles, nanowires and thin films of controlled size and composition. The optimum conditions for electrodepositing a fixed alloy CoPt composition over different substrates were obtained, which permitted the preparation of different geometries of the alloy on top of substrates suitable for magnetic measurements to be done. Morphology and crystal structure of the different samples were studied revealing that the same hcp cobalt distorted structure was obtained with slight differences in the preferred orientation. A clear effect of the geometrical structure of the deposits in the magnetic properties was observed for a fixed alloy composition (68–71 wt.% Pt). Hard magnetic properties can be enhanced by changing the deposit shape. The trend from highest to lowest anisotropy follows: nanoparticles > thin films > nanowires with high aspect ratio, although different anisotropy contributions should be taken into account depending on the geometry. However, a corrosion resis-

tance test is necessary to determine the viability of the prepared nanostructures. The increase tendency of the nanostructures to oxidize relative to films is due to their higher exposed surface area.

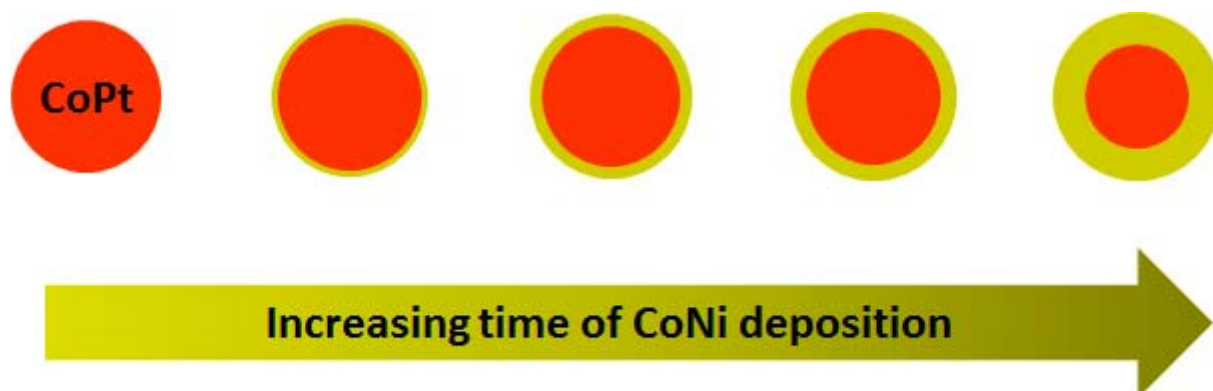
### Acknowledgments

This article was supported by contract CTQ2010-20726 (sub-program BQU) from the Comisión Interministerial de Ciencia y Tecnología (CICYT). The authors wish to thank the Serveis Científicocotècnics (Universitat de Barcelona) for the use of their equipment. Some substrates have been prepared in the Clean Room of the IMB-CNM (CSIC), supported by the IMB-CNM (CSIC)NGG-158 project. M.C. would also like to thank the Departament d'Innovació, Universitats i Empresa of the Generalitat de Catalunya and Fons Social Europeu for their financial support.

### References

- [1] S.Z. Chu, S. Inoue, K. Wada, K. Kurashima, *Electrochim. Acta* 51 (2005) 820.
- [2] A.I. Gapin, X.R. Ye, L.H. Chen, D. Hong, S. Jin, *IEEE Trans. Magn.* 43 (2007) 2151.
- [3] N.B. Chaure, F.M.F. Rhen, J.J.M. Hilton, D. Coey, *Electrochem. Commun.* 9 (2007) 155.
- [4] S. Shamaila, R. Sharif, S. Riaz, M. Khaleeq-ur-Rahman, X.F. Han, *Appl. Phys. A: Mater.* 92 (2008) 687.
- [5] Y. Peng, T. Cullins, G. Möbus, X. Xu, B. Inkson, *Nanotechnology* 18 (2007) 485704.
- [6] Y. Dahmane, L. Cagnon, J. Voiron, S. Pairis, M. Bacia, L. Ortega, N. Benbrahim, A. Kadri, *J. Phys. D: Appl. Phys.* 39 (2006) 4523.
- [7] W. Chen, Z. Li, G.B. Ji, S.L. Tang, M. Lu, Y.W. Du, *Solid State Commun.* 133 (2005) 235.
- [8] L. Cagnon, Y. Dahmane, J. Voiron, S. Pairis, M. Bacia, L. Ortega, N. Benbrahim, A. Kadri, *J. Magn. Mater.* 310 (2007) 2428.
- [9] J. Fu, S. Cherevko, C.H. Chung, *Electrochem. Commun.* 10 (2008) 514.
- [10] J.H. In, H.L. Liu, J.H. Lee, J.H. Wu, J.S. Ju, Y.K. Kim, *IEEE Trans. Magn.* 45 (2009) 2471.
- [11] S. Shamaila, R. Sharif, S. Riaz, M. Ma, M. Khaleeq-ur-Rahman, X.F. Han, *J. Magn. Mater.* 320 (2008) 1803.
- [12] M. Onoda, K. Shimizu, T. Tsuchiya, T. Wanabe, *J. Magn. Mater.* 126 (1993) 595.
- [13] T. Osaka, *Electrochim. Acta* 42 (1997) 3015.
- [14] T. Osaka, T. Sawaguchi, F. Mizutani, T. Yokoshima, M. Takai, Y. Okinaka, *J. Electrochem. Soc.* 146 (1999) 3295.
- [15] I. Tabakovic, V. Inturi, S. Riemer, *J. Electrochem. Soc.* 149 (2002) C18.
- [16] F. Lallemand, D. Comte, L. Ricq, P. Renaux, J. Pagetti, C. Dieppedale, P. Gaud, *Appl. Surf. Sci.* 225 (2004) 59.
- [17] E. Pellicer, E. Gómez, E. Vallés, *Surf. Coat. Technol.* 201 (2006) 2351.
- [18] E. Gómez, E. Pellicer, M. Duch, J. Esteve, E. Vallés, *Electrochim. Acta* 51 (2006) 3214.
- [19] P.L. Cavallotti, M. Bestetti, S. Franz, *Electrochim. Acta* 48 (2003) 3013.
- [20] L. Vieux-Rochaz, C. Dieppedale, B. Desloges, D. Gamet, C. Barragatti, H. Rostaing, J. Meunier-Carus, *J. Micromech. Microeng.* 16 (2006) 219.
- [21] N. Yasui, A. Imada, T. Den, *Appl. Phys. Lett.* 83 (2003) 3347.
- [22] K.H. Lee, S.W. Kang, G.H. Kim, W.Y. Jeung, *J. Magn. Mater.* 272 (2004) e925.
- [23] S. Kulkarni, S. Roy, *J. Appl. Phys.* 10109 (2007) K524.
- [24] H.D. Park, K.H. Lee, G.H. Kim, W.Y. Jeung, *J. Appl. Phys.* 99 (2006) 08N305-1.
- [25] O. Berh, Y. Rosenberg, Y. Shacham-Diamand, E. Gileadi, *Microelectron. Eng.* 84 (2007) 2444.
- [26] M. Cortés, S. Matencio, E. Gómez, E. Vallés, *J. Electroanal. Chem.* 627 (2009) 69.
- [27] M. Cortés, E. Gómez, E. Vallés, *Electrochem. Commun.* 12 (2010) 132.
- [28] G. Pattanaik, G. Zangari, J. Weston, *Appl. Phys. Lett.* 89 (2006) 112.
- [29] R.A. McCurrie, *Ferromagnetic Materials Structure and Properties*, Academic Press Inc., San Diego, 1994.
- [30] R. Skomski, *J. Phys.: Condens. Matter.* 15 (2003) R841.
- [31] T. Ouchi, Y. Arikawa, T. Homma, *J. Magn. Mater.* 320 (2008) 3104.
- [32] J. García-Torres, E. Gómez, X. Alcobé, E. Vallés, *Cryst. Growth Des.* 9 (2009) 1671.

5.4.5 Electrochemical preparation and magnetic properties of submicrometric core-shell CoPt-CoNi particles





Contents lists available at ScienceDirect

## Journal of Electroanalytical Chemistry

journal homepage: [www.elsevier.com/locate/jelechem](http://www.elsevier.com/locate/jelechem)

# Electrochemical preparation and magnetic properties of submicrometric core–shell CoPt–CoNi particles

M. Cortés, E. Gómez, E. Vallés\*

Electrodep, Departament de Química Física and Institut de Nanociència i Nanotecnologia (IN<sup>2</sup>UB), Universitat de Barcelona, Martí i Franquès 1, E-08028 Barcelona, Spain

## ARTICLE INFO

## Article history:

Received 16 July 2010

Received in revised form 7 September 2010

Accepted 9 September 2010

Available online 17 September 2010

## Keywords:

Magnetic properties

Electrodeposition

Core–shell particles

CoPt alloy

CoNi alloy

## ABSTRACT

Electrodeposition method has allowed the preparation of submicron CoPt particles covered with CoNi shells of different thicknesses. The magnetic properties of these particles have been analysed; a contribution of semi-hard magnetic behaviour and soft-magnetic behaviour, associated with the particles, and the CoNi shell, respectively, has been detected. Although a gradual decrease of the coercivity was observed by increasing the CoNi shell thickness, the CoPt core always dominates the magnetization–magnetic field curve shape.

© 2010 Elsevier B.V. All rights reserved.

## 1. Introduction

Extensive researches have been performed for the synthesis and characterization of nanoparticles due to their different properties regarding to the corresponding bulk material, which allows proposing their use for a great number of applications related to their special magnetic, optical, catalytic, chemical or biological abilities. Several methods of manufacturing nanoparticles were developed, based both on physical and chemical process [1–6]. Some of these particles are core–shell type in which the central material is surrounded by a different material. The external material could exert either as protective material [7–10] or to promote novel properties [11–14]. In particular, core–shell nanoparticles with magnetic core have been extensively prepared from different techniques in order to take advantage of the change of the properties of the ferromagnetic material when its size diminishes. Protective character of the shell is especially important when the ferromagnetic core is unstable toward oxidation in air, which easily occurs when their size becomes small.

However, in some occasions core–shell particles with intermediate dimensions (hundreds of nanometers) are of interest because they show magnetic properties greatly different with respect to either nanoparticles or bulk configurations for the same material system [15,16]. For example, when systems in which soft and hard magnetic materials are positioned in contact, these particles can be used in exchange-spring systems, which are based on the exchange

coupled of soft and hard ferromagnetic phases. These systems can combine the high magnetization of soft phase with the coercivity of hard phase to attain a high energy product to obtain a maximum magnetic energy product [17]. A system is recognized as an exchange spring magnet when both phases are coupled to each other [18,19]. In this case, the high saturation magnetization of the soft phase and the high coercivity of the hard phase confer better magnetic properties of the composite compared to the individual soft and hard phases, thus providing high magnetic energy product [20]. Although recently there has been an important increase in the interest of modulated magnetic properties, the study of these kinds of systems combining soft and hard ferromagnets has not improved significantly because of the lack of effective fabrication methods. It is desirable to work with moderate particle size of soft and hard phases, which guarantees a high remanence and sufficient high coercivity [18].

The aim of the present work is to investigate the possibilities of the electrodeposition method for preparing magnetic core–shell particles, with a core of CoPt alloy in intermediate dimensions (100–500 nm) (semi-hard magnetic response) and a shell of CoNi (soft-magnetic alloy) of controllable thickness and analyse the magnetic properties of the global structure. After the electrochemical preparation of the alloy core particles, the capability of recovering them with a shell of a second alloy (CoNi), avoiding its deposition onto the substrate will be tested. The variation of the magnetic properties of the particles as a function of the shell thickness will be analysed. The particles will be prepared using two different electrodeposition baths similar to other previously studied over silicon-doped substrate [21,22]. The lower conductivity of this

\* Corresponding author. Tel.: +34 403 92 38; fax: +34 402 12 31.

E-mail address: [e.valles@ub.edu](mailto:e.valles@ub.edu) (E. Vallés).

substrate, with respect to metallic or carbon substrates, can favour, at low deposition charges, a lower nucleation rate and hence, the formation of particles rather than continuous layers. The non-magnetic behaviour of the substrate will also permit the detection of the magnetic response of the particles prepared over it.

## 2. Experimental

Submicron CoPt particles have been prepared potentiostatically at  $-1050$  mV for 40 s at  $40$  °C and 100 rpm from a solution containing  $2.5 \times 10^{-3}$  M  $\text{CoCl}_2$  +  $1.2 \times 10^{-3}$  M  $\text{Na}_2\text{PtCl}_6$  +  $0.5 \times 10^{-2}$  M sodium citrate + 1 M  $\text{NH}_4\text{Cl}$  +  $30 \text{ g dm}^{-3}$   $\text{H}_3\text{BO}_3$  (the pH of the solution was adjusted at 4.5 with NaOH solutions) over a doped silicon (p-B Sitronix 11523–13012 with a resistivity of  $0.008$ – $0.012 \Omega \text{ cm}$ , supplied by IMB-CNM.CSIC) substrate. Silicon pieces of  $0.6 \text{ cm} \times 0.3 \text{ cm}$  were used as working electrode. The silicon substrate was etched with a 5% (p/v) HF solution for 60 s to remove the native silicon oxide. A fixed charge was maintained during the deposition in order to attain consistent particle sizes, also assuring that the deposition took place through the identical  $j$ – $t$  transient.

After electrodeposition of CoPt particles, the shell growth was performed in a second cell using a 0.2 M  $\text{CoCl}_2$  + 0.9 M  $\text{NiCl}_2$  +  $30 \text{ g dm}^{-3}$  boric acid +  $0.7 \text{ g dm}^{-3}$  saccharine, pH = 3, solution. Deposition was performed potentiostatically at  $-900$  mV,  $25$  °C and 100 rpm.

All the reagents were of analytical grade. Solutions were freshly prepared with water which was first doubly distilled and then treated with a Millipore Milli Q system. Solutions were de-aerated by argon bubbling before each experiment and maintained under argon atmosphere during it.

Electrodeposition was carried out using a microcomputer-controlled potentiostat/galvanostat Autolab with PGSTAT30 equipment and GPES software. A three-electrode cell with controlled temperature was used in each case. The reference electrode was an Ag/AgCl/ $1 \text{ mol dm}^{-3}$  NaCl electrode. All potentials were referenced to this electrode. The counter electrode was a platinum spiral.

Analysis of the deposits was performed by means of a Leica Stereoscan S-360 scanning electron microscope. A Hitachi H-4100FE (field emission scanning electron microscope) was used for the observation of the electrodeposited particles.

Magnetic properties of the deposits were characterized using a SQUID magnetometer at room-temperature. The magnetic field was applied parallel to the substrate.

## 3. Results and discussion

The voltammetric response of the CoPt system over the activated silicon substrate is shown in Fig. 1. Over this electrode, after some initial reduction current corresponding to platinum deposition, simultaneous deposition of Co and Pt takes place from around  $-850$  mV. The anodic scan showed, at around  $-0.5$  V, a peak assigned to the oxidation of molecular hydrogen retained over the electrode; this peak disappeared when the voltammogram was recorded in stirring conditions. The other oxidation current corresponded to the CoPt oxidation. From the voltammetric results, the deposition potential was selected to prepare CoPt particles. Platinum rich particles with a Pt wt.% in the range 65–75% were desired in order to enhance the magnetic anisotropy of the material [23]. The compositional analysis and the observation of the deposits prepared at different potentials led to select a deposition potential of  $-1050$  mV and a deposition time of 40 s to prepare submicrometric platinum-rich CoPt particles of fixed composition. A representative  $j$ – $t$  transient of the deposition (Fig. 2) shows a

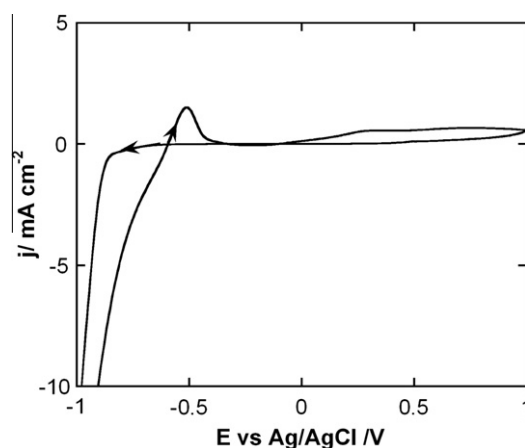


Fig. 1. Cyclic voltammogram of a  $2.5 \times 10^{-3}$  M  $\text{CoCl}_2$  +  $1.2 \times 10^{-3}$  M  $\text{Na}_2\text{PtCl}_6$  +  $0.5 \times 10^{-2}$  M citrate + 1 M  $\text{NH}_4\text{Cl}$  +  $30 \text{ g dm}^{-3}$   $\text{H}_3\text{BO}_3$ , pH = 4.5, solution over doped silicon electrode.

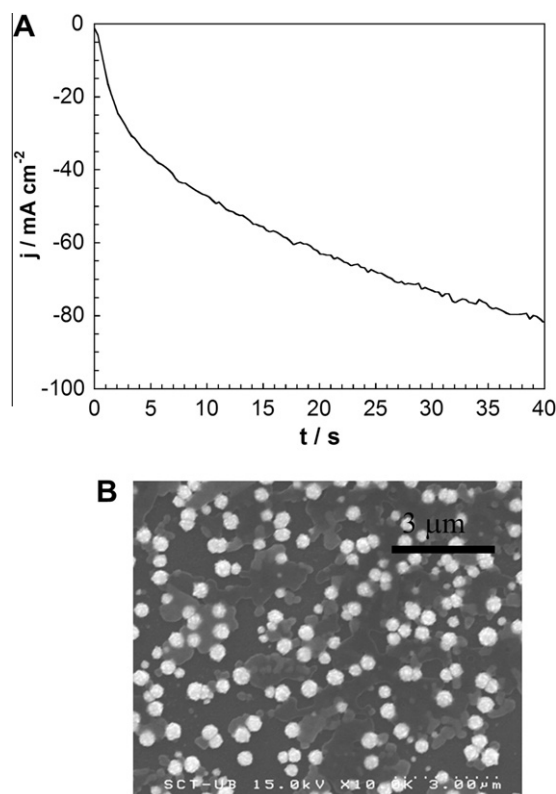
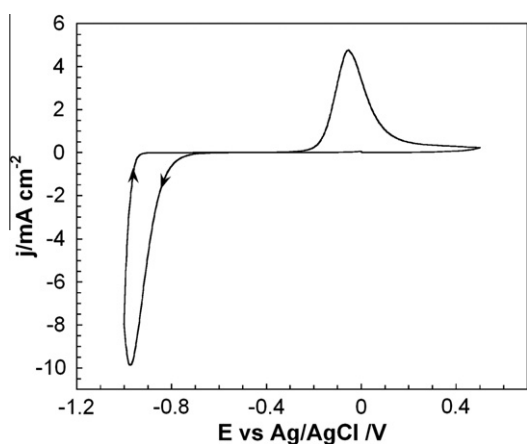


Fig. 2. (A) Galvanostatic curve and (B) FE-SEM images for CoPt particles obtained with stirring, over doped silicon electrode, at  $-1050$  mV for 40 s at  $40$  °C.

gradual increase of the current density with time. Platinum-rich CoPt particles (68–71wt. of Pt) were obtained in these conditions. For the fixed deposition charge ( $-0.5$  C), a distribution of rounded particles with sizes ranging from 150–500 nm was obtained over silicon substrate.

In order to select the optimum conditions to cover the particles with the CoNi alloy shell, a voltammetric study of the CoNi deposition was performed using continuous CoPt films freshly electrodeposited over the silicon substrate (Fig. 3). Typical response of the CoNi deposition, similar to that obtained from the selected bath over other substrates [22], was observed. The nucleation loop of the simultaneous codeposition of cobalt and nickel was registered.



**Fig. 3.** Cyclic voltammogram of a 0.2 M  $\text{CoCl}_2$  + 0.9 M  $\text{NiCl}_2$  + 30  $\text{g dm}^{-3}$  boric acid + 0.7  $\text{g dm}^{-3}$  saccharine, pH = 3, solution over doped silicon electrode with a 190 nm CoPt film on it.

Only one oxidation peak was detected in the positive scan, corresponding to the dissolution of the solid solution formed during the negative scan.

Different CoNi test deposits have been prepared at different potentials. From these results, a potential of  $-900$  mV, for which

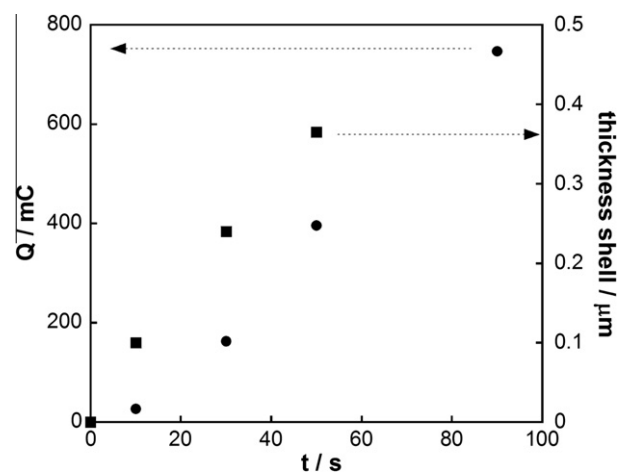


**Fig. 5.** Variation of the charge and thickness of the CoNi shell with time.

CoNi alloy of 59 wt.% Co was obtained, was selected to perform the shell deposition over the CoPt core particles. The sequence of electrochemical preparation of the CoPt–CoNi particles was: CoPt particles were prepared in the CoPt solution over the silicon substrate and immediately the samples were rinsed and introduced in the cell containing the CoNi solution to perform the CoNi

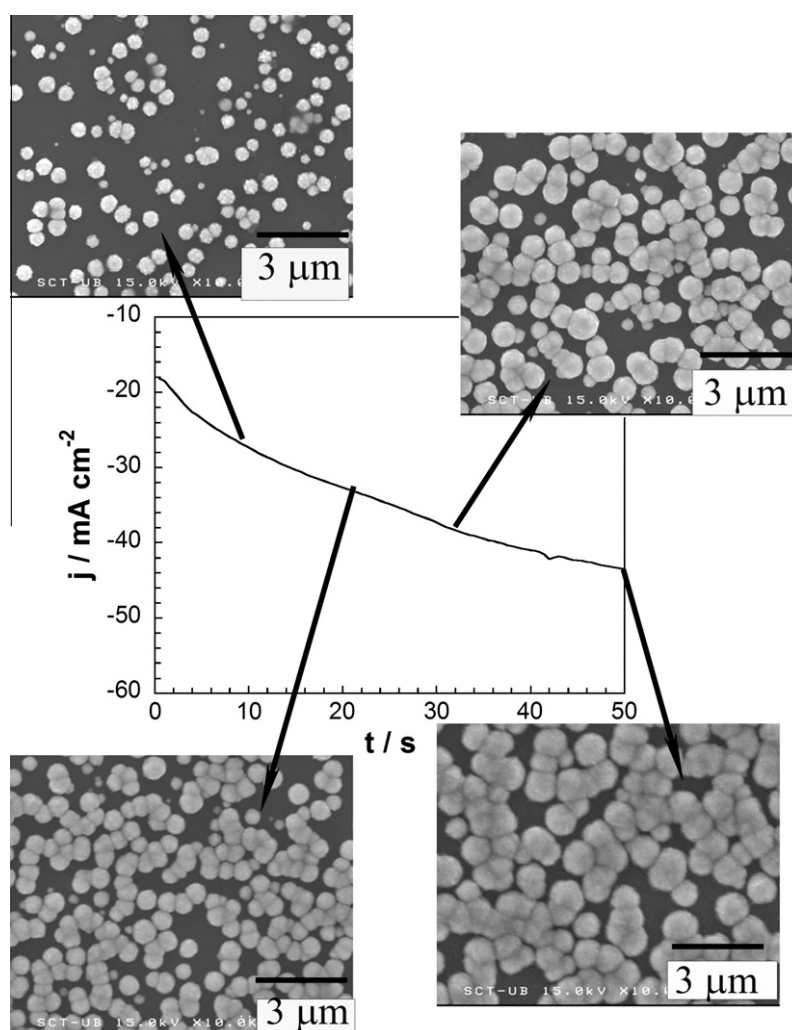


**Fig. 4.**  $j$ - $t$  Transients at  $-900$  mV and FE-SEM images of CoPt–CoNi particles obtained at different deposition times.

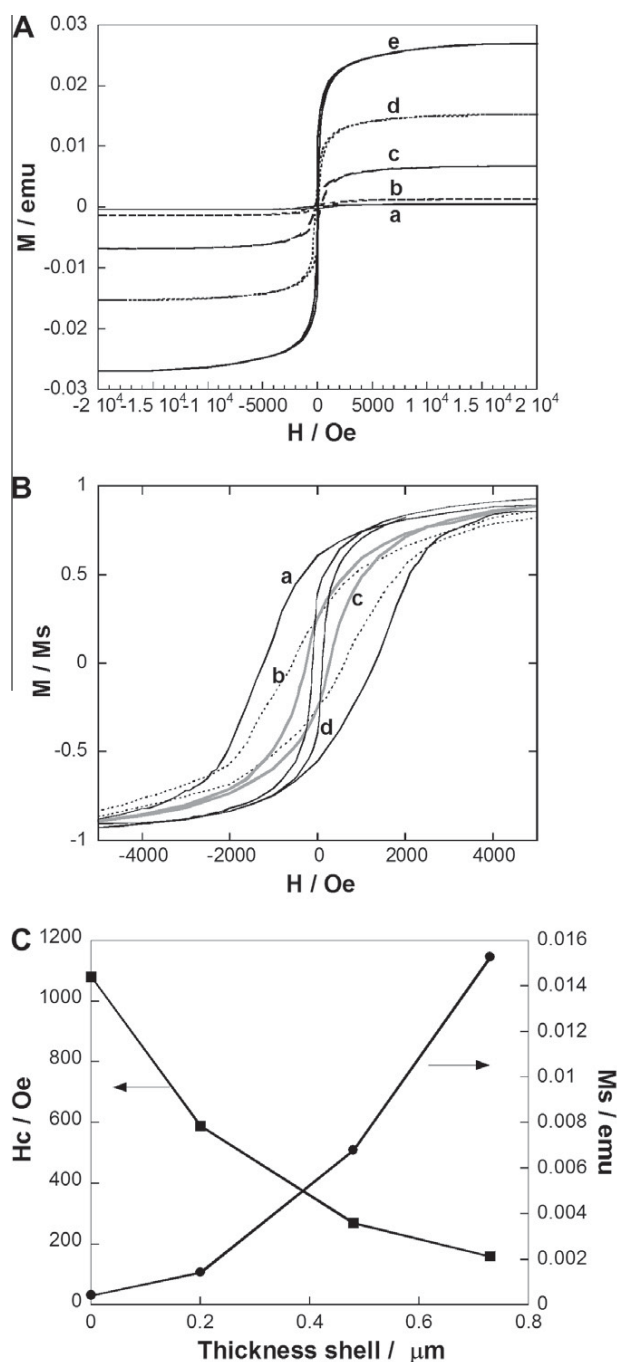


**Fig. 6.** Room-temperature magnetization curves taken with the applied field parallel to the samples (A) CoPt core particles obtained at  $-1050$  mV, 40 s,  $40$  °C (a) without CoNi shell (b) with a CoNi shell obtained at  $-900$  mV,  $25$  °C, 10 s (c) 40 s (d) 50 s (e) 90 s and (B) normalized magnetization curves of the same samples of (A) and (C) variation of the coercivity and the saturation magnetization with thickness shell.

electrodeposition. The observation of the samples after the deposition by means of scanning microscopy showed that CoNi only deposits on the CoPt particles since no new deposit was observed over the silicon substrate (Fig. 4); this result was confirmed by EDS analysis.

CoPt particles initially deposited onto the silicon substrate were covered by a CoNi shell, with a thickness that could be controlled

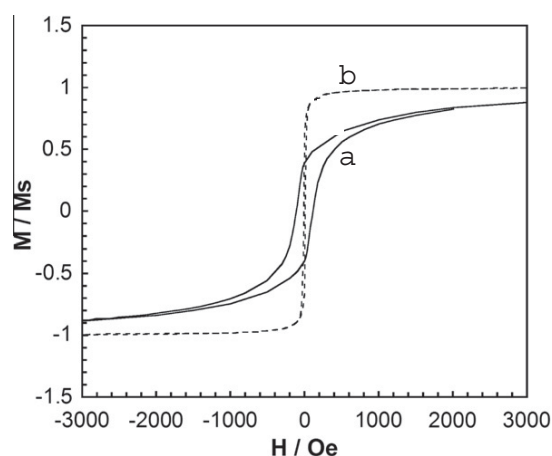


**Fig. 7.** Normalized room-temperature magnetization curves taken with the applied field parallel to the samples (a) CoPt core particles obtained at  $-1050$  mV, 40 s,  $40$  °C with a CoNi shell obtained at  $-900$  mV,  $25$  °C, 50 s and (b) thin film CoNi obtained at  $-900$  mV,  $25$  °C, 50 s, over the silicon activated substrate.

**Table 1**

Estimation of the magnetisation of saturation of the CoNi shell in the samples b, c, d, e of Fig. 6A.

Total Ms (emu)	Ms shell CoNi (emu)	Estimated CoNi g from the deposition charge	Ms shell ( $\text{emu g}^{-1}$ )
0.00143	0.00101	$8.24 \times 10^{-6}$	122.3
0.00681	0.00639	$4.97 \times 10^{-5}$	128.5
0.01527	0.01485	$1.21 \times 10^{-4}$	123.0
0.02703	0.02661	$2.28 \times 10^{-4}$	116.8

as a function of the deposition time (Fig. 5). A deposition rate of CoNi over the CoPt particles of  $7.2$  nm/s was measured, which allows controlling the thickness of the shell. The CoNi deposition time cannot exceed the 50 s to avoid coalescence of the core-shell particles observed at high deposition times. The compositional analysis demonstrated that a 60 wt.% Co was maintained for the CoNi deposition over the particles.

Magnetic properties of the core-shell particles were analysed by recording the magnetization-magnetic field applied response of the silicon samples containing the particles; the samples were placed parallel to the magnetic field applied. Fig. 6A reveals that the magnetization of saturation enhances by increasing the CoNi deposition charge, due to a higher amount of the electrodeposited magnetic material. A detail of the normalized magnetic curves is recorded in Fig. 6B. The magnetization curve does not show the superimposition of two loops corresponding to the two different systems (CoPt and CoNi) but a single step hysteresis loop. The core-shell particles showed a good single-magnetic behaviour, the hard and the soft-magnetic material are well exchange coupled. A decrease of the coercivity of the particles was observed by increasing the deposition charge of CoNi shell.

Fig. 6C gathers the effect of the increase of deposition charge of CoNi shell on both magnetization of saturation and coercivity. A relevant decrease of the coercivity is accompanied by an increase in the magnetization of saturation.

Although a drastic decrease of the coercivity was observed for CoPt-CoNi particles respect to the pure CoPt core, the core-shell particles still have a clear difference with pure CoNi films obtained from the same bath, which have lower coercivity ( $H_c = 10$  Oe) and higher magnetic susceptibility, even with thick shells ( $0.36$   $\mu\text{m}$ ). This is reflected in the high magnetization/magnetic field slope (Fig. 7).

The contribution of the CoNi shell to the total magnetization of saturation of the CoPt–CoNi systems was evaluated (Table 1). The estimated  $M_s$  value for the CoNi shell was in the range of the detected for electrodeposited CoNi films of similar composition (119–126 emu g<sup>-1</sup>) [24,25]. The estimation of the weight of the CoNi from the deposition charge was consistent with the high efficiency (around 90%) of the deposition process using the applied conditions. In summary, it is possible to prepare the core–shell particles with modulated/variable magnetic properties as a function of the shell thickness.

The magnetic results observed demonstrate the interaction between the semi-hard response of the CoPt core and the soft one of the CoNi shell. The presence of the core of CoPt always affects to the magnetic response of the CoNi shell, even for the greatest thickness of the shell. The core–shell particles can be considered as a composite comprising of both soft and hard magnetic material. The global system magnetically gives a good single-phase behaviour that allows controlling the magnetic behaviour of the particles as a function of the CoPt/CoNi ratio. The main interaction is between the hard and soft phases although some interaction between the soft phases could occur as short distances exist between particles. The energy product of the core–shell particles (area included in the hysteresis loop) can be regulated from the ratio of the core and shell phases. The electrodeposition method has been demonstrated useful to prepare core–shell particles than can actuate as an exchange-spring system as an easier and alternative method to other preparation ones [18,26].

#### 4. Conclusions

Electrodeposition has allowed the preparation of core–shell particles of around 0.2–1 μm diameter, with both core and shell of magnetic alloys. The size of core and shell can be controlled as a function of the deposition charge applied. Two electrolytic baths are necessary and silicon-doped electrode seems to be a suitable substrate for obtaining the particles without direct deposition of the second alloy over the substrate. The magnetic properties of the particles were a combination of the specific of the two alloys used, the semi-hard-magnetic behaviour of the core CoPt and the soft-magnetic behaviour of the CoNi shell. Nonsuperposition of the magnetic loops of the two systems was observed but a single step hysteresis loop was recorded. The global system magnetically gives a good single-phase behaviour that allows controlling the magnetic behaviour of the particles as a function of the core and shell thicknesses. The core–shell particles can be considered as a composite of both soft and semi-hard magnetic material in which the two magnetic phases are well exchange coupled to each other. Electrodeposition opens the possibility of preparation of magnetic

micrometric systems with well exchange coupled magnetic phases.

#### Acknowledgments

The authors wish to thank the Serveis Científicotècnics (Universitat de Barcelona) for the use of their equipment. This paper was supported by contract MAT2006-12913-C02-01 from the *Comisión Interministerial de Ciencia y Tecnología (CICYT)* and *IMB-CNM (CSIC) NGG-158 project*. Meritxell Cortés would also like to thank the *Departament d'Innovació, Universitats i Empresa* of the *Generalitat de Catalunya* and *Fons Social Europeu* for their financial support.

#### References

- [1] M.A. Lopez-Quintela, *Curr. Opin. Colloid In.* 8 (2003) 137–144.
- [2] M. Boutonnet, S. Logdberg, E.E. Svensson, *Curr. Opin. Colloid In.* 13 (2008) 270–286.
- [3] P.J. Kuleska, K. Miecznikowski, B. Baranowska, P. Bogdanoff, I. Dorbandt, *Electrochem. Commun.* 8 (2006) 904–908.
- [4] T. Hanemann, D.V. Szabo, *Materials* 3 (2010) 3468–3517.
- [5] Q. Huo, J.G. Worden, *J. Nanoparticle Res.* 9 (2007) 1013–1025.
- [6] Y. Mastai, A. Gedanken, *Chem. Mater.* 1 (2004) 113–169.
- [7] J. Lin, W. Zhou, A. Kumbhar, J. Wiemann, J. Fang, E.E. Carpenter, C.J. O'Connor, *J. Solid State Chem.* 159 (2001) 26–31.
- [8] X. Wang, L. Wang, I.S. Lim, K. Bao, M. Derrick, H.H. Park, J. Luo, H. Shunli, C.J. Zhon, *J. Nanosci. Nanotechnol.* 9 (2009) 3005–3012.
- [9] X. Teng, H. Yang, *J. Nanosci. Nanotechnol.* 7 (2007) 356–361.
- [10] J. Rivas, A.J. Garcia-Bastida, M.A. Lopez-Quintela, C. Ramos, *J. Magn. Magn. Mater.* 300 (2006) 185–191.
- [11] O. Iglesias, X. Batlle, A. Labarta, *J. Phys. D Appl. Phys.* 41 (2008) 134010/1–134010/5.
- [12] N. Lakshnu, H. Bhargava, O.P. Suwalko, K. Venugopalan, V. Sebastian, V.R. Reddy, A. Gupta, *Phys. Rev. B* 80 (2009) 174425/1–174425/6.
- [13] F. Jimenez-Villacorta, C. Prieto, *J. Phys.: Condens. Matter* 20 (2008) 085216/1–085216/10.
- [14] H. Zeng, S. Sun, J. Li, Z.L. Wang, J.P. Liu, *Appl. Phys. Lett.* 85 (2004) 792–794.
- [15] M.F. Hansen, K.S. Vecchio, F.T. Parker, F.E. Spada, A.E. Berkowitz, *Appl. Phys. Lett.* 82 (2003) 1574–1576.
- [16] A.M. Gabay, M. Marinescu, G.C. Hodjipanayis, *J. Appl. Phys.* 99 (2006) 08B506/1–08B506/3.
- [17] D. Roy, P.S.A. Kumar, *J. Appl. Phys.* 106 (2009) 073902-1–073902-4.
- [18] K.W. Moon, S.G. Cho, Y.H. Choa, K.H. Kim, J. Kim, *Phys. Status Solidi A* 204 (2007) 4141–4144.
- [19] Y. Wang, F.S. Li, J. Ariake, N. Honda, S. Ishio, K. Ouchi, *J. Magn. Magn. Mater.* 320 (2008) 3083–3087.
- [20] T. Tanaka, J. Matsuzaki, H. Kurisu, S. Yamamoto, *J. Magn. Magn. Mater.* 320 (2008) 3100–3103.
- [21] M. Cortés, E. Gomez, E. Vallés, *Electrochem. Commun.* 12 (2010) 132–136.
- [22] E. Gómez, J. Ramirez, E. Vallés, *J. Appl. Electrochem.* 28 (1998) 71–79.
- [23] M. Cortés, S. Matencio, E. Gómez, E. Vallés, *J. Electroanal. Chem.* 627 (2009) 69–75.
- [24] E. Gómez, E. Vallés, *J. Appl. Electrochem.* 29 (1999) 805–812.
- [25] M. Duch, J. Esreve, E. Gómez, R. Pérez-Castillejos, E. Vallés, *J. Electrochem. Soc.* 149 (2002) C201–C208.
- [26] D. Roy, C. Shivakumara, P.S.A. Kumar, *J. Magn. Magn. Mater.* 321 (2009) L11–L14.

## 5.5 Conclusions

From the electrochemical study of both binary CoPt and ternary CoPtP processes the optimum electrodeposition conditions for deposits preparation were found. Although there was a significant hydrogen evolution during the electrodeposition, it was possible to electrodeposit uniform CoPt and CoPtP films of different thicknesses over silicon/seed layer. The control of the electrodeposition conditions permitted the control of the composition of the deposits. CoPt deposits with Pt content in the range of 60-87 wt. % and CoPtP ones in the range of 25-45 wt. % Pt have been prepared. The efficiency of the process was a function of the composition of the films and the deposition potential applied. Low efficiencies of 3-5 % and 7-10 % were found for the different compositions of the CoPt and CoPtP deposits respectively over Si/Ti/Ni. In the case of CoPt films the efficiency increases to 20 % when using glass/ITO as working electrode, revealing a high dependence of the process efficiency with the substrate used. CoPtP probably showed a higher efficiency because there was less Pt content in these deposits and then less hydrogen evolution during deposition occurred.

The incorporation of P in the CoPt electrodeposits enhanced the cobalt deposition, which led to a decrease of the Pt percentage in the deposits. A maximum value of platinum of around 40 wt. % was obtained in presence of hypophosphite. The presence of hypophosphite in the bath did not affect the deposition rate, which is around 500-700 nm/h.

For CoPt deposits, it has been possible to obtain deposits with Pt compositions of around 60 wt. % . Deposits with Pt composition lower than 70 wt. % presented a highly distorted hcp Co phase where Pt was incorpo-

rated in the crystalline lattice of the hcp Co leading to an increase in the crystalline cell parameters. On the other hand deposits with more than 70 wt. % of Pt presented an fcc Pt phase. CoPtP films only showed the distorted hcp Co phase because in no case the Pt percentage attained was higher than 40 wt. % .

Films with the distorted hcp Co phase presented hard magnetic behaviour, whereas films containing the fcc phase presented soft magnetic behaviour. CoPt films with high Pt percentages but with hcp Co phase presented higher values of coercivity without annealing of the samples than the ones with low Pt percentage. CoPtP films presented higher coercivity values than CoPt ones for the same Pt composition. In fact, the maximum coercivity value (1,400 Oe) was obtained from CoPtP deposits with Pt percentages of 40 wt. % . This entails profits because greater coercivity values were obtained from CoPtP films with 40 wt. % than CoPt films with high Pt percentages (60 wt. % ), being more economic the preparation process. However, CoPt films presented higher magnetic susceptibility than CoPtP, thus providing a faster response and higher magnetic energy product, very interesting characteristics for MEMS applications.

Both alloys present high corrosion resistance, as corresponds to platinum alloys. The P incorporation slightly increases the corrosion resistance of the deposit probably as a consequence of P segregation between the magnetic grains.

The conclusions extracted in these studies open the possibility of preparing magnets that can be directly integrate on devices involving silicon substrates.

The selected bath, with and without citrate, is suitable for the electrodeposition of the different micro/nanostructures of platinum-rich CoPt alloy (60-70 wt. % of Pt) with a distorted hcp structure. In the cases photolithographed substrates or membranes were used the CoPt alloy perfectly filled the templates.

Well defined nanometric-thick, in the range of 100-400 nm, magnetic squared and lined patterned microstructures of test were obtained over patterned glass/ITO substrates with good adhesion of the deposited layer to the substrate after removing the resin mask. This system permitted a wide range of deposition potentials to be applied without variation of the alloy composition of the microstructure. Coercivity values of around 720 Oe were measured in all cases. However, different shape anisotropy leads to variations in the  $K_{an}$ . The magnetic response of the substrate-microstructure system could be modulated by the orientation of the applied magnetic field.

CoPt nanowires of 100 or 200 nm (nominal values) in diameter with lengths ranging from 700 nm to 14  $\mu\text{m}$  were electrodeposited by using both polycarbonate and alumina membranes sputtered with Au as substrate. The nanowires growth evolution was observed. The diameter of the channel pores used lead to arrays of nanowires with easy magnetization in the direction perpendicular to the axis of the wire. Nanowires of  $\varnothing = 200$  nm presented lower coercivity values (around 330 Oe) than nanowires of  $\varnothing = 100$  nm (around 700 Oe). Nanowires with the same diameter but different aspect ratio present very similar coercivity values but different magnetic susceptibility depending on the orientation of the external magnetic field. Higher anisotropy of the array was observed when alumina templates were

used, due to the increased interaction between adjacent nanowires.

Electrodeposition allowed us to obtain submicron CoPt particles over both graphite and silicon substrates and modulate the size and the magnetic properties as a function of the deposition potential. The deposit composition varied with time in the first stages of the process as a consequence of the initial Pt deposition over which simultaneous Co deposition occurred; Pt percentage in the deposits slightly decreased with time to attain a constant value. Magnetic behaviour depended on the size of the CoPt particles as well as of their composition. However, the most significant factor was the particles size, so controlling the size of the particles, magnetic properties can be modulated. The bigger the particles the higher the coercivity value as long as the particles are mono-domain. Particles of 150-250 nm showed the higher coercivity value (2,500 Oe) compared with other structures or with thick films.

By using electrodeposition methods it was also possible to obtain homogeneous thin films of controlled composition over ITO. The thickness of the films was varied by adjusting the deposition time. For 230 nm-thick films coercivity values of 850 Oe were obtained.

Hard magnetic properties can be enhanced by changing the deposit shape. The trend from highest to lowest anisotropy follows: nanoparticles of  $\varnothing = 150$  nm > thin films of 230 nm > squared and lined patterned microstructures 100-400 nm thick  $\approx$  nanowires  $\varnothing = 100$  nm, 14  $\mu$ m length > nanowires  $\varnothing = 200$  nm, 14  $\mu$ m length, although different anisotropy contributions should be taken into account depending on the geometry. Nanowires with different aspect ratio do not present differences in the

coercivity values. However, longer nanowires present higher anisotropy, because they have more shape anisotropy.

There is an increase tendency of the nanostructures to be oxidize relative to films because of their higher exposed surface area.

Core-shell particles of around 0.2-1  $\mu\text{m}$  diameter, with both core and shell of magnetic alloys were prepared by electrochemical methods over silicon-doped substrate. The magnetic properties of the particles were a combination of the specific of the two alloys used, the semi-hard-magnetic behaviour of the core CoPt and the soft-magnetic behaviour of the CoNi shell. The global system magnetically gave a good single-phase behaviour that allows controlling the magnetic behaviour of the particles as a function of the core and shell thicknesses. Electrodeposition opens the possibility of preparation of magnetic micrometric systems with well exchange coupled magnetic phases.

Modulation of the magnetic properties was possible by changing the shape and size of the magnetic CoPt alloy or by exchange coupling the alloy phase with a softer magnetic alloy.



## Chapter 6

# Formation of organic monolayers over electrodeposited magnetic materials as a first step for spintronics spin valves fabrication

### 6.1 Introduction

Spintronics is an emerging discipline based in the exploitation of the spin of the electrons and their associated magnetic moment to fabricate solid-state devices such as spin-valves, spin-transistors or diodes. Although it is a relatively new field of study, it has already seen some of its fundamental results turned into actual devices in a record time of 10 years and it holds great promises for the future [122, 123]. Spintronics could have various advantages over conventional electronics, in which only electronic charge is manipulated, including compactness, robustness and lower power consumption. Moreover, spintronic systems exploit the fact that spin electron can be used to encode information that persists when the device is switched

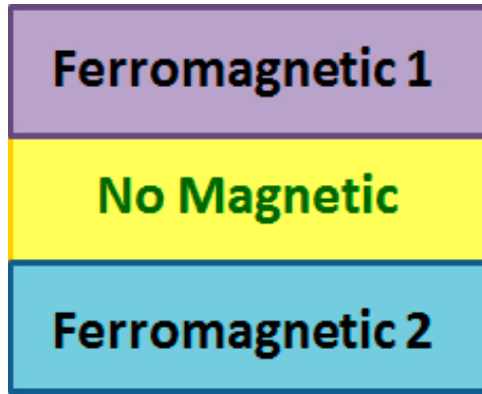


Figure 6.1: Schematic representation of a spin valve

off. These spins can be manipulated with and without using magnetic fields and using little energy.

Spin valves have tremendous potential applications as non volatile magnetic memories, hard-disks reading heads, magnetic sensors and spin valve transistors (figure 6.1). They consist in two magnetic material layers separated by a non-magnetic one (Co/Cu/NiFe, CoFe/Cu/Co, CoFeB/MgO/CoFeB, Fe/Al<sub>2</sub>O<sub>3</sub>/Fe, NiFe/Cu/Co, NiFe/Cu/NiFe, NiFe/Au/Co, NiFe/Cu/CoPt). These devices present magnetoresistance (MR), phenomenon that consists in the dependence of the electrical resistance with the spin electrons and this can be controlled by external applied magnetic fields. Depending on the middle material they will experiment giant magnetoresistance (GMR) or tunnel magnetoresistance (TMR).

In GMR the spacer is a conductive material (Cu, Ag, Au). If we consider that the current in a material is produced by two currents one of spin up and the other of spin down electrons, as suggested by Mott's model [124], when the magnetic materials are in antiferro configuration both spin up and down electrons will suffer scattering and the resistance will be high (figure 6.2). However, when applying a magnetic field that changes the

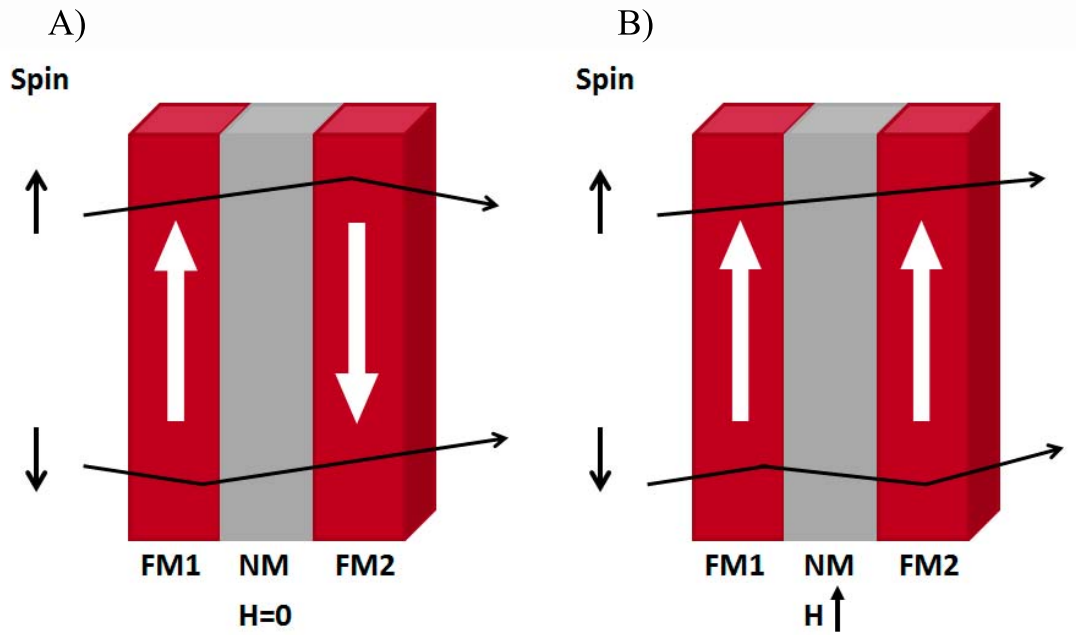


Figure 6.2: Schematic representation of A) Antiferro and B) Ferro configurations in GMR junctions and the scattering process in giant magnetoresistance phenomenon

configuration of the magnetic layer to ferromagnetic, electrons with the spin oriented parallel to the magnetic field will hardly suffer scattering and that decreases the resistance of the material. Even that the ones with spin antiparallel suffer more scattering, the sum of current measured is lower than with the antiferro configuration.

For TMR the middle material is a dielectric material (MgO, amorphous AlO, Al<sub>2</sub>O<sub>3</sub>/SrTiO<sub>3</sub>). In this case when the magnetic materials are in a ferro configuration the tunnel effect is higher because electrons are more likely to quantum mechanically tunnel (figure 6.3). According to Julliere's model [125], electron spin is conserved in the tunneling process, so tunneling of up and down spin electrons are two independent processes. It means that tunnel effect will take part between filled and unfilled states of the same spin in the two magnetic materials. When applying a magnetic field there is a splitting of the bands and not both spin configurations have

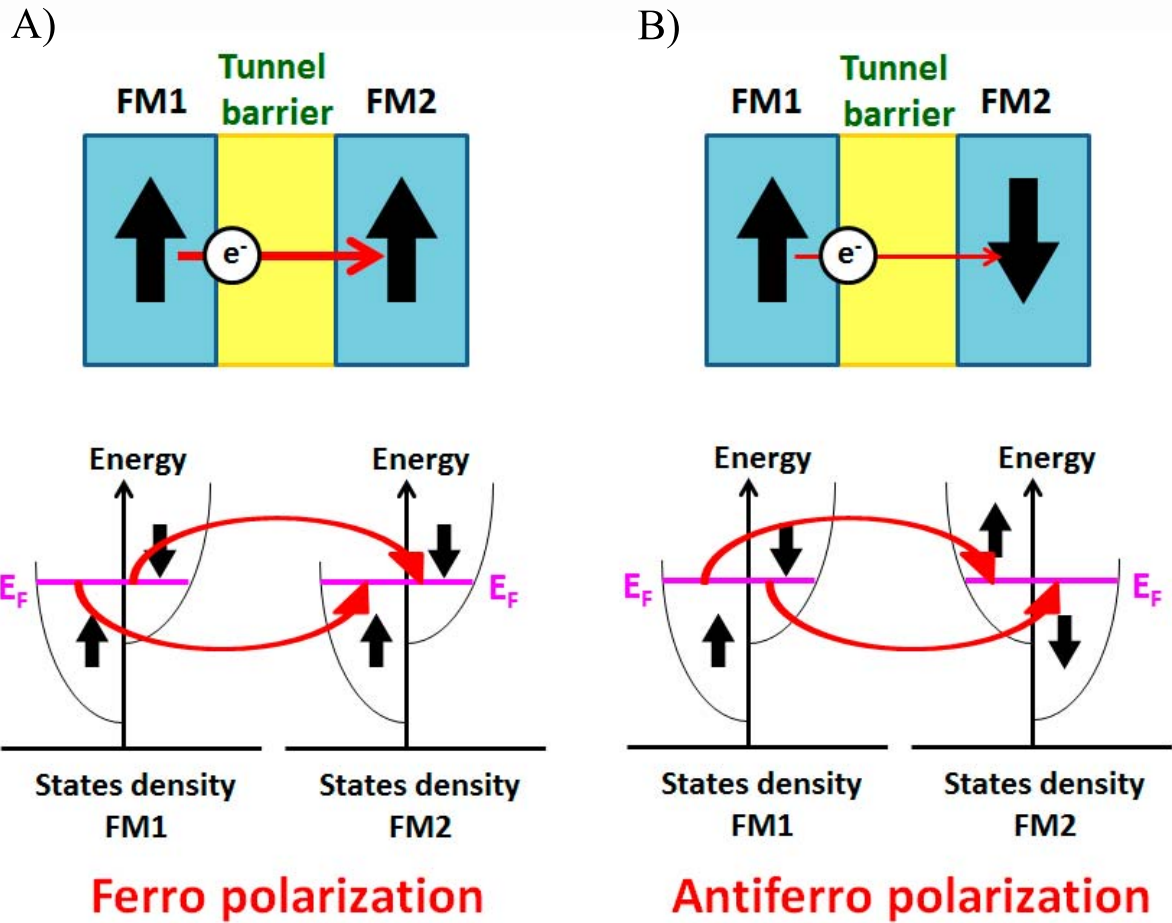


Figure 6.3: Schematic representation of A) Ferro and B) Antiferro configurations in TMR junctions and the tunnel process in tunnel magnetoresistance phenomenon

the same energy. If the magnetic materials are in ferro configuration the minority spins tunnel to the minority states and the majority spins tunnel to the majority states. On the contrary, when the two films are magnetized antiparallel the majority spins of one film tunnel to the minority states of the other film and vice versa. That causes a decrease in the tunnel effect and the resistance of the material increases [126].

However, for the spintronics revolution can take place, it is mandatory to find ways to inject, manipulate and detect the spin of electrons in the devices. The manipulation of the spins is, in theory, relatively simple, but

its injection and detection is extremely challenging in the coming years. There are different aspects to take into account such as: the spin polarization at the Fermi level of the ferromagnetic material, high spin polarized materials are more convenient, but also the spacer material plays a crucial role in the polarized spin injection. In that line, different spacer materials have been reported. At the beginning, metals (Cu, Ag, Au) were the more widely used for these applications; however more recently semiconductors (ZnO, MgO) [123, 127] and organic materials [128] have been studied. It has been found out that using organic materials instead of inorganic ones enhanced the phenomenon of magnetoresistance [128]. In order to observe magnetoresistance it is important that the spin information can survive long distance transport; otherwise the different ferro and antiferro configurations would not show any resistance difference. Organic molecules are made of very light atoms that present very weak spin-orbit and hyperfine interactions that permit a long spin lifetime. Moreover, even more important is the existence of a “clean” interface when using organic materials. When an inorganic material is used, a diffusion interlayer of one material into the other is usually observed. And there are other undesired problems as inhomogeneity of the thickness layers and roughness that may induce the spin to lose their polarization, so it severely hinders the polarized spin injection [129, 130]. Organic materials, such as self-assembled monolayers (SAMs), offer the possibility of bonding an organic molecule direct to the electrode to avoid all this problems. For that reason the interface between inorganic materials with a large spin-polarization and SAMs are likely to play a crucial role in which has been named molecular spintronics (figure 6.4) [131, 132].

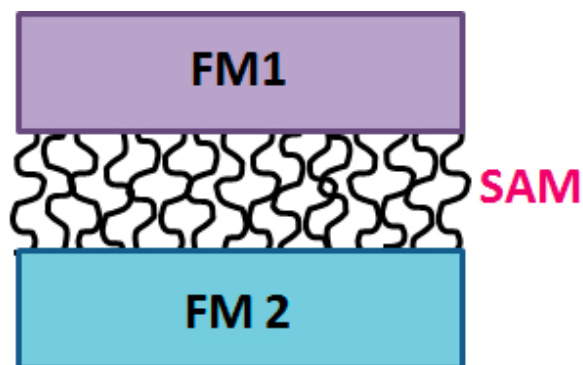


Figure 6.4: Schematic representation of a spin valve with a monolayer as spacer material

According to these results for improving spintronic devices, studies have already been carried out to optimize both the magnetic layers and the organic materials between them. Respect to the magnetic layers, studies of electrodeposited materials for spintronics applications have already been carried out, to take advantage of the low cost and other advantages of electrodeposition [133]. Electrodeposited layers could be used as magnetic components of the spintronic devices.

Monolayer formation over magnetic substrates was also studied to be used as non-magnetic components of the spintronic devices. The method used to obtain the monolayers was molecular self-assembly because it is a very effective and widely used method for forming molecular monolayers on metal surface [134–139]. It is a really easy method to be used and it permits to obtain homogeneous monolayers with high degree of internal molecular order. For that reason it has been widely used in many branches of science requiring well-defined molecular monolayers. One of the most studied examples of molecular self-assembly is alkanethiols monolayer formation typically over noble metals substrates such as gold [140–147] because the sulphur end group presents high affinity for gold and they can form densely packed highly crystalline monolayers [147, 148]. These monolayers have

been well-characterised using techniques such as infra-red spectroscopy, scanning tunnelling microscopy and x-ray photoelectric spectroscopy. Although they have been less studied, there are also some works of SAM over other materials [109, 149, 150].

In line with this, the work presented in this chapter reports the preparation by electrochemical method, of magnetic layers and the formation, over them, of organic monolayers, as the manner that the magnetic substrate/organic monolayer can be the base of spintronic valves. Two different substrates were selected to be electrodeposited, magnetite and CoP. Low roughness layers of these materials were prepared and monolayers of organic compounds were formed over them [109, 149, 151].

Monolayer deposition over magnetite ( $\text{Fe}_3\text{O}_4$ ) is a particularly promising example for spintronic applications [152], because it exhibits ferrimagnetism, and calculations predict complete spin polarization at the Fermi level [153, 154]. Moreover, the self-assembly method is straightforward to apply over it because it is not oxidized at room temperature at air.

First of all, magnetite layers of different thickness were electrodeposited using the method proposed by Switzer and co-workers [155]. The influence of the deposition rate on the roughness and morphology of the films was studied. The crystalline structure and magnetic properties of the films were analysed by X-ray diffraction (XRD) and SQUID magnetometry, respectively, in order to corroborate pure-magnetite formation and to analyse the magnetic properties of the films. Once the deposits were obtained the monolayers formation was carried out. In order to study the obtained monolayer, voltammetric response in a blank solution of bare-magnetite

and modified magnetite with a monolayer on top were compared. To complement the previous studies contact angles measurements of water over the as-deposited and modified magnetite films were also done. Finally, X-ray photoelectron spectroscopy (XPS) was used to corroborate the monolayer formation. The results of this part of the work are presented in the paper “*Adsorption of organic layers over electrodeposited magnetite ( $Fe_3O_4$ ) thin films*”.

Electrochemical methods have been shown to produce magnetite thin films with good control over purity; however, sometimes if the electrodeposition conditions are not the correct ones, codeposition of other iron oxides is produced. For that reason Raman spectroscopy measurements were realised on some of the magnetite films to ensure the purity of our deposits. The possibility of electrodeposition of low rough magnetic magnetite layers of high purity over which chemisorbed organic monolayers can be linked has been demonstrated. The results of this part of the work are presented in the section “*Raman Spectroscopy analysis of magnetite deposits*”.

In another study, CoP was the selected magnetic substrate to link the organic monolayers. CoP is an interesting alloy to be used in spintronics devices due to its magnetic properties [56, 156–158] and because it is possible to obtain very smooth thin films, which is important to obtain monolayers with high order and low defects density. However, molecular functionalisation by self-assembly under ambient conditions is far less straightforward over CoP, because it has more tendency than gold or magnetite to oxidise. In order to avoid problems relating to surface oxidation, UHV (ultra high vacuum) has been used but it is not a conventional method of self-assembly. To use direct self-assembly for monolayers formation onto these deposits

from solution phase, problems with surface oxidation need to be overcome.

For that reason, in this work, an electrochemical method of in-situ octanethiol layer formation from an acidic sodium sulphate solution over flat magnetic electrodeposited film was tested. First of all, CoP deposits were prepared and characterised. Then, the adsorption of octanethiol films over them was tested by adding in-situ an ethanol solution of the organic molecule in the supporting electrolyte. Finally, the formation and purification of the layers were analysed by means of electrochemical and EQCM methods. Contact angle as well as XPS measures were used to corroborate the monolayer formation. The results of this part of the work are presented in the section “*In-situ electrochemical method for octanethiol monolayer formation over amorphous CoP deposits*”.

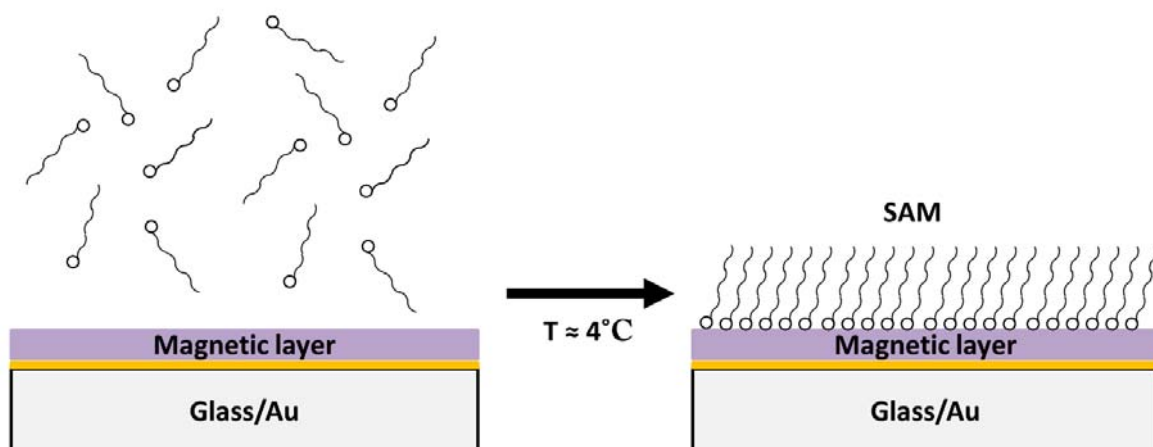


## 6.2 Results presented in this chapter

- Paper: “*Adsorption of organic layers over electrodeposited magnetite (Fe<sub>3</sub>O<sub>4</sub>) thin films*” M. Cortés, E. Gómez, J. Sadler and E. Vallés, *Electrochimica Acta* 56 (2011) 4087-4091
- “*Analysis of the purity of magnetite deposits*”
- “*In-situ electrochemical method for octanethiol monolayer formation over amorphous CoP deposits*”



### 6.2.1 Adsorption of organic layers over electrodeposited magnetite ( $\text{Fe}_3\text{O}_4$ ) thin films





# Adsorption of organic layers over electrodeposited magnetite (Fe<sub>3</sub>O<sub>4</sub>) thin films

M. Cortés<sup>a,\*</sup>, E. Gómez<sup>a,1</sup>, J. Sadler<sup>b</sup>, E. Vallés<sup>a,1</sup>

<sup>a</sup> *Electrodep, Departament de Química Física and Institut de Nanociència i Nanotecnologia (IN<sup>2</sup>UB), Universitat de Barcelona, Martí i Franquès 1, 08028 Barcelona, Spain*

<sup>b</sup> *H.H. Wills Physics Laboratory, Royal Fort, Tyndall Avenue, Bristol BS8 1TL, United Kingdom*

## ARTICLE INFO

### Article history:

Received 21 July 2010

Received in revised form 27 January 2011

Accepted 28 January 2011

Available online 4 February 2011

### Keywords:

Molecular spintronics

Electrodeposition

Magnetite

Magnetism

Monolayers

## ABSTRACT

The formation of monolayers of two organic compounds (oleic acid and dodecanethiol) over magnetite films was studied. Magnetite films ranging from 80 nm to 3.75 μm-thick were electrodeposited on Au on glass substrates under galvanostatic control, with deposition parameters optimized for minimum surface roughness. Films were characterised by SEM and AFM, showing granular deposits with a low rms roughness of 5–40 nm measured over an area of 1 μm<sup>2</sup>. The growth rate was estimated by measuring cross-sections of the thin films. Pure magnetite with an fcc structure is observed in XRD diffractograms. The adsorption of both oleic acid and dodecanethiol on the magnetite films was tested by immersing them in ethanol solutions containing the organic molecules, for different deposition time, temperature and cleaning procedure. Monolayer formation in both cases was studied by contact angle and voltammetric measurements, as well as XPS.

© 2011 Elsevier Ltd. All rights reserved.

## 1. Introduction

Spintronics is an emerging solid-state device technology in which electron spin is controlled and manipulated. Spintronics could have various advantages over conventional electronics, in which only electronic charge is manipulated, including compactness, robustness and lower power consumption. Studies of electrodeposited materials for spintronics applications have already been carried out, to take advantage of the low cost and other advantages of electrodeposition [1], and magnetite (Fe<sub>3</sub>O<sub>4</sub>) is a particularly promising example [2]. Magnetite contains Fe<sup>3+</sup> in its tetrahedral sites while octahedral sites are shared by an equal mixture of Fe<sup>2+</sup> and Fe<sup>3+</sup> ions. It exhibits ferrimagnetism, and calculations predict complete spin polarization at the Fermi level [3,4].

Just as molecular electronics is based on the use of inter-connected molecules to perform the basic functions of digital electronics, the aim of molecular spintronics is to exploit the weak spin–orbit and hyperfine interactions in organic molecules to gain enhanced spin transfer in spintronic devices [5]. For molecular spintronics the interface between inorganic materials with a large spin-polarization and SAMs (self-assembled monolayers) are likely to play a crucial role. In line with this, the aim of the present work is to prepare low roughness magnetite layers over which monolayers of two organic compounds (oleic acid and dodecanethiol) can be formed [6–8].

Electrochemical methods have been shown to produce magnetite thin films [2–9] with good control over purity, so magnetite was electrodeposited using the method proposed by Switzer and co-workers [10].

Magnetite deposits of different thickness were obtained, analysing the influence of the deposition rate on the roughness and morphology of the films. The crystalline structure and magnetic properties of the films were analysed by X-ray diffraction (XRD) and SQUID magnetometry, respectively. The formation of monolayers was detected by analysing the voltammetric response of the modified magnetite films in a blank solution as well as measuring contact angles of water over the as-deposited and modified magnetite films. Finally X-ray photoelectron spectroscopy (XPS) was used to corroborate the monolayer formation.

## 2. Experimental

The electrodeposition was performed in a conventional three-electrode cell from solutions containing Fe<sub>2</sub>(SO<sub>4</sub>)<sub>3</sub>, triethanolamine (TEA) and NaOH, all of analytical grade. The electrochemical study was performed using cyclic voltammetry. Magnetite deposits were obtained from a solution containing 0.09 M Fe(III) + 0.1 M TEA + 2 M NaOH. A temperature of 70 °C, as well as stirring of the solution, was maintained during the electrodeposition. Solutions were freshly prepared with ultrapure Milli Q water.

Electrodeposition was carried out using a microcomputer-controlled potentiostat/galvanostat Autolab PGSTAT30 with GPES software. An Au on glass substrate previously annealed to obtain a {1 1 1} Au orientation was selected as the working electrode. The

\* Corresponding author. Tel.: +34 934039241; fax: +34 934021231.

E-mail address: [m.cortes@ub.edu](mailto:m.cortes@ub.edu) (M. Cortés).

<sup>1</sup> ISE <fn0005>member.

reference electrode was Ag/AgCl/1 M NaCl. All potentials were referenced to this electrode. The counter electrode was a platinum spiral.

A Jeol JSM 5600LV scanning electron microscope (SEM) was used for morphology and section observation. Films roughness (rms) was analysed using a Veeco Dimension V atomic force microscope (AFM). Deposits thicknesses were measured using a Fogale-Nanotec ZoomSurf 3D white-light interferometer.

The structure of the deposits was studied using a Philips MRD diffractometer with parallel optical geometry, Cu  $K\alpha$  radiation ( $\lambda = 1.5418 \text{ \AA}$ ) and a texture goniometer that allows sample rotation about three axes. Magnetic properties were characterized by means of a SQUID magnetometer at room temperature.

For monolayer formation both oleic acid and dodecanethiol were used. In order to make the voltammetric study, solutions in analytical grade 0.05 M  $\text{Na}_2\text{SO}_4$  adjusted to pH 3 with  $\text{H}_2\text{SO}_4$  were used. Contact angle measurements were performed using home-built apparatus, and X-ray photoelectron spectroscopy (XPS) experiments were carried out in a PHI ESCA-5500 Multitechnique System from Physical Electronics.

### 3. Results and discussion

A voltammetric study of the Fe(III)-containing electrolyte was performed using Au on glass substrates, starting at a potential where no process took place. The potential was scanned first negative and then positive in order to study the reduction and oxidation processes, respectively. Fig. 1A shows a cyclic voltammogram recorded under stationary conditions using a potential sweep of  $50 \text{ mV s}^{-1}$ . The shape that was obtained is similar to that obtained by Switzer and co-workers [10], with slight differences in the current density values. From the voltammetric results, potentials and current densities were chosen to perform the electrodeposition.

Potentiostatically deposited layers presented poor adherence to the gold, and for that reason deposits were obtained galvanostatically by applying negative current densities in the range of  $10\text{--}23.3 \text{ mA/cm}^2$ . Different charges ranging from  $-0.5 \text{ C/cm}^2$  to  $-7.5 \text{ C/cm}^2$  were applied to prepare magnetite films of different thickness. Fig. 1B shows the chronopotentiometric curves corresponding to the preparation of deposits of fixed charge but different current densities. They demonstrate that the potential reached in the deposition increases with the current density.

X-ray diffraction results show that, in all cases, the deposits obtained correspond to pure fcc magnetite. A representative diffractogram of one of the samples is shown in Fig. 2A. As magnetite exhibited some peaks similar to those of maghemite, the cell parameter was calculated and compared. The lattice parameter estimated from the X-ray profiles was  $a = 0.842 (6) \text{ nm}$ , slightly higher than the standard value of  $a = 0.8396 \text{ nm}$  (JCPDS#19-0629), consistent with the results reported by Switzer and co-workers [10]. Maghemite has a cell parameter of  $a = 0.8352 \text{ nm}$  (JCPDS#39-1346), differing significantly from the value obtained in this work, enabling both oxides to be differentiated. In our case, the as-deposited magnetite films exhibit preferential orientation in the  $\{100\}$  and  $\{511\}$  directions as the peaks corresponding to these reflections show higher intensities (relative to the  $(311)$  peak) than those predicted (JCPDS#19-0629). The  $\{511\}$  orientation for magnetite electrodeposited on Au has been discussed previously [2].

Magnetization–magnetic field curves were recorded with the film parallel and perpendicular to the applied magnetic field (Fig. 2B). The higher value of magnetic field necessary to attain saturation magnetization in the latter case reveals the magnetic shape anisotropy of the deposited magnetic layers. The measured coercivity is 70 Oe, as observed in the expanded hysteresis loops shown in the inset of Fig. 2B.

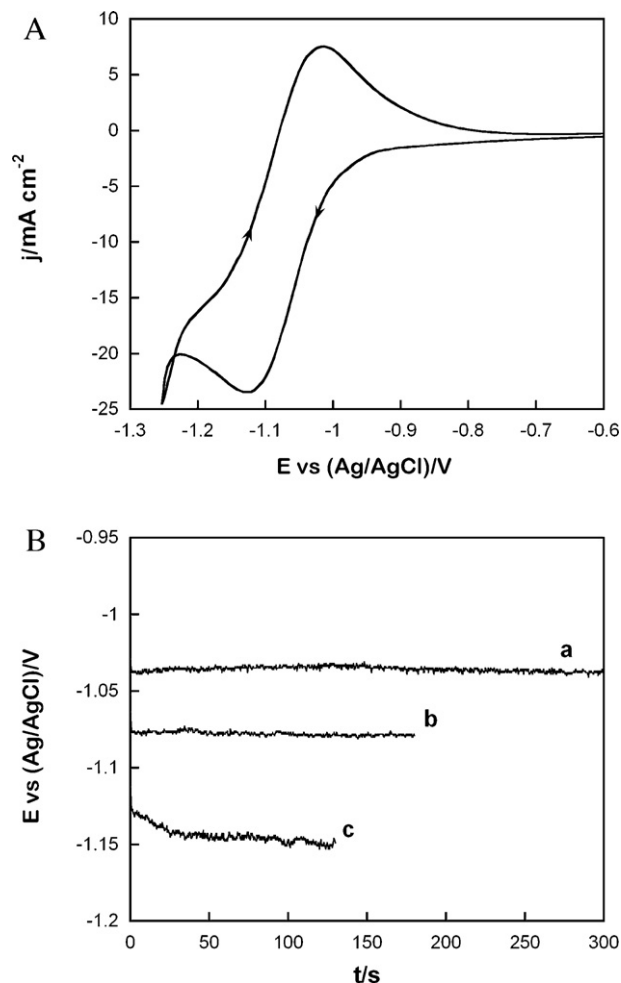
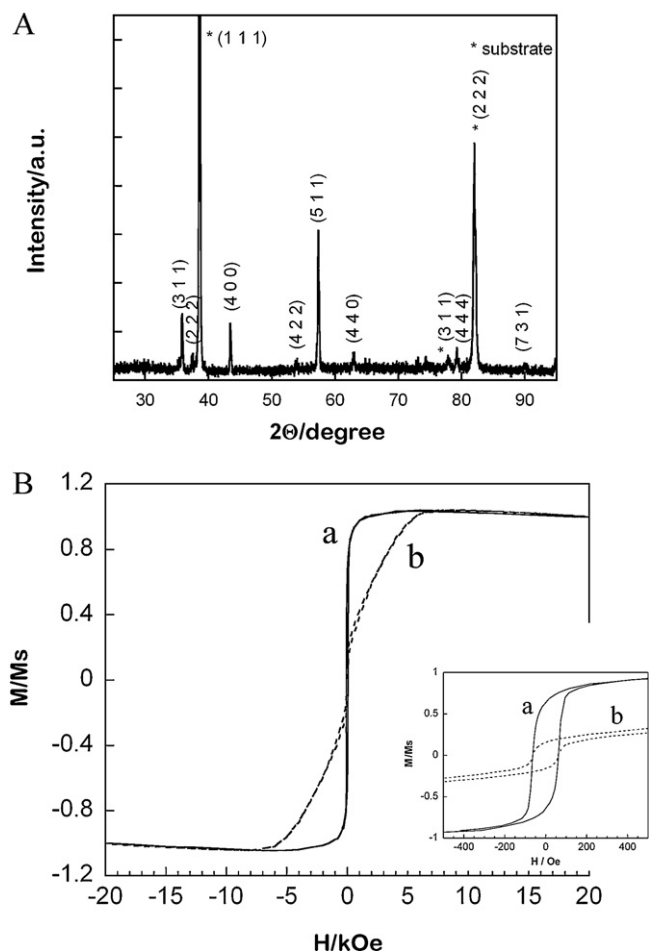


Fig. 1. (A) Cyclic voltammogram of a 0.09 M Fe(III) + 0.1 M TEA + 2 M NaOH solution.  $T = 70^\circ \text{C}$ . No stirring, Au on glass working electrode. (B) Potentiometric curves for deposits obtained with stirring, Au on glass working electrode, at (a)  $-10 \text{ mA/cm}^2$ , (b)  $-16.7 \text{ mA/cm}^2$ , and (c)  $-23.3 \text{ mA/cm}^2$ .  $Q = -3 \text{ C/cm}^2$ .

The roughness and morphology of the samples were studied by AFM and FE-SEM, respectively (Fig. 3A and B). Granular deposits with a roughness ranging from 5 to 40 nm were obtained. The thickness of the deposits was measured using an FE-SEM (Fig. 3C) and interferometer, enabling the estimation of a growth rate of  $7.5 \text{ nm/s}$  and an efficiency of 16% at a current density of  $-10 \text{ mA/cm}^2$ . We attribute the low current efficiency to the relatively high current density we used.

As a step towards their application in organic spintronic devices, we studied the adsorption of organic molecules on the electrodeposited magnetite thin films. Dodecanethiol and oleic acid were tested. The magnetite on Au on glass samples were immersed in 1 mM solution of oleic acid in ethanol for 24 h, and subsequently washed with ethanol five times for duration of 30 min each wash. The samples were washed as many times as necessary to ensure chemisorption of the organic layer over the magnetite films. The monolayer formation was controlled by means of contact angle measurements. The contact angle of water on the surface was measured after each cleaning in order to detect the change of the surface behaviour from hydrophilic to hydrophobic.

Following monolayer deposition at room temperature, the contact angle quickly decreased to the value measured before monolayer deposition after one or two washes. The monolayer needed a lower temperature to be formed because chemisorption is an exothermic process. Following monolayer deposition



**Fig. 2.** (A) X-ray diffractogram of a magnetite deposit obtained on Au on glass at  $-10 \text{ mA/cm}^2$ ,  $Q = -5 \text{ C/cm}^2$ . (B) Normalized room-temperature magnetization curves taken with the applied field parallel (a) and perpendicular (b) to a magnetite deposit obtained at  $-10 \text{ mA/cm}^2$ ,  $Q = -3 \text{ C/cm}^2$ , on Au on glass. An expanded view of the hysteresis loops is shown as an inset.

at a decreased temperature of  $4^\circ\text{C}$ , the contact angle did not change after the five washes, which indicates that the monolayer was obtained by chemisorption. A similar procedure was used for the dodecanethiol, using a 50 mM solution of dodecanethiol in ethanol. After cleaning the samples, they were completely dry after immersion in water, whereas they are wet after immersing them before the monolayer was deposited. Contact angle measurements in Table 1 show that hydrophobic behaviour was observed for the treated magnetite films, when organic layer of oleic acid or dodecanethiol was linked to the magnetite surface, whereas the as-deposited magnetite was hydrophilic. Fig. 4 illustrates this change in the hydrophobic character of the surfaces.

The presence of the oleic acid and dodecanethiol monolayer over the magnetite was also analysed from XPS and voltammetric experiments. XPS data was analysed with the program Multipak from Physical Electronics. We have used the sensitivity factor method to quantify these data. The standard sensitivity factors were corrected for the used geometry and analyzer's lenses. In relation to

**Table 1**  
Contact angle measurements.

	Contact angle ( $^\circ$ )
Magnetite without monolayer	22–45
Oleic acid monolayer	85–90
Dodecanethiol monolayer	88–105

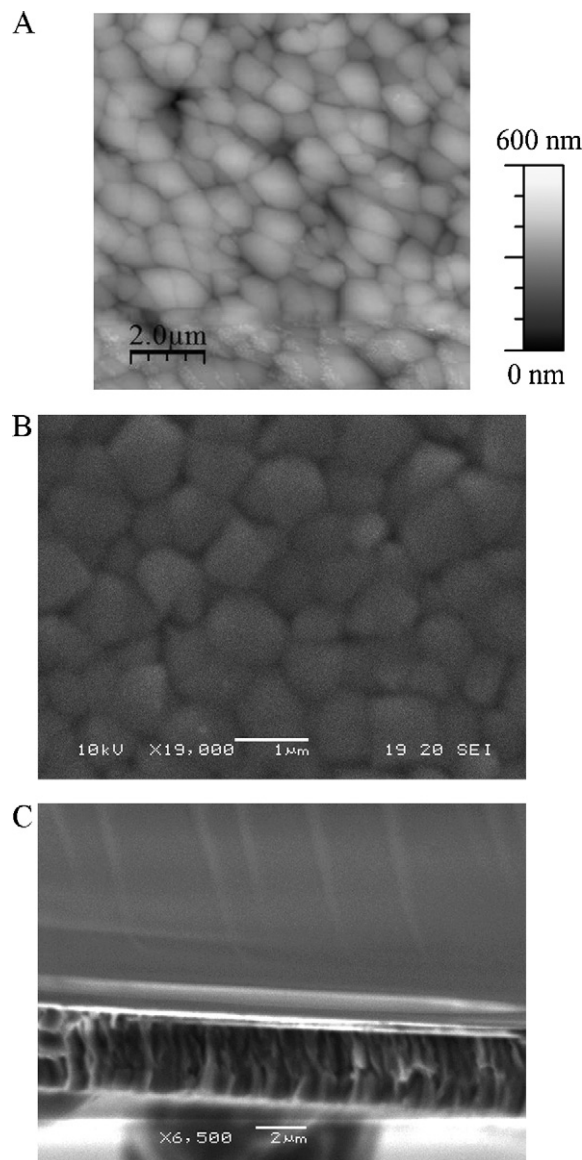


**Fig. 3.** (A) AFM and (B) FE-SEM images of a region of a magnetite deposit obtained at  $-10 \text{ mA/cm}^2$ ,  $Q = -5 \text{ C/cm}^2$ . (C) FE-SEM section of a magnetite deposit obtained at  $-15 \text{ mA/cm}^2$ ,  $Q = -7.5 \text{ C/cm}^2$ , on Au on glass.

the binding energies, they have been corrected by assuming that main peak of the C1s signal is related to physisorbed carbon at 284.8 eV. The recorded XPS spectra of Fe2p and S2p are shown in Fig. 5; from the area over the peaks and the corrected sensitivity factors, we have estimated the C/Fe and C/S ratios. A clear change in the C/Fe ratio was observed from the pure magnetite samples (4.6) to samples treated with oleic acid (7.3) and dodecanethiol (7.2). The Fe2p peak attenuation in the samples treated when oleic acid or dodecanethiol is attributed to the adsorbed layer on top (Fig. 5A). As only the surface part of the sample is analysed with this technique, there is less contribution of iron in the signal in those samples where monolayer was added. Moreover, for the samples with adsorbed dodecanethiol, a small peak in the 167 eV zone related to the S2p transition was observed (Fig. 5B) [11]; for this sample, a Fe/S ratio of 13.6 and a C/S ratio of 97.7 were observed, while for pure magnetite the sulphur content is zero. The small S proportion over the sample analysed leads to a very small peak, but it clearly appears at around the S–O bond position. The great width of the peak allows us to do a roughly estimation fit with two

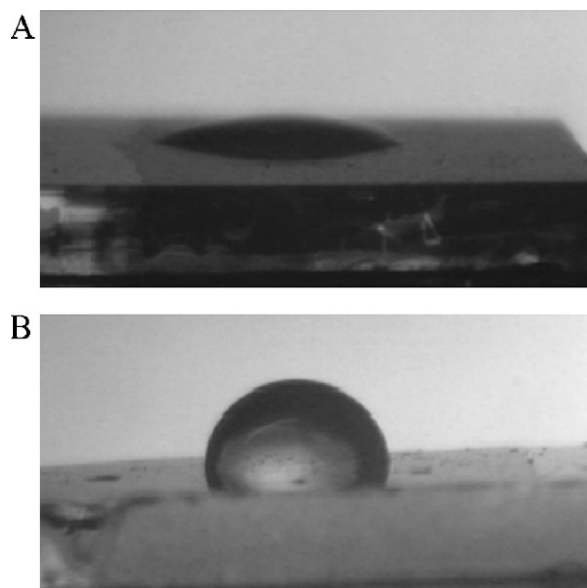


**Fig. 4.** (A) Hydrophilic behaviour of pure magnetite and (B) hydrophobic behaviour of magnetite with adsorbed oleic acid layer.

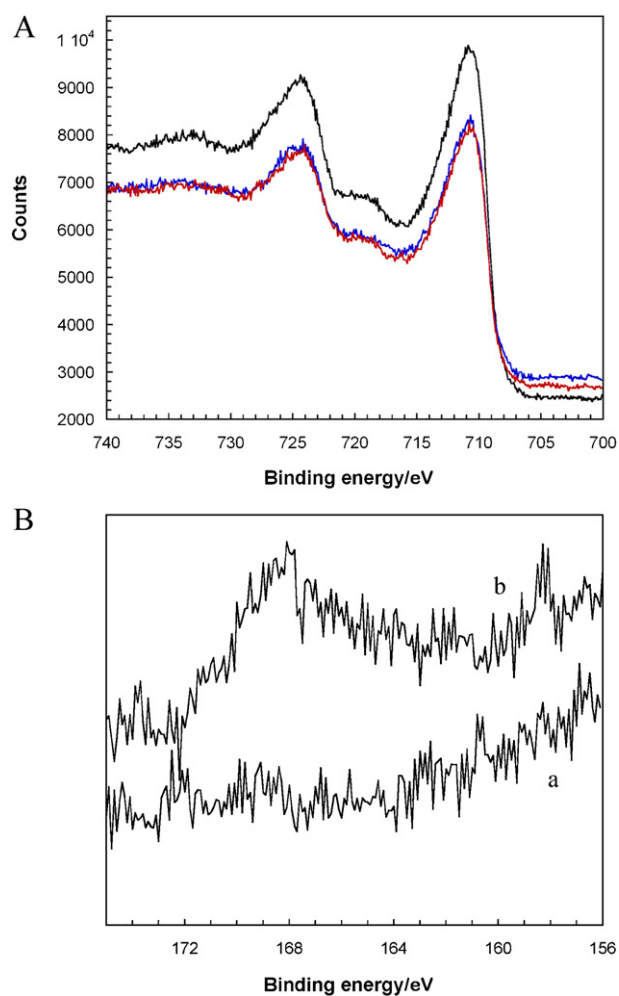


**Fig. 5.** XPS high resolution spectra of (A) Fe2p of pure magnetite (black line, a), magnetite/dodecanethiol monolayer (red line, b) and magnetite/oleic acid monolayer (blue line, c) and (B) S2p peak of pure magnetite (a), magnetite/dodecanethiol monolayer (b). (For interpretation of the references to color in the figure caption, the reader is referred to the web version of the article.)

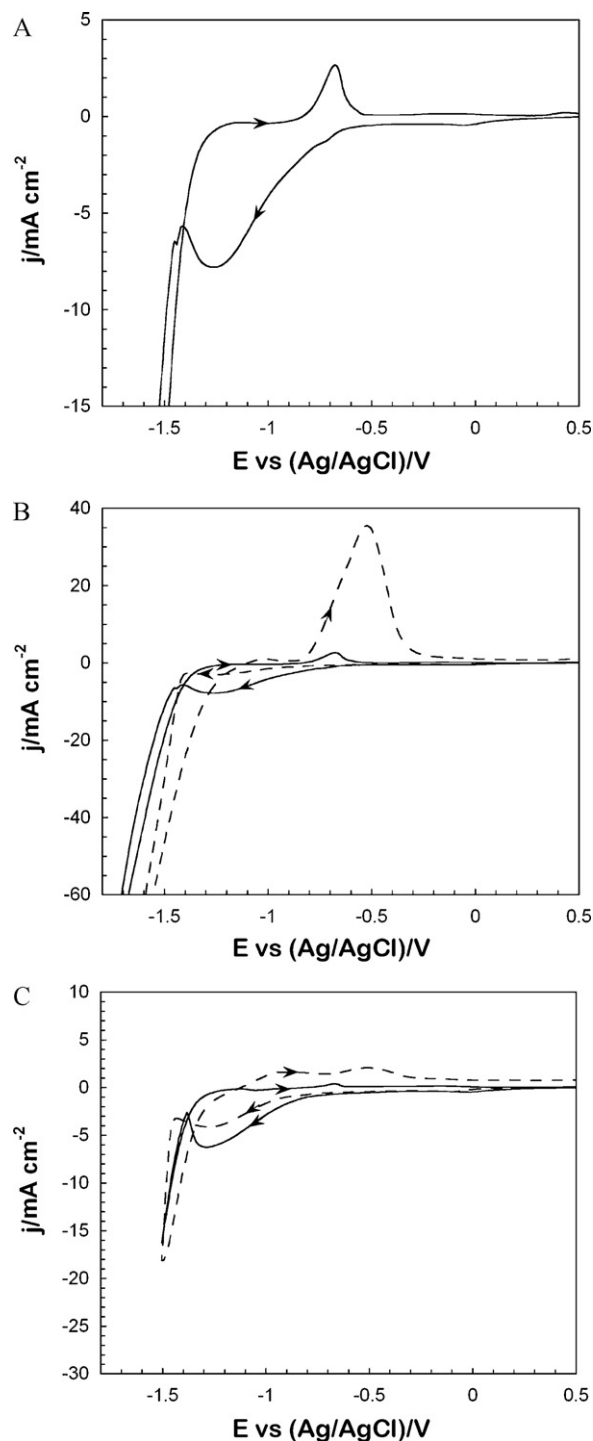
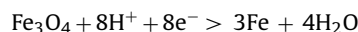


**Fig. 6.** Voltammetric curves in blank solution of (A) bare magnetite, cathodic limit =  $-1.8$  V. (B) Comparison of magnetite (solid line) and magnetite/oleic acid, cathodic limit =  $-1.8$  V (dashed line). (C) Comparison of magnetite (solid line) and magnetite/dodecanethiol (dashed line), cathodic limit =  $-1.5$  V.

peaks at 165.8 eV and 168.4 eV. These peaks might correspond to two different sulphur ways of bonding to oxygen, when the thiol is bonded to the magnetite surface.

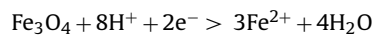
Voltammetric studies of the samples were performed in order to detect the presence of the organic layers adsorbed over the magnetite substrate. A reference cyclic voltammogram was recorded for bare magnetite in an acid blank solution which can supply the necessary protons for the magnetite reduction ( $0.05$  M  $\text{Na}_2\text{SO}_4$  adjusted to pH 3 with  $\text{H}_2\text{SO}_4$ ). The cyclic voltammetry of an as-

deposited magnetite film shows (Fig. 6A) two reduction features in which the magnetite reduces to iron according to the overall reaction [12,13]



before the simultaneous massive hydrogen evolution.

Fig. 6A shows that the magnetite reduction begins at around 0 V; in this first step magnetite reduces to Fe(II) probably through the reaction [14]:



followed for the Fe(II) reduction. From  $-0.6\text{ V}$  an increase of the reduction current was observed, as a consequence of magnetite and Fe(II) reduction and simultaneous  $\text{H}^+$  reduction. From around  $-1.4\text{ V}$ , massive hydrogen evolution occurs simultaneously. When the cathodic limit is negative enough, one oxidation peak was detected in the anodic scan. This peak was enhanced by making the cathodic limit more negative.

After the magnetite films were treated with oleic acid, the cyclic voltammograms detected changes with respect to the reference response, attributed to the presence of an oleic layer. The reduction current was decreased in the entire region 0 to  $-1.4\text{ V}$  (Fig. 6B). The presence of adsorbed oleic over the as-deposited magnetite surface limits the protons presence near the electrode, hindering the reduction of both magnetite and  $\text{H}^+$ . Scanning to negative potentials causes the oleic acid to desorb, resulting in a higher reduction current being detected from around  $-1.4\text{ V}$ , which is also reflected in the increase of the oxidation peak.

Similar voltammetric behaviour was observed when the dodecanethiol layer is adsorbed over the magnetite surface. Fig. 6C shows the voltammetric scan at shorter cathodic limit in which the decrease of the reduction current was also observed when dodecanethiol layer is present over the magnetite. The self-assembled monolayer therefore has a clear blocking effect of the test reduction processes, independent of whether oleic acid or dodecanethiol is used.

#### 4. Conclusions

Low roughness magnetite films were prepared by electrodeposition for the adsorption of organic monolayers. We have used the

triethanolamine electrolyte developed by Switzer and co-workers [10] to electrodeposit magnetite cathodically on Au substrates, finding a  $\{511\}$  orientation, as reported for magnetite prepared on similar substrates by anodic electrodeposition [2]. Both dodecanethiol and oleic acid are shown to adsorb on the magnetite prepared at low temperature, significantly inducing the hydrophobicity of the surface. XPS experiments enabled the interaction between the layers and the substrate to be detected. The voltammetric response of the magnetite in a blank solution has been used to demonstrate the presence of the organic monolayers. Further work is needed to establish the structure of the adsorbed layer, and establish whether or not ordered self-assembled monolayers (SAMs) are formed. Such SAMs are likely to find future application in spintronic devices.

#### Acknowledgments

The authors wish to thank the Serveis Científicotècnics (Universitat de Barcelona) and the Servei de Magnetoquímica (Universitat de Barcelona) for the use of their equipment. This paper was supported by contract MAT2006-12913-C02-01 from the Comisión Interministerial de Ciencia y Tecnología (CICYT) and IMB-CNM (CSIC)NGG-158 project.

#### References

- [1] R.G. Delatorre, M.L. Munford, V. Stenger, A.A. Pasa, W. Schwarzacher, M.S. Meruvia, I.A. Hümmelgen, *J. Appl. Phys.* 99 (2006) 08H704.
- [2] T.A. Sorenson, S.A. Morton, G.D. Waddill, J.A. Switzer, *J. Am. Chem. Soc.* 124 (2002) 7604.
- [3] Z. Zhang, S. Satpathy, *Phys. Rev. B* 44 (1991) 13319.
- [4] V.I. Anisimov, I.S. Elfimov, N. Hamada, K. Terakura, *Phys. Rev. B* 54 (1996) 4387.
- [5] A.R. Rocha, V.M. García-Suárez, S.W. Bailey, C.J. Lambert, J. Ferrer, S. Sanvito, *Nat. Mater.* 4 (2005) 335.
- [6] Z. Mekhalif, J. Riga, J.J. Pireaux, J. Delhalle, *Langmuir* 13 (1997) 2285.
- [7] S. Wang, F.J. Yue, D. Wu, F.M. Zhang, W. Zhong, Y.W. Du, *Appl. Phys. Lett.* 94 (2009) 012507.
- [8] M. Klokkenburg, J. Hilhorst, B.H. Erné, *Vib. Spectrosc.* 43 (2007) 243.
- [9] S. Chatman, A.J.G. Noel, K.M. Poduska, *J. Appl. Phys.* 98 (2005) 113902.
- [10] H.M. Kothari, E.A. Kulp, S.J. Limmer, P. Poizot, E.W. Bohannon, J.A. Switzer, *J. Mater. Res.* 21 (1) (2006) 293.
- [11] M. Descostes, F. Mercier, N. Thromat, C. Beaucaire, M. Gautier-Soyer, *Appl. Surf. Sci.* 165 (2000) 288.
- [12] P.D. Allen, N.A. Hampson, G.J. Bignold, *J. Electroanal. Chem.* 99 (1979) 299.
- [13] P.D. Allen, N.A. Hampson, G.J. Bignold, *J. Electroanal. Chem.* 111 (1980) 223.
- [14] A.M. Al Mayouf, *Corros. Sci.* 218 (2006) 898.

### 6.2.2 Analysis of the purity of magnetite deposits

One of the main difficulties in the preparation of magnetite is to obtain it pure, as sometimes some other iron oxides can be codeposited with magnetite. The presents of impurities of other oxides can lead to a change in some of the magnetite properties not desirable for its application in spintronic devices.

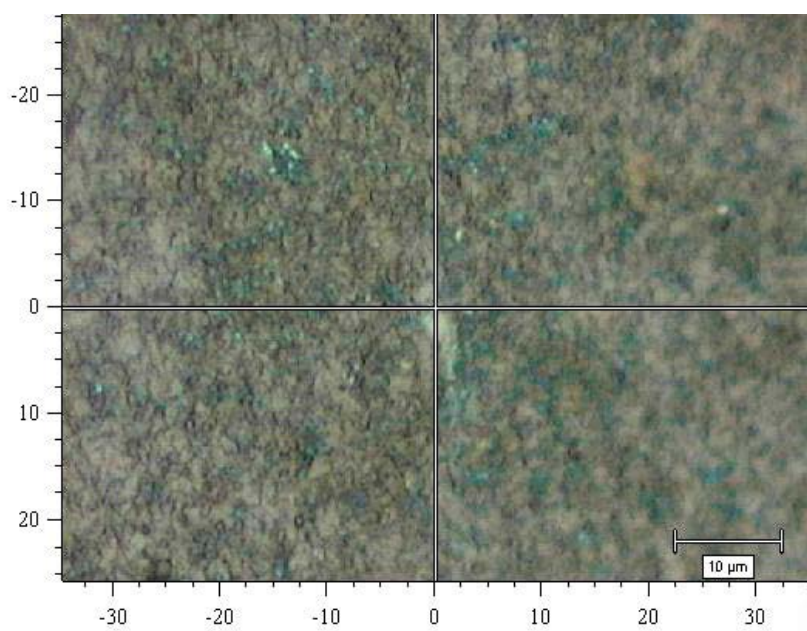


Figure 6.5: Optical image of the magnetite region where the spectrum was taken

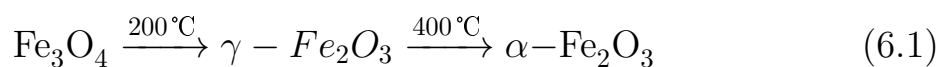
In order to study the purity of the deposits Raman spectra were recorded and compared with magnetite ( $\text{Fe}_3\text{O}_4$ ), maghemite ( $\gamma\text{-Fe}_2\text{O}_3$ ), goethite ( $\text{FeO}(\text{OH})$ ) and hematite ( $\alpha\text{-Fe}_2\text{O}_3$ ) ones reported in literature. In figure 6.5 an optical image of the region where the spectrum was taken is shown. Raman spectra were recorded at room temperature using a Renishaw Invia micro-Raman system. The samples were excited by the 488 nm line of an argon ion laser. The spectra were collected in a backscattering

geometry with spectral resolution of  $2 \text{ cm}^{-1}$ . The laser beam was focused on the sample by a x50 0.9NA (numerical aperture) objective to a spot size of 300 nm. The samples were exposed to both 3 mW and 0.5 mW incident laser powers, with unpolarised detection. One spectrum was recorded each time with an acquisition time of 300 s.

The scans were run between 123 and  $895 \text{ cm}^{-1}$ , since the iron oxides main vibration and rotational modes appeared in this range. In figure 6.6 Raman spectra recorded at 3 mW (A) and 0.5 mW (B) were shown. Significant differences in the spectra were observed depending on the incident laser power.

Hematite and magnetite spectra from RRUFF database are shown in figure 6.7 to facilitate the comparison with the experimental data. According to peak assignation reported by several workers for different iron oxides [159,160], in figure 6.6A bands assigned to hematite, maghemite and magnetite vibrational modes are recorded in the sample irradiated with 3 mW laser power, whilst only magnetite modes were detected in figure 6.6B correspondent to the sample irradiated with 0.5 mW laser power.

In our case the measurements were performed in air. In these conditions, if the power laser is too high, it can cause a temperature increase of the illuminated spot and consequently the magnetite oxidation. Under this conditions magnetite suffers the following phase transitions 6.1:



That is why in the spectrum recorded at higher power some maghemite

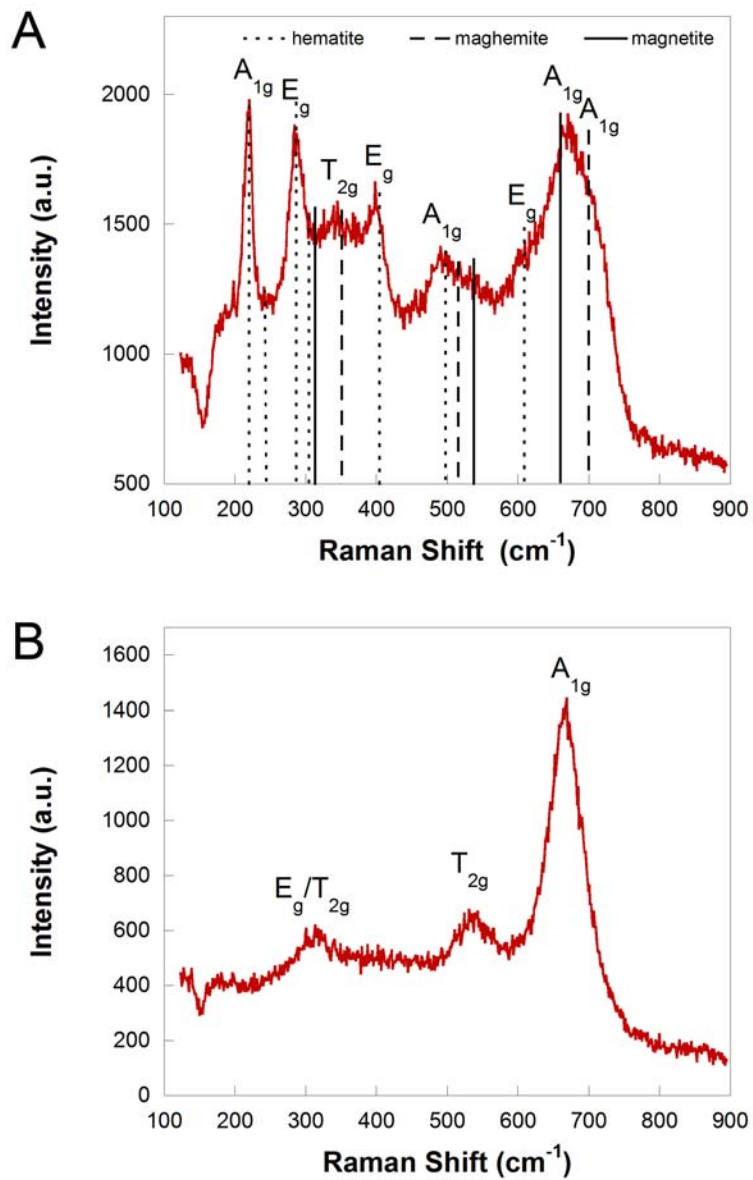


Figure 6.6: Raman spectra of a magnetite deposit obtained on glass/Au at  $-15 \text{ mA/cm}^2$ ,  $Q=-7.5 \text{ C/cm}^2$ , recorded at an incidence power of A) 3 mW and B) 0.5 mW

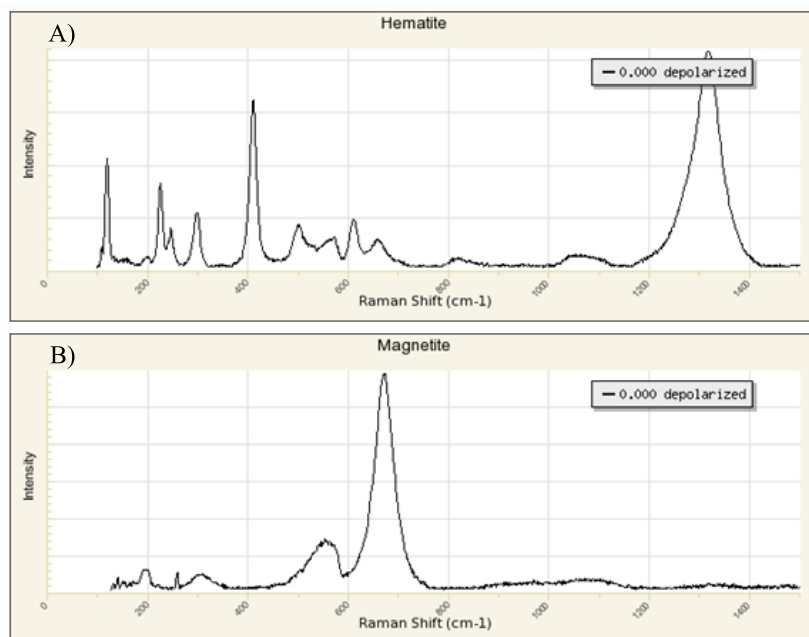


Figure 6.7: Reference Raman spectra of A) hematite R040024 and B) magnetite R060191 both from RRUFF Database

and hematite vibrational modes were detected. However, when using the low power laser only magnetite modes were detected which suggests that the electrodeposits obtained were pure magnetite. Faria et al. [160] had performed a comparison of light and heating effects on magnetite and had studied its transformation into maghemite and hematite with temperature increase by Raman spectroscopy. It is an important effect to take into account because it can lead to the misinterpretation of spectra.

From these results it might be deduced that electrodeposited samples correspond to pure magnetite, although the intense illumination of the samples causes their degradation and other species are detected in these conditions in Raman spectrum. This effect was also seen by Shebanova et al. [161].

Magnetite Raman spectrum showed two bands at 663 and 530 cm<sup>-1</sup>

assigned to  $A_{1g}$  and  $T_{2g}$  modes respectively and a third band at  $311\text{ cm}^{-1}$  that has been assigned to both  $E_g$  or  $T_{2g}$  modes in the literature [161]. These modes have been described:  $A_{1g}$  as a symmetric stretch of oxygen atoms along Fe-O bonds,  $E_g$  (for some authors  $T_{2g}$ , the one at  $311\text{ cm}^{-1}$ ) as a symmetric bend of oxygen with respect to Fe and finally  $T_{2g}$  (the one at  $530\text{ cm}^{-1}$ ) as an asymmetric stretch of Fe and O [161].



# In-situ electrochemical method for octanethiol monolayer formation over amorphous CoP deposits

M. Cortés,\* E. Gómez, and E. Vallés

*Electrodep, Departament de Química Física and Institut de Nanociència i Nanotecnologia (IN<sup>2</sup> UB),  
Universitat de Barcelona, Martí i Franquès 1, 08028 Barcelona, Spain.*

W. Schwarzacher

*H.H. Wills Physics Laboratory, Royal Fort, Tyndall Avenue, Bristol BS8 1TL, United Kingdom.*

An electrochemical method of in-situ octanethiol layer formation from an acidic sodium sulphate solution over magnetic CoP films was developed. CoP films of 1.5  $\mu\text{m}$ -thickness were electrodeposited on glass/Au substrates under potentiostatic control, which led to small grain deposits with low rms roughness (2-3 nm). The obtained CoP deposits containing 90-92 wt. % Co were amorphous and exhibited soft magnetic behaviour. The adsorption of octanethiol on the CoP films was performed after electrochemically cleaning the deposit surface and adding in-situ the octanethiol in ethanol solution. An electrochemical study reveals the formation of physisorbed or chemisorbed layers depending on the cleaning procedure. Glass/Au/CoP/octanethiol samples revealed an increase in the rms roughness of 4-6 nm, probably as a consequence of the electrochemical cleaning process. Chemisorbed monolayer formation over the CoP deposits was confirmed by XPS measurements and corroborated by contact angle measurements.

## I. INTRODUCTION

Molecular self-assembly (SAM) provides one of the most effective and widely used methods for forming molecular monolayers on metal surface<sup>1-6</sup>. It is usually straightforward to apply and facilitates the fabrication of homogeneous monolayer films with a high degree of internal molecular order. It has been wide used in many branches of science requiring well-defined molecular monolayers. Within electrochemistry, applications for these molecular monolayers include molecular sensors, surface passivation and corrosion inhibition, templates for electrodeposition, studies of interfacial electron transfer and surfaces for bioelectrochemistry. Usually the literature of self-assembled monolayers formation refers to noble metals substrates such as gold<sup>7-14</sup>, because the gold surface is stable in ambient conditions and it is electrochemically inert.

Moreover, alkanethiols are known to have a high affinity for gold due to the sulphur end group and form densely packed highly crystalline monolayers. Alkanethiols self-assembly onto gold has been well characterised using techniques such as infra-red spectroscopy, scanning tunnelling microscopy and x-ray photoelectric spectroscopy and has become the most studied example of molecular self-assembly<sup>14,15</sup>.

SAM onto other metals is less well studied<sup>16-19</sup>, because they have more tendency than gold to oxidise, depending on ambient conditions, which makes molecular functionalisation by self-assembly under ambient conditions far less straightforward. Metals such as nickel, cobalt and iron are of interest for their magnetic properties<sup>20-23</sup>, and self-assembled alkanethiol films on these metals are of interest for patterning, surface functionalisation, protection against oxidation, as well as in molecular electronics and spintronics<sup>24-26</sup>. Molecular

functionalisation of such base metals in UHV would avoid problems relating to surface oxidation; however it is not a conventional method of self-assembly. A more common method for SAM's formation is direct self-assembly onto base metals from solution phase but this method needs to overcome the problems with surface oxidation.

In this work, an electrochemical method of in-situ octanethiol layer formation from an acidic sodium sulphate solution over flat magnetic electrodeposited film is studied. CoP was chosen as the magnetic substrate because the feasibility to obtain very smooth deposits of this material. For this purpose, deposits of CoP are prepared and characterised. The adsorption of octanethiol films over them is tested by adding in-situ an ethanol solution of the organic molecule in the supporting electrolyte. The formation and purification of the layers will be analysed by means electrochemical and EQCM methods. Contact angle as well as XPS measures will be used to characterise the monolayer formation.

## II. EXPERIMENTAL

Electrodeposition has been carried out using a potentiostat/galvanostat Autolab PGSTAT302 with GPES software in a three-electrode cell. A glass/Au substrate was selected as the working electrode; samples of 5x5 cm<sup>2</sup> were used. The reference electrode was a saturated calomel electrode (SCE). The counter electrode was a platinum spiral. CoP deposits were prepared potentiostatically at -1200 mV for 30 seconds at 75 °C without stirring using a 62 g/l H<sub>3</sub>PO<sub>3</sub>, 58 g/l H<sub>3</sub>PO<sub>4</sub>, 180 g/l CoCl<sub>2</sub> 6H<sub>2</sub>O, 40 g/l CoCO<sub>3</sub> solution.

Leica Stereoscan S-360 scanning electron microscope was used to analyse deposits composition. Films roughness (rms) was analysed using a Veeco Dimension V

atomic force microscope (AFM).

The structure of deposits was studied by means of a Philips MRD diffractometer with parallel optical geometry using Cu K $\alpha$  radiation ( $k = 1.5418 \text{ \AA}$ ). Magnetic properties were characterised by means of a SQUID magnetometer at room temperature in helium atmosphere.

Before monolayer deposition, electrochemical cleaning of the CoP surface in a 0.05 M Na $_2$ SO $_4$  adjusted to pH = 3 with H $_2$ SO $_4$  solution was performed. For monolayer formation a 10 $^{-2}$  M octanethiol in ethanol solution was used. EQCM and chronoamperometry were used to follow the formation process. Contact angle measurements were performed using home-built apparatus, and X-ray Photoelectron Spectroscopy (XPS) experiments were carried out in a PHI ESCA-5500 Multitechnique System from Physical Electronics and the recorded data was analysed with the program Multipak from Physical Electronics.

### III. RESULTS AND DISCUSSION

Figure 1A shows a chronoamperometric curve corresponding to the preparation of CoP deposits under static conditions. Granular and compact 1.5  $\mu\text{m}$ -thick deposits of low rms roughness (2-3 nm measured over an area of 100  $\mu\text{m}^2$ ) were obtained and resolved by AFM (figure 1B). The EDX analysis of these CoP films revealed a 8-10 wt. % of P. XRD diffractograms (figure 1C) confirm the amorphous nature of the deposited CoP, revealed by the band between 40 and 50  $2\theta$  which corresponds with the data found in the literature about amorphous deposits with such an amount of P $^{27}$ . Normalized magnetization curves with the field applied parallel to the samples were recorded; soft-magnetic behaviour is revealed (figure 1D). The measured coercivity was 4 Oe.

CoP is susceptible of being superficially oxidised in contact with air, which makes it necessary to remove the possible oxide formed over these deposits before covering them with an octanethiol monolayer. In order to clean the deposits by removing the superficial oxides, electrochemical reduction was made: cyclic voltammetry was selected as a tool to both detect and remove oxide formation. Two consecutive scans from -0.2 to -1 V were recorded in 50 ml of a 0.05 M Na $_2$ SO $_4$  solution at pH = 3 (figure 2). In the first scan, a reduction peak attributed to both oxide and proton reduction was detected $^{28,29}$ . From the second scan, the reduction current decreased as a consequence of oxide removal. Once the CoP deposit has been cleaned, the sample was maintained inside the sulphate solution at a potential of -0.6 V referred to SCE; this potential value was selected after previous experiments because it maintains a negative polarization of the surface avoiding any possible oxide formation and it is a potential at which low proton reduction took place.

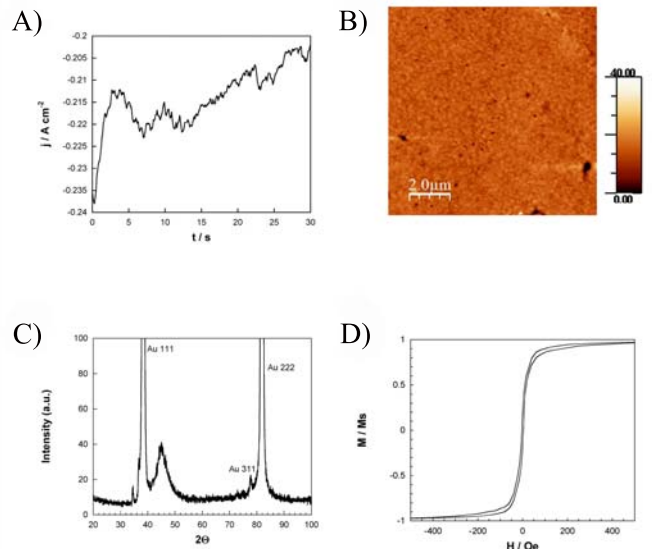


FIG. 1: A) Chronoamperometric curve, B) AFM image, C) XRD diffractogram and D) normalized room-temperature magnetization curve for a CoP deposit obtained, glass/Au working electrode, at -1200 mV for 30 seconds at 75°C

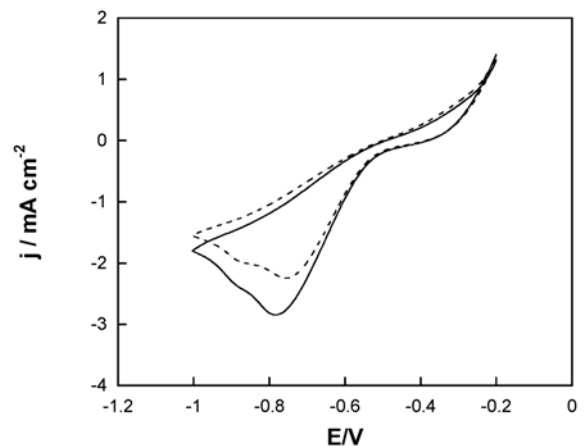


FIG. 2: Voltammetric curves in an acidic sodium sulphate solution of a deposit of CoP, first scan (solid line), second scan (dashed line)

The formation of layers was monitored by potentiostatic method as well as by EQCM. Figure 3 shows the potentiostatic curve over the glass/Au/CoP substrate recorded at -0.6 V and the dependency of the frequency shift response during the formation of the octanethiol layers. In both cases, it is observed that around 5 minutes were required to stabilize the signal when applying

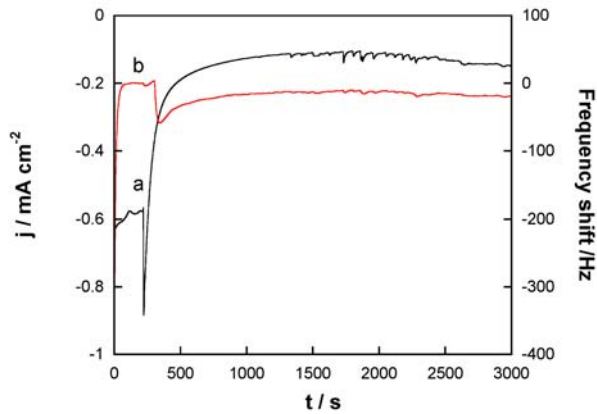


FIG. 3: Chronoamperometric curve (a) and frequency shift response (b) during the formation of the octanethiol layers at  $-0.6$  V

the fixed potential. Once the stabilization was attained, one ml of the octanethiol dissolution was added and a perturbation of both signals was recorded, after that the system evolved to a new equilibrium, forming the organic layer. A decrease of the current density is observed after the layer formation, as a consequence of the reduction of the electroactive area of the electrode in contact with the solution which minimizes proton reduction. Also, a reduction of the capacitive current is expected after adsorption. Analogous behaviour was observed for the frequency shift response, as there is more matter mass on top of the crystal after the organic molecule was adsorbed, decreasing the resonant frequency.

Once the octanethiol layer was formed, the samples were cleaned to remove the excess of organic molecule that was not adsorbed and then they were electrochemically studied. Two different methods were tested, method I consisted of rinsing the sample in ethanol a few times for 30 minutes during each wash and method II was sonicating the sample in ethanol for 5 minutes. Cyclic voltammograms were recorded, applying the same potential range as that in figure 2, in order to compare the electrochemical response of the reduction proton process in the samples with and without monolayer.

Significant differences in the response were observed (figure 4) depending on the cleaning procedure applied. When the glass/Au/CoP/octanethiol samples were washed with ethanol, a blocking of the hydrogen evolution reaction was observed (figure 4A), which suggest the formation of thiol multilayers. However, when the excess of the adsorbed thiol is removed by sonicating the samples, an enhancement of the proton reduction reaction was observed (figure 4B); this behaviour has been observed by different authors when a monolayer

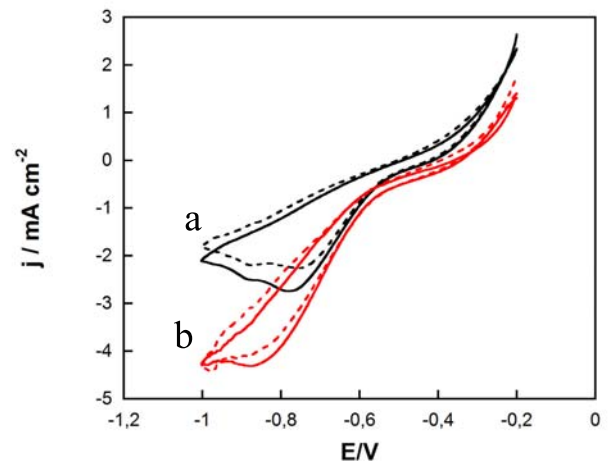
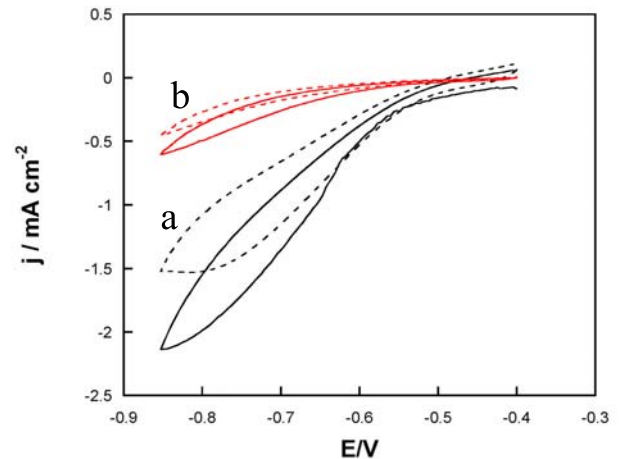


FIG. 4: Voltammetric curves in an acidic sodium sulphate solution of (A) pure CoP (a) and CoP with organic layer on top washed with ethanol (b), (B) pure CoP (a) and CoP with organic layer on top sonicated in ethanol (b). First scan (solid line), second scan (dashed line)

of thiol is chemisorbed on a metallic substrate<sup>29–31</sup>; we select method II in order to assure monolayer formation after removing the excess of thiol.

The CoP/octanethiol monolayer samples were characterised by AFM and an increase in the rms roughness of 4-6 nm was detected (figure 5), probably as a consequence of the electrochemical cleaning process.

Contact angle measurements show that hydrophobic behaviour was observed when octanethiol monolayer was linked to the CoP surface, whereas the as-deposited CoP was hydrophilic (table I). The measurement of the contact angle of water on the surface of both pure CoP samples and CoP/ octanethiol monolayer samples allows the change of the surface behaviour from hydrophilic to hy-

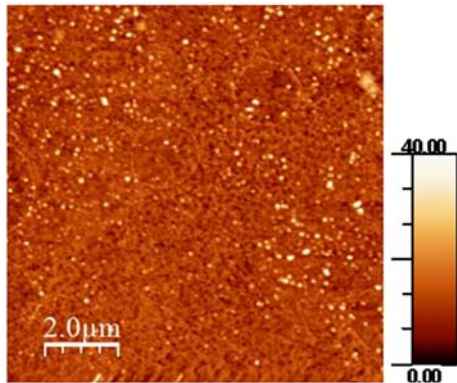


FIG. 5: AFM image of a CoP with an octanethiol monolayer

TABLE I: Theoretical values of  $I$  and  $2\theta$  of an fcc Cu powder and experimental values for the Cu deposit obtained over Si/SiO<sub>2</sub>/Ti/Cu

	Contact angle /°C
CoP without monolayer	23-31
CoP with octanethiol monolayer	78-85

drophobic to be detected, which corroborated the layer formation. Figures 6A and 6B illustrate this change in the character of the surfaces.

The presence of the octanethiol monolayer over the CoP was also analysed by XPS. We have used the sensitivity factor method to quantify these data. The standard sensitivity factors were corrected for the used geometry and analyzer's lenses. The binding energies have been corrected by assuming that main peak of the C<sub>1s</sub> signal is related to physisorbed carbon at 284.8 eV. Figure 7 shows the recorded XPS spectra of S<sub>2p</sub> for both pure CoP and CoP/octanethiol surfaces. In both cases, a peak at 168 eV appears, associated to the transition of the sulphate. However, a new peak at 160 eV appears in the sample containing the monolayer but not in the pure CoP one in which only the background line is recorded at that energy range. This peak is a doublet with a gap of 1.60 eV related to the sulphur of the monolayer adsorbed on top. From the area under the peaks and the corrected sensitivity factors, we have estimated the C/S ratio. A clear change in the C/S ratio was observed from the pure CoP samples (1257.5) to samples treated with octanethiol (18.3), which corroborates octanethiol monolayer formation over the CoP deposit.

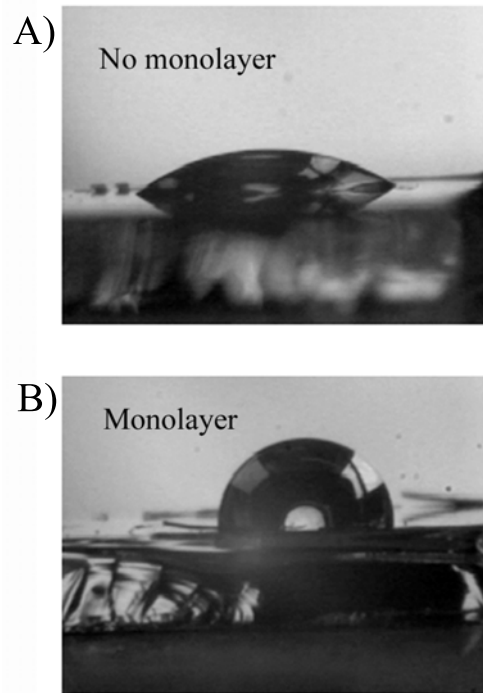


FIG. 6: (A) Hydrophilic behaviour of pure CoP and (B) hydrophobic behaviour of CoP with adsorbed octanethiol layer

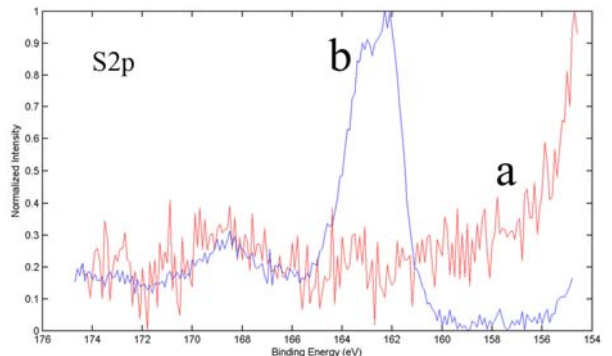


FIG. 7: XPS high resolution spectra of S<sub>2p</sub> peak of pure CoP (a), CoP/octanethiol monolayer (b)

#### IV. CONCLUSIONS

An electrochemical preparation method of octanethiol monolayers over flat CoP deposits has been developed. Amorphous CoP films showing low roughness and soft magnetic behaviour were prepared by electrodeposition for the adsorption of organic monolayers. In-situ octanethiol layer formation over CoP films from an acidic sodium sulphate solution was performed: Native oxides

over the CoP surface were electrochemically removed and a negative polarization was maintained during the monolayer formation to prevent new oxide formation. The octanethiol layer formation was followed by potentiostatic methods as well as by EQCM, revealing a decrease in the current density as well as in the frequency shift as a consequence of the formation of the layer on top of the electrode. To obtain a monolayer, the samples were sonicated in ethanol in order to remove the octanethiol excess. The voltametric response in a blank solution showed an enhancement in the current density of the hydrogen evolution. XPS experiments confirm the presence of the octanethiol monolayer over the CoP. Hydrophobicity of the surface was induced by adding the monolayer.

The results obtained open the possibility of using electrochemical methods for the formation of thiol monolay-

ers over magnetic films, which are able to be used in molecular spintronic devices.

## V. ACKNOWLEDGMENTS

This article was supported by contract CTQ2010-20726 (subprogram BQU) from the Comisin Interministerial de Ciència y Tecnología (CICYT). The authors wish to thank the Centres Científics i Tecnològics de la Universitat de Barcelona (CCiTUB) for the use of their equipment. M. C. would also like to thank the Departament dInnovació, Universitats i Empresa of the Generalitat de Catalunya and Fons Social Europeu for their financial support.

---

\* Electronic address: m.cortes@ub.edu

- <sup>1</sup> C. Xie, H. Li, S. Li, J. Wu, Z. Zhang, *Anal. Chem.* **2010**, *82*, 241–249.
- <sup>2</sup> T. Clark, R. Ferrigno, J. Tien, K. Paul, G. Whitesides, *J. Am. Chem. Soc.* **2002**, *124*, 5419–26.
- <sup>3</sup> B. Diaconescu, T. Yang, S. Berber, M. Jazdyk, G. Miller, D. Tomnek, K. Pohl, *Phys. Rev. Lett.* **2009**, *102*, 056102(1)–056102(4).
- <sup>4</sup> S. Jensen, A. Baber, H. Tierney, E. H. Sykes, *ACS Nano.* **2007**, *1*, 423–428.
- <sup>5</sup> R. Michalitsch, C. Noguez, A. Najari, A. ElKassmi, A. Yassar, P. Lang, F. . Garnier, *Synthetic Met.* **1999**, *101*, 5–6.
- <sup>6</sup> M. Fonticelli, O. Azzaroni, G. Benitez, M. Martins, P. Carro, R. Salvarezza, *J. Phys. Chem. B* **2004**, *108*, 1898–1905.
- <sup>7</sup> E. Baldrich, O. Laczka, F. Del-Campo, F. Munoz, *J. Immunol. Methods* **2008**, *336* (2), 203–212.
- <sup>8</sup> S. Lei, M. Lanqun, *Talanta* **2006**, *70*, 68–74.
- <sup>9</sup> T. Luczak, M. Beltowska-Brzezinska, *Microchim. Acta.* **2011**, *174*, 19–30.
- <sup>10</sup> T. Masadome, A. Ueda, M. Kawakami, *Anal. Lett.* **2004**, *37*, 225–233.
- <sup>11</sup> L. Velleman, J. Shapter, D. Losic, *J. Membrane Sci.* **2009**, *328*, 121–126.
- <sup>12</sup> F. Hubenthal, N. Borg, T. Weidner, U. Siemeling, F. Trager, *Appl. Phys. A: Mater* **2009**, *94*, 11–17.
- <sup>13</sup> M. Sheffer, V. Vivier, D. Mandler, *Electrochem. Commun.* **2007**, *9*, 2827–2832.
- <sup>14</sup> M. Silva, I. Cavalcanti, M. Barroso, M. Sales, R. Dutra, *J. Chem. Sci.* **2010**, *122*, 911–917.
- <sup>15</sup> H. Aoki, Y. Umezawa, A. Vertova, S. Rondinini, *Anal. Sci.* **2006**, *22*, 1581–1584.
- <sup>16</sup> M. Cortes, E. Gomez, J. Sadler, E. Valles, *Electrochim. Acta* **2011**, *56*, 4087–4091.
- <sup>17</sup> Z. Mekhalif, J. Riga, J. Pireaux, J. Delhalle, *Langmuir* **1997**, *13*, 2285–2290.
- <sup>18</sup> S. Wang, F. Yue, D. Wu, F. Zhang, W. Zhong, Y. Du, *Appl. Phys. Lett.* **2009**, *94*, 012507(1)–012507(3).
- <sup>19</sup> J. Petta, S. Slater, D. Ralph, *Phys. Rev. Lett.* **2004**, *93*, 136601–136604.
- <sup>20</sup> J. M. Garcia-Torres, E. Gomez, E. Valles, *J. Appl. Electrochem.* **2009**, *39*, 233–240.
- <sup>21</sup> P. Evans, G. Yi, W. Schwarzacher, *Appl. Phys. Lett.* **2000**, *76*, 481–483.
- <sup>22</sup> M. Munford, L. Seligman, M. Sartorelli, E. Voltolini, L. Martins, W. Schwarzacher, A. Pasa, *J. Magn. Magn. Mater.* **2001**, *226*, 1613–1615.
- <sup>23</sup> M. Duch, J. Esteve, E. Gomez, R. Perez-Castillejos, E. Valles, *J. Micromech. Microeng.* **2002**, *12*, 400–405.
- <sup>24</sup> M. Halik, A. Hirsch, *Adv. Mater.* **2011**, *23*, 2689–2695.
- <sup>25</sup> S. Mallajosyula, S. Pati, *J. Phys. Chem. B* **2008**, *112*, 16982–16989.
- <sup>26</sup> W. Naber, S. Faez, W. van der Wiel, *J. Phys. D: Appl. Phys.* **2007**, *40*, R205–R228.
- <sup>27</sup> R. da Silva, A. Pasa, J. Mallett, W. Schwarzacher, *Surf. Sci.* **2005**, *576*, 212–216.
- <sup>28</sup> G. Kozhina, A. Ermakov, V. Fetisov, A. Fetisov, K. Yu, *Shunyaev Russ. J. Electrochem.* **2009**, *45*, 1170–1175.
- <sup>29</sup> J. Sadler, D. Szumski, A. Kierzkowski, S. Catarelli, K. Stella, R. Nichols, M. Fonticelli, G. Benitez, B. Blum, R. Salvarezza, W. Schwarzacher, *Phys. Chem. Chem. Phys.* **2011**, *13*, 17987–17993.
- <sup>30</sup> T. Suzuki, T. Yamada, K. Itaya, *J. Phys. Chem. B* **1996**, *100*, 8954–8961.
- <sup>31</sup> C. Taubert, D. Kolb, U. Memmert, H. Meyer, *J. Electrochem. Soc.* **2007**, *154*, D293–D299.



### 6.3 Conclusions

Deposits of both magnetite and CoP with soft magnetic behaviour were electrodeposited over glass/Au substrates and their morphology and crystalline structure were characterised. A solution containing 0.09 M Fe(III) + 0.1 M TEA + 2 M NaOH was used to obtain magnetite deposits and a 62 g/l  $\text{H}_3\text{PO}_3$ , 58 g/l  $\text{H}_3\text{PO}_4$ , 180 g/l  $\text{CoCl}_2 \cdot 6\text{H}_2\text{O}$ , 40 g/l  $\text{CoCO}_3$  solution was selected for CoP formation. In the case of magnetite films of different thickness between 80 nm and 4  $\mu\text{m}$  have been prepared and the growth rate was determined. CoP deposits obtained were 1.5  $\mu\text{m}$ -thick.

In both cases, deposits obtained presented low roughness which permitted to obtain very flat films suitable for the organic monolayers adsorption. Different organic compounds were studied.

Magnetite purity was corroborated by Raman Spectroscopy. Both dodecanethiol and oleic acid are shown to adsorb on magnetite by immersing the films in a solution containing the organic molecule for 24 hours at low temperature.

In the case of CoP films, native oxides were electrochemically removed before the octanethiol layer formation and negative polarization was maintained during the process to prevent new oxide formation. The octanethiol layer formation was followed by potentiostatic methods as well as by EQCM, revealing a decrease in the current density as well as in the frequency shift as a consequence of the formation of the layer on top of the electrode.

Physisorbed molecules were removed by sonicating the samples in ethanol, as corroborated by contact angle measurements that took the same value

than in as-deposited films after washing the sample few times. The monolayer remains over the both magnetic layers after successive cleaning of the samples with ethanol. Hydrophobicity of the surface was induced when a monolayer was formed, even after washing the samples several times.

XPS experiments enabled the interaction between the layers and the substrate to be detected. Peaks corresponding to sulphur bonding to the different films were detected, confirming the presence of the monolayers over them.

The voltammetric response of the different films in a blank solution has been also used to demonstrate the presence of the organic monolayers. Several differences were observed in the case of magnetite and an enhancement in the current density of the hydrogen evolution was detected in CoP.

Although further work is needed to study the structure of the adsorbed monolayer, the results presented here show a possible application for electrochemical methods in molecular spintronic devices.

## Chapter 7

# Conclusions

The specific conclusions extracted of each one of the three sections have been already presented. The general conclusions referred to the overall work are:

- Electrodeposition has been demonstrated to be a useful technique for the design and fabrication of micro/nanomaterials with specific properties that allow them to be implemented in biosensors, MEMS and molecular spintronic devices. Then, electrochemistry can be said to be a versatile technique that it can be used in new applications such as the preparation of sensors and actuators.
- Planar copper coils to be implemented in an inductive biosensor have been designed, obtained and characterised. For that reason it has been necessary to perform simulations of the resistance and inductance of the coils. An optimum bath, the electrodeposition conditions and the fabrication processes to obtain adherent and low stressed copper coils of several microns thick, with the adequate number of turns and thickness have been found. The variation of the resonance frequency

of coils when placing magnetic particles on top of them have been measured as the first test of their sensing ability.

- Deposition of CoPt hard magnetic alloy for MEMS application has been performed. The basic study of the electrodeposition process of the CoPt alloy has permitted to find the optimum bath and optimum electrodeposition conditions. Based on the previous electrochemical results, it has been possible to obtain CoPt thin films, microstructures, nanoparticles, nanowires and CoPt@CoNi over different substrates. The influence of the electrodeposition/preparation conditions on the properties of the CoPt alloy (morphology, composition, crystalline structure, magnetic properties) has been studied for each one of the shapes of the micro/nanostructures.
- As the first step to fabricate a molecular spintronic device, smooth magnetic thin films of magnetite and cobalt-phosphorous alloy by means of electrodeposition have been prepared. Over them, organic monolayers formation has been possible. The formation of the monolayer has been studied by using contact angle measurements, cyclic voltametry and XPS.

## Appendix A

### Resum en català

#### **Electrodeposició:**

L'electrodeposició implica fenòmens químics associats amb la separació i la transferència de càrrega. Aquesta es pot produir de forma homogènia en solució, o heterogènia sobre les superfícies dels elèctrodes. Com a mínim han de tenir lloc dues semireaccions de transferència de càrrega per tal d'assegurar l'electroneutralitat de la dissolució . En el cas de reaccions redox heterogènies, aquestes semireaccions es produeixen en dos elèctrodes submergits en una solució.

L'electrodeposició és un procés en el qual els ions metàl·lics presents en la solució es redueixen per recobrir un objecte conductor amb una capa del material de gruix dependent de la càrrega aplicada. La reacció química que té lloc és A.1:



Aquest procés implica l'aplicació d'un corrent elèctric a través de la

solució que conté els ions i que seran reduïts sobre el substrat. Aquesta reacció és heterogènia i es porta a terme a la regió interfacial entre l'elèctrode i la solució. Els electrons transferibles des de l'elèctrode han de tenir un mínim d'energia per què es produeixi la transferència, aquesta energia vindrà associada a un potencial prou negatiu. Cada semireacció té associat un potencial d'elèctrode estàndard  $E^\circ$ . Per les semireaccions en equilibri, tenim el potencial d'equilibri,  $E_{eq}$ , que està relacionat amb el potencial estàndard a través de l'equació de Nernst A.2:

$$E_{eq} = E^\circ - \frac{RT}{nF} \sum \nu_i \ln a_i \quad (\text{A.2})$$

On  $\nu_i$  són els nombres estequiomètrics i  $a_i$  són les activitats de les espècies.

Normalment és necessari aplicar un potencial superior al d'equilibri per tal de superar la barrera d'activació i permetre que la reacció de reducció tingui lloc. El potencial addicional al qual es produeix la deposició s'anomena sobrepotencial,  $\eta$  i és necessari realitzar un estudi electroquímic bàsic per tal d'establir els potencials adients per què cada procés tingui lloc.

Hi ha alguns elements que són bàsics per dur a terme l'electrodeposició, com ara: L'electròlit, la cel·la electrolítica, els elèctrodes i la font de corrent o potencial. L'electròlit és la solució que conté els ions del metall o metalls que volem dipositar, generalment coneguts com a espècies electroactives. En general, és una solució aquosa i pot contenir altres espècies que controlin el pH o bé augmentin la conductivitat de la solució o millorin

les característiques dels dipòsits. La cel·la electrolítica és el recipient on està contingut l'electròlit. Per dur a terme l'electrodeposició són necessaris com a mínim dos elèctrodes: un elèctrode de treball que actui com a càtode i on es porta a terme la reducció dels ions metàl·lics, per tal de que es produeixi l'electrodeposició és necessari que el substrat sigui conductor. El segon elèctrode necessari és l'auxiliar que actua com l'ànode del procés. Per tal de tenir un millor control del procés es pot utilitzar un tercer elèctrode, aquest s'anomena elèctrode de referència i permet controlar el potencial de l'elèctrode de treball al qual s'inicia la reacció i com es va modificant al anar augmentant el sobrepotencial. Finalment, per aplicar i mesurar el senyal durant l'electrodeposició es fa servir una font de corrent o potencial.

Tot i que la tècnica d'electrodeposició pot semblar un mètode fàcil per a la preparació de materials, s'han de controlar una gran quantitat de paràmetres del procés, com ara la composició de l'electròlit, el pH, la temperatura, l'agitació, el potencial aplicat o el corrent. La variació de qualsevol d'aquests paràmetres pot afectar les característiques dels dipòsits ja siguin l'espessor, la composició, la mida del gra o l'estructura cristal·lina, entre d'altres. Aquestes característiques a la vegada afectaran a les propietats magnètiques, elèctriques o òptiques del material.

### **Additius:**

Com ja s'ha esmentat anteriorment, en algunes ocasions és necessari afegir algunes espècies en el bany per tal de modificar algunes de les característiques dels dipòsits. Aquestes espècies es denominen additius i són substàncies químiques que afegides en una proporció molt petita al bany,

permeten modificar les característiques dels dipòsits, com ara: morfologia, rugositat, duresa, estructura i resistència a la corrosió.

L'ús dels additius apropiats en una concentració apropiada permetrà obtenir recobriments amb els requisits desitjats. No obstant això, un excés o un mal ús dels additius pot produir dipòsits opacs, fràgils o amb stress. Hi ha molts tipus d'additius i normalment es classifiquen com:

- **Abrillantadors.** Aquests tipus d'additius disminueixen la rugositat del dipòsit, ja que modifiquen el procés de nucleació generant un gra més fi.
- **Anivelladors.** Relanteixen la velocitat de creixement, ja que són adsorbits en els punts on el dipòsit està creixent massa ràpid, i inhibeixen el creixement.
- **Modificadors d'estructura.** En aquest cas els additius redueixen l'stress dels dipòsits.
- **Carriers.** Faciliten la desorció de l'hidrogen i redueixen la tensió superficial del dipòsit.
- **Agents complexants.** Complexen els cations metàl·lics, el que permet controlar l'arribada dels ions a la superfície de l'elèctrode. Això desfavoreix el creixement dendrític no desitjat, que produeix dipòsits opacs, rugosos i porosos.

### **Electrodeposició: avantatges i inconvenients**

Electrodeposició presenta diversos avantatges sobre altres tècniques. Un d'aquests avantatges és el seu baix cost, l'equip utilitzat és barat i pràctica-

ment no requereix manteniment.

D'altra banda, la temperatura que normalment s'utilitza per fer créixer el material sol ser inferior a 100°C. Aquesta característica evita problemes produïts durant el refredament del substrat com per exemple que els dipòsits presentin tensió.

Un altre avantatge és que es pot assolir una velocitat de deposició superior respecte a les tècniques de buit, el que permet obtenir dipòsits més gruixuts en un lapse de temps relativament baix. Això fa que la galvanoplàstia sigui insubstituble en certes aplicacions. A més, utilitzant les tècniques de buit una alta quantitat del material precursor es diposita en les parets de la cambra, situació que no es produeix en l'electrodeposició, en la que en una sola etapa s'aconsegueix recobriment 3D donat que només diposita sobre el substrat.

Però potser un dels avantatges més importants de l'electrodeposició i segurament la característica que ha contribuït en gran mesura a la seva incorporació a la indústria microelectrònica és la capacitat de dipositar el material només a la part conductora del substrat deixant lliures les zones aïllants. En aquest sentit, aquesta tècnica permet aconseguir patrons sobre substrats litogràfics sense cap necessitat de tractaments posteriors.

Per contra, l'electrodeposició també presenta alguns inconvenients. D'una banda, la uniformitat dels dipòsits electrodepositats (composició química i gruix) depèn de la geometria de la cel·la i de la hidrodinàmica del procés, factors de vegades difícils de controlar.

D'altra banda, també és important considerar l'esgotament de la com-

posició d'electròlits, ja que en aquests processos la concentració és un dels paràmetres crítics.

### **Història de l'electrodeposició:**

No és possible determinar amb precisió l'origen de l'electrodeposició, però hi ha indicis de que es remunta almenys tres mil anys. De fet, la presència en les antigues tombes de Tebes i Memphis de diversos objectes coberts amb una capa prima de coure, com ara gerros i estatuets d'argila, fulles d'espases i puntes de fletxa, ... permet suposar que en l'antiguitat els egipcis van usar mètodes similars a l'actual galvanoplàstia del coure. Cal admetre que aquestes obres no podien ser dutes a terme mitjançant la deposició de coure utilitzant una font d'alimentació externa i una solució concentrada d'una sal del metall. En lloc d'això, era suficient submergir una estàtua tallada de fusta on la superfície hagués estat prèviament metal·litzada mitjançant l'aplicació de pols d'or de gra molt fi o per aplicació d'or (o plata) batut en fulles primes juntament i una placa de zinc en una solució de coure i connectar-les, d'aquesta manera es produïa un intercanvi de ions. Quan el dipòsit de coure de l'estàtua era prou gruixut es retirava del bany, s'assecava a foc lent i a continuació es procedia a un escalfament progressiu per eliminar-ne les cendres del suport de fusta. No obstant això només són conjectures.

L'electroquímica moderna va ser inventada pel químic italià Luigi V. Brugnatelli el 1805. Brugnatelli va explotar la invenció que cinc anys abans havia fet el seu col·lega Alessandro Volta, la pila de Volta, per dur a terme la primera electrodeposició. Aquest fenomen, que va ser ignorat per l'Acadèmia Francesa de les Ciències, va ser investigat uns anys més tard

per Spencer a Anglaterra, La Rive a Sussa (1825) i Antoine Becquerel a França (1829). D'altra banda, el físic rus Jacobi, partint de la investigació de Delarue sobre el funcionament de la pila de Daniell, va inventar al 1837 els processos utilitzats actualment per a la galvanoplàstia del coure.

La galvanoplàstia ràpidament es va fer popular a Rússia, amb gent com l'inventor Bagrationi Pere, el científic Heinrich Lenz i l'autor de ciència ficció Vladimir Odóyevski, tots ells van contribuir al desenvolupament de la tecnologia. Un exemple dels usos de galvanoplàstia durant la segona meitat del segle XIX a Rússia són les escultures galvanitzades gegants de la Catedral de Sant Isaac a Sant Petersburg i la cúpula daurada de la catedral de Crist Salvador a Moscou, l'Església Ortodoxa més alta del món.

Més tard, John Wright de Birmingham, Anglaterra, van descobrir que el cianur de potassi és un electròlit adequat per a la galvanoplàstia d'or i de plata. George i Elkington Henry, els associats de Wright, i el comte Henri de Ruolz-Montchal a França van aconseguir obtenir un dipòsit adherent d'or o de plata connectant un elèctrode al pol negatiu de la font de corrent, tot fent servir solucions de sals d'or o plata.

Aquest moment podria ser considerat com la invenció dels recobriments daurats i platejats per electròlisi. De fet és el naixement de galvanoplàstia. Les primeres patents de galvanoplàstia van ser fetes al 1840 per George i Henry Elkington, per a la deposició d'or i plata. Llavors es va fundar la indústria de galvanoplàstia a Birmingham des d'on es va estendre per tot el món.

Alguns mesos més tard, Ruolz, va fer una patent a França. El desenvolupament de l'electrodeposició de metalls preciosos es va produir a partir

de 1850, però a mesura que la ciència electroquímica es va anar desenvolupant el procés d'electrodeposició es va anar entenent i es van desenvolupar altres processos de galvanoplàstia per fins no decoratius. El níquel electrolític, llautó, estany i zinc comercials van ser desenvolupats durant la dècada de 1850. La Norddeutsche Affinerie a Hamburg va ser la primera planta de galvanoplàstia moderna que va iniciar la seva producció el 1876. Un dels inconvenients de la galvanoplàstia en aquell moment eren les extremadament lentes velocitats de deposició que s'obtenien. Malgrat això, va ser possible obtenir excel·lents resultats ja que la deposició lenta afavoria l'obtenció d'un gra fi i la cohesió del metall.

A mitjans del segle XIX, la modelització i estudi de l'electroquímica, van ser duts a terme per Michael Faraday i John Daniell.

A partir de l'arribada del desenvolupament de generadors elèctrics a finals del segle XIX, la indústria de la galvanoplàstia va rebre un gran impuls, ja que es va acabar la limitació de potència DC i tot es va convertir en possible. L'aplicació de corrents més altes permetia processar a granel components metàl·liques de màquines i d'automòbils que requereixen protecció contra la corrosió i/o millorar les propietats, juntament amb una millor aparença.

Les dues guerres mundials i la creixent indústria de l'aviació van donar un impuls als nous avenços i millores, incloent processos com ara el cromat dur, el xapat d'aliatge de bronze, el níquel sulfamat, juntament amb nombrosos altres processos de recobriments. L'equipament per dur a terme l'electrodeposició va evolucionar dels tancs d'accionament manual a equips automatitzats capaços de processar milers de quilograms per hora.

Durant l'última part del segle XX, l'electroquímica i la deposició electroquímica s'han estès a diferents aplicacions, tant en el món de la indústria com en el de la investigació.

### **L'Electrodeposició a la indústria:**

Avui dia l'electrodeposició s'utilitza en una àmplia gamma d'aplicacions pel processament i acabat de metalls:

Els mètodes electrolítics s'utilitzen per extreure i refinar metalls com ara: plom, estany, coure, or i plata. L'avantatge d'extreure o refinar metalls per processos electrolítics és que el metall obtingut és d'alta puresa. Una aplicació industrial important de l'electròlisi és el forn elèctric, que s'utilitza per a la fabricació d'alumini, un dels elements més abundants en l'escorça terrestre, però que només pot ser extret per electròlisi. Altres metalls que poden ser extrets són el magnesi i el sodi. En aquest forn, les sals metàl·liques s'escalfen fins que es fonen i són ionitzades. A continuació, el metall es diposita electrolíticament.

L'electroformació i el mecanitzat electromecànic són dos tipus de processament de metalls. En el primer cas, un metall es electrodepositat sobre d'un motlle que es retira després. Els metalls més comunament usats són el níquel i el coure. Per contra el mecanitzat electromecànic també conegut com electroerosió s'utilitza quan el mecanitzat mecànic no és possible i consisteix en dissoldre l'objecte que actua com ànode mitjançant l'ús d'un càtode amb la forma d'un motlle adequat per a obtenir aquest objecte. Aquest mètode s'utilitza en la fabricació de components, com ara pales per turbines.

La galvanoplàstia és un procés àmpliament utilitzat en la indústria per revestir objectes de metall amb una capa prima d'un metall diferent. És un dels processos més importants en termes de volum de producció, i també té un dels majors impactes econòmics. El propòsit d'aquests recobriments és proporcionar a l'objecte de metall recobert alguna propietat desitjada que no té. Per exemple, el cromat es porta a terme en molts objectes, com ara peces d'automòbils, aixetes de bany, llantes de rodes i molts altres.

Una aplicació habitual d'aquest procediment és la joieria, on una peça feta amb material barat es recobreix amb una capa d'or o plata, per protegir-lo de la corrosió i per augmentar-ne el valor. De fet, aquesta va ser la primera aplicació de galvanoplàstia en la indústria, tal i com s'ha comentat anteriorment. Alguns exemples de processos de galvanoplàstia són: El zinc electrolític, que consisteix en un recobriment de zinc que actua com una barrera que es sacrifica per evitar la corrosió del metall de sota. Els processos d'estanyat que són utilitzats per evitar la corrosió de les llaunes i altres recipients d'ús alimentari. El cromat, que s'utilitza pel seu aspecte decoratiu i perquè proporciona resistència a la corrosió i facilita els procediments de neteja. També es fa servir àmpliament per a peces que requereixen resistència al desgast, ja que augmenta la duresa de la superfície. Un sector de la indústria on s'ha aplicat amb èxit la galvanoplàstia és la indústria naval o la de l'automoció per recobrir xapes, para-xocs, pistons hidràulics i cilindres, anelles de pistó, components de motors i aplicacions similars. Un procediment relativament nou és l'electrodeposició de peces de plàstic amb capes de metall, que dota a la superfície de la peça de plàstic de propietats típiques dels metalls.

L'electrodeposició també pot ser usada a més petita escala, com per ex-

emple, el níquel electrolític, que s'utilitza en la rellotgeria i en l'electrònica a causa de la seva resistència a la corrosió i el seu aspecte decoratiu. També es pot utilitzar com a base per a altres revestiments galvanoplàstics.

### **Noves aplicacions de l'electrodeposició:**

Electrodeposició ha recorregut un llarg camí des dels seus inicis, el desenvolupament de noves tècniques n'ha augmentat el rang d'aplicacions de la mateixa. En aquest capítol es proporciona un breu resum d'algunes d'aquestes noves aplicacions.

L'electrodeposició també es pot utilitzar per sintetitzar polímers conductors (CP) a partir de la seva polimerització tot utilitzant l'oxidació electroquímica. En els darrers anys s'ha observat un augment de l'interès en l'ús de CP com a protecció contra la corrosió. Per això s'han realitzat diferents intents de sintetitzar-los electroquímicament sobre metalls actius en lloc del sobre metalls nobles, alguns d'aquests intents han estat duts a terme en dissolvents orgànics o disminuint el sobrepotencial de l'electropolimerització, ja sigui per mitjà de la presència de mediadors d'electrons o per la passivació del metall abans de la formació de la capa de polímer. També s'han aconseguit recents avenços en la síntesi i aplicacions de compostos de PC/CCG (grafens químicament convertits). Per exemple, han estat preparats per polimerització electroquímica compostos de PANI (polianilina)/CCCG i de PPy (polipirrol)/CCG. A causa de l'estructura i les propietats d'aquests materials compostos les seves aplicacions s'han estès més enllà de la mera protecció contra la corrosió i han estat utilitzats en diferents dispositius electroquímics, com a materials d'emmagatzematge d'energia en supercondensadors, per a la conversió d'energia en cel·les so-

lars de tercera generació i en detecció electroquímica.

A causa de la gran utilitat que presenten les nanoestructures, hi ha hagut un gran interès en la recerca de mètodes per a l'obtenció de nanoestructures d'alta qualitat. Des de fa unes dècades l'electrodeposició es considera com una alternativa real als mètodes de deposició física. Alguns exemples de materials nanoestructurats són: capes fines, patrons nanomètrics, multicapes, nanofils, etc... S'ha realitzat la deposició electroquímica de nanofils de Bi,  $\text{Bi}_2\text{Te}_3$ , PbSe,  $\text{PbSe}_{1-x}\text{Te}_x$  i  $\text{CoSb}_3$  per a ser utilitzats en generadors d'energia termoelèctrica i refrigeradors. Per exemple, Lim i col·laboradors han fabricat un dispositiu termoelèctric basat en l'ús de l'electrodeposició de nanofils de  $\text{Bi}_2\text{Te}_3$  de tipus n i nanofils de  $\text{Bi}_{2-x}\text{Sb}_x\text{Te}_3$  de tipus p. En un altre exemple, nanotubs de  $\text{TiO}_2$  preparats per oxidació electroquímica van ser investigats per la fotodegradació de fenol, taronja de metil, blau de metilè o acetaldehid gasós.

Hi ha diversos exemples de capes magnètiques i dipòsits obtinguts mitjançant l'electrodeposició utilitzats en (MEMS) sistemes microelectromecànics. Leith i col·laboradors han realitzat l'electrodeposició de NiFe a través d'un motlle per obtenir components de MEMS amb composició uniforme. Diferents autors han preparat capes primes de diferents aliatges com ara aliatges de fòsfor, tungstè, platí i cobalt. La necessitat d'obtenir materials magnètics durs capaços de retenir les seves propietats magnètiques fins a gruixos de desenes de micres utilitzant processos de deposició compatibles amb el silici ha portat Kulkarni i col·laboradors a electrodepositar capes de CoPtP de fins a 82 micres de gruix. Nombrosos grups han investigat el procés de creixement de microestructures d'aliatges i la correlació amb les seves propietats magnètiques. Wang i col·laboradors han presentat un nou

mètode per millorar l'adhesió de capes de Ni mitjançant l'ús de polsos de corrent.

Els dipòsits que resegueixen un patró i els arranjaments de nanofils han estat utilitzats per a fabricar memòries no volàtils d'alta densitat, alguns exemples són les nanoestructures de  $\text{Ag}_2\text{Se}$  obtingudes per Ann i col·laboradors i els arranjaments de nanofils de  $\text{Ni}_x\text{Pb}_{1-x}$  fabricats per Ji i col·laboradors i de nanofils de Co-Cu preparats per Lin i col·laboradors.

L'electrodeposició de capes múltiples que mostren magnetoresistència gegant (GMR) similar a la que sol obtenir-se per mètodes físics han permès utilitzar l'electroquímica per a la preparació de dispositiu d'espíntrònica. La majoria dels estudis sobre multicapes electrodepositades per obtenir GMR s'han dut a terme sobre mostres preparades per tècniques de doble pols a partir d'un sol bany que contenia tant les espècies magnètiques com les no magnètiques. En els últims 15 anys s'ha realitzat una alta activitat de recerca sobre multicapes electrodepositades amb comportament GMR. Una prova d'aquesta investigació és l'elevat nombre de papers que hi ha hagut sobre el tema i l'àmplia gamma de multicapes estudiades: CoCu/Cu, NiCu/Cu, CoAg/Ag, CoAu/Au, CoRu/Ru, CoNiCu/Cu, FeNiCu/Cu, FeCoCu/Cu, Co(Cu)Zn/Cu i FeCoNiCu/Cu.

D'altra banda, s'ha aconseguit la preparació electroquímica de *composites* magnètics. L'interès de la preparació d'aquests *composites* rau en la millora de certes propietats, com ara la resistència mecànica, la protecció contra la corrosió, l'hidrofòbia, una major duresa o produir canvis en el magnetisme. En el nostre grup s'ha estudiat la preparació de *composites* que consistien en nanopartícules magnètiques incrustades en una matriu

metàl·lica dúctil. Pané i col·laboradors han preparat un *composite* de micropartícules de ferrita de bari atrapades en una matriu electrodepositada de CoNi i Roldan i col·laboradors han estudiat pel·lícules compostes de partícules magnètiques en una matriu de coure.

Avui en dia, les tècniques electroquímiques han estat integrades en els sistemes de micro-anàlisi total ( $\mu$ -TAS) per a assajos bioquímics. Es tracta d'un mètode simple, ràpid, barat, específic i sensible i que consumeix poca potència, característiques que fan que l'electroquímica sigui adequada per ser utilitzada com a mètode de detecció. S'ha realitzat la fabricació de microxips que combinen múltiples estratègies de detecció, una d'elles l'electroquímica. Lapos i col·laboradors han presentat un microxip que combinava l'electroforesi amperomètrica i la fluorescència com a mètodes de detecció. També s'han descrits xips que combinaven tant la fluorescència o la detecció de conductivitat sense contacte amb la detecció electroquímica o l'electroquimioluminiscència en un sol microxip. No obstant això, aquesta no és l'única aplicació de l'electroquímica en assaigs bioquímics, s'han emprat microelèctrodes en els xips de microfluidica i altres microdispositius per a la manipulació elèctrica de fluids i analits bioquímics com ara ADN, proteïnes, cèl·lules, microorganismes, nanopartícules, i possiblement molècules individuals en solucions aquoses. Finalment s'han documentat la combinació de mètodes electroquímics amb substàncies biològiques receptores (anticossos, enzims, ADN, àcid nucleic, etc...) en una gran varietat de biosensors electroquímics. Però per a la realització de biosensors electroquímics no només s'han utilitzat receptors biològics, més recentment, s'han aplicat materials en la nanoescala com elèctrodes o marcadors biomoleculars en el diagnòstic de malalties i organismes infecciosos i en la

detecció d'agents nocius. Les nanopartícules també han jugat un paper crucial en biosensors electroquímics basats en nanomaterials.

Per una altra banda, les tècniques electroquímiques normalment utilitzades per realitzar l'electrodeposició de diversos materials es poden utilitzar per dur a terme estudis fonamentals de cinètica de transferència d'electrons per l'electrònica molecular. Per aquest propòsit s'han combinat elèctrodes modificats amb monocapes autoassemblades (SAM) i tècniques electroquímiques com ara la voltametria cíclica, la voltametria d'AC, la cronoamperometria i l'espectroscòpia d'impedància electroquímica.

### **Objectius:**

Aquesta tesi es centra principalment en les noves aplicacions i usos de l'electrodeposició com a eina de fabricació de nous materials que poden ser integrats en diferents tipus de dispositius com ara sensors i actuadors. L'electrodeposició presenta diversos avantatges respecte a altres tècniques, sobre tot respecte aquelles que utilitzen el buit. Especialment per la seva altra versatilitat pel que fa als materials que es poden utilitzar i a les estructures que es poden obtenir, fet que permet la seva integració en diferents processos.

Els objectius específics plantejats en aquesta tesi han estat en primer lloc el disseny, preparació i caracterització de bobines planes per fabricar biosensors inductius. Per això ha calgut escollir el bany i les condicions de treball òptims, així com els processos de fabricació més adequats a seguir per tal de preparar bobines planes de coure resistents, robustes, ben definides i adherents amb diferents relacions d'aspecte, que siguin capaces de detectar partícules magnètiques. També s'han realitzat càlculs simulant

els principals paràmetres de les bobines per millorar-ne la sensibilitat. En una etapa posterior, s'han fabricat les noves bobines dissenyades i s'han dut a terme les primeres proves de la capacitat de detecció.

En segon lloc, es va proposar la deposició d'un aliatge magnètic dur per a la seva aplicació en MEMS. L'aliatge escollit va ser el CoPt. Per tal de trobar un bany òptim per a la seva deposició s'ha dut a terme l'estudi bàsic del procés d'electrodeposició de l'aliatge. S'han preparat estructures amb diferents formes i geometries (dipòsits, pel·lícules primes, microestructures, nanopartícules, nanofilis, ...) sobre diferents substrats i s'ha estudiat la influència de les condicions d'electrodeposició sobre les propietats de l'aliatge de CoPt (morfologia, composició, estructura cristal·lina, propietats magnètiques, ...) i s'ha realitzat l'anàlisi de la relació entre aquestes propietats.

Per últim, s'ha dut a terme un estudi inicial de la formació de monocapes orgàniques sobre diferents substrats magnètics, com al primer pas per fabricar un dispositiu d'espintrònica molecular. Per aquest motiu s'han preparat pel·lícules primes de magnetita i d'aliatge CoP per mitjà de l'electrodeposició i s'ha dut a terme l'estudi de la formació de les monocapes d'octanotiol i d'àcid oleic sobre els substrats.

Aquesta tesi s'ha desenvolupat principalment en el Laboratori d'Electrodeposició i Corrosió (Electrodep) del Departament de Química Física de la Universitat de Barcelona sota la supervisió de la Dra. Elisa Vallès i la Dra. Elvira Gómez. Part d'aquesta tesi es va dur a terme en el grup de Física de Superfícies del Laboratori de Física HH Wills de la Universitat de Bristol al Regne Unit durant dos estades de tres mesos sota la supervisió del Dr.

Walther Schwarzacher.

### **Electrodeposició de bobines planes de coure per a sensors inductius:**

La possibilitat de realitzar anàlisis in situ i sobre el terreny, que permeten la detecció d'espècies tòxiques o agents patògens, com ara pesticides o antibiòtics en els aliments, és un requisit important en sectors com les indústries alimentària i farmacèutica, la biotecnologia, la salut pública i d'anàlisis clíniques. És per això que els últims anys han estat testimonis d'un creixent interès en biosensors que presenten no només una alta sensibilitat i especificitat, però també un baix cost, fàcil maneig, i portabilitat. Les tècniques d'immunoassaig es basen en el reconeixement biològic de l'analit per ser detectat per un antigen específic o un anticòs, que està vinculat a un marcador adequat amb propietats radioactives, enzimàtics o luminescent. Aquestes tècniques de detecció proporcionen una alta sensibilitat i especificitat. Durant els anys, diversos marcadors han estat utilitzats, com per exemple: marcadors radioactius en radioimmunoassaig, marcadors enzimàtics i marcadors fluorescents.

No obstant donat els desavantatges d'aquests marcadors les partícules magnètiques (MP) es presenten com una alternativa interessant als marcadors prèviament esmentats, ja que presenten una alta estabilitat, baix cost, baixa toxicitat i poden ser detectades de forma molt senzilla. Als biosensors immunomagnètics, basats en l'ús de MP, se'ls coneix amb el nom de biosensors inductius, ja que l'activitat sensora ve donada pels canvis en la inductància d'una bobina plana a causa de la presència de les MP en la mostra sota anàlisi. Tant la superfície de les MP com de la

bobina han de ser funcionalitzades amb un antigen específic per a l'anàlisi a detectar. Aquest tipus de dispositius presenta un alt potencial per al desenvolupament de sistemes amb una sensibilitat molt alta, baix cost i alta especificitat. A més, el fet de no necessitar aplicar un camp magnètic permanent quan el sensor està operant simplifica el disseny d'aquests dispositius i també permet una integració més fàcil en tot el sistema.

En treballs previs, realitzats en el departament d'Electrònica de la Universitat de Barcelona, es van fabricar bobines d'Al formades per anells concèntrics de dos nivells de 1,5 micres de gruix, tot utilitzant processos compatibles amb la tecnologia estàndard CMOS (Complementary Metal Oxide Semiconductor). No obstant això, aquestes bobines mostraven falta de correlació entre els canvis de inductància i la densitat de MP quan es comparaven amb els valors simulats. El problema es devia a una elevada resistència de la bobina que comprometia l'exactitud de les mesures de inductància. Aquest és un problema molt comú i inherent a la tecnologia planar de micro sistemes i un inconvenient important, ja que dificulta la mesura dels canvis en la inductància mitjançant els mètodes comuns basats en la mesura de la freqüència de ressonància. Per tal de minimitzar el problema de l'alta resistència intrínseca, era necessari desenvolupar tècniques fiables per la fabricació de capes metàl·liques amb gruixos de diverses micres o fins i tot superiors a 10 micres. Una alternativa interessant pel creixement d'aquestes capes és l'ús de tècniques de deposició electroquímica. L'electrodeposició és totalment compatible amb les tecnologies CMOS, sent possible realitzar la deposició a través de màscares de resina. Per tant, es va proposar la deposició electroquímica de Cu com a alternativa a l'Al. En principi, el Cu és adequat per la seva baixa resistivi-

tat, cost moderat i la facilitat per créixer electroquímicament d'una forma controlada. Donada la naturalesa del substrat, el creixement electroquímic de Cu sobre silici requereix l'ús d'una capa llavor superficial.

El treball presentat en aquest capítol descriu el disseny, fabricació i caracterització de microdispositius elèctrics d'inducció, des dels primers passos del procés de deposició a la caracterització dels biosensors. Com a pas previ a la fabricació de bobines, va ser necessari trobar un bany i optimitzar les condicions d'electrodeposició i els diferents aspectes del procés de fabricació.

En aquest sentit, es van desenvolupar banys electrolítics que contenien coure (II), àcid sulfúric i diversos additius. Per a cada bany seleccionat es van escollir les condicions de deposició a partir d'un estudi electroquímic. Per tal de trobar el bany que conduïa a unes característiques de dipòsit òptimes per a la fabricació de les bobines, es van preparar dipòsits tot utilitzant diferents banys amb quantitats variables d'electròlits i additius i es van analitzar la morfologia, l'orientació preferencial i l'estrès de cada un d'ells. Els gruixos dels dipòsits van ser controlats en funció de la càrrega de reducció. Els millors dipòsits es van obtenir a partir de solucions àcides que contenien elevades concentracions de Cu (II) i quantitats moderades de tres additius.

Un altre aspecte que va caldre tenir en compte va ser la capa llavor. Com ja s'ha comentat abans, és necessària una capa llavor per tal de fer que el substrat (Si/SiO<sub>2</sub>) sigui suficientment conductor i pugui tenir lloc el procés d'electrodeposició. Per aquesta raó, en aquest treball es van utilitzar dues capes llavor diferents: Ti/Ni i Ti/Cu. El nostre interès s'ha

centrat en l'anàlisi de l'estrès i l'adherència dels dipòsits en cada cas per tal d'assegurar que els dipòsits romanien adherits al substrat després de les diferents etapes de fabricació. Els millors resultats es van obtenir pels substrats Si/SiO<sub>2</sub>/Ti/Cu.

No obstant això, no es poden considerar finalitzades l'optimització del bany ni de la capa llavor sense corroborar els resultats provant de dipositar microestructures. Per a això, es van dipositar bobines de prova de forma quadrada sobre substrats fotolitografiats (Si/SiO<sub>2</sub>/capa llavor/màscara de resina) usant els diferents banys i les diferents capes llavor. Un cop més el gruix de les pistes es va poder controlar ajustant la càrrega de deposició. Un cop obtingudes les bobines, es van eliminar tant la màscara de resina com la capa llavor, cal que la capa llavor sigui eliminada per tal d'evitar el curtcircuit de les bobines. Es van provar dos tipus d'atacs (plasma i químic) per a cada capa, però els millors resultats es van observar amb l'atac químic.

Una de les raons per a fer servir coure per fabricar les bobines era reduir les altes resistències en sèrie inherents a la tecnologia planar. Per tal de comprovar si s'havia aconseguit reduir aquesta resistència, es van caracteritzar elèctricament de les bobines de prova i es van comparar els valors amb els d'Al. Els valors de la resistència elèctrica de les bobines electrodepositades de Cu van ser significativament més baixos que els obtinguts a partir de les bobines d'Al fabricades utilitzant els processos estàndard de la tecnologia de silici. Això va demostrar que l'electrodeposició del Cu és una bona alternativa als materials i a les tècniques utilitzades anteriorment per a la fabricació de les bobines i obre la possibilitat de dissenyar i desenvolupar biosensors inductius.

L'estudi bàsic es va realitzar en una cel·la electroquímica de 250 ml utilitzant peces petites (1x2 cm<sup>2</sup>) com a substrats i un espiral de platí com contraelèctrode. Com que l'objectiu final del treball era fer servir aquestes bobines en el procés de fabricació d'un biosensor, es va procedir a l'escalat del procés. Va ser possible escalar el procés i obtenir bobines amb una bona definició de les parets i que resseguien perfectament els motlles de la foto-resina.

Un segon objectiu era l'obtenció de les bobines sobre substrats flexibles, econòmics i d'un sol ús, que permetien fabricar un biosensor per a ser utilitzat en anàlisi de camp. El bany i els resultats anteriorment optimitzats van ser un bon punt de partida per posar a prova la viabilitat de la proposta. Els plàstics escollits inicialment van ser: PEEK, PEN, PMMA, PS, Tefló i Kapton. En aquest cas també va ser necessària una capa llavor per a realitzar el procés d'electrodeposició. L'anàlisi de la morfologia, estructura i l'estrès dels dipòsits obtinguts sobre els diferents substrats va determinar que el PEN era el millor candidat per a la fabricació de biosensors.

Finalment, es va proposar un nou disseny de bobina a partir de les simulacions de les condicions necessàries per a aconseguir una resistència elèctrica mínima i una màxima sensibilitat. Segons les simulacions, la màxima sensibilitat i la linealitat del circuit s'aconseguien treballant a prop de la freqüència de ressonància ( $f_p$ ), per tant es va haver de tenir en compte que la forma i la posició del pic de ressonància depenen dels paràmetres elèctrics del circuit A.3:

$$f_p = \left(\frac{f_o}{\sqrt{2}}\right) \left(1 + \sqrt{1 + \frac{1}{2} \left(\frac{R}{f_o \Pi L}\right)^2}\right)^{\frac{1}{2}} \quad (\text{A.3})$$

On  $f_o = \omega_o/2\Pi$  és la freqüència natural del circuit, R la resistència intrínseca de la bobina i  $\omega_o$  és la freqüència harmònica  $= (1/LC)^{1/2}$ , on L és la inductància i C la capacitat. La forma del pic de ressonància ve determinada pel factor Q, un factor Q elevat porta a un pic de ressonància estret i intens. El factor de qualitat està determinada per A.4:

$$Q = \left(\frac{L\omega_o}{R}\right) \quad (\text{A.4})$$

Per tant, la disminució de la capacitat i la resistència fan augmentar el factor de qualitat. No obstant, això implica també un increment en la fp, que pot prendre valors fora del rang de mesura dels dispositius comuns. Per aquesta raó, es van realitzar simulacions de la resistència en sèrie intrínseca, del factor de qualitat i de les freqüències de ressonància. D'acord amb els resultats de les simulacions, es van triar les diferents dimensions de la bobina per tal d'assolir el millor compromís entre un valor de inductància alta, un factor de qualitat alt i freqüències de treball raonables.

Usant la nova màscara amb el disseny optimitzat, es van ajustar les condicions d'electrodeposició per preparar bobines de prop de 15 micres de gruix, amb una bona definició de les pistes. Després de la preparació de les bobines, es van eliminar la resina i les capes llavor i es va procedir a la caracterització elèctrica de les bobines. Les mesures mostraven baixes resistències elèctriques que eren en bona concordança amb els valors òptims simulats.

Es va analitzar la viabilitat de les bobines de coure per al seu ús com a biosensors en una configuració de circuit de filtre de segon ordre diferencial

que treballa en condicions pròximes a la ressonància. Tant els valors de la inductància com els valors de la freqüència de ressonància obtinguts a partir de les bobines preparades concorden amb els valors de la simulació i presenten una baixa desviació estàndard.

Es va realitzar una caracterització preliminar de la capacitat de detecció del dispositiu mitjançant l'ús de pols de ferro neodimi bor. Les bobines es van recobrir amb un vernís de base acrílica per aïllar-les abans de la caracterització amb la pols, ja que aquesta pot causar el curtcircuit de les bobines. Els resultats van revelar un canvi en la freqüència de ressonància, el que va permetre detectar la presència de la pols magnètica. Es van realitzar simulacions addicionals per estudiar els efectes de les dimensions de la bobina i la densitat de pistes, per seguir millorant el disseny en un futur treball. Aquests dispositius van demostrar un gran potencial per aplicacions immunomagnètiques.

### **Estudi del procés d'electrodeposició de l'aliatge binari CoPt i ternari CoPtP:**

Els sistemes microelectromecànics (MEMS) són la integració d'elements mecànics, sensors, actuadors i electrònics en un substrat, generalment de silici, a través de la tecnologia de microfabricació. Algunes de les aplicacions comercials dels MEMS inclouen: impressores d'injecció de tinta, acceleròmetres en dispositius electrònics, telèfons mòbils i càmeres digitals, micròfons en dispositius portàtils, sensors de pressió dels pneumàtics en automòbils, sensors de pressió de la sang, commutació òptica, aplicacions Bio-MEMS, acceleració de fluids, micro-refrigeració, etc...

Un actuator és un dispositiu que utilitza una força per moure o contro-

lar un mecanisme o sistema per tal de generar un efecte en un procés automatitzat. Pot operar amb diferents fonts d'energia: elèctrica, hidràulica, o magnètica. Per tal d'utilitzar camps magnètics per operar el mecanisme cal utilitzar sistemes d'imants. No obstant això, la col·locació d'un imant permanent en un microactuator no és fàcil. Per aquesta raó, recentment hi ha hagut un interès creixent en la miniaturització dels materials magnètics durs i en la seva integració en MEMS perquè aquest fet permetria millorar l'eficiència d'aquests dispositius.

Els mètodes electroquímics es poden utilitzar per preparar materials magnètics compatibles amb el processament de MEMS. L'electrodeposició és completament compatible amb els processos de microfabricació i s'ha utilitzat per preparar diversos dipòsits de micres de gruix de metalls, aliatges i compostos sobre diversos substrats.

Encara que la majoria dels microactuadores magnètics desenvolupats utilitzen materials magnètics tous, els materials magnètics durs també són útils en algunes aplicacions (motors, minibombes, microactuadors). La preparació de dipòsits magnètics durs per mitjà de tècniques electroquímiques, que són diferents de les normalment utilitzades en actuadors magnètics, és un repte. Un exemple de l'intent de preparar capes magnètiques dures és la incorporació de partícules ferromagnètiques en una matriu d'aliatge CoNi mitjançant electrodeposició. Els materials magnètics durs més comuns són CoPt, FePt, i terres rares com  $\text{Nd}_2\text{Fe}_{14}\text{B}$  o  $\text{SmCo}_5$ , però, la codeposició de capes primes magnètiques de terres rares implica l'ús de dissolvents orgànics i l'aplicació de potencials molt negatius. S'han depositat aliatges de base Co com: CoNiP, CoFePt, CoPt o CoPtP, donant com a resultat capes de baixa coercitivitat. Per obtenir materials

magnètics durs es necessari obtenir estructures cristal·lines, sovint ordenades, que presentin anisotropia. Generalment es necessària una etapa de recuit posterior a l'electrodeposició per tal d'obtenir un canvi en la fase cristal·lina que doni la desitjada resposta magnètica.

L'objectiu d'aquest treball és estudiar el procés d'electrodeposició dels sistemes CoPt i CoPtP amb la finalitat de controlar la preparació de capes binaries o ternaries sobre sustrats de silici/capa llavor per tal de modular-ne les propietats magnètiques.

En aquest sentit, es van seleccionar solucions que contenen  $\text{CoCl}_2$ ,  $\text{Na}_2\text{PtCl}_6$ ,  $\text{NaH}_2\text{PO}_2$ ,  $\text{H}_3\text{BO}_3$  i  $\text{NH}_4\text{Cl}$ . Es van estudiar sobre carboni vitri els processos de reducció de cada metall, així com de la solució blanc per separat. El procés de reducció del platí es produeix a potencials més positius que el de cobalt, quan es dipositen ambdós metalls simultàniament l'inici de la reducció de cobalt s'avança a causa de que el platí prèviament dipositat facilita la nucleació del cobalt.

Un efecte semblant es va observar al afegir quantitats moderades de hipofosfit en el bany, el que revela que la incorporació de P en les primeres etapes de la deposició catalitza la reducció de Co. El P s'incorpora a l'aliatge, ja que es atrapat en la cel·la cristal·lina mentre la deposició es duu a terme. A causa de la presència de platí a l'aliatge es va observar una evolució d'hidrogen significativa. No obstant això, aquest procés té lloc a potencials més negatius de l'inici de la codeposició d'ambdós metalls per tant va ser possible obtenir l'aliatge.

Es van realitzar estudis de la deposició de l'aliatge sobre un substrat de Si/Ti/Ni i es van obtenir dipòsits de CoPtP potenciostàticament amb un

baix contingut de fòsfor (0,5-6 wt. %) i diferents wt. % de Pt, així com alguns dipòsits de CoPt. Es va analitzar la influència de les condicions de deposició (potencial aplicat, composició del bany, pH, temperatura, càrrega) sobre l'estructura, composició i la coercitivitat de les capes magnètiques.

Les diferències en la quantitat de platí van revelar canvis significatius en l'estructura dels dipòsits i conseqüentment en la seva coercitivitat. Es van obtenir dipòsits de CoPt i CoPtP amb diferents propietats magnètiques des de tou a dur. També es van estudiar l'efecte de recuit però no es van observar diferències significatives abans i després del tractament tèrmic, probablement perquè no es va aplicar suficient temperatura.

En un segon treball, es va estudiar més àmpliament l'efecte de la incorporació de P en el dipòsit. Es van utilitzar tant tècniques galvanostàtiques com potencioestàtiques per obtenir capes de CoPt riques en platí, per tal d'obtenir capes magnètiques dures dipositades sobre substrats de silici/capa llavor sense la necessitat d'un recuit posterior de les capes dipositades. Els resultats indiquen que són necessaris alts percentatges de Pt per tal de millorar l'anisotropia magnètica de la fase de cobalt. Es van analitzar les diferents condicions de deposició per tal d'obtenir capes amb una composició i estructura optimitzada per tal d'obtenir la màxima coercitivitat, màxima permeabilitat i bona resistència a la corrosió, propietats desitjables per al seu ús en microdispositius magnètics.

Es van realitzar estudis de la influència de la incorporació de P en les propietats magnètiques, estructurals, morfològiques i en la resistència a la corrosió dels electrodeposits de CoPt, també es van analitzar els canvis

en el procés de deposició i en la velocitat de deposició. L'eficiència del procés en tots dos casos va ser calculada comparant la càrrega teòrica i l'experimental. Per al càlcul la càrrega experimental, es van utilitzar les dimensions del dipòsit i la seva densitat. Els resultats van revelar que hi havia una dependència significativa de l'eficiència segons el substrat utilitzat. La densitat es va poder estimar a partir de la fase cristal·lina i la posició dels pics enregistrats en els difractogrames de raigs X.

Aquests estudis van demostrar la possibilitat de preparar imants que podien ser integrats directament en els dispositius amb substrats de silici.

### **Electrodeposició de micro o nanoestructures de CoPt. Modulació de les propietats magnètiques:**

En els últims anys l'estudi de sistemes magnètics nanoestructurats ha suscitat un gran interès per les seves propietats físiques i químiques i les seves aplicacions tecnològiques. Aquests sistemes poden ser utilitzats com a suports per a la gravació magnètica d'alta densitat o incorporar-se a microdispositius. Un dels punts principals en l'estudi d'aquests sistemes és com canvien les propietats magnètiques en funció de la seva forma i mida. És evident que, pel desenvolupament de dispositius magnètics basats en matrius de nanoestructures, cal estudiar les propietats de les nanoestructures magnètiques, el seu comportament magnètic quan es troben formant part d'una matriu.

Els sistemes més estudiats han estat les nanopartícules i els arranjaments de nanofils. Diferents tècniques han estat utilitzades per a la seva fabricació, una d'aquestes tècniques ha estat l'electrodeposició. Els mètodes electroquímics es poden utilitzar per a preparar imants permanents de

nivell nanomètric per al seu ús en dispositius micro.

Tenint en compte els avantatges i desavantatges d'ambdós sistemes estudiats fins ara (CoPt i CoPtP), la resta de l'estudi es va realitzar amb l'aliatge de CoPt ja que presentava una resposta més ràpida al camp magnètic aplicat i major energia magnètica encara que la resistència a la corrosió i la coercitivitat fossin una mica menors que pel CoPtP. No obstant, aquest últim inconvenient es podia compensar preparant capes amb majors percentatges de Pt i el CoPt és un sistema més senzill. L'electrodeposició de l'aliatge de CoPt es va dur a terme a partir d'un bany que contenia:  $2,5 \cdot 10^{-3} \text{ M CoCl}_2 + 1,2 \cdot 10^{-3} \text{ M Na}_2\text{PtCl}_6 + 1 \text{ M NH}_4\text{Cl} + 30 \text{ g dm}^{-3} \text{ H}_3\text{BO}_3$  a pH 4,5 i es va estudiar la dependència de les propietats magnètiques amb la composició. La major coercitivitat es va obtenir en els dipòsits amb estructura hcp amb alt percentatge de platí.

Es van obtenir diferents micro/nanoestructures riques en platí de l'aliatge de CoPt. La dificultat de preparar estructures ben definides depèn de les dimensions del patró (si s'utilitza) i les característiques del bany electrolític. En la literatura es va trobar que utilitzant banys que contenien citrat es podia millorar la coercitivitat dels dipòsits, per això, es van preparar alguns dipòsits afegint un cert percentatge de citrat al bany, però en el nostre cas no es van detectar diferències significatives. Per a cada tipus d'estructura, es va seleccionar l'electrode adequat no magnètic que permetia simultàniament l'electrodeposició de l'aliatge i la mesura de les propietats magnètiques. En alguns casos es van utilitzar màscares de fotolitografia o membranes de policarbonat i d'alúmina, ja que aquestes permetien el control tant de la separació entre les nanoestructures com de la seva relació d'aspecte.

Les micro/nanoestructures preparades van ser:

- Microestructures amb forma de quadrats i de línies
- Nanocables de diferent longitud i amplada i diferent separació entre ells
- Partícules submicromètriques
- Capes primes
- Partícules nucli-escorça

El substrat seleccionat per la fabricació de capes primes va ser vidre/ITO. Com no es tracta d'un substrat molt conductor va caldre aplicar potencials de reducció alts per tal d'induir la formació de nuclis significatius. La baixa conductivitat del substrat va permetre obtenir capes primes en lloc de gruixudes ja que la velocitat de deposició va ser prou petita.

Per obtenir microestructures amb forma de quadrats i de ratlles es va utilitzar una màscara fotolitografiada de 1,2 micres de gruix sobre un substrat de ITO. Encara que en alguns casos la presència d'una resina pot dificultar el procés de deposició, en aquest cas els potencials utilitzats van ser similars al de la preparació de capes primes, ja que els patrons definits en la màscara eren prou grans per permetre l'arribada de les espècies electroactives.

Els nanofils es van obtenir mitjançant l'ús de membranes tant de policarbonat com d'alúmina sputteritzades per una cara amb Au per fer-les conductores. Encara que el moviment de les espècies electroactives en els canals porosos és normalment difícil, en el nostre cas, la presència de la

capa llavor conductora d'or i la mida del porus va fer que l'inici del procés de deposició fos fàcil. A causa de que la membrana d'alúmina comercial presentava una major hidrofobicitat va ser necessari aplicar un potencial més negatiu en aquestes membranes, per tal d'assolir un corrent de reducció similar a les de policarbonat i afavorir el flux de ions a través de la membrana.

Finalment, es van utilitzar elèctrodes de grafit i de silici per la preparació de partícules submicromètriques. El substrat de silici es va submergir en un 5% (p/v) de una solució de HF durant 60 s per tal d'eliminar l'òxid de silici natiu abans de l'electrodeposició. En el cas del grafit es va poder utilitzar un potencial menys negatiu, encara que aquests potencials no van ser tan alts com en el cas dels substrats de ITO perquè per tal d'obtenir partícules es desitjable una velocitat de nucleació baixa.

En tots els casos es va estudiar la morfologia, la composició i la fase cristal·lina. A causa de la mida de les estructures i l'alta proporció d'àtoms en la seva superfície, aquestes estructures poden ser susceptibles a ser oxidades, per aquesta raó es van realitzar proves de resistència a la corrosió revelant una bona resistència a l'oxidació en tots els casos. Les propietats magnètiques van ser analitzades i comparades.

Un altre sistema interessant són les partícules nucli-closca en les que un material central està envoltat d'un material diferent. El material extern pot actuar com a material de protecció o aportar noves propietats al material del nucli. En particular, les nanopartícules magnètiques han estat àmpliament preparades a partir de diferents tècniques per actuar com a nucli magnètic de les nucli-closca, per tal d'aprofitar el canvi de les propietats

del material ferromagnètic quan la seva mida disminueix. El caràcter protector de la closca és especialment important quan el nucli ferromagnètic és inestable pel que fa a l'oxidació amb l'aire, fet que es produeix més fàcilment a mesura que la mida es redueix. A mesura que la mida es va reduint, el comportament s'acosta al paramagnetisme. Per això, en algunes ocasions és interessant estudiar partícules amb nucli i closca de dimensions intermèdies (centenars de nanòmetres) per que les propietats magnètiques que presenten són molt diferents respecte a les de nanopartícules o el material *bulk* del mateix sistema. Per exemple, quan dos materials magnètics tou i dur es posen contacte, aquests sistemes poden combinar la alta magnetització de la fase tova amb la alta coercitivitat de la fase dura per tant d'assolir un producte de màxima energia magnètica. L'estudi d'aquests tipus de sistemes que combinen ferromagnetos tous i durs no ha evolucionat significativament a causa de la falta de mètodes de fabricació eficaços i és per això que vam considerar la seva preparació.

En aquesta línia, partícules del tipus nucli-closca, amb un nucli de l'aliatge de CoPt en dimensions intermèdies (100-500 nm) (resposta magnètica semidura) i una closca de CoNi (aliatge magnèticament tou) de gruix controlable van ser preparades amb mètodes electroquímics. El dipòsit de la closca es va preparar utilitzant un bany de: 0,2 M  $\text{CoCl}_2$  + 0,9 M  $\text{NiCl}_2$  +  $30 \text{ g dm}^{-3}$   $\text{H}_3\text{BO}_3$  +  $0,7 \text{ g dm}^{-3}$  sacarina, pH = 3, sobre un substrat de silici. La baixa conductivitat d'aquest substrat comparada amb els substrats metàl·lics o de carboni, afavoreix una velocitat de nucleació més baixa i per tant, la formació de partícules en lloc de capes contínues i permet el recobriment de les partícules del nucli del primer aliatge (CoPt) amb un segon aliatge (CoNi), evitant la seva deposició sobre el substrat.

Es va realitzar l'anàlisi de la variació de les propietats magnètiques de l'estructura global en funció del gruix del dipòsit de la closca. El comportament no magnètic del substrat va permetre la detecció de la resposta magnètica de les partícules preparades sobre ell.

### **La formació de monocapes orgàniques electrodepositades sobre materials magnètics com un primer pas per la fabricació de les vàlvules d'espíntrònica:**

L'espíntrònica és una disciplina emergent, basada en l'explotació de l'espín dels electrons i del seu moment magnètic associat per a la fabricació de dispositius d'estat sòlid, tals com vàlvules d'espín, espín-transistors o díodes. La espíntrònica podria tenir diversos avantatges sobre l'electrònica convencional, en què es manipula només la càrrega dels electrons, que són: més compactat, robustesa i baix consum d'energia. A més, el fet que els sistemes espíntrònics explotin l'espín de l'electró pot ser utilitzat per codificar informació que persisteixi quan els dispositius estiguin apagats. Aquests espíns poden ser manipulats amb i sense l'ús de camps magnètics i l'ús de poca energia.

En concret, les vàlvules d'espín tenen un enorme potencial com a memòries volàtils no magnètiques, caps de lectura de discs durs, sensors magnètics i transistors d'espín. Consisteixen en dues capes de material magnètic, separades per un no magnètic (Co/Cu/NiFe, CoFe/Cu/Co, CoFeB/MgO/Co/FeB, Fe/Al<sub>2</sub>O<sub>3</sub>/Fe, NiFe/Cu/Co, NiFe/Cu/NiFe, NiFe/Au/Co, NiFe/Cu/CoPt). Aquests dispositius presenten magnetoresistència (MR), un fenomen que consisteix en la dependència de la resistència elèctrica amb l'espín dels electrons i pot ser controlada per camps magnètics externs. De-

penent del material entremig es parla de magnetoresistència gegant (GMR) o magnetoresistència túnel (TMR).

No obstant això, per a que la revolució de l'espíntrònica pugui tenir lloc, és imprescindible trobar la manera d'injectar, manipular i detectar l'espín dels electrons en els dispositius. La manipulació dels espins és, en teoria, relativament simple, però la seva injecció i detecció és extremadament difícil. Hi ha diferents factors que juguen un paper crucial en la injecció dels espín polaritzats, com ara: la polarització de l'espín en el nivell de Fermi del material ferromagnètic i el material espaiador. En aquesta línia s'han descrit diferents materials separadors. Al principi, els metalls (Cu, Ag, Au) van ser els més utilitzats per a aquestes aplicacions, però, més recentment, s'han comenat a estudiar alternatives com semiconductors (ZnO, MgO) i materials orgànics. S'ha trobat que l'ús de materials orgànics en lloc d'inorgànics millora el fenomen de la magnetoresistència. Per tal d'observar magnetoresistència és important que la informació de l'espín sobrevisqui al ser transportada a llarga de la distància que separa els dos materials magnètics, en cas contrari les configuracions ferro i anti-ferro no mostren cap diferència en la resistència. Les molècules orgàniques estan fetes d'àtoms molt lleugers que presenten interaccions espín-òrbita molt febles que permeten una vida llarga de l'espín. D'altra banda, un fet encara més important és l'existència d'una interfície "neta". Quan s'utilitzen materials inorgànics normalment es produeix una capa intermitja de difusió d'un material en l'altre, a part d'altres problemes no desitjats com ara la falta d'homogeneïtat en el gruix i la rugositat de les capes. Tots aquests problemes poden induir a l'espín a perdre la seva polarització, fet que obstaculitza seriosament la injecció d'espín polaritzats.

Els materials orgànics, com ara les monocapes autoensamblades (SAMs), ofereixen la possibilitat d'evitar tots aquests problemes. És per això que la interfície entre materials inorgànics amb un alt nivell de polarització d'espín i SAM (monocapes autoensamblades) és una bona opció per desenvolupar dispositius anomenats d'espíntrònica molecular.

D'acord amb aquests resultats, per tal de millorar els dispositius espíntrònics, s'han dut a terme estudis per optimitzar tant les capes magnètiques com els materials orgànics a dipositar entre ells. Pel que fa a les capes magnètiques, alguns materials electrodepositats ja han estat testats per a aplicacions d'espíntrònica.

També s'ha estudiat la formació de monocapes sobre substrats magnètics per tal de ser utilitzades com components no magnètics dels dispositius d'espíntrònica. El mètode utilitzat per obtenir les monocapes va ser l'autoensamblatge molecular (SAM), ja que és un mètode molt eficaç i àmpliament utilitzat per a la formació de monocapes moleculars sobre la superfície de metalls. És un mètode molt fàcil d'utilitzar i que permet obtenir monocapes homogènies amb un alt grau d'ordenament molecular intern. Un dels exemples més estudiats en autoensamblatge molecular ha estat típicament la formació de monocapes d'alcanotriols sobre substrats de metalls nobles com ara l'or, ja que el sofre del grup final presenta una elevada afinitat per l'or i es poden formar denses monocapes altament cristal·lines. Aquestes monocapes han estat ben caracteritzades mitjançant tècniques com la espectroscòpia infraroja, microscòpia d'efecte túnel i la fotoespectroscòpia de raigs X. Tot i que han estat menys estudiades, també hi ha alguns exemples de SAM en altres materials.

En aquesta línia, el treball presentat en aquest capítol descriu la preparació de capes magnètiques mitjançant l'electroquímica i la formació sobre aquestes capes magnètiques de monocapes orgàniques com la base de les vàlvules d'espíntrònica. Amb aquest fi es van seleccionar dos substrats diferents com a capa magnètica: magnetita i CoP. Es van preparar capes d'aquests materials de baixa rugositat i sobre ells es van formar monocapes de compostos orgànics.

La deposició de monocapa sobre magnetita ( $\text{Fe}_3\text{O}_4$ ) és un exemple particularment prometedor per aplicacions d'espíntrònica, ja que aquesta presenta ferrimagnetisme, i els càlculs prediuen una polarització d'espín completa en el nivell de Fermi. A més, és senzill aplicar el mètode d'autoensamblatge pel fet que no s'oxida en aire a temperatura ambient.

En primer lloc, es van electrodepositar capes de magnetita de diferents gruixos utilitzant el mètode proposat per Switzer i col·laboradors. Es va estudiar la influència de la velocitat de deposició en la rugositat i la morfologia dels dipòsits. Es van analitzar l'estructura cristal·lina i les propietats magnètiques de les capes per difracció de raigs-X (DRX) i magnetometria SQUID, respectivament, per tal de corroborar la formació de magnetita pura i analitzar les propietats magnètiques de les capes. Una vegada es van obtenir els dipòsits es va dur a terme la formació de les monocapes. Per tal d'estudiar la monocapa obtinguda es van enregistrar les respostes voltamètriques en una solució blanc tant de la magnetita pura com de la magnetita recoberta amb una monocapa i es van comparar. Per complementar els estudis anteriors es van realitzar mesures d'angle de contacte de l'aigua. Finalment, es va utilitzar l'espectroscòpia de raigs X (XPS) per corroborar la formació de les monocapes.

S'ha demostrat que a partir de mètodes electroquímics es poden produir capes primes de magnetita amb un bon control sobre la puresa, però, de vegades, si les condicions d'electrodeposició no són les correctes, es produeix la codeposició d'altres òxids de ferro. És per això que es van realitzar mesures d'espectroscòpia Raman en algunes de les capes de magnetita, per assegurar la puresa dels nostres dipòsits. Els resultats van confirmar que es tractava de capes de magnetita d'alta puresa.

En un altre estudi, es va utilitzar CoP com a substrat magnètic per depositar les monocapes orgàniques. El CoP és un aliatge interessant per ser utilitzat en dispositius d'espíntrònica a causa de les seves propietats magnètiques i perquè és possible obtenir capes primes molt llises, la qual cosa és important per obtenir monocapes amb un alt ordre i una baixa densitat de defectes. No obstant això, la funcionalització amb monocapes pel mètode de l'autoensamblatge en condicions ambientals és molt menys directa sobre l'aliatge de CoP, perquè té més tendència que l'or o la magnetita a oxidar-se. Sovint s'utilitza ultra alt buit (UHV) per tal d'evitar problemes relacionats amb l'oxidació de la superfície, no obstant no és un mètode convencional d'autoensamblatge. Per utilitzar l'autoensamblatge en dissolució per a la formació de monocapes en aquests dipòsits cal superar els problemes que causa l'oxidació de la superfície.

Per aquesta raó, en aquest treball es va provar un mètode electroquímic per a la formació in situ d'una capa d'octanotiol a partir d'una solució àcida de sulfat de sodi. En primer lloc, es van preparar i caracteritzar dipòsits de CoP. Un cop obtinguts els dipòsits, es va procedir a l'adsorció de les monocapes d'octanotiol mitjançant l'addició in situ d'una solució d'etanol de la molècula orgànica en l'electròlit suport. Finalment es va

analitzar la formació i la purificació de les capes mitjançant voltamperometries cícliques i una balança electroquímica de cristall de quars. Es van realitzar mesures de l'angle de contacte i de XPS per corroborar la formació de les monocapes.

### **Conclusions finals:**

- S'ha demostrat que l'electrodeposició és una tècnica útil per al disseny i la fabricació de micro/nanomaterials amb propietats específiques que els permeten ser implementats en biosensors, MEMS i dispositius d'espíntrònica. Per tant, es pot afirmar que l'electroquímica és una tècnica versàtil que pot ser utilitzada en noves aplicacions com ara la preparació de sensors i actuadors.
- S'han dissenyat, obtingut i caracteritzat bobines planes de coure per ser implementades en un biosensor inductiu. Per aquesta raó, ha estat necessari realitzar simulacions de la resistència i la inductància de les bobines. S'ha trobat un bany òptim, així com les condicions d'electrodeposició i els processos de fabricacions per l'obtenció de bobines de coure amb baix estrès i bona adherència, de diverses micres de gruix, amb el nombre adequat de voltes i amplada de pista. Com a primer test de la capacitat de detecció de les bobines s'ha mesurat la variació de la seva freqüència de ressonància al col·locar-hi partícules magnètiques a la part superior.
- S'ha dut a terme la deposició d'un aliatge magnètic dur de CoPt per a la seva aplicació en MEMS. L'estudi bàsic del procés d'electrodeposició de l'aliatge de CoPt ha permès optimitzar el bany i trobar les condicions adequades d'electrodeposició. Basant-se en els resultats anteri-

ors, ha estat possible obtenir capes primes de CoPt, microestructures, nanopartícules, nanofil·ls i CoPt@CoNi a partir de diferents substrats. Per a cadascuna de les formes de les micro / nanoestructures s'ha estudiat l'influència de les condicions d'electrodeposició/preparació en les propietats de l'aliatge de CoPt (morfologia, composició, estructura cristal·lina, propietats magnètiques, etc...).

- Com a primer pas per a fabricar un dispositiu d'espíntrònica molecular, s'han preparat capes fines magnètiques de magnetita i CoP amb una baixa rugositat mitjançant l'electrodeposició. Sobre aquestes capes ha estat possible la formació de monocapes orgàniques. La formació de les monocapes s'ha estudiat mitjançant l'ús de mesures d'angle de contacte, voltamperometries cícliques i XPS.

# Bibliography

- [1] P. RIPKA, S. KAWAHITO, S. CHOI, A. TIPEK and M. ISHIDA. *Micro-fluxgate sensor with closed core*. *Sensor. Actuat. A-Phys.* **91**, 65–69 (2001).
- [2] J. PRIETO, P. SANCHEZ, C. AROCA, E. LOPEZ, M. SANCHEZ, O. DE ABRIL and L. PEREZ. *Improving the characteristics in magnetostrictive-piezoelectric sensors when the viscous interface is removed*. *Sensor. Actuat. A-Phys.* **84 (3)**, 338–341 (2000).
- [3] A. T. KUHN, editor. *Industrial electrochemical processes*. Elsevier (Amsterdam 1971).
- [4] J. O. BOCKRIS, B. E. CONWAY, E. YEAGER and R. E. WHITE. *Comprehensive treatise of electrochemistry*. VCH Weinheim (New York 1981).
- [5] A. R. BURKIN, editor. *Production of aluminum and alumina, critical reports on applied chemistry*. Wiley (Chichester 1987).
- [6] C. M. A. BRETT and A. M. OLIVEIRA-BRETT. *Electrochemistry. Principles, methods and applications*. Oxford University Press (Oxford 1993).
- [7] S. BIALLOZOR and A. KUPNIEWSKA. *Conducting polymers electrodeposited on active metals*. *Synthetic Met.* **155**, 443–449 (2005).
- [8] C. LI and G. SHI. *Synthesis and electrochemical applications of the composites of conducting polymers and chemically converted graphene*. *Electrochim. Acta* **56**, 10737–10743 (2011).
- [9] C. ROSS. *Electrodeposited Multilayer Thin Films*. *Annu. Rev. Mater. Sci* **24**, 159–188 (1994).
- [10] E. GOMEZ, E. PELLICER and E. VALLES. *Electrochemical Behavior of NiMo Electrocatalyst for Water Electrolysis*. *Electrochem. Commun.* **7(3)**, 275–281 (2005).
- [11] S. ARMYANOV. *Crystallographic structure and magnetic properties of electrodeposited cobalt and cobalt alloys*. *Electrochim. Acta* **45 (20)**, 3323–3335 (2000).

- [12] E. TOTH-KADAR, L. PETER, T. BECSEI, J. TOTH, L. POGANY, T. TARNOCZI, P. KAMASA, G. LANG, A. CZIRAKI and W. SCHWARZACHER. *Preparation and Magnetoresistance Characteristics of Electrodeposited Ni -Cu Alloys and Ni-Cu/Cu Multilayers*. J. Electrochem. Soc. **147**, 3311–3318 (2000 (9)).
- [13] Y. HAYASHI, S. KASHIWABARA and Y. JYOKO. *Preparation and characterization of electrodeposited metallic multilayers*. Physica B **239 (1-2)**, 35–40 (1997).
- [14] C. ROSS, M. HWANG, M. SHIMA, H. SMITH, M. FARHOUD, T. SAVAS, W. SCHWARZACHER, J. PARROCHON, W. ESCOFFIER, H. BERTRAM, F. HUMPHREY and M. REDJDAL. *Magnetic properties of arrays of electrodeposited nanowires*. J. Magn. Mater. **249**, 200–207 (2002).
- [15] F. XIAO, C. HANGARTER, B. YOO, Y. RHEEM, K.-H. LEE and N. V. MYUNG. *Recent progress in electrodeposition of thermoelectric thin films and nanostructures*. Electrochim. Acta **53**, 8103–8117 (2008).
- [16] A. D. PAOLA, E. GARCIA-LOPEZ, G. MARCI and L. PALMISANO. *A survey of photocatalytic materials for environmental remediation*. J. Hazardous Mat. **211-212**, 3–29 (2012).
- [17] S. LEITH and D. SCHWARTZ. *High-Rate through-Mold Electrodeposition of Thick ( $\geq 200$  microm) NiFe MEMS Components with Uniform Composition*. J. Microelectromech. S. **8(4)**, 384–392 (1999).
- [18] N. MYUNG, D. PARK, M. SCHWARTZ, K. NOBE, H. YANG, C. YANG and J. JUDY. *Electrodeposited hard magnetic thin films for MEMS applications*. Proc. Electrochem. Soc. **PV 2000-29**, 506–521 (2000).
- [19] S. GUAN and B. NELSON. *Pulse reverse electrodeposited nanograined CoNiP thin films and microarrays for MEMS actuators*. J. Electrochem. Soc. **152**, C190–C195 (2005).
- [20] S. KULKARNI and S. ROY. *Deposition of thick Co-rich CoPtP films with high energy product for magnetic microelectromechanical applications*. J. Magn. Mater. **322**, 1592–1596 (2010).
- [21] G. PATTANAIK, D. KIRKWOOD, X. XU and G. ZANGARI. *Electrodeposition of hard magnetic films and microstructures*. Electrochim. Acta **52**, 2755–2764 (2007).

- [22] P. COJOCARU, L. MAGAGNIN, E. GOMEZ, E. VALLES, F. LIU, C. CARRARO and R. MABOUDIAN. *Magnetic micromechanical structures based on CoNi electrodeposited alloys*. J. Micromech. Microeng. **20**, 125017(1)–125017(6) (2010).
- [23] X. SUN, Q. YUAN, D. FANG and H. ZHANG. *Electrodeposition and characterization of CoNiMnP permanent magnet arrays for MEMS sensors and actuators*. Sensor. Actuat. A-Phys. page In press (2012).
- [24] P. KIM, A. EPSTEIN, M. KHAN, L. ZARZAR, D. LIPOMI, G. WHITESIDES and J. AIZENBERG. *Structural transformation by electrodeposition on patterned substrates (STEPS): A new versatile nanofabrication method*. Nano Lett. **12**, 527–533 (2012).
- [25] H. WANG, R. LIU, W. JIANG, J. ZHU, J. FENG, G. DING and X. ZHAO. *A novel method for improving the adhesion strenght of the electrodeposited Ni films in MEMS*. Appl. Surf. Sci. **257**, 2203–2207 (2011).
- [26] B. ANN, H. JI, J. WU, M. CHO, K. YANG, H. LEE and Y. KIM. *Phase changeable silver selenide thin films fabricated by pulse electrodeposition*. Current Applied Physics **9**, 1338–1340 (2009).
- [27] G. JI, J. CAO, F. ZHANG, G. XU, H. SU, S. TANG, B. GU and Y. DU. *NixPb1-x Nanowire Arrays: Effects of Annealing*. J. Phys. Chem. B **109**, 17100–17106 (2005).
- [28] X. LIN, G. JI, T. GAO, J. NIE and Y. DU. *Magnetic properties of CoCu nanowire arrays fabricated in different conditions by SC electrodeposition*. Solid State Commun. **152**, 1585–1589 (2012).
- [29] I. BAKONYI and L. PETER. *Electrodeposited multilayer films with giant magnetoresistance (GMR): progress and problems*. Prog. Mater. Sci. **55**, 107–245 (2010).
- [30] S. PANE, E. GOMEZ and E. VALLES. *Enhanced magnetism in electrodeposited-based CoNi composites containing high percentage of micron hard-magnetic particles*. Electrochem. Commun. **9**, 1755–1760 (2007).
- [31] A. ROLDAN, E. GOMEZ, S. PANE and E. VALLES. *Electrodeposition of copper magnetite magnetic composite films*. J. Appl. Electrochem. **37**, 575–582 (2007).
- [32] X. XU, S. ZHANG, H. CHEN and J. KONG. *Integration of electrochemistry in micro-total analysis systems for biochemical assays: Recent developments*. Talanta **80**, 8–18 (2009).
- [33] M. HERVAS, M. A. LOPEZ and A. ESCARPA. *Electrochemical immunosensing on board microfluidic chip platforms*. Trac-Trend. Anal. Chem. **31**, 109–128 (2012).

- [34] S. A. ANSARI and Q. HUSAIN. *Potential applications of enzymes immobilized on/in nano materials: A review*. *Biotechnology Advances* **30**, 512–523 (2012).
- [35] M. F. BARROSO, N. DE-LOS SANTOS-ALVAREZ, C. DELERUE-MATOS and M. OLIVEIRA. *Towards a reliable technology for antioxidant capacity and oxidative damage evaluation: Electrochemical (bio)sensors*. *Biosens. Bioelectron.* **30**, 1–12 (2011).
- [36] B. PEREZ-LOPEZ and A. MERKOCI. *Nanomaterials based biosensors for food analysis applications*. *Trends Food Sci. Tech.* **22**, 625–639 (2011).
- [37] A. L. ECKERMANN, D. J. FELD, J. SHAW and T. J. MEADE. *Electrochemistry of redox-active self-assembled monolayers*. *Coordin. Chem. Rev.* **254**, 1769–1802 (2010).
- [38] B. D. CULLITY. *Elements of X-ray diffraction*. ADDISON-WESLEY PUBLISHING COMPANY, Inc. (1956).
- [39] C. SERRE, A. PEREZ-RODRIGUEZ, N. FONDEVILLA, E. MARTINCIC, S. MARTINEZ and J. E. J.R. MORANTE, J. MONTSERRAT. *Design and implementation of mechanical resonators for optimized inertial electromagnetic microgenerators..* *Microsyst. Technol.* **14**, 653–658 (2008).
- [40] R. YALLOW and S. BERSON. *Assay of plasma insulin in human subject by immunological methods*. *Nature* **184**, 1648–1649 (1959).
- [41] D. ANDERSON, B. GUO, Y. XU, L. NG, L. KRICKA, K. SKOGERBOE, D. HAGE, L. SCHOEFF, J. WANG, L. SOKOLL, D. CHAN, K. WARD and K. DAVIS. *Clinical chemistry*. *Anal. Chem.* **69**, 165R–229R (1997).
- [42] S. BAGLIO, A. PEREZ-RODRIGUEZ, S. MARTINEZ, C. SERRE, J. R. MORANTE, J. ESTEVE and J. MONTSERRAT. *Microinductive Signal Conditioning With Resonant Differential Filters: High-Sensitivity Biodetection Applications*. *IEEE T. Instrum. Meas.* **56**, 1590–1595 (2007).
- [43] K. LARSSON, K. KRIZ and D. KRIZ. *Magnetic Transducers in Biosensors and Bioassays*. *Analisis.* **27**, 617–621 (1999).
- [44] D. GRAHAM, H. FERREIRA and P. FREITAS. *Magnetoresistive-based biosensors and biochips*. *Trends Biotechnol.* **22**, 455–462 (2004).
- [45] M. GIJS. *Magnetic bead handling on-chip: new opportunities for analytical applications*. *Microfluid. Nanofluid.* **1**, 22–40 (2004).

- [46] C. KRIZ, K. RADEVIK and D. KRIZ. *Magnetic permeability measurements in bioanalysis and biosensors*. Anal. Chem. **68**, 1966–1970 (1996).
- [47] RICHARDSON, P. HAWKINS and R. LUXTON. *The use of coated paramagnetic particles as a physical label in a magneto-immunoassay*. Biosens. Bioelectron. **16**, 989–993 (2001).
- [48] J. RICHARDSON, A. HILL, R. LUXTON and P. HAWKINS. *A novel measuring system for the determination of paramagnetic particle labels for use in magneto-immunoassays*. Biosens. Bioelectron. **16**, 1127–1132 (2001).
- [49] C. SERRE, S. MARTINEZ, A. PEREZ-RODRIGUEZ, J. MORANTE, J. ESTEVE and J. MONTSERRAT. *Si technology based microinductive devices for biodetection applications*. Sensor. Actuat. A-Phys. **132**, 499–505 (2006).
- [50] T. OSAKA. *Electrochemical formation and microstructure in thin films for high functional devices*. Electrochim. Acta **42**, 3015–3022 (1997).
- [51] C. NEAGU, J. GARDENIERS, M. ELWENSPOEK and J. KELLY. *An electrochemical active valve*. Electrochim. Acta **42**, 3367–3373 (1997).
- [52] L. ROMANKIW. *A path: from electroplating through lithographic masks in electronics to LIGA in MEMS*. Electrochim. Acta **42**, 2985–3005 (1997).
- [53] M. DATTA and D. LANDOLT. *Fundamental aspects and applications of electrochemical microfabrication*. Electrochim. Acta **45**, 2535–2558 (2000).
- [54] H. CHO and C. AHN. *A bidirectional magnetic microactuator using electroplated permanent magnet arrays*. J. Microelectromech. S. **11**, 78–84 (2002).
- [55] E. GOMEZ, E. PELLICER, M. DUCH, J. ESTEVE and E. VALLES. *Molybdenum alloy electrodeposits for magnetic actuation*. Electrochim. Acta **51**, 3214–3222 (2006).
- [56] M. DUCH, J. ESTEVE, E. GOMEZ, R. PEREZ-CASTILLEJOS and E. VALLES. *Electrodeposited Co-Ni alloys for MEMS*. J. Micromech. Microeng. **12**, 400–405 (2002).
- [57] M. DUCH, J. ESTEVE, E. GOMEZ, R. PEREZ-CASTILLEJOS and E. VALLES. *Development and characterization of Co-Ni alloys for microsystems applications*. J. Electrochem. Soc. **149**, C201–C208 (2002).
- [58] A. COUTROT, E. DUFOUR-GERGAM, J. QUEMPEL, E. MARTINCIC, J. GILLES, J. GRANDCHAMP, M. MATLOSZ, A. SANCHEZ, L. DARASSE and J. C. GINEFRI. *Copper micromoulding process for NMR microinductors realization*. Sensor. Actuat. A-Phys. **99**, 49–54 (2002).

- [59] C. SERRE, N. YAAKOUBI, S. MARTNEZ, A. PREZ-RODRGUEZ, J. MORANTE and J. M. J. ESTEVE. *Electrochemical deposition of Cu and Ni/Cu multilayers in Si Microsystem Technologies*. Sensor. Actuat. A-Phys. **123124**, 633–639 (2005).
- [60] K. D. DE LEZAMA, A. GARCIA-ARRIBAS, J. BARANDIARAN and J. GUTIERREZ. *Comparative study of alternative circuit configurations for inductive sensors*. Sensor. Actuat. A-Phys. **91**, 226–229 (2001).
- [61] S. BAGLIO, S. CASTORINA and N. SAVALLI. *Strategies and circuits for micro inductive biosensor conditioning*. Eurosensors XVI: Proceedings of the 16th European Conference on Solid-State Transducers pages 604–607 (2002).
- [62] H. DOLLE. *The Influence of Multiaxial Stress States, Stress Gradients and Elastic Anisotropy on the Evaluation of (Residual) Stresses by X-rays*. J. Appl. Cryst. **12**, 489–501 (1979).
- [63] T. OSAKA, T. SAWAGUCHI, F. MIZUTANI, T. YOKOSHIMA, M. TAKAI and Y. OKINAKA. *Effects of Saccharin and Thiourea on Sulfur Inclusion and Coercivity of Electroplated Soft Magnetic CoNiFe Film Articles*. J. Electrochem. Soc. **146**, 3295–3299 (1999).
- [64] I. TABAKOVIC, V. INTURI and S. RIEMER. *Composition, Structure, Stress, and Coercivity of Electrodeposited Soft Magnetic CoNiFe Films: Thickness and Substrate Dependence*. J. Electrochem. Soc. **149**, C18–C22 (2002).
- [65] F. LALLEMAND, D. COMTE, L. RICQ, P. RENAUX, J. PAGETTI, C. DIEPPEDALE and P. GAUD. *Effects of organic additives on electroplated soft magnetic CoFeCr films*. Appl. Surf. Sci. **225**, 59–71 (2004).
- [66] T. CHIN. *Permanent magnet films for micro-electro-mechanical system applications*. J. Magn. Magn. Mater. **209**, 75–79 (2000).
- [67] D. PARK, N. MYUNG, M. SCHWARTZ and K. NOBE. *Nanostructured magnetic CoNiP electrodeposits: structureproperty relationships*. Electrochim. Acta **47**, 2893–2900 (2002).
- [68] N. MYUNG, D. PARK, B. YOO and P. SUMODJO. *Development of electroplated magnetic materials for MEMS*. J. Magn. Magn. Mater. **265**, 189–198 (2003).
- [69] D. NIARCHOS. *Magnetic MEMS: key issues and some applications*. Sensor. Actuat. A-Phys. **109**, 166–173 (2003).
- [70] S. GUAN and B. NELSON. *Fabrication of hard magnetic microarrays by electroless codeposition for MEMS actuators*. Sensor. Actuat. A-Phys. **118**, 307–312 (2005).

- [71] S. GUAN and B. NELSON. *Electrodeposition of low residual stress CoNiMnP hard magnetic thin films for magnetic MEMS actuators*. J. Magn. Magn. Mater. **292**, 49–58 (2005).
- [72] Y. SU, H. WANG, G. DING, F. CUI, W. ZHANG and W. CHEN. *Electroplated hard magnetic material and its application in microelectromechanical systems*. IEEE Trans Magn **41**, 4380–4383 (2005).
- [73] F. PIGAZO, F. PALOMARES, F. CEBOLLADA and J. GONZALEZ. *Preparation of hard magnetic materials in thin film form*. J. Magn. Magn. Mater. **320**, 1966–1971 (2008).
- [74] K. LEW, M. RAJA, S. THANIKAIKARASAN, T. KIM, Y. KIM and T. MAHALINGAM. *Effect of pH and current density in electrodeposited CoNiP alloy thin films*. Mater. Chem. Phys. **112**, 249–253 (2008).
- [75] Q. XU, Y. KAGEYAMA and T. SUZUKI. *Ion-beam-induced chemical-vapor deposition of FePt and CoPt particles*. J. Appl. Phys. **97**, 10K308(1)–10K308(3) (2005).
- [76] X. CHEN, Z. JIANG, L. ZHANG, Y. CHEN, F. BAI, H. CHEN and J. ZHU. *Study on the Magnetic Properties and Microstructure of Nd-Fe-B Nanocomposite Permanent Magnets*. Mater. Sci. Forum **426-432**, 2381–2386 (2003).
- [77] Y. LIU, M. DALLIMORE, P. MCCORMICK and T. ALONSO. *Synthesis of SmCo<sub>5</sub> by chemical reduction during mechanical alloying*. Appl. Phys. Lett. **60**, 3186–3187 (1992).
- [78] K. ZUZEK-ROZMAN, A. KRAUSE, K. LEISTNER, S. FHLER, L. SCHULTZ and H. SCHLORB. *Electrodeposition and hard magnetic properties of CoPt films in comparison to FePt films*. J. Magn. Magn. Mater. **314**, 116–121 (2007).
- [79] P. CAVALLOTTI, M. BESTETTI and S. FRANZ. *Microelectrodeposition of CoPt alloys for micromagnetic applications*. Electrochim. Acta **48**, 3013–3020 (2003).
- [80] I. ZANA, G. ZANGARI, J. PARK and M. ALLEN. *Electrodeposited CoPt micron-size magnets with strong perpendicular magnetic anisotropy for MEMS applications*. J. Magn. Magn. Mater. **272276**, E1775– E1776 (2004).
- [81] K. LEE, S. KANG, G. KIM and W. JEUNG. *Fabrication of multi-layered CoPtP alloy with high coercivity and squareness by electrochemical deposition*. J. Magn. Magn. Mater. **272276**, E925–E926 (2004).
- [82] H. PARK, K. LEE, G. KIM and W. JEUNG. *Microstructure and magnetic properties of electrodeposited CoPtP alloys*. J. Appl. Phys. **99**, 08N305(1)–08N305(3) (2006).

- [83] L. VIEUX-ROCHAZ, C. DIEPPEDALE, B. DESLOGES, D. GAMET, C. BARRAGATTI, H. ROSTAING and J. MEUNIER-CARUS. *Electrodeposition of hard magnetic CoPt material and integration into magnetic MEMS*. J. Micromech. Microeng. **16**, 219–224 (2006).
- [84] N. YASUI, A. IMADA and T. DEN. *Electrodeposition of (001) oriented CoPt L10 columns into anodic alumina films*. Appl. Phys. Lett. **83**, 3347–3349 (2003).
- [85] Y. DAHMANE, L. CAGNON, J. VOIRON, S. PAIRIS, M. BACIA, L. ORTEGA, N. BENBRAHIM and A. K. AND. *Magnetic and structural properties of electrodeposited CoPt and FePt nanowires in nanoporous alumina templates*. J. Phys. D: Appl. Phys. **39**, 4523–4528 (2006).
- [86] M. A. WILLARD, L. K. KURIHARA, E. E. CARPENTER, S. CALVIN and V. G. HARRIS. *Chemically prepared magnetic nanoparticles*. Int. Mater. Rev. **49**, 125–170 (2004).
- [87] J. GALLOWAY, J. BRAMBLE, A. RAWLINGS, G. BURNELL, S. EVANS and S. STANILAND. *Biotemplated Magnetic Nanoparticle Arrays*. Small **8** (2), 204–208 (2012).
- [88] H. BOYEN, G. KASTLE, K. ZURN, T. HERZOG, F. WEIGL, P. ZIEMANN, O. MAYER, C. JEROME, M. MOLLER, J. SPATZ, M. GARNIER and P. OELHAFEN. *A Micellar Route to Ordered Arrays of Magnetic Nanoparticles: From Size-Selected Pure Cobalt Dots to CobaltCobalt Oxide CoreShell Systems*. Advanced Functional Materials **13** (5), 359–364 (2003).
- [89] Z. ZHONG, B. GATES, Y. XIA and D. QIN. *Soft Lithographic Approach to the Fabrication of Highly Ordered 2D Arrays of Magnetic Nanoparticles on the Surfaces of Silicon Substrates*. Langmuir **16** (26), 10369–10375 (2000).
- [90] J. RYBCZYNSKI, U. EBELS and M. GIERSIG. *Large-scale, 2D arrays of magneticnanoparticles*. Colloids Surface A **219** (13), 1–6 (2003).
- [91] X. LIU, L. FU, S. HONG, V. DRAVID and C. MIRKIN. *Arrays of Magnetic Nanoparticles Patterned via Dip-Pen Nanolithography*. Advanced Materials **14** (3), 231–234 (2002).
- [92] B. D. TERRIS and T. THOMSON. *Nanofabricated and self-assembled magnetic structures as data storage media*. J. Phys. D: Appl. Phys. **38**, R199–R222 (2005).
- [93] T. CHEN, F. PAN, J. HUNG, L. CHANG, S. WU and C. CHEN. *Amorphous Carbon Coated Silicon Nanotips Fabricated by MPCVD Using Anodic Aluminum Oxide as the Template*. J. Electrochem. Soc. **154**, D215–D219 (2007).

- [94] G. ZHANG and J. CHEN. *Synthesis and Application of La<sub>0.59</sub>Ca<sub>0.41</sub>CoO<sub>3</sub> Nanotubes Batteries, Fuel Cells, and Energy Conversion*. J. Electrochem. Soc. **152**, A2069–A2073 (2005).
- [95] R. INGUANTA, S. PIAZZA and C. SUNSERI. *Novel procedure for the template synthesis of metal nanostructures*. Electrochem. Commun. **10**, 506–509 (2008).
- [96] R. INGUANTA, S. PIAZZA and C. SUNSERI. *Template electrosynthesis of CeO<sub>2</sub> nanotubes*. Nanotechnology **18**, 485605(1)–485605(6) (2007).
- [97] B. YANG, Y. WU, B. ZONG and Z. SHEN. *Electrochemical Synthesis and Characterization of Magnetic Nanoparticles on Carbon Nanowall Templates*. Nano Lett. **2** (7), 751–754 (2002).
- [98] C. ROSS. *Patterned magnetic recording media*. Annu. Rev. Mat. Res. **31**, 203–235 (2001).
- [99] M. MOTOYAMA, Y. FUKUNAKA, T. SAKKA and Y. OGATA. *Initial stages of electrodeposition of metal nanowires in nanoporous templates*. Electrochim. Acta **53**, 5766–5773 (2008).
- [100] H. MASUDA and K. FUKUDA. *Ordered Metal Nanohole Arrays Made by a Two-Step Replication of Honeycomb Structures of Anodic Alumina*. Science **268**, 1466–1468 (1995).
- [101] E. A. DALCHIELE, R. E. MAROTTI, A. CORTES, G. RIVEROS, H. GOMEZ, L. MARTINEZ, R. R. D. LEINEN, F. MARTIN and J. R. RAMOS-BARRADO. *Silver nanowires electrodeposited into nanoporous templates: Study of the influence of sizes on crystallinity and structural properties*. Physica E **37**, 184–188 (2007).
- [102] G. RIVEROS, S. GREEN, A. CORTES, F. GOMEZ, R. E. MAROTTI and E. A. DALCHIELE. *Silver nanowire arrays electrochemically grown into nanoporous anodic alumina templates*. Nanotechnology **17**, 561–570 (2006).
- [103] S. CHU, S. INOUE, K. WADA and K. KURASHIMA. *Fabrication of integrated arrays of ultrahigh density magnetic nanowires on glass by anodization and electrodeposition*. Electrochim. Acta **51**, 820–826 (2005).
- [104] A. GAPIN, X. YE, L. CHEN, D. HONG and S. JIN. *Patterned media based on soft/hard composite nanowire array of Ni/CoPt*. IEEE Trans. Magn. **43**, 2151–2153 (2007).
- [105] N. CHAURE, F. RHEN, J. HILTON and D. COEY. *Design and application of a magnetic field gradient electrode*. Electrochem. Commun. **9**, 155–158 (2007).

- [106] S. SHAMAILA, R. SHARIF, S. RIAZ, M. K. UR RAHMAN and X. HAN. *Fabrication and magnetic characterization of  $\text{Co}_x\text{Pt}_{1-x}$  nanowire arrays*. Appl. Phys. A: Mater. **92**, 687–691 (2008).
- [107] L. ROMANKIW, I. CROLL and M. HATZAKIS. *Batch-fabricated thin-film magnetic recording heads*. IEEE Trans. Magn. **3**, 597–601 (1970).
- [108] J. LIN, W. ZHOU, A. KUMBHAR, J. WIEMANN, J. FANG, E. CARPENTER and C. OCONNOR. *Gold-Coated Iron ( $\text{Fe@Au}$ ) Nanoparticles: Synthesis, Characterization, and Magnetic Field-Induced Self-Assembly*. J. Solid State Chem. **159**, 26–31 (2001).
- [109] S. WANG, F. YUE, D. WU, F. ZHANG, W. ZHONG and Y. DU. *Enhanced magnetoresistance in self-assembled monolayer of oleic acid molecules on  $\text{Fe}_3\text{O}_4$  nanoparticles*. Appl. Phys. Lett. **94**, 012507(1)–012507(3) (2009).
- [110] X. TENG and H. YANG. *Iron Oxide Shell as the Oxidation-Resistant Layer in  $\text{SmCo}_5\text{@Fe}_2\text{O}_3$  CoreShell Magnetic Nanoparticles*. J. Nanosci. Nanotechnol. **7**, 356–361 (2007).
- [111] J. RIVAS, A. GARCIA-BASTIDA, M. LOPEZ-QUINTELA and C. RAMOS. *Magnetic properties of  $\text{Co/Ag}$  core/shell nanoparticles prepared by successive reactions in microemulsions*. J. Magn. Magn. Mater. **300**, 185–191 (2006).
- [112] O. IGLESIAS, X. BATLLE and A. LABARTA. *Particle size and cooling field dependence of exchange bias in core/shell magnetic nanoparticles*. J. Phys. D: Appl. Phys. **41**, 134010(1)–134010(5) (2008).
- [113] N. LAKSHMI, H. BHARGAVA, O. SUWALKO, K. VENUGOPALAN, V. SEBASTIAN, V. REDDY and A. GUPTA. *Magnetic properties resulting from core-shell interactions in nanosized  $\text{Ni}_{0.25}\text{Co}_{0.25}\text{Zn}_{0.5}\text{Fe}_2\text{O}_4$* . Phys. Rev. B **80**, 174425(1)–174425(6) (2009).
- [114] F. JIMENEZ-VILLACORTA and C. PRIETO. *Magnetic properties and interaction mechanisms of iron-based coreshell structures prepared by sputtering at low substrate temperatures*. J. Phys.: Condens. Matter **20**, 085216(1)–085216(10) (2008).
- [115] H. ZENG, S. SUN, J. LI, Z. WANG and J. LIU. *Tailoring magnetic properties of core-shell nanoparticles*. Appl. Phys. Lett. **85**, 792–794 (2004).
- [116] M. HANSEN, K. VECCHIO, F. PARKER, F. SPADA and A. BERKOWITZ. *Exchange-spring permanent magnet particles produced by spark erosion*. Appl. Phys. Lett. **82**, 1574–1576 (2003).

- [117] A. GABAY, M. MARINESCU and G. HADJIPANAYIS. *Enhanced  $M_r$  and  $(BH)_{max}$  in anisotropic  $R_2Fe_{14}B/Fe$  composite magnets via intergranular magnetostatic coupling*. J. Appl. Phys. **99**, 08B506(1)–08B506(3) (2006).
- [118] D. ROY and P. KUMAR. *Enhancement of  $(BH)_{max}$  in a hard-soft-ferrite nanocomposite using exchange spring mechanism*. J. Appl. Phys. **106**, 073902(1)–073902(4) (2009).
- [119] K. MOON, S. CHO, Y. CHOA, K. KIM and J. KIM. *Synthesis and magnetic properties of nano  $Ba$ -hexaferrite/ $NiZn$  ferrite composites*. Phys. Status Solidi A **204**, 4141–4144 (2007).
- [120] Y. WANG, F. LI, J. ARIAKE, N. HONDA, S. ISHIO and K. OUCHI. *Effect of the effective anisotropy field of soft layer on magnetic properties of soft/hard stacked media*. J. Magn. Magn. Mater. **320**, 3083–3087 (2008).
- [121] T. TANAKA, J. MATSUZAKI, H. KURISU and S. YAMAMOTO. *Magnetization behavior of hard/soft-magnetic composite pillar*. J. Magn. Magn. Mater. **320**, 3100–3103 (2008).
- [122] S. WOLF, D. AWSHALOM, R. BUHRMAN, J. DAUGHTON, S. VON MOLNR, M. ROUKES, A. Y. CHTCHELKANOVA and D. TREGGER. *Spintronics: a spin-based electronics vision for the future*. Science **294**, 1488–1495 (2001).
- [123] D. AWSHALOM and M. FLATT. *Challenges for semiconductor spintronics*. Nat. Phys. **3**, 153–159 (2007).
- [124] N. MOTT. *The transition to the metallic state*. Proc. Roy. Soc. **153**, 699–717 (1939).
- [125] M. JULLIERE. *Tunneling between ferromagnetic films*. Phys. Lett. **54A**, 225–226 (1975).
- [126] J. S. MOODERA and J. NASSAR. *Spin-tunneling in ferromagnetic junctions*. Annu. Rev. Mater. Sci. **29**, 381–432 (1999).
- [127] H. DERY, P. DALAL, L. CYWINSKI and L. SHAM. *Spin-based logic in semiconductors for reconfigurable large-scale circuits*. Nature **447**, 573–576 (2007).
- [128] Z. XIONG, D. WU, Z. V. VARDENY and J. SHI. *Giant magnetoresistance in organic spin-valves*. Nature **427**, 821–824 (2004).
- [129] E. HOLMSTROM, L. NORDSTROM, L. BERGQVIST, B. SKUBIC, B. HJORVARSSON, P. S. I. A. ABRIKOSOV and O. ERIKSSON. *On the sharpness of the interfaces in metallic multilayers*. PNAS **101** (14), 4742–4745 (2004).

- [130] S. PARKIN. *Spin-polarized current in spin valves and magnetic tunnel junctions*. MRS Bulletin **31**, 389–394 (2006).
- [131] A. R. ROCHA, V. M. GARCIA-SUAREZ, S. W. BAILEY, C. J. LAMBERT, J. FERRER and S. SANVITO. *Towards molecular spintronics*. Nat. mater. **4**, 335–339 (2005).
- [132] S. SANVITO. *Molecular Spintronics*. Chem:Soc.Rev. **40**, 3336–3355 (2011).
- [133] R. DELATORRE, M. MUNFORD, V. STENGER, A. PASA, W. SCHWARZACHER, M. MERUVIA and I. HUMMELGEN. *Electrodeposited p-type magnetic metal-base transistor*. J. Appl. Phys. **99**, 08H704–08H707 (2006).
- [134] C. XIE, H. LI, S. LI, J. WU and Z. ZHANG. *Surface molecular self-assembly for organophosphate pesticide imprinting in electropolymerized poly(p-aminothiophenol) membranes on a gold nanoparticle modified glassy carbon electrode*. Anal. Chem. **82**, 241–249 (2010).
- [135] T. CLARK, R. FERRIGNO, J. TIEN, K. PAUL and G. WHITESIDES. *Template-directed self-assembly of 10-microm-sized hexagonal plates*. J. Am. Chem. Soc. **124**, 5419–26 (2002).
- [136] B. DIACONESCU, T. YANG, S. BERBER, M. JAZDZYK, G. MILLER, D. TOMNEK and K. POHL. *Molecular Self-Assembly of Functionalized Fullerenes on a Metal Surface*. Phys. Rev. Lett. **102**, 056102(1)–056102(4) (2009).
- [137] S. JENSEN, A. BABER, H. TIERNEY and E. H. SYKES. *Dimethyl Sulfide on Cu111: Molecular Self-Assembly and Submolecular Resolution Imaging*. Acs. Nano. **1**, 423–428 (2007).
- [138] R. MICHALITSCH, C. NOGUES, A. NAJARI, A. ELKASSMI, A. YASSAR, P. LANG and F. . GARNIER. *beta-functionalized oligothiophenes for molecular self-assembly*. Synthetic Met. **101**, 5–6 (1999).
- [139] M. FONTICELLI, O. AZZARONI, G. BENITEZ, M. MARTINS, P. CARRO and R. SALVAREZZA. *Molecular Self-Assembly on Ultrathin Metallic Surfaces: Alkanethiolate Monolayers on Ag(1x1)-Au(111)*. J. Phys. Chem. B **108**, 1898–1905 (2004).
- [140] E. BALDRICH, O. LACZKA, F. DEL-CAMPO and F. MUNOZ. *Gold immunofunctionalisation via self-assembled monolayers: study of critical parameters and comparative performance for protein and bacteria detection*. J. Immunol. Methods **336** (2), 203–212 (2008).

- [141] S. LEI and M. LANQUON. *Gold nanoparticle/alkanedithiol conductive films self-assembled onto gold electrode: Electrochemistry and electroanalytical application for voltammetric determination of trace amount of catechol*. *Talanta* **70**, 68–74 (2006).
- [142] T. LUCZAK and M. BELTOWSKA-BRZEZINSKA. *Gold electrodes modified with gold nanoparticles and thio compounds for electrochemical sensing of dopamine alone and in presence of potential interferents. A comparative study*. *Microchim. Acta.* **174**, 19–30 (2011).
- [143] T. MASADOME, A. UEDA and M. KAWAKAMI. *Gold Electrode Modified with a Self-Assembled Monolayer of 11-Amino-1-undecanethiol Hydrochloride for the Determination of Anionic Surfactants*. *Anal. Lett.* **37**, 225–233 (2004).
- [144] L. VELLEMAN, J. SHAPTER and D. LOSIC. *Gold nanotube membranes functionalised with fluorinated thiols for selective molecular transport*. *J. Membrane Sci.* **328**, 121–126 (2009).
- [145] F. HUBENTHAL, N. BORG, T. WEIDNER, U. SIEMELING and F. TRAGER. *Gold nanoparticle growth on self-assembled monolayers of ferrocenyl-substituted terpyridine on graphite*. *Appl. Phys. A: Mater* **94**, 11–17 (2009).
- [146] M. SHEFFER, V. VIVIER and D. MANDLER. *Self-assembled monolayers on Au microelectrodes*. *Electrochem. Commun.* **9**, 2827–2832 (2007).
- [147] M. SILVA, I. CAVALCANTI, M. BARROSO, M. SALES and R. DUTRA. *Gold electrode modified by self-assembled monolayers of thiols to determine DNA sequences hybridization*. *J. Chem. Sci.* **122**, 911–917 (2010).
- [148] H. AOKI, Y. UMEZAWA, A. VERTOVA and S. RONDININI. *Ion-channel sensors based on ETH 1001 ionophore embedded in charged-alkanethiol self-assembled monolayers on gold electrode surfaces*. *Anal. Sci.* **22**, 1581–1584 (2006).
- [149] Z. MEKHALIF, J. RIGA, J. PIREAUX and J. DELHALLE. *Self-Assembled Monolayers of n-Dodecanethiol on Electrochemically Modified Polycrystalline Nickel Surfaces*. *Langmuir* **13**, 2285–2290 (1997).
- [150] J. PETTA, S. SLATER and D. RALPH. *Spin-Dependent Transport in Molecular Tunnel Junctions*. *Phys. Rev. Lett.* **93**, 136601–136604 (2004).
- [151] M. KLOKKENBURG, J. HILHORST and B. ERNE. *Surface analysis of magnetite nanoparticles in cyclohexane solutions of oleic acid and oleylamine*. *Vib. Spectrosc.* **43**, 243–248 (2007).

- [152] T. SORENSON, S. MORTON, G. WADDILL and J. SWITZER. *Epitaxial Electrodeposition of Fe<sub>3</sub>O<sub>4</sub> Thin Films on the Low-Index Planes of Gold*. J. Am. Chem. Soc. **124**, 7604–7609 (2002).
- [153] Z. ZHANG and S. SATPATHY. *Electron states, magnetism, and the Verwey transition in magnetite*. Phys. Rev. B **44**, 13319–13331 (1991).
- [154] V. ANISIMOV, I. ELFIMOV, N. HAMADA and K. TERAKURA. *Charge-ordered insulating stage of Fe<sub>3</sub>O<sub>4</sub> from first-principles electronic structure calculations*. Phys. Rev. B **54**, 4387–4390 (1996).
- [155] H. KOTHARI, E. KULP, S. LIMMER, P. POIZOT, E. BOHANNAN and J. SWITZER. *Electrochemical deposition and characterization of Fe<sub>3</sub>O<sub>4</sub> films produced by the reduction of Fe(III)-triethanolamine*. J. Mater. Res. **21** (1), 293–301 (2006).
- [156] J. M. GARCIA-TORRES, E. GOMEZ and E. VALLES. *Modulation of magnetic and structural properties of cobalt thin films by means of electrodeposition*. J. Appl. Electrochem. **39**, 233–240 (2009).
- [157] P. EVANS, G. YI and W. SCHWARZACHER. *Current perpendicular to plane giant magnetoresistance of multilayered nanowires electrodeposited in anodic aluminum oxide membranes*. Appl. Phys. Lett. **76**, 481–483 (2000).
- [158] M. MUNFORD, L. SELIGMAN, M. SARTORELLI, E. VOLTOLINI, L. MARTINS, W. SCHWARZACHER and A. PASA. *Electrodeposition of magnetic thin films of cobalt on silicon*. J. Magn. Magn. Mater. **226**, 1613–1615 (2001).
- [159] A. M. JUBB and H. C. ALLEN. *Vibrational Spectroscopic Characterization of Hematite, Maghemite, and Magnetite Thin Films Produced by Vapor Deposition*. Appl. mat. inter. **2** (10), 2804–2812 (2010).
- [160] D. L. A. DE FARIA, S. V. SILVA and M. T. DE OLIVEIRA. *Raman Microspectroscopy of Some Iron Oxides and Oxyhydroxides*. J. Raman Spectrosc. **28**, 873–878 (1997).
- [161] O. N. SHEBANOVA and P. LAZOR. *Raman spectroscopic study of magnetite (Fe<sub>3</sub>O<sub>4</sub>): a new assignment for the vibrational spectrum*. J. Solid State Chem. **174**, 424–430 (2003).